UNIVERSITY OF CALIFORNIA SAN DIEGO

Cortical replay, hippocampal ripples, and cortico-hippocampal communication in human sleep

A dissertation submitted in partial satisfaction of the
requirements for the degree Doctor of Philosophy

in

Neurosciences

with a Specialization in Computational Neurosciences

by

Xi Jiang

Committee in charge:

Professor Eric Halgren, Chair
Professor Jill Leutgeb
Professor Terrence Sejnowski
Professor Bradley Voytek
Professor John Wixted

2018

The Dissertation of Xi Jiang is approved, and it is acceptable in quality and form for publication on microfilm and electronically:

_____

_____

_____

_____

_____

Chair

University of California San Diego

2018

DEDICATION

To ten-year-old me, who wanted to be a comedian;

To twelve-year-old me, who wanted to be a novelist;

And to fifteen-year-old me, who wanted to be a philosopher:

Better luck next time!

EPIGRAPH

No one applauded after Zhang San-Feng's demonstration of sword forms: how could such slow and powerless techniques—if indeed they could be called that—be worth anything in a fight? Some thought it must be that Master Zhang deliberately slowed down his movements for his pupil Wu-Ji's sake, lest he miss the details.

San-Feng spoke up: "Did you watch carefully, my child?"

Wu-Ji replied: "I did."

"Do you remember everything?"

"I've forgotten a little bit."

"Well, must be hard for you then. Think on it a little more."

Wu-Ji kept quiet. After a few moments, San-Feng asked again: "How about now?"

"I've forgotten more than half."

Zhou Dian, who served under Wu-Ji, was rattled: "That's terrible; he just kept forgetting! Master Zhang, your swordsmanship was too profound to be learned through one demonstration alone! Won't you please go through the forms again?"

San-Feng smiled and said: "Sure; I'll go through them again." He held up the sword and began anew. After a few forms, everyone was confused: none of the forms were the same as the ones in the last demonstration! Zhou Dian was desperate: "No, no! This makes the problem even worse!" San-Feng drew back the sword with a circular swipe, and asked again: "My child, how about now?"

Wu-Ji replied: "I still haven't forgotten three forms."

San-Feng nodded, sheathed the sword, and returned to his seat.

Wu-Ji walked around the hall for a few more moments, first in a small circle, then in a half-circle, before stopping altogether. Suddenly he raised his head, face beaming with pleasure, and shouted: "I have completely forgotten everything!"

"Wonderful!" Said San-Feng: "You have forgotten very quickly! Now you are ready to face the Eight-Armed Swordmaster."

—Translated (liberally) from "The Heaven Sword and Dragon Saber", by Jin Yong

TABLE OF CONTENTS

LIST OF ABBREVIATIONS

Ant: anterior

DS: downstate

ECoG: electrocorticography

EEG: electroencephalography

GE: graphoelement

HC: hippocampus

HG: high gamma

LFP: local field potential

NC: neocortex

NREM: non-rapid eye movement (sleep)

N2: stage 2 of NREM sleep

N3: stage 3 of NREM sleep

PLV: phase-locking value

Post: posterior

REM: rapid eye movement (sleep)

ROI: (neocortical) region of interest

SEEG: stereotactic electroencephalography

Sleep-Post: NREM sleep periods after a given waking period

Sleep-Pre: NREM sleep periods before a given waking period

SS: spindle

SSR: spindle-ripple

SWR: sharpwave-ripple

SWS: slow-wave sleep

TB: theta burst

US: upstate

LIST OF FIGURES

LIST OF TABLES

ACKNOWLEDGEMENTS

I would like to acknowledge Professor Eric Halgren for his support as the chair of my committee; I greatly appreciate of his magnanimity, his scientific acumen, and his biking skills.

I would also like to acknowledge the rest of my committee for their invaluable advice, and to express my gratitude for my lab mates putting up with me along the way: C. D., Q. D., C. G., M. H., E. K., D. M., R. M., A. N., B. R., and I. S. Special thanks to T., G., and V.—our cohort of lab crayfish, now unfortunately deceased—and to Dog, my poorly named cat.

Chapter 1, in full, is a reprint of the material as it appears in Scientific Reports, Article number: 17380 (2017), under the title "Replay of large-scale spatio-temporal patterns from waking during subsequent NREM sleep in human cortex", Jiang, Xi; Shamie, Isaac; Doyle, Werner; Friedman, Daniel; Dugan, Patricia; Devinsky, Orrin; Eskandar, Emad; Cash, Sydney S.; Thesen, Thomas; Halgren, Eric, Nature Research, 2017. The dissertation author was the primary investigator and author of this paper.

Chapter 2, in full, is currently being prepared for submission for publication of the material. Jiang, Xi; Gonzalez-Martinez, Jorge; Cash, Sydney S.; Chauvel, Patrick; Halgren, Eric. The dissertation author was the primary investigator and author of this paper.

Chapter 3, in full, is currently being prepared for submission for publication of the material. Jiang, Xi; Gonzalez-Martinez, Jorge; Halgren, Eric. The dissertation author was the primary investigator and author of this paper.

Chapter 4, in full, is currently being prepared for submission for publication of the material. Jiang, Xi; Gonzalez-Martinez, Jorge; Halgren, Eric. The dissertation author was the primary investigator and author of this paper.

VITA

2013 Bachelor of Science, Emory University

2015 Master of Science, University of California San Diego

2018 Doctor of Philosophy, University of California San Diego

PUBLICATIONS

"Replay of large-scale spatio-temporal patterns from waking during subsequent NREM sleep in human cortex" Scientific Reports, article number 17380, December 2017.

"Toward a database of intracranial electrophysiology during natural language presentation" Language, Cognition and Neuroscience, July 2018.

FIELDS OF STUDY

Major Field: Neuroscience

Computational Neuroscience Specialization
Professor Eric Halgren

ABSTRACT OF THE DISSERTATION

Cortical replay, hippocampal ripples, and cortico-hippocampal communication in human sleep

by

Xi Jiang

Doctor of Philosophy in Neurosciences with a Specialization in Computational Neurosciences

University of California San Diego, 2018

Professor Eric Halgren, Chair

Non-rapid eye movement (NREM) sleep is crucial for memory formation in mammals. Cortical replay of awake neural activity in NREM sleep, coordinated by hippocampal ripples (high-frequency oscillations that mark hippocampal replay of waking neuronal firing sequences), is thought to facilitate the consolidation of novel experience. However, direct human electrophysiological evidence for replay is lacking. Moreover, hippocampal ripples and their connection to cortical activity are not well characterized in humans, partly owing to the difficulty in accessing the human hippocampus; while some reports show human sharpwave-ripples as

found in animals, others report hippocampal sleep spindles that modulate ripples and co-occur with scalp EEG spindles. Thus, I performed analyses on human intracranial electrophysiological data, separating high-gamma power-based neocortical population firing peaks and hippocampal ripples from interictal activity. In Chapter 1, consistent sequences of high-gamma peaks ("Motifs") across neocortex were captured during waking. These Motifs were then compared to activity patterns in sleeps preceding (Sleep-Pre) and following (Sleep-Post) waking. Motifs predominantly resembled patterns in Sleep-Post than in Sleep-Pre, thereby constituting human cortical replay. In Chapter 2, hippocampal sharpwave-ripples were characterized in terms of their morphology, spectral characteristics, occurrence rate, and spread. While some traits were shared with animals, such as LFP morphology, others were potentially unique to humans, e.g. preferential occurrence in anterior hippocampus. In Chapter 3, the relationship between hippocampal sharpwave-ripples and neocortical sleep graphoelements in NREM was explored, whereby sharpwave-ripples were found to associate with neocortical theta bursts, spindles, downstates and upstates across the whole cortex, often with characteristic temporal latencies. Neocortical events near sharpwave-ripples also tended to follow specific sequences, i.e. theta burst-downstate-spindle "triplets". In Chapter 4, the previously published claim of human ripples organized by hippocampal spindles was investigated. While new evidence did support hippocampal spindles modulating ripples, both sharpwave-ripples and spindle-ripples were found in the same hippocampal locations, as well as transitional forms. Hippocampal spindles and spindle-ripples preferentially occurred in posterior hippocampus, were coordinated with cortical NREM graphoelements, and tended to phase-lock with co-occurring neocortical (especially parietal) spindles. In sum, human sharpwave-ripples and spindle-ripples may constitute separate, if complementary, routes toward organization of cortical reactivation and memory consolidation.

www.nature.com/scientificreports

SCIENTIFIC REPORTS

OPEN

Received: 14 August 2017
Accepted: 27 November 2017
Published online: 12 December 2017

Replay of large-scale spatio-temporal patterns from waking during subsequent NREM sleep in human cortex

Xi Jiang[1], Isaac Shamie[2], Werner K. Doyle[3], Daniel Friedman[3], Patricia Dugan[3], Orrin Devinsky[3], Emad Eskandar[4], Sydney S. Cash[5], Thomas Thesen[3,6] & Eric Halgren[2,7]

Animal studies support the hypothesis that in slow-wave sleep, replay of waking neocortical activity under hippocampal guidance leads to memory consolidation. However, no intracranial electrophysiological evidence for replay exists in humans. We identified consistent sequences of population firing peaks across widespread cortical regions during complete waking periods. The occurrence of these "Motifs" were compared between sleeps preceding the waking period ("Sleep-Pre") when the Motifs were identified, and those following ("Sleep-Post"). In all subjects, the majority of waking Motifs (most of which were novel) had more matches in Sleep-Post than in Sleep-Pre. In rodents, hippocampal replay occurs during local sharp-wave ripples, and the associated neocortical replay tends to occur during local sleep spindles and down-to-up transitions. These waves may facilitate consolidation by sequencing cell-firing and encouraging plasticity. Similarly, we found that Motifs were coupled to neocortical spindles, down-to-up transitions, theta bursts, and hippocampal sharp-wave ripples. While Motifs occurring during cognitive task performance were more likely to have more matches in subsequent sleep, our studies provide no direct demonstration that the replay of Motifs contributes to consolidation. Nonetheless, these results confirm a core prediction of the dominant neurobiological theory of human memory consolidation.

"Replay" of spatio-temporal neuronal activity patterns from waking during slow-wave sleep (SWS) was first demonstrated in rat hippocampal place cells[1,2]. Hippocampal replay is hypothesized to play a crucial role in memory consolidation, orchestrating cortical replay during sleep, resulting in synaptic plasticity and thus memory consolidation[1,3]. Indeed, replay coordinated with the hippocampus occurs in visual[4] and prefrontal[5,6] cortices, and memory strength can be modulated by disrupting or augmenting replay[7]. While most replay studies were conducted in rats, one study found replay of firing-patterns across motor, somatosensory, and parietal cortices in macaques[8], where both within-area and across-area (parietal and motor) neural ensembles were seen to reactivate. Reactivation of local hemodynamic patterns evoked by previously studied stimuli have been demonstrated in humans[9–13]. However, hemodynamic signals are too sluggish to detect temporal (i.e. sequential activation) patterns that are critical for memory encoding and consolidation, or to allow identification of fine temporal correlations with sleep graphoelements relevant to memory processing. Replay may also occur in scalp EEG[14] or MEG[15] recordings, but their poor spatial resolution and correlation with neuronal firing limit their interpretation. Similarly, average correlation patterns of ECoG broadband gamma power over sensory areas during NREM was reported to resemble the correlation patterns during awake movie-watching periods[16]. While supportive of spatial pattern reactivations in the human cortex specifically during NREM, such full-night average methods

[1]Neurosciences Graduate Program, University of California at San Diego, La Jolla, CA, 92093, USA. [2]Department of Radiology, University of California at San Diego, La Jolla, CA, 92093, USA. [3]Comprehensive Epilepsy Center, New York University School of Medicine, St George's, NY, 10016, USA. [4]Department of Neurosurgery, Massachusetts General Hospital, Harvard Medical School, Boston, MA, 02114, USA. [5]Department of Neurology, Massachusetts General Hospital, Harvard Medical School, Boston, MA, 02114, USA. [6]Department of Physiology & Neuroscience, St. George's University, West Indies, Grenada. [7]Department of Neurosciences, University of California at San Diego, La Jolla, CA, 92093, USA. Correspondence and requests for materials should be addressed to X.J. (email: x4jiang@ucsd.edu) or E.H. (email: ehalgren@ucsd.edu)

were insufficient for investigating whether, like animal replay, fine temporal structures/sequences could be established for widespread cortical reactivations. Here we utilized long-term (>4 days) recordings using intracranial electrodes placed for the localization of seizure onset and eloquent cortex in subjects with focal epilepsy. Electrode contacts were either within the cortex and hippocampus (stereoelectroencephalography, SEEG), or were on the cortical surface (electrocorticography, ECoG). We measured High Gamma (HG) activity (70–190 Hz) across widespread cortical locations. HG amplitude tracks local neuronal firing[17], and predicts declarative memory encoding[18] and retrieval[19]. Across cognitive tasks and conditions, HG amplitude is strongly correlated with hemodynamics, but has much faster (millisecond) resolution[20].

We simultaneously recorded Local Field Potentials (LFP) from multiple cortical sites to detect the widespread cortical modulations characteristic of NREM. LFPs are generated by spatially organized and temporally-coherent trans-membrane currents, and can be seen at the scalp as EEG and MEG[21]. The NREM characteristics we identified include sleep spindles (~500–2000 ms bursts of 10–17 Hz waves) and delta activity[22,23]. Delta is comprised of rhythmic "downstates" and "upstates", wherein the cortex alternates at ~0.5–2 Hz between near-silence and firing similar to quiet waking[24]. Cortical replay in rodents is associated with spindles and down-to-upstates[22,23], and memory consolidation in humans is associated with their density in the EEG[9,25]. In addition to spindles and delta activities, whose phasic coupling to ripples appears to enhance consolidation[26], there have also been reports of cortical theta oscillations coordinating sequential encoding of episodic memory[27] and their occurrence in NREM sleep being predictive of successful verbal memory recall[28]. We also related possible replay events to hippocampal sharp-wave ripples, which in rodents mark the occurrence of cellular replay[29].

Our strategy for detecting candidate spatiotemporal patterns for replay was based on several previous observations. In humans, hemodynamic patterns specific for particular memories are distributed during encoding and retrieval[30]. In rodents, c-Fos up-regulation is widespread across multiple cortical areas after learning[31,32], with a delayed wave of hippocampal c-Fos expression, peaking 18–24 hours after training regimens that produce long lasting memories[33]. Therefore, we reasoned that distributed spatio-temporal patterns of sequential HG amplitude peaks would be found if we searched in 6–19 hours of continuous waking ECoG/SEEG. Based on their spatio-temporal similarity, we clustered these patterns into recurring "Motifs". We hypothesized that these Motifs would be more prevalent during NREM periods following the waking period ("Sleep-Post") than those preceding it ("Sleep-Pre"), thus indicating a "replay" of the day's neural activities during subsequent sleeps.

Results

For each subject, widespread cortical Motifs were identified during waking, and spatiotemporal activity patterns similar to those Motifs (and therefore considered putative *reactivations* of Motifs) were identified from the two NREM periods (including both N2 and N3, but not N1; see "Preprocessing and SWS sleep period selection" in Methods) that comprise Sleep-Post (i.e. subsequent to the waking period) and the two NREM periods that comprise Sleep-Pre (i.e. preceding the waking period). A significant majority of those Motifs were more likely to occur more often in Sleep-Post than in Sleep-Pre. Novel Motifs, or Motifs identified during active cognition, were more likely to be preferentially re-activated during Sleep-Post. Motif recurrence was associated with increased cortical spindles and slow oscillation power, as well as broadband hippocampal activation. A list of which subjects were involved in each analysis can be found as Supplementary Table S1.

Identification of consistent spatiotemporal Motifs of cortical activity during waking. For each subject, temporal sequences comprising HG peaks across multiple cortical locations ("Events") (Supplementary Fig. S1, Fig. 1) were detected in both the single central waking period (W_0) and the four NREM periods (Supplementary Fig. S2), two preceding W_0 (thus comprising "Sleep-Pre") and two following W_0 (thus comprising "Sleep-Post"). Consistent Motifs of cortical activity were derived from waking Events using measures of similarity in the spatial distribution of active locations across the cortex, and the sequential order in which different cortical locations become active. Please note that we use the term "Event" to refer to a particular observed spatiotemporal sequence of HG peaks, and the term "Motif" to refer to the inferred consistent spatiotemporal pattern which could appear as several different Events with similar HG peak sequences. Our analysis detected Events and inferred Motifs during waking, then assimilated Events to Motifs during NREM in order to statistically compare their occurrence in different sleep periods. The spatial similarity of these Events was quantified using channel ensemble-wise correlation coefficients adopted from rodent studies of cortical patterns and memory replay[34]. The temporal similarity of the Events was computed using matching indices[4], which required at least four distinct elements in a sequence; only Events containing at least 4 HG peaks from unique cortical loci were therefore involved in the identification of Motifs. Using these metrics, hierarchical clustering reduced the initial set of Events to a set of Motifs which consistently repeated during waking.

Based on the observed duration of cortical replay events from rodent data[4], we defined our Event selection criteria as having a total duration (i.e. time between the occurrence of the first and the last HG peak) of <2000 milliseconds, with no temporal overlap between any two Events. In order to test whether the occurrence of such Events is different from what would be expected under the null hypothesis of no consistent relationship in the activity of different cortical locations, the same Event detection procedure was applied to 1000 bootstrap replicates with shuffled inter-peak intervals. Because the HG peaks in different channels after shuffling no longer were temporally related to each other, the number of Events increased (Fig. 2a). However, because these Events no long resembled each other as often, the number of Motifs declined (Fig. 2b), and the number of channels contributing peaks to Events which were detected after shuffling was correspondingly smaller (Fig. 2c). These effects were all significant at the $p < 0.001$ level (i.e., all 1000 shuffles produced numbers outside the range of the actually observed data). This result held in all six subjects and also for each of the four NREM periods. These observations

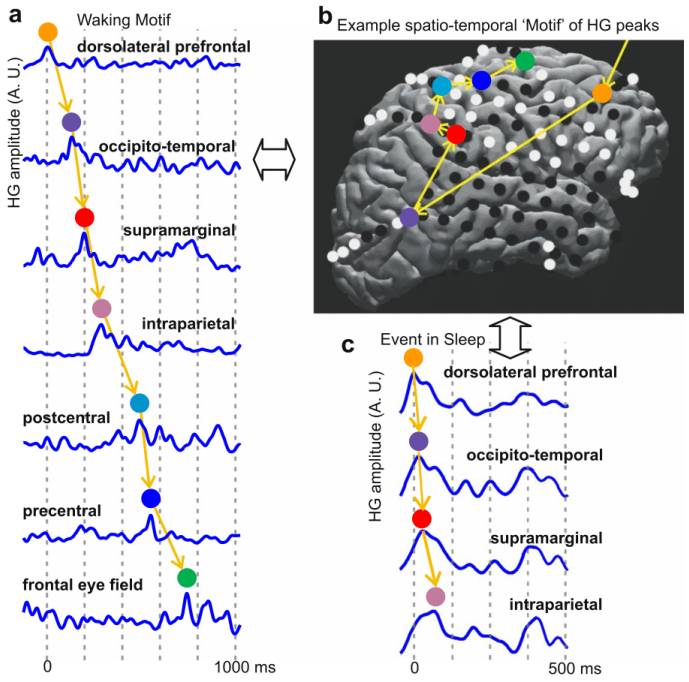

Figure 1. Spatio-temporal cortical activity Events and Motifs. (**a**) Example Waking Event, comprising a sequence of HG peaks occurring within 2s. A.U.: arbitrary units. (**b**) Example spatio-temporal Motif of HG peaks. Events were spatially- and temporally-clustered to obtain 60–250 representative Motifs for each subject, each with >20 Events (see "Motif selection and matching index analysis" in Methods and Fig. S1). Motifs with the most representative temporal order were matched against Events found in NREM (Fig. 3a). (**c**) Example NREM Event whose HG peaks come from channels involved in the Motif to the left and are in the same temporal order as the same channels' HG peaks in the Motif.

suggest that the detected Events represent non-random consistent spatio-temporal sequences of large peaks of cortical population firing.

Recurrence of Motifs in the form of Motif-Event matches during sleep. These highly distributed cortical activity Motifs identified during waking were then matched with Events during NREM in two preceding ("Sleep-Pre") and two subsequent ("Sleep-Post") nights. We concentrated our analysis on N2 and N3 rather than lighter NREM or REM sleep because it is characterized by the spindles and slow oscillations which are correlated with replay in rodents[22,23] and consolidation in humans[25,35]. Stages N2 and N3 were combined because both contain spindles and slow oscillations (with delta power increasing and spindle power decreasing as N2 progresses into N3)[36–38]. Also, combining N2 and N3 increased comparability to rodents who do not display that distinction during SWS[26,39]. NREM was identified by increased low delta (<2 Hz) and spindle (9–17 Hz) and decreased high gamma (70–190 Hz) power (Supplementary Fig. S3). Sleep depth was quantitatively matched using these characteristics in the Sleep-Pre vs. Sleep-Post epochs entered into analysis (Supplementary Fig. S3). Further confirmation of subject sleep/wake states was provided by state separation via PCA[40] (Supplementary Fig. S3).

We identified Event matches to waking Motifs (Motif-Event matches) using the stringent criterion that all common channels must show gamma activity in the exact same temporal order, and sub-selected the Motifs under the consistency criteria, which remain unchanged for all subsequent analyses and are detailed as follows: we derived waking Motifs from the central waking period W_0, and for each Motif, the number of Event matches were computed for S_{-2}, S_{-1}, S_1, and S_2 separately (Fig. 3a), with normalization to the total number of Events for each sleep period. However, if we denote the number of matches, or number of replaying frames (NRF) for a given sleep n, as NRF-S_n, then for a given Motif to be considered for subsequent analyses, it needs to satisfy either of the following:

(1) NRF-S_1 > NRF-S_{-1}, NRF-S_1 > NRF-S_{-2}, NRF-S_2 > NRF-S_{-1}, and NRF-S_2 > NRF-S_{-2}.
(2) NRF-S_1 < NRF-S_{-1}, NRF-S_1 < NRF-S_{-2}, NRF-S_2 < NRF-S_{-1}, and NRF-S_2 < NRF-S_{-2}.

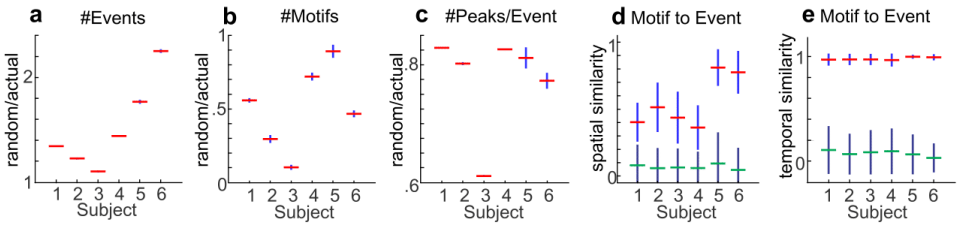

Figure 2. Waking Events and Motifs do not arise from chance, and are spatio-temporally similar. (**a**) The number of Events obtained from actual data is less than expected numbers from chance. Pseudo-Events were obtained from 1000 data shuffles (with the inter-peak intervals of each channel randomly permuted). For each subject, the distribution of ratios between the number of Events from shuffles and the actual number of Events is summarized. In this and all panels, the red horizontal line marks the mean, and the blue vertical line marks the standard deviation (SD). (**b**) The number of Motifs obtained from actual data is greater than expected numbers from chance. Pseudo-Motifs were obtained from >300 of the shuffles performed in (**a**) The distribution of ratios between the number of pseudo-Motifs from shuffles and the actual number of Motifs is summarized similar to (**a**). (**c**) The number of channels involved in waking Events are thus greater than expected from chance. The distribution of ratios between the mean numbers of channels from pseudo-Events in (**a**) and the actual means are summarized as in (**a** and **b**). (**d**,**e**) Events are more similar spatio-temporally to the Motifs they matched to than the other Motifs. (**d**), The distribution of spatial similarity indices calculated for Motif-to-Event matches (with red mean lines) and the distribution of indices calculated between Motifs and Events that are not matched to them (with green mean lines). The spatial index for each Motif-Event pair is defined as 2 x (number of channels in common)/(total number of channels in both the Motif and the Event). (**e**), The distribution of temporal similarity indices for the Motif-Event pairs from (**d**). The temporal index for each Motif-Event pair is defined as $[1+(m-n)/(m+n)]/2$, where m is the number of Event channel pairs in the same temporal order as the same channels in the Motif, and n is the number of such channel pairs in the opposite temporal order. For both (**d** and **e**, the blue distributions are significantly different from the black (two-sample Kolmogorov-Smirnov test, $p < 0.0001$), and the blue distributions have significantly greater medians (Mann-Whitney U test, $p < 0.0001$).

In particular, criterion 1 ensures that both NRFs from Sleep-Pre could not be greater than any NRFs from Sleep-Post for a given Motif to be considered "replaying", and criterion 2 the opposite. In terms of both spatial and temporal similarity, the Events were more similar to their matched Motifs than to other Motifs with whom they did not match. In other words, for each subject, the distribution of spatial or temporal distance metrics for Motif-to-Event matches appeared to be significantly different (two-sample Kolmogorov-Smirnov test, $p < 0.0001$) and to have a significantly greater median (Mann-Whitney *U* test, $p < 0.0001$) when compared to the distribution of distances between unmatched Motifs and Events (Fig. 2d,e).

Our major finding was that in all six subjects (abbreviated as "Sub"), significantly more waking Motifs showed greater numbers of matches to activity in Sleep-Post than that in Sleep-Pre (Fig. 3c, $p = 0.0368$ for Sub. 1, $p = 0.0022$ for Sub. 2, $p = 0.0061$ for Sub. 4, $p < 0.0001$ for Sub. 3 and Sub. 6, $p = 0.0007$ for Sub. 5). Thus, the majority of distributed spatiotemporal Motifs of cortical activity observed during waking occur more often in the following nights, as compared to the preceding nights. While replay sequences in rodents appear to be temporally compressed compared to waking events[1,4], the inter-peak intervals of our waking Motifs that recurred (i.e. had more Sleep-Post matches) were not significantly greater than those of the matching Events during NREM (Wilcoxon rank sum test) (Supplementary Fig. S4).

Preferential re-activation during Sleep-Post is robust. We tested whether this finding of more Motifs with preferential re-activation during Sleep-Post was robust by varying our analysis in three ways. First, since replay Motifs during sleep (i.e. Events in sleep that matched waking Motifs) are not necessarily exactly identical to those during waking, we relaxed our criterion for a Motif-Event match. Rather than requiring that the activation order of all channels match exactly, we required only that the number of channel-pairs in the correct order was significantly above chance[4]. Again, all subjects displayed a significant propensity to have Motifs with more Sleep-Post matches (Fig. 3d, $p = 0.3806$ for Sub. 4, $p = 0.0048$ for Sub. 1, $p = 0.0035$ for Sub. 2, $p = 0.0036$ for Sub. 5, $p < 0.0001$ for Sub. 3 and Sub. 6). Second, we modified our criterion for considering a Motif to have occurred more often in Sleep-Post than Sleep-Pre periods. Rather than simply comparing the normalized number of Motif-Event matches in the two Sleep-Post periods to the number in the two Sleep-Pre periods, we required that the total number of matches exceed a threshold established by comparing Sleep-Pre and -Post Events to the same Motifs, whose channel orders were randomly shuffled[4]. Only the four ECoG subjects had a sufficient number of Motifs to repeat our analysis with the stringent (Fig. 3e, $p < 0.0001$ for each subject) and combinatorial requirements (Fig. 3f, $p < 0.0001$ for each subject) after the shuffle tests. In all four subjects, more Motifs had a greater number of significant Sleep-Post matches than Sleep-Pre matches.

Third, we altered the criteria used to identify Events: we repeated our initial exact match analyses with different maximum Event duration in seconds (from 500 ms to 4000 ms, in 500 ms steps) and with different HG peak percentile thresholds (95^{th} to 99^{th} percentile, in 1 percentile steps). For all six subjects, we observed significant

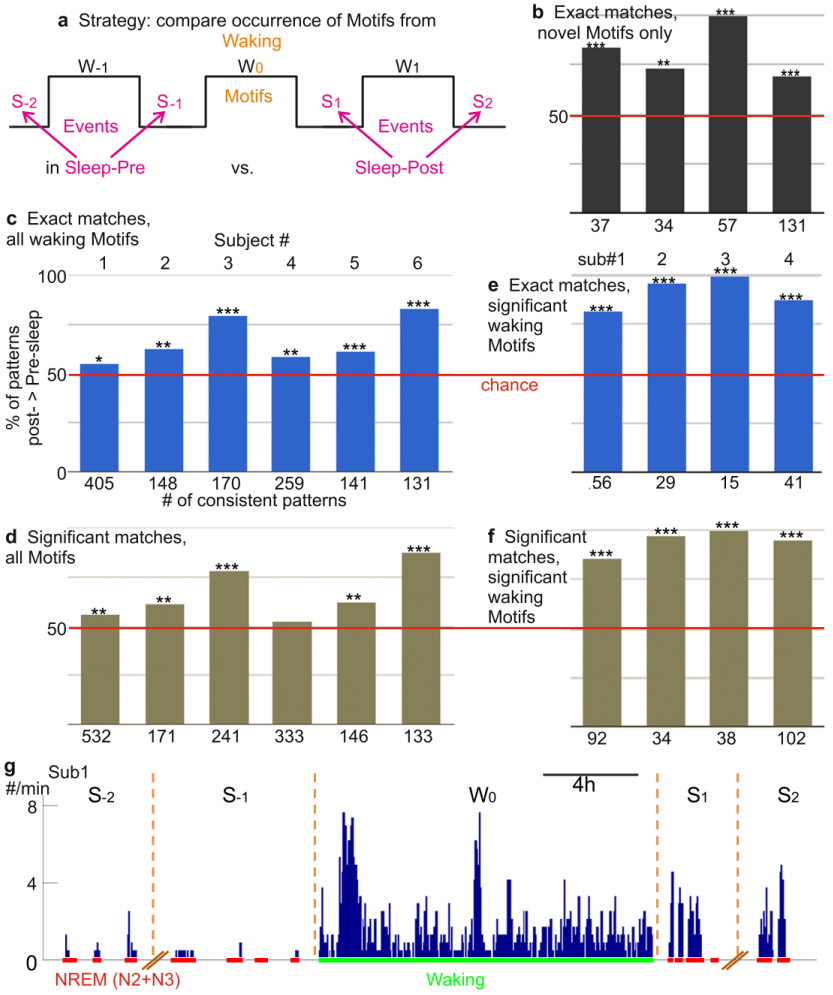

Figure 3. Events similar to waking cortical spatiotemporal activity Motifs occur more often in Sleep-Post than Sleep-Pre. (**a**) Schematic for Motif-Event matching. HG activity Motifs in the waking period W_0 were matched to the Events found in four consecutive NREM periods: Sleep-Pre (S_{-2}, S_{-1}) and Sleep-Post (S_1, S_2). **(b–f)**, Motif-Event matching results. Among waking Motifs with consistent (i.e. more Sleep-Pre than Sleep-Post matches for both S_{-2} and S_{-1}, or *vice versa*) matches found across four nights, a higher percentage has more Sleep-Post matches than Sleep-Pre matches. The data are counts, and the null hypothesis is that the counts of Motifs showing greater occurrence in Sleep-Post than Sleep-Pre would be equal to those showing the converse, so a simple binomial test was performed on each subject. In (**b**) only Motifs found in W_0 that did not occur in W_{-1} were used; for (**b**,**c** and **d**) exact matches were required; for (**e**) and (**f**) significant non-exact matches were also accepted; (**b**,**d** and **f**) only include waking Motifs that passed a significance test (see main text). SEEG subjects 5 and 6 did not have sufficient channels for the analyses in (**b**,**d** and **f**). Red lines represent chance (equal percentage of patterns with more Sleep-Post or more Sleep-Pre matches). (2-tailed binomial tests: (**b**) $^{**}p = 0.009$, $^{***}p < 0.0001$; (**c**) $^{*}p = 0.0368$, $^{**}p = 0.0022$ for 2, $p = 0.0061$ for 4, $^{***}p < 0.0001$ for 3 and 6, $p = 0.0007$ for 5; (**d**) $^{***}p < 0.0001$; (**e**) $p = 0.3806$ for 4, $^{**}p = 0.0048$ for 1, $p = 0.0035$ for 2, $p = 0.0036$ for 5, $^{***}p < 0.0001$; (**f**) $^{***}p < 0.0001$). (**g**) The occurrence of exact matches across four nights (S) and one waking period (W) to waking Motifs that matched to more Events in Sleep-Post than Sleep-Pre. Histogram bin size: 8 min.

Sub.ID	Age	Sex	Electrode Types	Waking Period Length (hours)	NREM (N2 + N3) Period Average Length (hours)	# of Channels Used/ Available	Median # of Channels in Waking Event/ Motif	Median # of Channels in Novel Waking Event/ Motif	# of Waking Motifs/ Novel Waking Motifs	# of Waking Events/ Novel Waking Events	# of Waking Events Matched to Motif	# of Novel Waking Events Matched to Novel Motif	Median # of Channels in Waking/ NREM Event Matched to Any Motif	Median # of Channels in Unmatched Waking Event	Median # of Channels in Unmatched NREM Event	Overall Rate for Waking Motifs (/h)	Overall Rate for Motifs in NREM (/h)
1	27	M	ECoG (grid + strip), SEEG	19.6	2.1 ± 0.68	52/124	6/8	9/13	1677/116	14620/1731	4184	255	8/8	6	5	214	595
2	52	F	ECoG (grid + strip), SEEG (hippocampus only)	6.6	5.3 ± 1.9	44/96	6/7	5/9	411/67	3440/1277	1062	234	7/8	5	5	161	253
3	47	M	ECoG (grid + strip) SEEG (hippocampus only)	15.2	4.2 ± 0.83	65/124	7/9	5/10	481/146	4040/2080	1158	655	9/9	6	5	78	277
4	54	F	ECoG (grid + strip), SEEG	10.1	4.4 ± 1.2	75/121	7/9	7/15	774/350	8427/4285	1805	2289	10/11	7	5	184	590
5	53	M	SEEG	16.1	5.1 ± 0.62	12/80	4/4	NA	451/NA	2119/NA	1073	NA	4/5	4	4	67	58
6	24	F	ECoG (strip), SEEG	11.6	2.3 ± 1.0	18/116	4/5	NA	315/NA	2173/NA	689	NA	5/6	4	4	54	63
7	33	F	ECoG (grid + strip)	9.6	5.3 ± 1.5	60/126	6/8	NA	628/NA	6709/NA	1453	NA	8/9	5	5	98	433

Table 1. List of subjects, age, sex, the types of electrodes used, the lengths of waking/sleep period recordings used, the median number of channels in an Event/Motif, the numbers of used (i.e. not dominated by epileptiform activity) versus available (i.e. the recorded voltage traces appear biological) cortical contacts, the number of waking Events/Motifs, and the overall occurrence rates of Motifs (i.e. Motif-to-Event matches). For subjects 5 and 6, only bipolar channels with clearly defined polarity inversions were kept for subsequent analyses. Hippocampal leads were too contaminated by epileptiform activity in subjects 1 and 4 to be used in this study. NA: not available. For a column with "/" separating numeric values and the column header, the numbers preceding the "/" symbol are described by the first part of this column's header (i.e. the part that also precedes the "/" symbol), and the numbers following "/" are described by the second part of the header.

replay effect outside the initial parameter set of 99th percentile, 2000 ms Event max duration (Supplementary Fig. S5). All subjects showed significant replay effect at the following parameter sets ([HG percentile, Event size]): [97th, 1 s], [98th, 1 s], [99th, 2 s], [99th, 2.5 s]. Further, out of the 36 replay analyses with 99th percentile threshold and max Event sizes from 1s to 3.5 s (6 parameter sets, 6 subjects), 29 showed significant replay effect, and 0 showed significance in the opposite direction (i.e. majority of waking Motifs matching Sleep-Pre Events more often than Sleep-Post Events). Similarly, out of the 24 analyses with max Event size 1s and percentile thresholds from 96th to 99th, 20 showed significant replay effect, and 0 showed significance in the other direction. In summary, our finding that more spatiotemporal Motifs of HG activity observed during waking occur more often in Sleep-Post than in Sleep-Pre is robust to different methods for identifying matching HG Motifs, for judging differences in occurrence rate, and for identifying initial HG Events.

As an additional control, we reversed sleep and waking periods and repeated our analyses. Specifically, we used identical parameters as in our initial analyses (exact match, 99th percentile, 2000 ms max Event duration), but with a central sleep period as our source of Motifs, two preceding waking periods as the equivalent of "Sleep-Pre", and two subsequent waking periods as the equivalent of "Sleep-Post". In contrast to our original results, where all six subjects showed the replay effect, our control analyses yielded 3 subjects with no significant "replay" or "pre-play" (i.e. the majority of sleep "Motifs" matched more often to Events in preceding waking periods), two subjects with significant "replay" ($p = 0.043$ for Sub. 2, $p < 0.0001$ for Sub. 4), and one subject with significant "pre-play" ($p = 0.01$ for Sub. 1).

Since HG activity in epileptic patients is prone to contamination by interictal events, we eliminated >50% of the channels because they were located in the epileptogenic or adjacent zones (Table 1). For the remaining channels, we constructed an artifact detector based on wavelet decomposition (Supplementary Fig. S6) that was able to identify >99% of human expert hand-marked interictal events. Furthermore, the number of detected artifacts did not change significantly from Sleep-Pre to Sleep-Post (one-way ANOVA with each sleep as a "treatment group" and the percentage of interictal-containing 2000 ms time bins as the dependent variable, F-statistic: 2.493 on 3 and 1287 DF, $p > 0.05$), and indeed showed a slight nonsignificant decrease (median interictal rate across channels for Sleep-Pre was 5.41%, whereas the median rate for Sleep-Post was 4.96%), indicating that these events alone could not explain the increase in repeating Motifs (i.e. Motif-Event matches) from Sleep-Pre to Sleep-Post.

Novel Motifs are more likely to show greater Sleep-Post replay. Reasoning that novel experiences are more likely to require replay for consolidation, we attempted to restrict the analysis to novel Motifs by including only those that had not occurred in the previous waking period. With this requirement, the four ECoG subjects had significantly more novel Motifs (which passed the random shuffle test) with greater numbers of

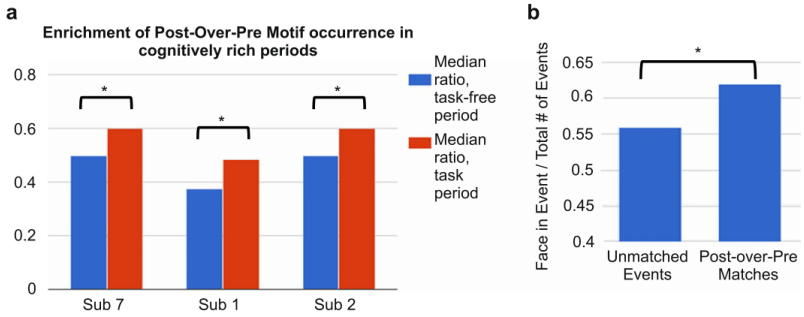

Figure 4. Motif occurrence enrichment in cognitively rich periods. (**a**) Motifs that matched more often to Events in Sleep-Post than to Events in Sleep-Pre (Post-over-Pre Motifs) preferentially occurred during task times in waking. For each randomly chosen 5-minute segment in waking, we calculated the following ratio: the number of Events similar to Post-over-Pre Motifs over the number of Events matched to all Motifs. 2000 random waking segments were selected, half within and half outside of the time for task performance. *$p < 0.001$ (Wilcoxon rank-sum test). (**b**) Motifs whose occurrences (i.e. waking Event matches) overlapped with face-including movie frames were more likely than non-overlapping Motifs to have more matches in Sleep-Post. *Two-tailed p-value (Chi-square test) = 0.0292.

Sleep-Post than Sleep-Pre Motif-Event matches (Fig. 3b, with shuffle tests and exact matches, $p = 0.009$ for Sub. 2, $p < 0.0001$ for others; SEEG subjects could not be examined because of too few qualifying Events due to low channel count). This result proves robust to different methods for identifying matching HG Motifs (i.e. allowing combinatorial matches and/or performing shuffle tests to evaluate Motifs) as well. Interestingly, more than 90% of the waking Motifs used in our initial analyses were actually novel in all four subjects.

Enrichment of putative replay Motifs during cognitive activity. Waking period activity was recorded continuously during the uninterrupted clinical and personal activities typical of a patient in a hospital room under no acute distress. However, we were able to identify periods in 3 subjects when their mental engagement might be expected to be relatively greater due to cognitive testing or watching a movie. Thus, we tested if the HG Motifs with wake-sleep matches were related to cognitive activity in three subjects with information-rich waking time periods (>30 min) of cognitive task performance (including two of the subjects described above, and one additional subject not included in previous replay analyses because only data from one preceding and one subsequent sleep was available; see Supplementary Table S1). While the exact tasks performed differ across subjects because they were not specifically performed for the current study, we were able to identify task types and time periods based on experimental notes (see "Data collection" in Methods). Using a bootstrapping procedure (see "Statistical analysis for Events and Motifs" in Methods), we found that for all three subjects, Motifs occurring during information-rich periods were more likely than Motifs found elsewhere in waking to have more Motif-Event matches in Sleep-Post than in Sleep-Pre ($p < 0.0001$ for each subject, Wilcoxon rank sum test) (Fig. 4a). In addition to this apparent "enrichment" of putative replay by cognitive task performance, we also observed that for subject 7, who watched an entire movie, HG Motifs overlapping with face-including movie frames were more likely than non-overlapping Motifs to have more Motif-Event matches in Sleep-Post (2×2 chi-square test, $p = 0.03$) (Fig. 4b).

Relation of putative replay to cortical sleep spindles, theta bursts, and slow oscillations. In rats, replay by specific neuron ensembles occurs in the context of sharp wave-ripples in the hippocampus[29]; and spindles/delta activity in the neocortex[22,23]. We thus examined delta power, theta oscillations, and spindle occurrences in cortical channels during the 3 s surrounding putative replay Events in NREM, i.e. Events that matched Motifs with more Sleep-Post than Sleep-Pre matches (using "exact match" criterion, without applying shuffle thresholds). The HG amplitude peaks in these putative replay Events were generally associated with a ~200 ms increase in broadband power surrounded by a prolonged increase in delta (Fig. 5a,b) in all subjects. In addition to elevated delta during putative replay Events, five of the six subjects displayed significant increases in theta and spindle occurrence in the period surrounding HG peaks from Motif-Event matches (the sixth was not included because too few spindles or theta bursts were detected, but showed similar trends). Theta occurrences consistently increased between 600 and 200 ms prior to the match peaks ($p < 0.001$, using permutation tests with 1000 iterations, see "Time-frequency analysis and sleep graphoelement detection/analysis" in Methods). In contrast, the significant ($p < 0.001$) increases in spindle likelihood could occur after 500 ms following the Motif-Event match peaks (in subjects 1, 4, 5), or in the 200 ms preceding the match peaks (in subjects 2, 3) (Fig. 5c,d).

Relation of putative replay Events to hippocampal activity. Simultaneous cortical ECoG and hippocampal SEEG recordings were available in three of our six subjects (Table 1), where we detected hippocampal sharp-wave ripples (Fig. 6a–c). Using the first (among the channels that matched the waking templates) HG peaks of putative cortical replay Events as triggers (Events were obtained under "exact match" criterion, without

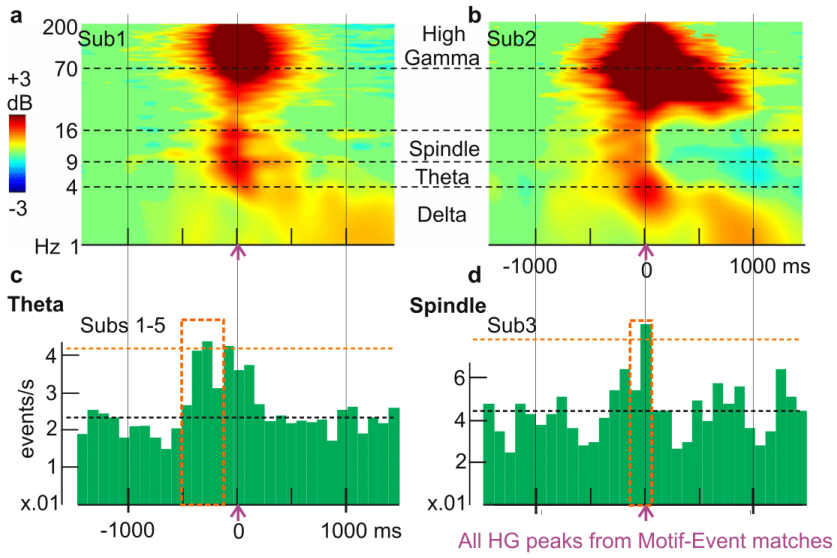

Figure 5. Putative replay frames are associated with spindle, delta, and theta activity. (**a**,**b**) Neocortical activity during sleep triggered on peaks of putative replay Events (i.e., Events matched to waking Motifs with "exact matches" criterion and no shuffle thresholds). Cortical theta, alpha, beta and gamma power increases for up to 1000 ms during putative replay events. Green mask for $p > 0.05$ (two-tailed bootstrap) from baseline period (−1500 ms to −1000 ms). Vertical solid lines/horizontal dash lines indicate shared X- or Y- axes across subplots, respectively. (**c**,**d**) Peri-HG-peak histograms of theta and spindle occurrences. Theta centers preferentially occur prior to Event peaks (Sub. 1–5 grand average: $p < 0.001$ from 600 ms before to 200 ms before Event HG peaks; FDR-corrected permutation tests), and spindles preferentially occur near Event peaks (Sub. 2–3: $p < 0.001$ in the 0.2 s before the HG Event peaks; FDR-corrected permutation test). Orange boxes: significant time stretches. Putative replay frames are from the first Sleep-Post period. Similar effects were found for the second period (not shown). The black horizontal dash line indicates median ripple rate, and the orange horizontal dash line indicates the 99th percentile.

applying shuffle thresholds), a sharp transient was noted in the average hippocampal LFP (Fig. 6d). In all three subjects, posterior hippocampal LFP showed slow activity coincident with significant broadband activation including frequencies over 100 Hz (Fig. 6e). This frequency range could reflect both ripples and unit firing. In rats, hippocampal sharp waves coincide with cortical transitions to up-states during SWS[41], and with coordinated replay in both cortex and hippocampus[4]. In our study, the prolonged (~1000 ms) increase in hippocampal HG suggests continuing hippocampal-cortical interaction as the successive cortical nodes in a Motif-Event match are activated. Indeed, in all three subjects (Sub. 2, 3, 5) with hippocampal contacts (left and right posterior hippocampi), morphologically typical sharp-wave ripples were recorded (but Sub. 2 had 10 times less than the others), with similar frequency profiles to previously reported primate[42] and human[37] ripples (Fig. 6f,g). In both Sub. 3 and Sub. 5, we observed a significant prolonged (up to at least 4s post-trigger) elevation in ripple occurrence rates after Motif-Event match peaks (Fig. 6h,i; $p = 0.039$ at [−2 s, 2 s] and $p < 0.001$ at [0, 4 s] for Sub. 5; $p = 0.013$ at [−2 s, 2 s], $p = 0.0446$ at [0, 4 s], $p = 0.039$ at [16 s, 20 s] and at [24 s, 28 s] for Sub. 3).

Selective involvement of cortical areas in putative replay Events. Visual inspection suggests that some cortical locations were involved more frequently in putative replay Events, and/or selectively at the onset of such Events (Fig. 7). We tested in subjects 1–6 whether the amount of HG peaks (which are from both waking and NREM Events that matched to waking Motifs with higher occurrence in Sleep-Post than in Sleep-Pre) found at each cortical location was significantly different from chance by a modified binomial test ($p < 0.05$ with FDR correction, see "Statistical analysis for Events and Motifs" in Methods). For all subjects, more than 50% of channels showed a significant difference, either greater or less than expected under the null hypothesis that all channels contributed equally to motifs. Similarly, the likelihood for each cortical location to have high gamma peaks in the beginning of an Event was found to be significantly different than chance for 20–80% of each subject's channels (permutation tests, $p < 0.05$ with FDR correction). Despite this evidence of nonrandom distribution of sites with more or less involvement in Motifs, earlier or later in the sequence, there was no obvious anatomical focus consistent across all subjects. However, in subjects 1, 2, and possibly 4, there seemed to be a tendency for the parietal-temporo-occipital junctions to have more HG peaks than expected by chance.

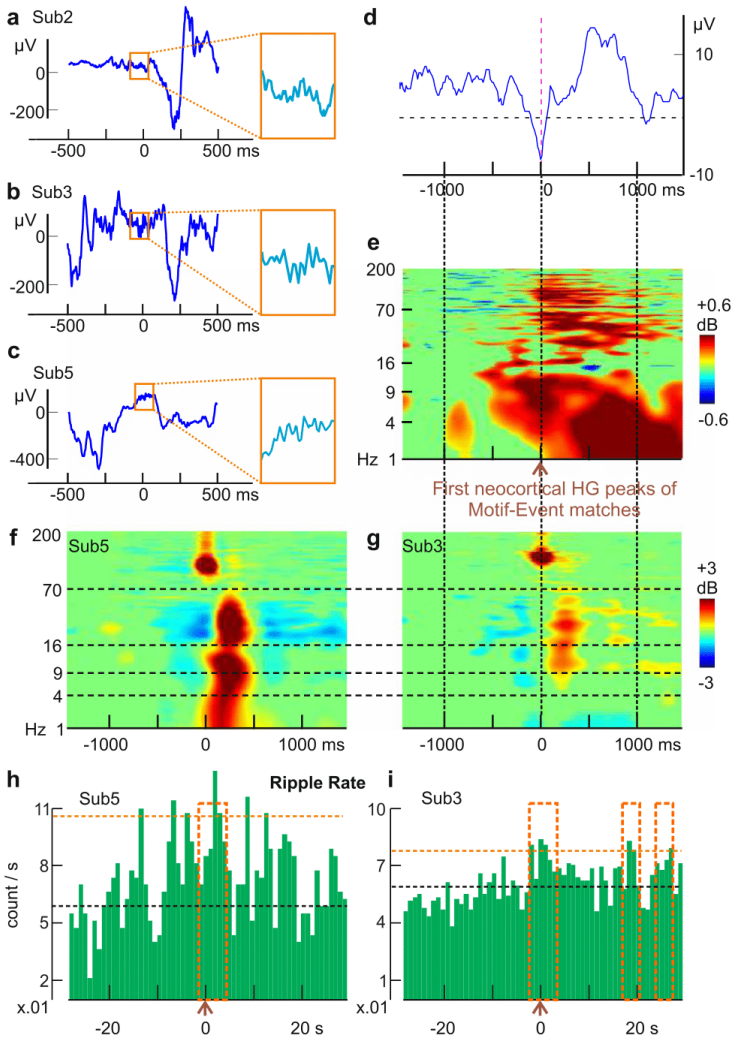

Figure 6. Putative replay frames are associated with hippocampal activity. (**a**,**c**) Examples of automatically detected hippocampal ripples (in orange squares, which covers 125 ms) and the surrounding LFP from subjects 2, 3, and 5, respectively. (**d**) Hippocampal LFP average triggered on 1st cortical HG peaks of matched Events (exact matches, no shuffle thresholds). (**e**) Aggregate time-frequency plot with all three subjects (470 randomly selected trials each); broadband hippocampal activity increases for ~1000 ms during matched Events. Power from 1–200 Hz (linear scale), with green mask for $p > 0.05$ (two-tailed bootstrap) from baseline period (−1500 ms to −1000 ms). (**f**,**g**) Time-frequency analysis of automatically detected ripples from posterior hippocampus shows power in the ripple frequency range (70–100 Hz). Vertical solid lines/horizontal dash lines that go across panels indicate shared X- or Y- axes across subplots, respectively. (**h**,**i**) Ripple occurrence rates become elevated near and after Motif-Event match peaks. The black horizontal dash line indicates median ripple rate, and the orange horizontal dash line indicates the 99th percentile. Time windows that show significance are described here as [start,end] in milliseconds, where negative/positive values refer to the temporal distance from trigger times: $p = 0.039$ at [−2000, 2000] and $p < 0.001$ at [0, 4000] for Sub. 5; $p = 0.013$ at [−2000, 2000], $p = 0.0446$ at [0, 4000], $p = 0.039$ at [1600, 2000] and at [2400, 2800] for Sub. 3 (FDR-corrected permutation tests). Orange boxes: significant time stretches. Due to the long time-base, only the first HG peak from a given Event would be used in this analysis. All Events are from the first Sleep-Post period. Similar effects were found for the second period (not shown).

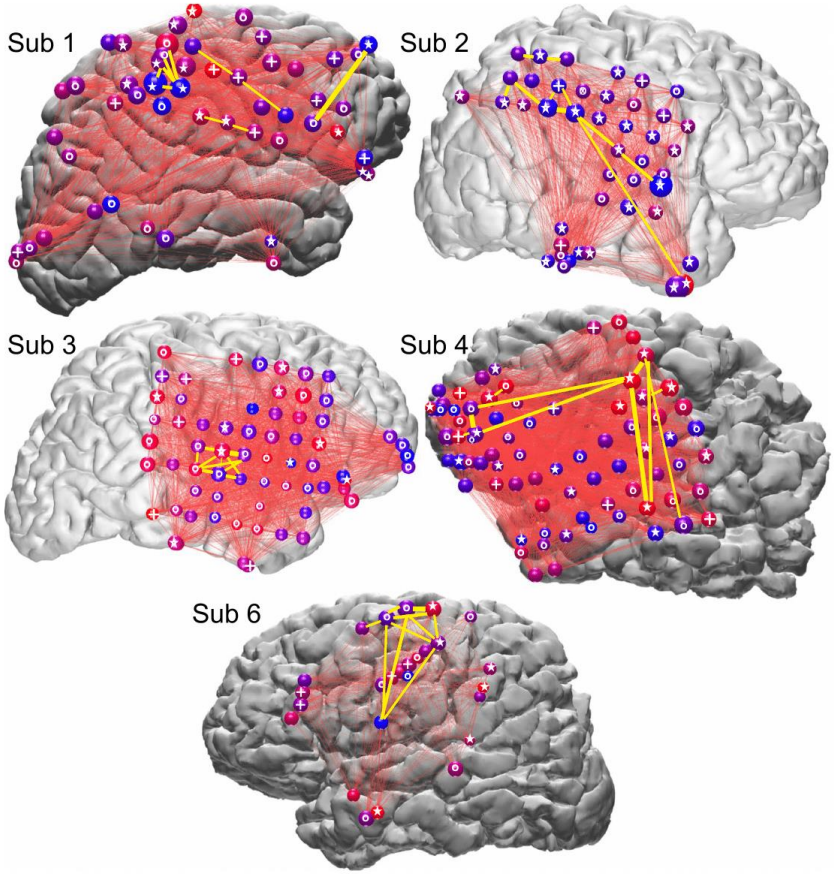

Figure 7. Participation of widespread cortical areas in Motifs. Spheres represent ECoG electrodes, with circles (o), plusses (+), or stars (☆) on the spheres indicating that they showed a significant deviation from chance (FDR corrected $p < 0.05$) in their occurrence rate, in their temporal order in the motifs, or in both, respectively. Specifically, a circle indicates that the amount of high gamma peaks seen at this cortical location was significantly different (more or less) from expected value based on chance alone. Similarly, a plus indicates that the likelihood for this cortical location to have high gamma peaks in the first quarter of an Event was significantly different (higher or lower) from chance, i.e. 25%. The size of each sphere indicates HG peak occurrence rate; color indicates the likelihood of HG peaks being early versus late in an Event (red: early, blue: late). Thin red lines connect the electrode pairs that produced temporally adjacent HG peaks within Events. Yellow lines connect the ten electrode pairs that produced the largest numbers of temporally adjacent HG peaks. Plotted are HG peaks from Motifs occurring in all waking and sleep periods (i.e. from both waking and NREM (the two Sleep-Post periods) Events that matched to waking Motifs with higher occurrence in Sleep-Post than in Sleep-Pre).

Discussion

We present the first clear demonstration of locally-recorded cortical replay in humans, in the form of large-scale spatio-temporal HG activity identified during waking and recurring during subsequent sleep periods. Each Motif typically involved widespread sensory, motor and association areas. While consistent with some primate recordings[8] and human hemodynamic studies[30], the current study is the first to our knowledge showing that both the initial waking representation and the subsequent sleep replay could involve widespread dynamic sequences using intracranial electrophysiology.

In order to demonstrate replay of widespread cortical spatio-temporal activity patterns, it was necessary to first demonstrate them in our recordings. We used clustering and statistical methods adapted from unit recordings studies in rodents to identify consistent spatiotemporal patterns of HG peaks ('Motifs'), and then tested if they were different from chance by comparing them to Motifs found when the temporal relationship between HG

peaks was disrupted with randomization. Randomization resulted in a highly significant decrease in the number and size of Motifs were found. While consistent spatio-temporal patterns have been observed to occur spontaneously with hemodynamic measures over widespread cortical areas[43], and locally using multi-microelectrode recordings[34,44], we are not aware of their having previously demonstrated in human cortical electrophysiological recordings. When the intervals between HG peaks were randomized fewer and smaller Motifs were found. This finding of highly distributed recurring spatiotemporal activity patterns confirms a basic assumption of cortical processing models[45].

Our finding of Motif replay was robust to different statistical criteria for identifying Events in sleep that matched waking Motifs, for determining if Motif occurrence rate differed between Sleep-Pre and Sleep-Post periods, and when only novel Motifs were considered. In fact, most of the recurring Motifs had not occurred in previous waking periods. Furthermore, preferential replay in Sleep-Post were generally replicated when the maximum pattern durations ranging from 1000 ms to 3000 ms (rather than the 2000 ms we initially used) and HG peak selection from 97 to 99th percentiles (Supplementary Fig. S5). As an additional control, no consistent results were obtained when we reversed sleep and waking periods and repeated our analyses. The electrophysiological context of recurring Motifs is thus consistent with those reported in rodents and humans to be associated with replay and/or consolidation. Notably, recurring Motifs (i.e. sleep Events that matched to waking Motifs) were associated with increased cortical sleep spindle and delta activity which are associated with not only unit firing replay in rodents[22,23] but also memory consolidation in humans[25,28,35]. Critically, the putative replay Events in our study were accompanied by strong sustained hippocampal activation, resembling sharp waves and ripples. Hippocampal sharp wave-ripples have a strong relationship to hippocampal unit replay in rodents[4], and presumably that is also true in humans. Thus, their association with cortical Motifs provides a neurophysiological mechanism for the hypothesized temporary hippocampal trace to contribute to the construction of the recurring cortical Motif.

We observed that putative replay continued for at least 2 nights after the waking period in which the Motif was originally detected (Fig. 3, Supplementary Fig. S7). This is consistent with the prolonged retrograde amnesia that occurs after hippocampal damage, suggesting an extended consolidation period[46]. The putative replay events lasted about 1000–2000 milliseconds in humans, consistent with rodent data[4]. This duration may reflect the algorithm used to identify spatiotemporal Motifs; longer or shorter Motifs could be found when we altered our maximum Event duration (Supplementary Fig. S5). Unlike rodents, the replaying Motifs we observed did not appear to be accelerated compared to their waking occurrence. This could reflect differences in approach and/or actual species differences. Humans typically live about 70 years and have one long sleep period every night. Rats typically live about 2 years and have many sleep periods throughout the day, staying in each state for as little as a few minutes[47]. Furthermore, compared to rats, humans have about 30 times more neocortical cells per hippocampal pyramidal neuron[48–51]. Thus, hippocampal orchestration of neocortical replay may be modified in humans, and the characteristics of replay occurrence may therefore differ substantially.

Strong circumstantial evidence supports a key role for replay during sleep for memory consolidation in rodents. For example, the reactivation of spatial goal-related firing during SWRs after learning predicts later memory recall, an effect which is depends on NMDA-mediated reactivation of goal-related firing pattern reactivations during ripples[3]. In addition, biasing behavior with external modulation of replay has been demonstrated by pairing spontaneous firing of hippocampal place cells with reward signal[7], as well as by auditory cueing of spatial preference during NREM sleep[52]. In our study, recurring Events during NREM showed a strong preference to arise from more cognitively rich periods in waking, but further work is needed to determine their experiential content, which would provide the leverage to obtain direct behavioral evidence that their replay is associated with memory consolidation.

We demonstrate here replay during sleep in humans, and its similarity in certain key features to replay in rodents (occurrence in NREM, close relation to hippocampal activity and to cortical sleep graphoelements), but its role in memory consolidation remains unexplored. Regardless of their relationship to memory consolidation, our results demonstrate the existence of consistent widespread spatiotemporal patterns of cortical population firing. Such patterns are fundamental to associationist perspectives on cortical function[53], but have not previously been described in humans.

Materials and Methods

Data collection. Seven subjects (3 male, 4 female) with long-standing drug-resistant partial seizures underwent ECoG macro-electrode (subdural grid and strip) and/or SEEG depth electrode implantation (4 with ECoG and limited SEEG, 2 with SEEG only, 1 with ECoG only). Subjects were all right-handed except for patient 5, who was ambidextrous. For patients 2–5 and 7, drugs were either no longer given to the patients by the time the recordings used in analysis had begun, or were provided in exactly the same dosage every day analyzed. Subjects 1 and 6 had changes to their medical regimen after the day of the first Sleep-Pre, but not for the other three days used in this study: subject 1 discontinued 200 mg oral carbamazepine and subject 6 started 50 mg oral quetiapine. For subjects 1, 3, 5, 6, and 7, quantitative clinical neuropsychology information was available, and subjects 2 and 4 were noted by clinicians to be cognitively normal. Subjects 1 and 7 had average scores on the Wechsler Adult Intelligence Scale (WAIS-IV) in Verbal Comprehension Index (Sub. 1: 100, Sub. 7: 105) and Perceptual Organization Index (Sub. 1: 107, Sub. 7: 100). Subject 6, who had lower scores (~80) on WAIS-IV, was a native Arabic speaker who did not speak English fluently. Subjects 3 and 4 received evaluation on WAIS-III: subject 3 had average (86) Verbal IQ, high (124) Performance IQ, and average Wechsler Memory Scale (WMS) recent memory test scores; subject 4 had low average scores (74/79) in Verbal/Performance IQ and in WMS.

Electrode targets and implantation duration were chosen entirely on clinical grounds. All methods were carried out in accordance with clinical guidelines and regulations at Comprehensive Epilepsy Center (New York University School of Medicine) and at Massachusetts General Hospital. All subjects gave fully informed consent

for data usage. All experiment protocols were monitored and approved by the Institutional Review Boards at New York University and Partners HealthCare. After implantation, electrodes were located using CT and MRI[54,55]. Continuous recordings from grid and strip macro-electrode arrays were made over the course of clinical monitoring for spontaneous seizures, with sampling rates at 500 or 512 Hz, using 128-channel clinical cable telemetry systems. All SEEG contacts were converted to a bipolar montage. Each pair of contacts (separated by 3.5 mm center-to-center) was only included if one contact was near the pial surface and the other near the white-to-gray transition, according to preoperative MRI aligned with postoperative CT[56], confirmed with neurophysiological criteria (high amplitude, coherence and inversion of spontaneous activity between the contacts). These bipolar transcortical derivations ensure that activity is locally generated[38]. During part of the recording periods, subjects 1, 2, and 7 engaged in cognitive activities (>30 min on one given day of their stays) as research participation for other groups; the patients' spontaneous waking behaviors were not interfered with otherwise. Subject 1 watched movie trailers (full video/audio) and performed a name-face association task, subject 2 performed an auditory pattern detection task and an auditory sequence discrimination task, and subject 7 watched the movie "Zoolander" (full video/audio) without interruption. Detailed task setup/descriptions and movie processing steps can be found in the Supplementary Methods.

Preprocessing and sleep period selection. Recordings were anonymized and converted into the European Data Format (EDF). Subsequent data preprocessing was performed in MATLAB; the Fieldtrip toolbox (RRID:SCR_004849)[57] was used for bandpass filters, line noise removal, and visual inspection. High gamma amplitude (HG) over time was estimated by smoothing the analytic amplitude of 70–190 Hz bandpassed data with a 100 ms 1D Gaussian kernel (Supplementary Fig. S1). Raw data corresponding to all NREM periods in each sleep were concatenated prior to HG peak detection. The top 1 percent of all local HG maxima for each channel was used for subsequent analyses. Given the lack of access to clinical hypnograms, patient monitoring videos, scalp EEG, electrooculogram, or any form of sleep staging hand marks for most subjects, instead of following the popular AAMS manual criteria[58], Sleep periods (as a combination of NREM sleep stages N2 and N3, where N2 and N3 forms a temporal continuum with progressively increased slow oscillation content) were identified by prolonged (>5 min) elevations in low delta band (<2 Hz) activity amplitude and corresponding declines in HG and initially high but gradually decreasing spindle band (9–17 Hz) amplitudes (Supplementary Fig. S3). Each NREM period was then verified by visual inspection for the presence of sleep graphoelements. Sleep-wake boundaries were defined as 1 hour before the first in a series of NREM periods (which are considered as in the same "sleep" if less than 2 hours apart), or 1 hour after the last in a series. Time segments between bouts of NREM and with no sleep graphoelements were considered REM or transient waking, and were removed from analyses.

Confirmation of subject sleep/wake states was provided by methods adapted from an early rodent behavioral state separation study[40], where periods of wakefulness and different sleep stages were identified as clusters on 2D histograms of the first principal components (PCs) for two frequency ratios, computed from Fourier transform integrals over different frequency bands. For the current analysis, these methods were modified as follows: one PC was computed from the ratio of the Fourier transform integral for 0.5–16 Hz over the integral for 0.5–55 Hz, and the other PC from the ratio of the 0.5–3 Hz integral over the 0.5–16 Hz integral. This method was validated against manual classification of sleep stages in subjects 2 and 3, by experienced clinicians (Supplementary Fig. S3). To ensure that the depth of sleep is equal for Sleep-Pre and Sleep-Post, normalized differences were calculated from the channel-wise z-scored differences between Sleep-Pre and Sleep-Post delta amplitudes (sum of two Sleep-Pre NREM periods minus sum of two Sleep-Post NREM periods) for each subject, and evaluated via one-sample sign tests. Randomly centered 1second time bins with greater than or less than median delta amplitude were discarded iteratively from Sleep-Pre and Sleep-Post as needed, until no significant difference between Sleep-Pre and Sleep-Post remained (Supplementary Fig. S3).

Artifact rejection. Since HG peaks may sometimes arise from artifacts or epileptiform activity, prior to bandpassing signal over the HG band, 2000 milliseconds of data centered around each HG peak underwent 1-D wavelet (Haar and Daubechies) decomposition for the detection and removal of sharp transients (i.e. signal discontinuities) that might contaminate the HG band. In addition, HG peaks that occurred in close temporal proximity (<100 ms) across more than 20% of all channels were discarded. Within each channel, HG peaks whose amplitudes exceeded 20 standard deviations above the mean were also excluded, and the minimum distance between same-channel HG peaks eligible for downstream analysis was set to 100 ms. Channels were not analyzed if the local cortex consistently displayed or was marked by clinicians as prone to interictal (or otherwise abnormal) activity (Table 1).

Event selection. HG peak Events in the form of vectors with integers designating different channels were created as follows: 2000-millisecond sliding windows were moved across the 4 NREM periods (two preceding the waking period, two subsequent) and the waking period data in 50 ms increments, with each movement yielding a different number of outlier HG peaks within the current window (Supplementary Fig. S1). The windows that yielded local maxima of HG peak numbers were taken as Events. A minimum of 4 peaks was required for an activity Event.

In the analysis limited to novel Events, the same initial procedure was followed except that the requirement that the Event represent a local maximum of HG peak numbers was relaxed to increase the sensitivity to all patterns that might recur. Instead, Events were defined by using each HG peak outlier as the starting point, and extending the Event to include subsequent peaks unless the inclusion of another peak would increase the Event length beyond 2000 milliseconds. The novel Event search was therefore not performed with a sliding window, but with a "saltatory" window (with a maximum length of 2000 milliseconds) that starts at the first (in temporal

order) HG peak in the data, reaches for up to 2000 milliseconds to include subsequent HG peaks, terminates, and restarts at the next HG peak in the data. This search procedure would be terminated either when all HG peaks belong to some elastic window, or when the last saltatory window would contain less than 4 HG peaks.

In all analyses, each Event was then binarized (0 for no HG in a channel, 1 for having at least one HG in a channel), and converted further into a 2-by-n spatio-temporal representation (one column for time indices, the other for channel number), where n is the number of total HG peaks in the pattern (Supplementary Fig. S1). In cases where a channel had more than one HG outlier peak within the same Event, the multiple peaks from this channel were replaced with a single peak located at the median position in time for all peaks from this channel, so that each Event contains only one HG peak per channel.

Motif selection and matching index analysis. Spatiotemporal activity Motifs were selected via metrics derived from rat cortical electrophysiology studies as follows: hierarchical clustering of the waking period Events was performed in R (with the packages Fast Hierarchical Clustering Routine[59] and Dynamic Tree Cut[60] using Phi-coefficient-derived distance matrices[34] and Ward's method[59] to group Events according to spatial distribution similarity. To select waking Motifs by further grouping Events according to HG peak order, and to match waking Motifs to NREM Events, temporal order similarity for waking Events in each cluster was then obtained via the matching index (MI) algorithm, which was implemented (using HG peaks in place of spike train convolutions) as previously described[4] (in MATLAB with custom scripts and in R with the TraMineR toolbox[61]), with the additional heuristic criterion that for each comparison, only the channels in common were used to calculate MI. Note that our measure of pattern similarity requires that each spatial location has a unique position in the temporal sequence, since this measure relies on counting the number of unit pairs (ECoG channel pairs in our case) in the same versus opposite order from a given Motif-Event match[4]. We therefore combined multiple HG peaks from the same channel in a given Event to a single peak at the median position in time of all HG peaks from that channel. This is a potential drawback in terms of Motif-Event match fidelity, as multiple HG peaks from the same channel in a stereotypical temporal order might be a key aspect of a given recurring Motif. However, if true, such stereotypy across multiple iterations/Events may also lead to similar median peak positions for that particular channel, relative to HG peak positions from other channels.

Based on the MI outcome (a distance matrix of match probabilities), each cluster of spatially similar waking Events was split into subclusters. Representative Motifs were chosen as those that include 90% of a given subcluster's Events in their neighborhoods, which were defined as 20% of the maximum distance between two Events for a given subcluster. These were then matched with MI to the Events in NREM, and each representative was associated with a certain number of replay frames (i.e. sleep Events that matched the waking Motif, or "Motif-Event matches") for each NREM period. If multiple Motifs were matched to the same NREM Event, for statistical purposes, the number of replay frames associated with each waking Motif for that night was incremented by 1/N instead of 1, where N equals the number of waking Motifs that matched to this common Event. So, if there were exactly three Motifs matched to the same Event, each Motif would have its number of replay frames incremented by only a third. Thus, the total count increments from any given Event would equal exactly 1 regardless of how many Motifs it matched, as long as it matched at least one. The resulting replay frame numbers for each NREM period were then normalized by the total number of Events found in that NREM period. For the random shuffle test of replay frame number significance[4], the two subjects with only SEEG contacts used for matching were not examined, since only Motif-Event matches with >6 channels satisfy the test's requirement, and few Motif-Event matches from these subjects exceed 6 channels in length.

Note that our analysis did not search for repetition during sleep of Events which occurred only once during waking. We required that Motifs were matched during waking by at least 2 Events, and such Events only comprised ~30% of waking Events on average across subjects. The possibility that these unique activity patterns also replay during subsequent sleep was not explored in the current study because it appeared prudent for us to perform our analyses on only the consistently recurring patterns that would be more likely to reflect reactivation of waking experiences. One requirement of such an investigation would be to determine if the unique Events are significantly non-random. In rodents, hippocampal replay was observed not only in NREM, but also during waking[62]; in humans, fMRI evidence suggests that event-specific reactivation, which predicts later successful recall, occurs in both hippocampus and cortex spontaneously after learning during waking[12]. Thus, while we could not exclude the possibility that rare activity patterns might also be involved in consolidation, we refrained from performing our novel analyses on unique, one-off patterns.

Statistical analyses for Events and Motifs. All statistical analyses involving hypothesis testing described under this section and the following section (LFP analysis) have $\alpha = 0.05$. Putative replay of waking Motifs was statistically evaluated as follows. First, Motifs were counted which had more Motif-Event matches during each of the Sleep-Pres (S_{-2} and S_{-1}) than in either of the Sleep-Posts (S_1 and S_2). This was compared to the number with the opposite pattern (more matches during each of the Sleep-Posts than in either of the Sleep-Pres), using 2-tailed binomial tests (hypothesized success rate set to 0.5). In order to test the sensitivity of the analysis to the choices described above regarding inclusion of Motifs and criteria for Motif-Event matches, binomial tests were also performed after supplementary analyses with the following restrictions that produced different numbers of matches or different sets of Motifs. First, we required the common cortical loci in matching Events and Motifs to have the exact same HG peak temporal order ("stringent") or not ("combinatorial"). Second, following Ji and Wilson[4], we used only Motifs whose total number of Motif-Event matches across all nights exceeded Motif-wise thresholds established by matching Sleep-Pre and -Post Events to the same Motifs with their channel order randomly shuffled 1000 times. Third, we used only novel Motifs.

In order to test if the numbers of waking/sleep Events observed, the mean number of HG peaks in Events, and the kurtosis of HG peak number distributions were greater than expected from the null hypothesis that HG peaks

occur randomly across the cortex, we compared the number of observed Events (with maximum duration of 2000 ms and at least 4 unique cortical locations), mean HG peak numbers, and kurtosis values from the original data to the numbers derived from 1000 sets of shuffled peak locations, where the total number of HG peaks and the location of the first HG peak from each channel remained the same as in the original, but the inter-peak intervals were shuffled randomly in temporal order over the same waking/sleep periods. The threshold for bootstrapping significance was set at 0.05.

In order to test if the task periods were enriched in waking Motifs that had more Motif-Event matches in Sleep-Post than in Sleep-Pre (note that, unlike previous replay analyses, only one Sleep-Post and one Sleep-Pre periods were used), we performed the following bootstrapping procedure: template-matching analyses were performed with one Sleep-Pre and one Sleep-Post per subject, using 10,000 random (allowing overlap) 5-minute time bins selected from either task or no-task waking periods. We then computed for each time bin a ratio between the number of waking Motifs with more Sleep-Post matches and the total number of Motifs with at least one match in sleep. These ratios were compared between task-on and task-off periods using the Wilcoxon signed-rank test.

In order to test if a given cortical location produced significantly more or less HG peaks than expected from chance, we took all the waking Motifs with more Motif-Event matches in Sleep-Post and the sleep Motifs they matched to and obtained, for each channel, the numbers of Motifs involving ("successes") and not involving ("failures") that channel. Each success-failure ratio was then evaluated via binomial test, with the expected success probability set as follows: for each subject, the mean number of HG peaks involved in a Motif-Event match was divided by the total number of channels. Thus, the null hypothesis was that all channels contributed equally to all motifs. Similarly, in order to test if a given cortical location was significantly more or less likely to produce HG peaks early (i.e. the first 1/4 of all channels involved), the number of successes and failures obtained from each channel was evaluated via binomial test with the expected success probability set as 25%. Because multiple comparisons were done for each subject, the p-values obtained were FDR-adjusted[63].

LFP analysis. Spectral content of the LFP data from cortical contacts of all six subjects and from hippocampal depth electrode recordings from three subjects was evaluated using EEGLAB (RRID:SCR_007292) routines that applied wavelet transforms[64]. Spectral power was calculated over 1 to 200 Hz across each individual time period ("trial") centered around ECoG HG peaks found in NREM patterns by convoluting each trial's signal with complex Morlet wavelets, and averages were then taken across trials. The resulting time-frequency matrices were normalized with respect to the mean power at each chosen frequency and masked with two-tailed bootstrap significance, with the pre-trigger times (−1500 ms to −1000 ms) as baseline.

For automatic theta oscillation detection, data from NREM periods were bandpassed from 5–9 Hz, and the amplitude envelope from Hilbert transform was used alongside detection thresholds based on standard-deviation-over-mean[36]. The theta events thus selected were further pruned by counting the number of zero-crossings over the duration of each event and calculating the zero-crossing-based frequency estimate, whereby if a given event's estimate fell outside the bandpass range, it was removed from analysis. Automatic spindle detection was performed using previously published methods for SEEG spindle identification, with parameters tuned for cortical spindles[65]: a 10–16 Hz bandpass was applied to the data and the analytic amplitude of the band passed signal was convolved with an average Tukey window of 600 ms. A channel-wise cutoff set at mean + 2s.d. was applied to each channel's convolved bandpass envelope to identify local maxima that would be "peaks" of putative spindles. To define the onset and offset of putative spindles, a 400 ms Tukey window was applied to the previously computed Hilbert amplitude, and the maximum FFT amplitude of the putative spindle signal at the spindle peak was used to set edge thresholds (50% of peak amplitude). Finally, the putative spindle segments were evaluated with four different criteria for rejection: 1, the spindle duration needs to be longer than 400 ms; 2, the spectral power outside the spindle frequency band on the lower end (4–8 Hz) or the higher end (18–30 Hz) should not exceed 14 dB; 3, each spindle should consist of at least 3 unique oscillation peaks in the 10–16 Hz bandpass; 4, the time between successive zero-crossings should be within the range of 40–100 ms.

Hippocampal sharp-wave ripples were detected following earlier published methods[37], with some modifications. First, data from NREM were filtered between 80–100 Hz (6th order Butterworth IIR bandpass filter). Root-mean-square (RMS) over time of the filtered signal was calculated using a moving average of 20 ms, with the 99% percentile of RMS values for each hippocampal channel being set as a heuristic cut-off. Whenever a channel's signal exceeded this cut-off continuously for at least 38 ms, a ripple event was detected. Since RMS peaks could arise from artifacts or epileptiform activity, 2000 milliseconds of hippocampal LFP data centered on each ripple event underwent 1-D wavelet (Haar and Daubechies 1–5) decomposition for the detection and removal of sharp transients (i.e. signal discontinuities). For each wavelet decomposition type, a scale threshold was established via iterative optimization for the best separation between ~550 hand-marked true ripple events and ~350 interictal events in the same NREM period. Automatic selections for theta bursts, spindles and ripples were visually reviewed for accuracy in the raw traces and confirmed for each subject and NREM period.

For our analyses involving graphoelements and Motifs/Events, we used Motif-Event matches that were obtained under the exact match (without shuffle) setup. To statistically evaluate the theta/spindle likelihood around all Motif-Event match HG peak times, we first made peri-stimulus histograms of theta/spindle occurrences with HG peaks as triggers (only peaks from Events that matched to waking Motifs and actually were part of the match were used). We used the midpoint of the theta/spindle occurrences as their times for histogram construction. For each HG peak, the theta/spindle counts to be added to the histogram only included the theta/spindle occurrences from the same channel. To obtain average histograms across multiple subjects, we first normalized individual subject's histogram, dividing the count of each histogram bin by the total number of theta/spindle occurrences within the histogram time window (+−2 s) to yield the observed likelihood for each subject, and averaged the observed likelihood across subjects. We then obtained the estimated average

rates by multiplying the bin-wise average likelihood with the average number of total theta/spindle occurrences. Finally, we converted the counts into occurrence rates (dividing counts by the number of trials). We calculated the expected histograms under the null hypothesis that there is no relationship between Motif peak and theta/spindle occurrences: null hypotheses were constructed for consecutive time bins across the entire histogram (200 ms bins with 100 ms overlap): over each given time bin preceding/at/following Motif-Event match peaks. We then compared the observed likelihoods for each subject/graphoelement type to the numbers derived from 1000 sets of randomly initiated pseudo-HG peak locations in the same Sleep-Post, where the total number of HG peaks and the number of HG peaks from each channel remained the same as in the original, and the inter-peak intervals from real Motif-Event matches were preserved. The threshold for bootstrapping significance was set at 0.05, and the p-values thus obtained were FDR-adjusted.

Similarly, in order to statistically evaluate the ripple event likelihood around Motif-Event match HG peak times, we made peri-stimulus histograms of ripple occurrences with HG peaks as triggers, but using only the first peaks from Motif-Event matches and the histogram time window was expanded to $+-40$ s. The null hypothesis for ripple histograms, in turn, were constructed using 4s bins with 50% overlap, and 1000 sets of random pseudo-HG peak locations, each set containing the same number of pseudo-HG peaks as the actual number of Motif-Event matches for the given Sleep-Post period.

Data Availability. Because clinical data sets are used in this study, raw electrophysiological recordings and neuroimaging files will be shared on a case-by-case basis in accordance with IRB agreements. All computer programs/scripts used in this study will be available upon request.

References

1. Pavlides, C. & Winson, J. Influences of hippocampal place cell firing in the awake state on the activity of these cells during subsequent sleep episodes. *J. Neurosci. Off. J. Soc. Neurosci.* **9**, 2907–2918 (1989).
2. Wilson, M. A. & McNaughton, B. L. Reactivation of hippocampal ensemble memories during sleep. *Science* **265**, 676–679 (1994).
3. Rasch, B. & Born, J. About Sleep's Role in Memory. *Physiol. Rev.* **93**, 681–766 (2013).
4. Ji, D. & Wilson, M. A. Coordinated memory replay in the visual cortex and hippocampus during sleep. *Nat. Neurosci.* **10**, 100–107 (2007).
5. Peyrache, A., Khamassi, M., Benchenane, K., Wiener, S. I. & Battaglia, F. P. Replay of rule-learning related neural patterns in the prefrontal cortex during sleep. *Nat. Neurosci.* **12**, 919–926 (2009).
6. Johnson, L., Euston, D., Tatsuno, M. & McNaughton, B. Stored-trace reactivation in rat prefrontal cortex is correlated with down-to-up state fluctuation density. *J. Neurosci. Off. J. Soc. Neurosci.* **30**, 2650–2661 (2010).
7. de Lavilléon, G., Lacroix, M. M., Rondi-Reig, L. & Benchenane, K. Explicit memory creation during sleep demonstrates a causal role of place cells in navigation. *Nat. Neurosci.* **18**, 493–495 (2015).
8. Hoffman, K. L. & McNaughton, B. L. Coordinated reactivation of distributed memory traces in primate neocortex. *Science* **297**, 2070–2073 (2002).
9. Bergmann, T. O., Mölle, M., Diedrichs, J., Born, J. & Siebner, H. R. Sleep spindle-related reactivation of category-specific cortical regions after learning face-scene associations. *NeuroImage* **59**, 2733–2742 (2012).
10. van Dongen, E. V. *et al*. Memory stabilization with targeted reactivation during human slow-wave sleep. *Proc. Natl. Acad. Sci.* **109**, 10575–10580 (2012).
11. Deuker, L. *et al*. Memory consolidation by replay of stimulus-specific neural activity. *J. Neurosci. Off. J. Soc. Neurosci.* **33**, 19373–19383 (2013).
12. Staresina, B. P., Alink, A., Kriegeskorte, N. & Henson, R. N. Awake reactivation predicts memory in humans. *Proc. Natl. Acad. Sci. USA* **110**, 21159–21164 (2013).
13. Tambini, A. & Davachi, L. Persistence of hippocampal multivoxel patterns into postencoding rest is related to memory. *Proc. Natl. Acad. Sci. USA* **110**, 19591–19596 (2013).
14. Schönauer, M. *et al*. Decoding material-specific memory reprocessing during sleep in humans. *Nat. Commun.* **8**, ncomms15404 (2017).
15. Piantoni, G., Van Der Werf, Y. D., Jensen, O. & Van Someren, E. J. W. Memory traces of long-range coordinated oscillations in the sleeping human brain. *Hum. Brain Mapp.* **36**, 67–84 (2015).
16. Ramot, M. *et al*. Emergence of Sensory Patterns during Sleep Highlights Differential Dynamics of REM and Non-REM Sleep Stages. *J. Neurosci.* **33**, 14715–14728 (2013).
17. Manning, J. R., Jacobs, J., Fried, I. & Kahana, M. J. Broadband shifts in local field potential power spectra are correlated with single-neuron spiking in humans. *J. Neurosci. Off. J. Soc. Neurosci.* **29**, 13613–13620 (2009).
18. Greenberg, J. A., Burke, J. F., Haque, R., Kahana, M. J. & Zaghloul, K. A. Decreases in theta and increases in high frequency activity underlie associative memory encoding. *NeuroImage* **114**, 257–263 (2015).
19. Yaffe, R. B. *et al*. Reinstatement of distributed cortical oscillations occurs with precise spatiotemporal dynamics during successful memory retrieval. *Proc. Natl. Acad. Sci.* **111**, 18727–18732 (2014).
20. Lachaux, J.-P., Axmacher, N., Mormann, F., Halgren, E. & Crone, N. E. High-frequency neural activity and human cognition: past, present and possible future of intracranial EEG research. *Prog. Neurobiol.* **98**, 279–301 (2012).
21. Jones, S. R. Local Field Potential, Relationship to Electroencephalography (EEG) and Magnetoencephalography (MEG). In *Encyclopedia of Computational Neuroscience* (eds Jaeger, D. & Jung, R.)1–6, https://doi.org/10.1007/978-1-4614-7320-6_727-1 (Springer New York, 2013).
22. Siapas, A. G. & Wilson, M. A. Coordinated interactions between hippocampal ripples and cortical spindles during slow-wave sleep. *Neuron* **21**, 1123–1128 (1998).
23. Mölle, M., Yeshenko, O., Marshall, L., Sara, S. J. & Born, J. Hippocampal sharp wave-ripples linked to slow oscillations in rat slow-wave sleep. *J. Neurophysiol.* **96**, 62–70 (2006).
24. Csercsa, R. *et al*. Laminar analysis of slow wave activity in humans. *Brain J. Neurol.* **133**, 2814–2829 (2010).
25. Mednick, S. C. *et al*. The critical role of sleep spindles in hippocampal-dependent memory: a pharmacology study. *J. Neurosci. Off. J. Soc. Neurosci.* **33**, 4494–4504 (2013).
26. Latchoumane, C.-F. V., Ngo, H.-V. V., Born, J. & Shin, H.-S. Thalamic Spindles Promote Memory Formation during Sleep through Triple Phase-Locking of Cortical, Thalamic, and Hippocampal Rhythms. *Neuron*, https://doi.org/10.1016/j.neuron.2017.06.025 (2017).
27. Heusser, A. C., Poeppel, D., Ezzyat, Y. & Davachi, L. Episodic sequence memory is supported by a theta-gamma phase code. *Nat. Neurosci.* **19**, 1374–1380 (2016).
28. Schreiner, T. & Rasch, B. Boosting Vocabulary Learning by Verbal Cueing During Sleep. *Cereb. Cortex* **25**, 4169–4179 (2015).

29. O'Neill, J., Pleydell-Bouverie, B., Dupret, D. & Csicsvari, J. Play it again: reactivation of waking experience and memory. *Trends Neurosci.* **33**, 220–229 (2010).
30. Rissman, J. & Wagner, A. D. Distributed representations in memory: insights from functional brain imaging. *Annu. Rev. Psychol.* **63**, 101–128 (2012).
31. Cowansage, K. K. *et al.* Direct Reactivation of a Coherent Neocortical Memory of Context. *Neuron* **84**, 432–441 (2014).
32. Mayford, M. & Reijmers, L. Exploring Memory Representations with Activity-BasedGenetics. *Cold Spring Harb. Perspect. Biol.* **8**, a021832 (2016).
33. Katche, C. *et al.* Delayed wave of c-Fos expression in the dorsal hippocampus involved specifically in persistence of long-term memory storage. *Proc. Natl. Acad. Sci. USA* **107**, 349–354 (2010).
34. Miller, J. K., Ayzenshtat, I., Carrillo-Reid, L. & Yuste, R. Visual stimuli recruit intrinsically generated cortical ensembles. *Proc. Natl. Acad. Sci. USA* **111**, E4053–4061 (2014).
35. Marshall, L., Helgadóttir, H., Mölle, M. & Born, J. Boosting slow oscillations during sleep potentiates memory. *Nature* **444**, 610–613 (2006).
36. Andrillon, T. *et al.* Sleep Spindles in Humans: Insights from Intracranial EEG and Unit Recordings. *J. Neurosci.* **31**, 17821–17834 (2011).
37. Staresina, B. P. *et al.* Hierarchical nesting of slow oscillations, spindles and ripples in the human hippocampus during sleep. *Nat Neurosci* **18**, 1679–1686 (2015).
38. Mak-McCully, R. A. *et al.* Distribution, Amplitude, Incidence, Co-Occurrence, and Propagation of Human K-Complexes in Focal Transcortical Recordings. *eneuro* **2** (2015).
39. Eschenko, O., Mölle, M., Born, J. & Sara, S. J. Elevated Sleep Spindle Density after Learning or after Retrieval in Rats. *J. Neurosci.* **26**, 12914–12920 (2006).
40. Gervasoni, D. *et al.* Global forebrain dynamics predict rat behavioral states and their transitions. *J. Neurosci. Off. J. Soc. Neurosci.* **24**, 11137–11147 (2004).
41. Battaglia, F. P., Sutherland, G. R. & McNaughton, B. L. Hippocampal sharp wave bursts coincide with neocortical 'up-state' transitions. *Learn. Mem. Cold Spring Harb. N* **11**, 697–704 (2004).
42. Skaggs, W. E. *et al.* EEG sharp waves and sparse ensemble unit activity in the macaque hippocampus. *J. Neurophysiol.* **98**, 898–910 (2007).
43. Liu, X. & Duyn, J. H. Time-varying functional network information extracted from brief instances of spontaneous brain activity. *Proc. Natl. Acad. Sci. USA* **110**, 4392–4397 (2013).
44. Ikegaya, Y. *et al.* Synfire Chains and Cortical Songs: Temporal Modules of Cortical Activity. *Science* **304**, 559–564 (2004).
45. Hebb, D. O. *The Organization of Behavior*. (Wiley & Sons, 1949).
46. Squire, L. R., Clark, R. E. & Knowlton, B. J. Retrograde amnesia. *Hippocampus* **11**, 50–55 (2001).
47. Torterolo, P., Lagos, P. & Monti, J. M. Melanin-concentrating hormone: a new sleep factor? *Front. Neurol.* **2**, 14 (2011).
48. Korbo, L. *et al.* An efficient method for estimating the total number of neurons in rat brain cortex. *J. Neurosci. Methods* **31**, 93–100 (1990).
49. West, M. J. & Gundersen, H. J. Unbiased stereological estimation of the number of neurons in the human hippocampus. *J. Comp. Neurol.* **296**, 1–22 (1990).
50. West, M. J., Slomianka, L. & Gundersen, H. J. Unbiased stereological estimation of the total number of neurons in thesubdivisions of the rat hippocampus using the optical fractionator. *Anat. Rec.* **231**, 482–497 (1991).
51. Pakkenberg, B. & Gundersen, H. J. Neocortical neuron number in humans: effect of sex and age. *J. Comp. Neurol.* **384**, 312–320 (1997).
52. Bendor, D. & Wilson, M. A. Biasing the content of hippocampal replay during sleep. *Nat. Neurosci.* **15**, 1439–1444 (2012).
53. Markram, H., Gerstner, W. & Sjöström, P. J. A history of spike-timing-dependent plasticity. *Front. Synaptic Neurosci.* **3**, 4 (2011).
54. Dykstra, A. R. *et al.* Individualized localization and cortical surface-based registration of intracranial electrodes. *NeuroImage* **59**, 3563–3570 (2012).
55. Yang, A. I. *et al.* Localization of dense intracranial electrode arrays using magnetic resonance imaging. *NeuroImage* **63**, 157–165 (2012).
56. Princich, J. P. *et al.* Rapid and efficient localization of depth electrodes and cortical labeling using free and open source medical software in epilepsy surgery candidates. *Front. Neurosci.* **7** (2013).
57. Oostenveld, R., Fries, P., Maris, E. & Schoffelen, J.-M. FieldTrip: Open source software for advanced analysis of MEG, EEG, and invasive electrophysiological data. *Comput. Intell. Neurosci.* **2011**, 156869 (2011).
58. Silber, M. *et al.* The visual scoring of sleep in adults. *J. Clin. Sleep Med. JCSM* **3**, 121–131 (2007).
59. Müllner, D. fastcluster: Fast Hierarchical, Agglomerative Clustering Routines for R and Python. *J. Stat. Softw. Vol 1 Issue 9 2013* (2013).
60. Langfelder, P., Zhang, B. & Horvath, S. Defining clusters from a hierarchical cluster tree: the Dynamic Tree Cut package for R. *Bioinforma. Oxf. Engl.* **24**, 719–720 (2008).
61. Gabadinho, A., Ritschard, G., Müller, N. S. & Studer, M. Analyzing and Visualizing State Sequences in R with TraMineR. *J. Stat. Softw. Vol 1 Issue 4 2011* (2011).
62. Karlsson, M. P. & Frank, L. M. Awake replay of remote experiences in the hippocampus. *Nat. Neurosci.* **12**, 913–918 (2009).
63. Benjamini, Y. & Hochberg, Y. Controlling the False Discovery Rate: A Practical and Powerful Approach to MultipleTesting. *J. R. Stat. Soc. Ser. B Methodol.* **57**, 289–300 (1995).
64. Delorme, A. & Makeig, S. EEGLAB: an open source toolbox for analysis of single-trial EEG dynamics including independent component analysis. *J. Neurosci. Methods* **134**, 9–21 (2004).
65. Mak-McCully, R. A. *et al.* Coordination of cortical and thalamic activity during non-REM sleep in humans. *Nat. Commun.* **8**, ncomms15499 (2017).

Acknowledgements

The authors would like to thank the following for their support: Qianqian Deng, Darlene Evardone, Chris Gonzalez, Don Hagler, Milan Halgren, Erik Kaestner, Adam Niese, Burke Rosen, Rachel Mak-McCully, and Anna Sargsyan. This work was supported by the U.S. Office of Naval Research (N00014-13-1-0672).

Author Contributions

W.D. and E.E. performed surgical implantations; D.F., P.D., O.D., S.C. and T.T. recruited subjects, and collected data; I.S., S.C. and T.T. were involved in study design; E.H. and X.J. designed the study; X.J. and I.S. analyzed the data; X.J. and E.H. wrote the paper. All authors reviewed and approved the manuscript.

Additional Information

Supplementary information accompanies this paper at https://doi.org/10.1038/s41598-017-17469-w.

Competing Interests: The authors declare that they have no competing interests.

Publisher's note: Springer Nature remains neutral with regard to jurisdictional claims in published maps and institutional affiliations.

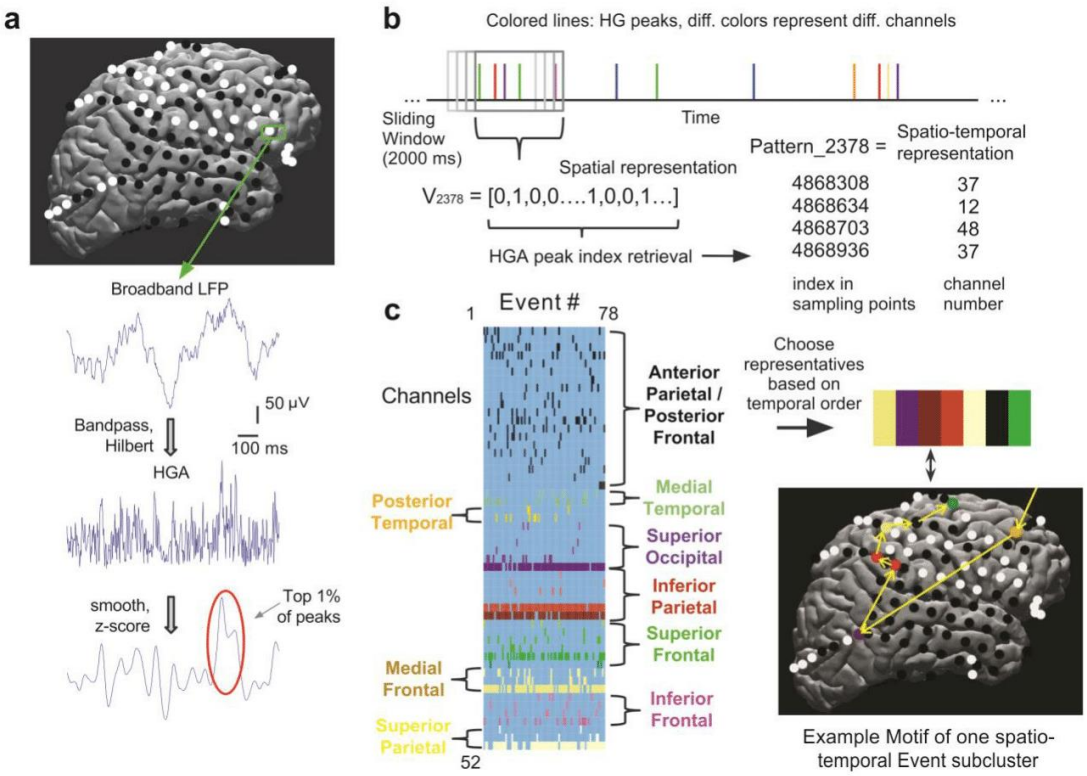

Supplementary Figure S1. Selection of Motifs representing consistent spatiotemporal patterns of HG peaks. ***a***, Selection of HC peaks. Top: ECoG electrode map (right hemisphere) for subject 1, black circles indicating contacts/channels discarded for downstream processing due to interictal activity or, rarely, poor recording quality. Bottom: An example data segment recorded from a grid electrode. The raw time series (LFP) was bandpassed (70-190 Hz), and the Hilbert transform was applied to obtain the HG analytic amplitude. Red circle: a local maximum/peak in HG. Only the top 1 % of all peaks was chosen for each channel as signals of cortical activation. ***b***, Selection of waking activity Events. 2-second sliding windows were moved across time to produce time segments with different numbers of HG peaks ("Events"). The segments that yielded local maxima of HG peak numbers were then transformed into their

corresponding spatial and spatio-temporal representations. ***c***, Clustering of Events into Motifs. The binary representations of waking activity underwent hierarchical clustering based on the spatial information (i.e. channels active). Using the matching index algorithm, Events in each cluster were further divided into subclusters based on the temporal order in which channels produce HG peaks. The representative Events in each subcluster were then chosen as template Motifs, to be matched to the Events found in NREM (N2+N3) periods. In summary, we use "Events" to refer to recurring spatiotemporal patterns of HG peaks, and "Motifs" to refer to clusters of Events with relatively minor differences which are grouped together for analysis.

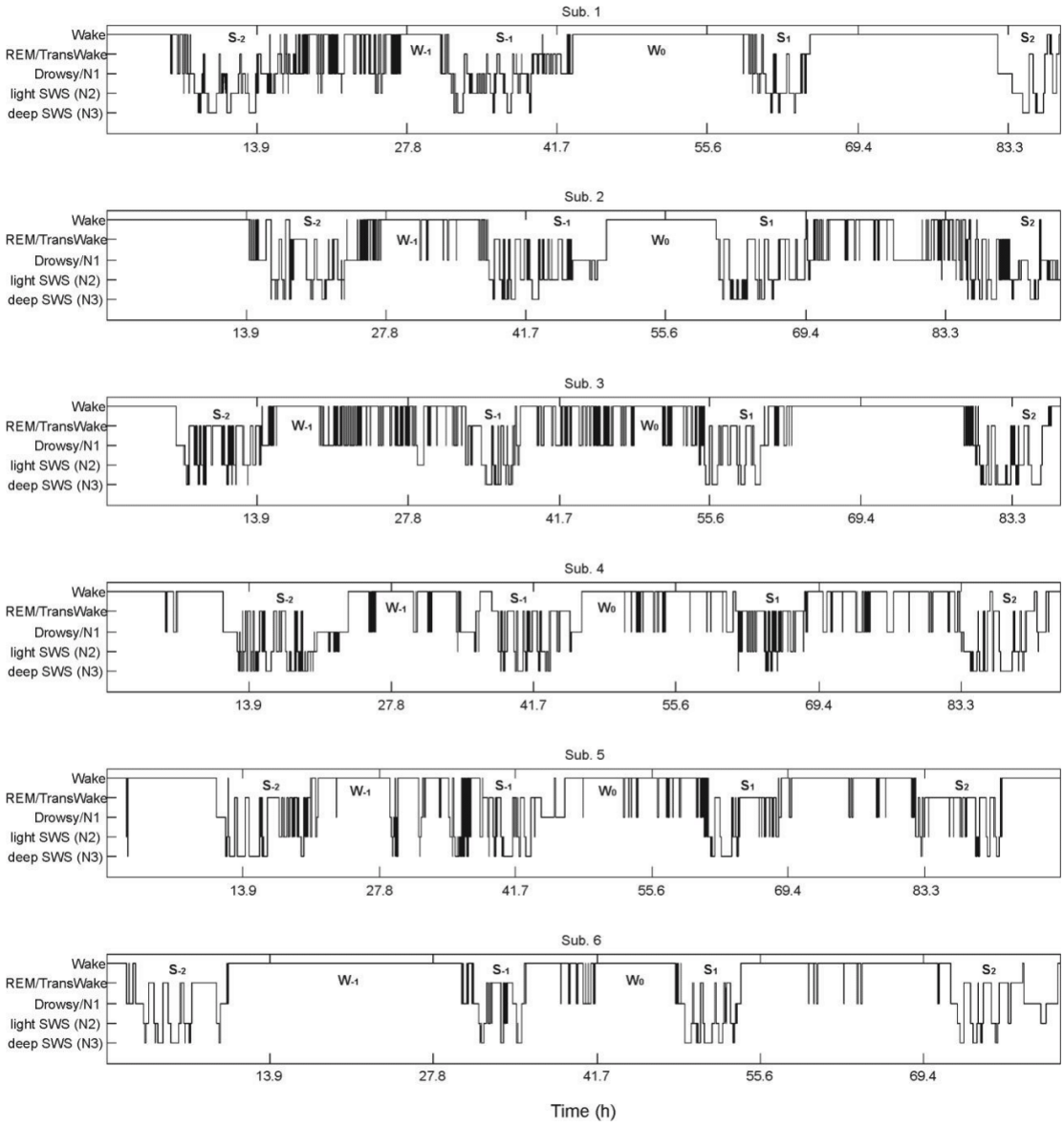

Supplementary Figure S2. Reconstructed hypnograms over four nights based on LFP characteristics resemble normal sleep structure. The separation of NREM and waking was achieved with the same methods used for Supplementary Fig. S3c. Time periods (< 2h) within the waking cluster of the PC state space that followed deep SWS (N3) periods and contain no

NREM sleep graphoelements were marked as REM/TransWake: REM or transitory waking period.

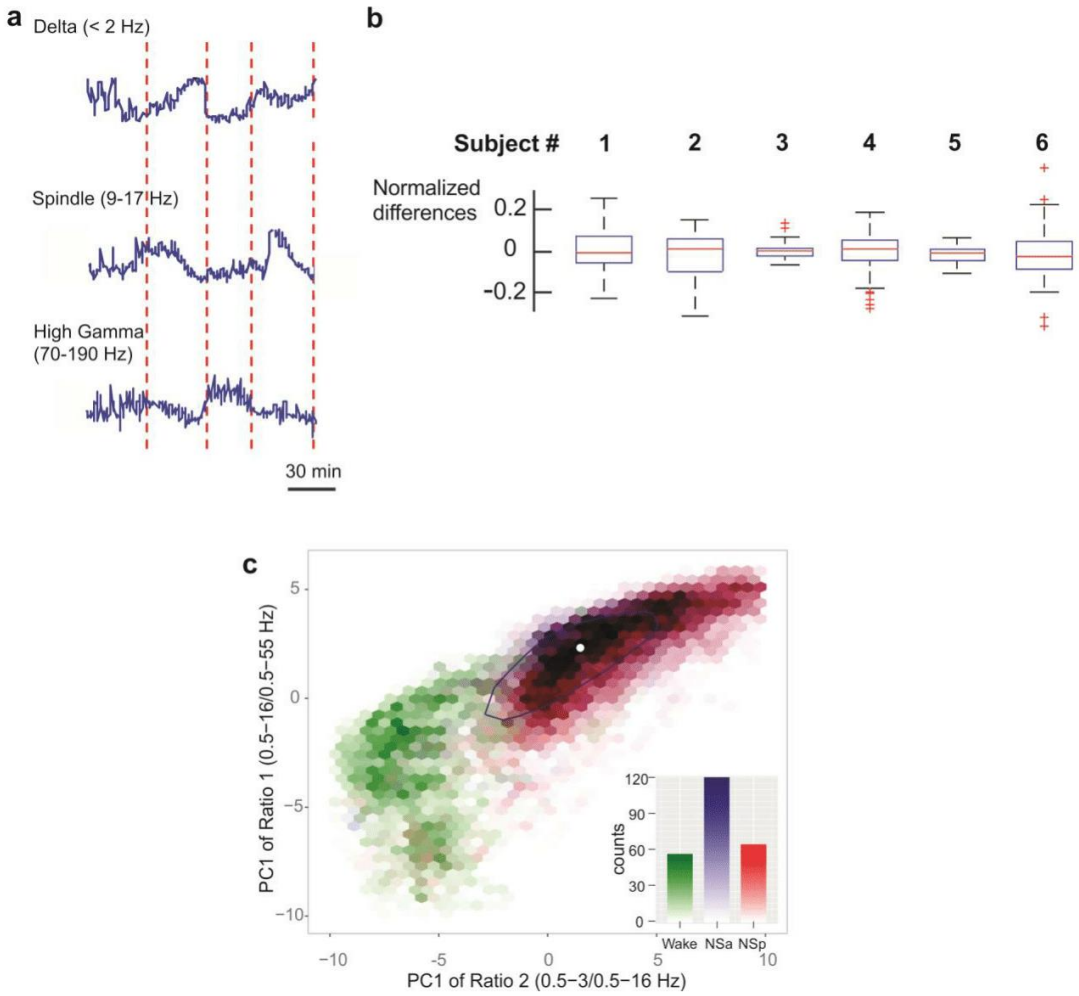

Supplementary Figure S3. **Selection of NREM periods**. ***a***, Identification of NREM sleep (stages N2+N3) using spectral power. The Hilbert analytic amplitudes of sleep LFP in the spindle (9-17 Hz), low delta (0.1-2 Hz), and HG (70-190 Hz) frequency bands were calculated, and the medians of consecutive 30s time windows were obtained. Prolonged delta amplitude

elevations in conjunction with drops in HG and generally high but gradually decreasing spindle frequency amplitude were used to identify NREM. ***b***, Similar depth of Sleep-Pre *versus* Sleep-Post NREM periods. The Normalized Difference was calculated from the channel-wise z-scored differences between Sleep-Pre and Sleep-Post delta amplitudes (sum of two Sleep-Pre NREM periods minus sum of two Sleep-Post NREM periods). For each subject, the blue box marks the range in Normalized Difference that covers the 25 % to 75 % percentile (interquartile range). The red lines mark the medians. The whiskers mark the maximum/minimum values except for outliers (+), i.e. channels with Normalized Difference values exceeding the blue box boundaries by 1.5 times the interquartile range. None of the subjects' medians were significantly different from 0 (one-sampled sign test, α=0.05). ***c***, NREM /wake separation via principal component analysis validates Hilbert amplitude-based NREM selection. Classifications by different methods of 2-second sleep epochs from the two subjects who were scored by polysomnographers are displayed as a 2D histogram. The first principal components (PCs) for two frequency ratios were computed across epochs and channels. Each hexagon represents all epochs with a particular value for PC1 of these ratios. RGB color blending for each hexagonal bin represents the proportion of sleep/wake epoch counts within the bin, with intensely single-colored bins representing frequently visited positions in state space. Lower right legend: NSa: epochs marked as NREM via Hilbert amplitude; NSp: epochs marked as NREM by qualified polysomnographers; Wake: epochs marked as waking by polysomnographers. There is substantial overlap (> 95 %) between NSa and NSp in PC space. The elliptic contour contains 50 % of all blue (NSa) epochs for each histogram, the white dot being the location of 2d median for blue epochs.

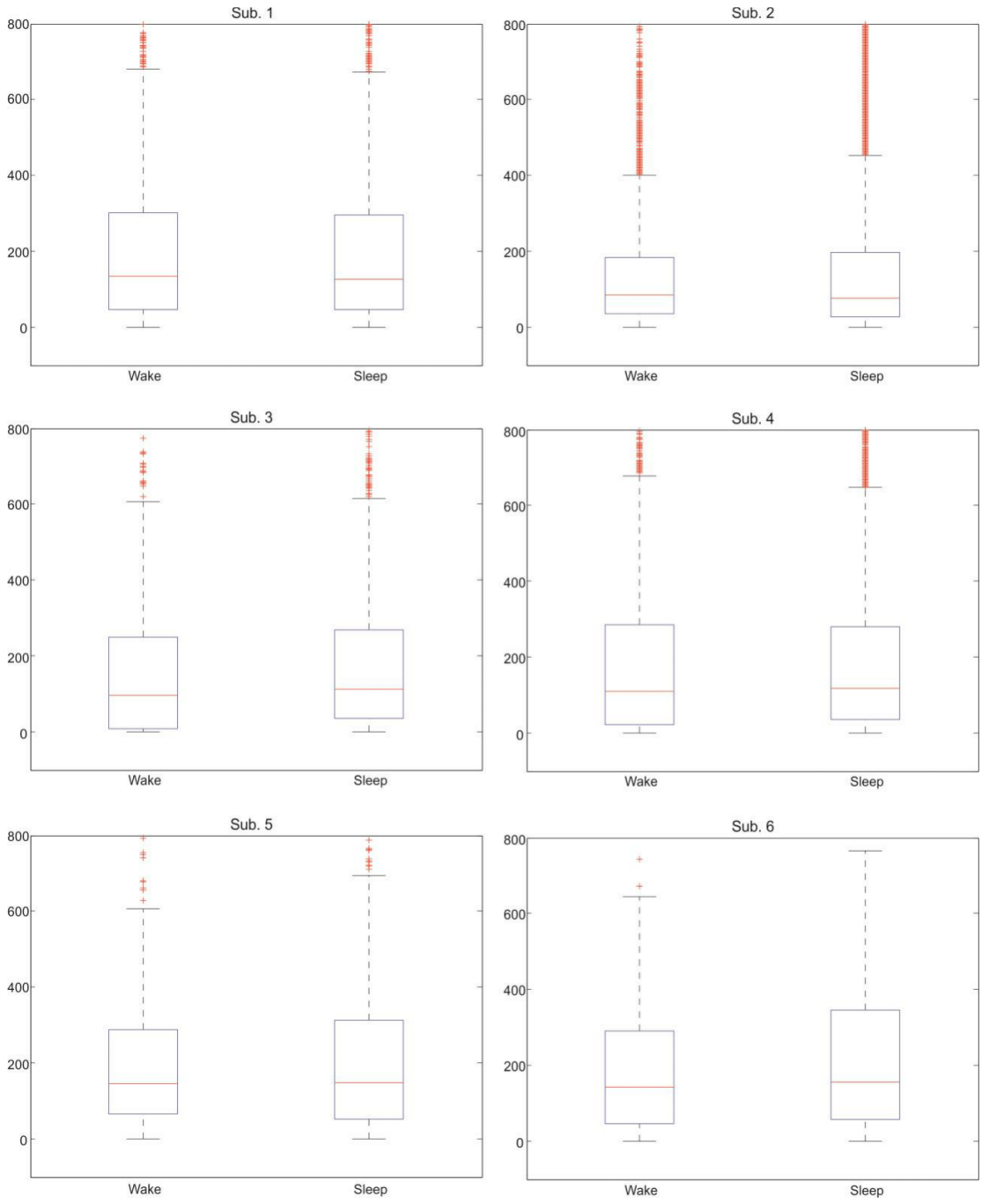

Supplementary Figure S4. Similar distribution of inter-peak intervals (IPIs, in milliseconds) within Events during waking and NREM. For each subject, the blue boxes mark

the ranges in waking or sleep Event IPIs that covers the 25 % to 75 % percentile (interquartile range). The red lines mark the medians. The whiskers mark the maximum/minimum values except for outliers (+), i.e. IPIs exceeding the blue box boundaries by 1.5 times the interquartile range. None of the subjects' waking Event IPI medians were significantly greater than the NREM Event IPI medians (Wilcoxon rank sum test, $\alpha = 0.05$).

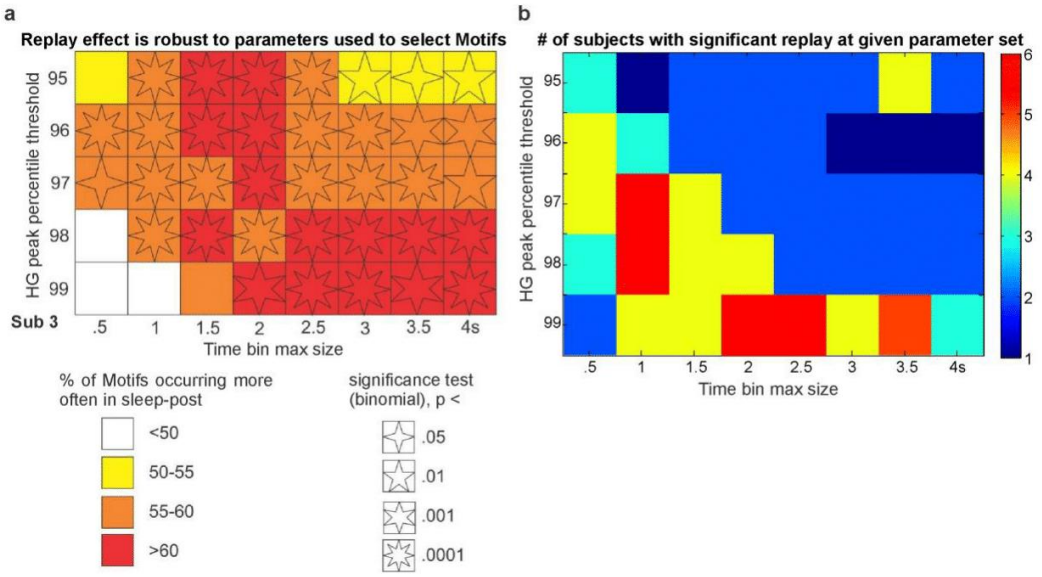

Supplementary Figure S5. Summary of significant replay observed under different HG peak thresholds and different maximum Event sizes. ***a***, Example summary of significant replay from subject 3. An identified waking Motif was considered replaying if it had more matching Events in Sleep-Post than in Sleep-Pre; the "replay effect" previously observed with HG peak threshold at 99th percentile and maximum Event size at 2 seconds was that the majority of waking Motifs were replaying. This effect is generally robust to changes in two crucial parameters used to select Motifs: HG peak threshold (from 95th to 99th percentile, in 1 percentile increments) and maximum Event size (from 0.5 s to 4 s, in 0.5 s increments). ***b***, Summary of the number of subjects, ranging from 1 to 6, showing a significant replay effect at each parameter set. All subjects showed significant replay effect at the following parameter sets ([HG percentile, Event size]): [97th, 1 s], [98th, 1 s], [99th, 2 s], [99th, 2.5s]. Note that, out of the 36 replay analyses with 99th percentile threshold and max Event sizes from 1 s to 3.5 s (6 parameter sets, 6 subjects), 29 showed significant replay effect, and 0 showed significance in the opposite direction (i.e. majority of waking Motifs matching Sleep-Pre Events more often than Sleep-Post

Events). Similarly, out of the 24 analyses with max Event size 1 s and percentile thresholds from 96^{th} to 99^{th}, 20 showed significant replay effect, and 0 showed significance in the other direction.

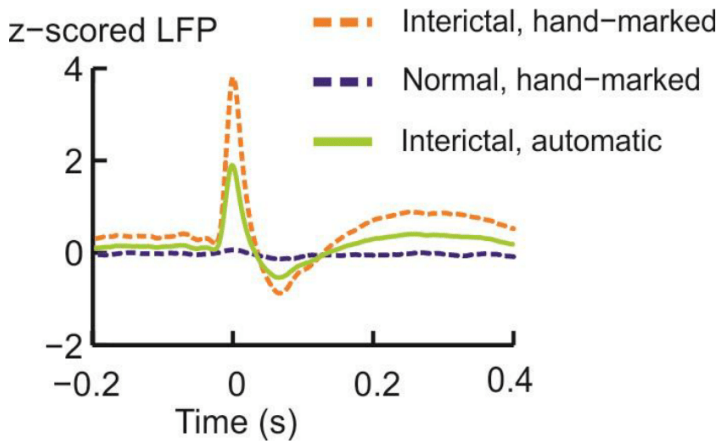

Supplementary Figure S6. Epileptic artifact rejection. ***b***, Artifact rejection via wavelet decomposition is sensitive and accurate. Out of a population of 990 2-second epochs (equal amounts of expert hand-marked interictal events/non-interictal random segments) taken from 3 channels of patient 2 with 0.1 Hz interictal occurrence rate, the artifact detector was able to capture most of the interictal events (53 false positives and 2 false negatives; d'=4.49). Consequently, the hand-marked and automatically-detected average waveforms are highly similar.

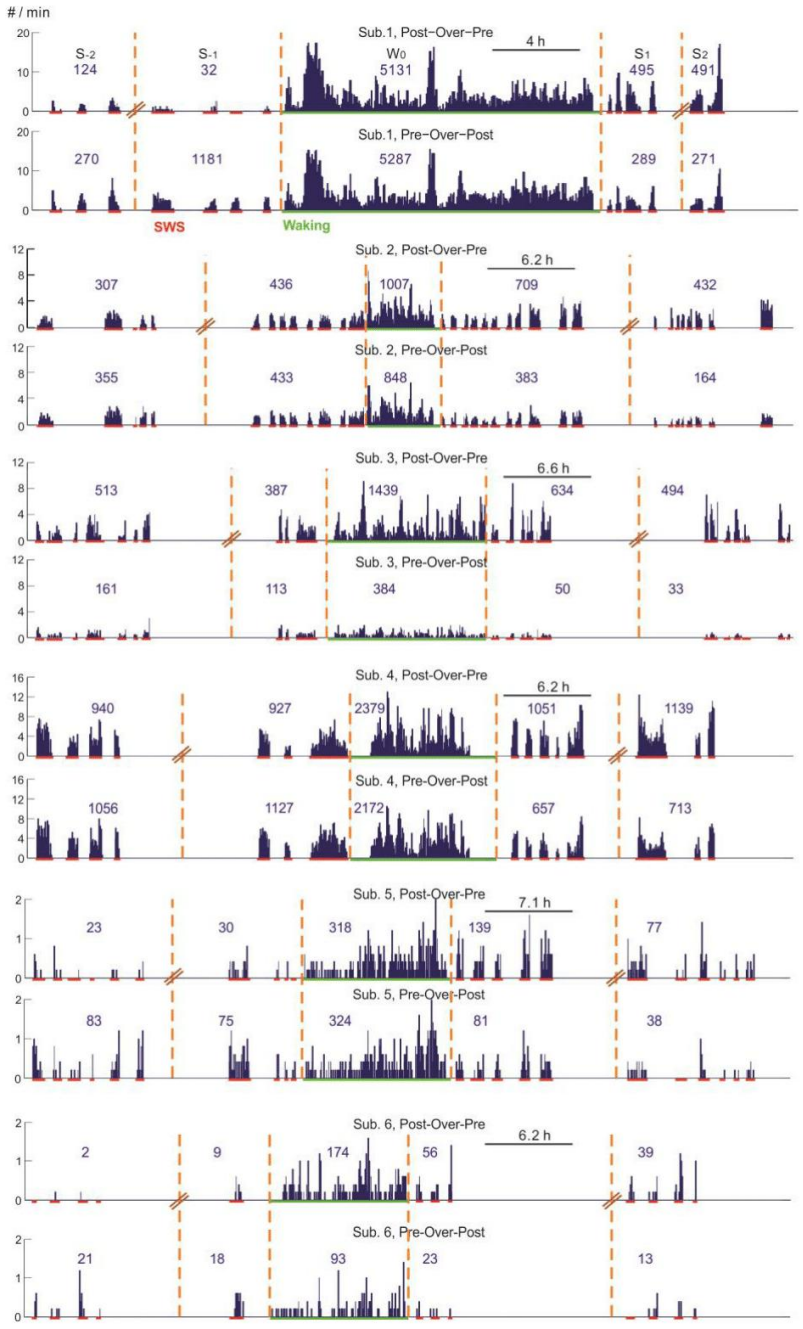

Supplementary Figure S7. The occurrence of significant (based on the combinatorial matching index) Motif-to-Event matches across four nights (S) and one waking period (W) to waking Motifs. NREM sleep (stages N2 and N3) segments are marked in red; waking

segments in green. Every two panels linked by orange dash lines belong to the same subject, with the diagonal double lines indicating separation between time periods. Histogram bin size: 5 min. Post-over-Pre: only showing Event matches to Motifs that matched more often to Events in Sleep-Post than to Events in Sleep-Pre. Pre-over-Post: only showing Event matches to Motifs that matched more often to Events in Sleep-Pre than to Events in Sleep-Post. The number of Event matches for each wake/sleep period is marked in blue above the corresponding period.

Subject ID	Replay analysis: Motif-Event matching (both exact and combinatiorial)	Replay analysis: Novel Motif-Event matching	Association of cortical graphoelements with Motifs	Association of hippocampal graphoelements with Motifs	Time-frequency analysis of hippocampal recording at Motif times	Enrichment of Motifs during task performance waking segments
1	Y	Y	Y	N	N	Y
2	Y	Y	Y	N	Y	Y
3	Y	Y	Y	Y	Y	N
4	Y	Y	Y	N	N	N
5	Y	N	Y	N	N	N
6	Y	N	Y	Y	Y	N
7	N	N	N	N	N	Y

Supplementary Table S1. List of subjects and the analyses performed with their electrophysiological recordings. Subject 7 was not used to perform the standard Motif-Event matching analyses since only one Sleep-Pre period was available (two would be required to perform replay analyses in the same manner as other subjects).

Supplementary Methods.

Waking Task Descriptions

The following tasks were performed by some of our subjects for other research groups, and we did not participate in the design or administration of these tasks. However, the electrophysiological recordings we received from our collaborators contained timing pulses, and we therefore were able to identify times of task participation during waking for three subjects.

NF task (subject 1): The Name-Face paired associate learning task consists of four consecutive phases: Nap1, Learning, Nap2, and Test, performed on the same day. At the Learning phase, the subject would learn to associate 3 unfamiliar name-face pairs. Some names would be presented also during Naps. No recordings from naps were analyzed in the current study.

AS task (subject 2): Subject heard a series of 7-10 s long tone sequences, each comprised of two pitches, and forming either a galloping rhythm or two parallel series, and the subject would report their experience.

Movie watching (subjects 1 and 7): Subjects 1 and 7 were provided with a laptop computer that contained movie content. Individual movie frames were aligned to trigger pulses sent to the clinical system, thus giving each movie frame a time stamp in electrophysiological data. Subject 1 watched a movie trailer lasting about 2.5 minutes four times, and was instructed to pay attention to different features each time before giving an oral report: 1. the characters, 2. the plot, 3. character/plot details not mentioned in previous oral reports, and 4. other details such as buildings and environmental sounds. Subject 7 was instructed to watch the movie “Zoolander” with no need for additional actions. Subject 7 completed viewing in one sitting, and did not

rewind or take breaks. The individual “Zoolander” movie frames were then extracted as jpeg images using the FFmpeg software, and all movie frames were loaded onto Google Picasa (version 3.9) to make use of its semiautomatic facial recognition feature (with 20 rounds of rescans and 20-40 hand marks per round), allowing each movie frame (and its associated electrophysiological data segment) to be marked as face-containing or not. Movie frames where both eyes were not visible on the same face were excluded from analysis to improve recognition accuracy.

Chapter 1, in full, is a reprint of the material as it appears in Scientific Reports, Article #17380 (2017), under the title “Replay of large-scale spatio-temporal patterns from waking during subsequent NREM sleep in human cortex”, Jiang, Xi; Shamie, Isaac; Doyle, Werner; Friedman, Daniel; Dugan, Patricia; Devinsky, Orrin; Eskandar, Emad; Cash, Sydney S.; Thesen, Thomas; Halgren, Eric, Nature Research, 2017. The dissertation author was the primary investigator and author of this paper.

CHAPTER 2: Characteristics of human hippocampal sharp-wave ripples

Title: Characteristics of human hippocampal sharp-wave ripples during NREM sleep

Abstract:

In rodents, pyramidal cell firing patterns from waking may be replayed in NREM sleep during hippocampal sharpwave-ripples (HC-SWR). In humans, HC-SWR have only been recorded with electrodes implanted to localize epileptic seizures. Here, we characterize human HC-SWR with rigorous rejection of epileptiform activity, requiring multiple oscillations and coordinated sharpwaves, distinguishing anterior and posterior HC, and NREM stages N2 and N3. We found that SWR do occur in those rare HC recordings which lack interictal epileptiform spikes (IIS), and with no or minimal seizure involvement. These HC-SWR have a similar rate (~12/min) and intra-HC topography (ripple maximum in putative stratum pyramidale, slow wave in radiatum) as rodents. Like rodents, human SWR are followed by locally-decreased broadband spectral power; in humans this decrease also precedes SWR. Human SWR ripple frequency is lower (~85Hz) than rodents (~140Hz). Similar SWR are found in HC with IIS, but no significant seizure involvement. In humans, SWR have 32% higher density in anterior than posterior HC, 53% higher density in N3 than N2, and do not occur significantly in waking. N2 and N3 cannot be distinguished in rodents, who produce SWR during quiet waking. Human SWR are focal, co-occurring in anterior and posterior HC only ~5% above chance, and bilaterally <2% above chance. In rodents, SWR usually propagate dorsal to ventral; in humans, propagation could be bi-directional. Despite basic similarities, human SWR may differ from rodent SWR due to differences in scale, sleep organization, and hemispheric specialization.

Introduction:

Hippocampal (HC) sharpwave-ripples (SWR) are composed of a large negative ~50-100ms "sharpwave" with superimposed 80-200Hz 'ripples', followed by ~200ms positive delta-wave (Buzsáki, 2015). During SWR, hippocampal pyramidal cells "replay" spatio-temporal firing patterns from waking (Wilson and McNaughton, 1994). Memory is impaired by disruption of hippocampal replay (de Lavilléon et al., 2015), or of SWR (Ego-Stengel and Wilson, 2010; Suh et al., 2013; Rothschild et al., 2016), supporting SWR's role in offline consolidation. The experiments above were in rodents, but SWR also occur in humans (Bragin et al., 1999), in whom hippocampal lesions also disrupt memory consolidation (Squire et al., 2001). However, differences between humans and rodents may lead to human-specific SWR characteristics.

Rodent SWR occur in non-rapid eye movement sleep (NREM) and Quiet Waking periods of immobility with large amplitude EEG. Unlike rodents, human sleep is nocturnal and quasi-continuous, with distinct stages of N2 characterized by sleep spindles and K-complexes, and N3 characterized by rhythmic upstates and downstates (Cash et al., 2009). Humans also appear to lack a stage comparable to rodent Quiet Waking (Poulet and Petersen, 2008). It is unknown if human SWR differ between N2 and N3, or if they occur during Quiet Waking.

Initial studies emphasized the synchrony of SWR across substantial portions of the rodent hippocampus (Chrobak and Buzsáki, 1996). However, Patel et al. (Patel et al., 2013) recently reported that HC-SWR seldom co-occur in dorsal and ventral HC. When they do co-occur, propagation is usually in the dorso-ventral direction. Although SWR waveform and density in dorsal and ventral HC were similar, they differed in amplitude and ripple frequency. In humans, it is unclear if the HC, which is entirely temporal, corresponds to rodent ventral HC, or if it has rotated such that human posterior HC corresponds to rodent dorsal HC, and human anterior HC

to rodent ventral HC (Strange et al., 2014). Thus, it is unclear if the differences found in rodents between dorsal versus ventral HC-SWR will be found in human posterior versus anterior HC-SWR.

Humans also differ from rodents in our strong hemispheric language specialization. Accordingly, unilateral medial temporal lobe lesions cause material-specific deficits, for verbal material after dominant lesions and visuospatial after nondominant (Weber et al., 2006; Iglói et al., 2010). This suggests functional independence of the two hippocampi, in contrast to rodents, where ~50% are bilaterally synchronous (Chrobak and Buzsáki, 1996). Human HC also differ from rodent in scale, with 30 times more pyramidal cells than mice (Korbo et al., 1990; West and Gundersen, 1990; West et al., 1991; Pakkenberg and Gundersen, 1997).

Human SWR have be recorded from electrodes implanted to localize epileptogenesis. Interictal spikes (IIS) are common in such recordings, often outside the ictal onset zone. IIS have high frequency components which overlap with ripples, leading to a variety of strategies for their separation (Wilson and Emerson, 2002). In addition to whether or how to distinguish IIS from SWR, criteria for selecting SWR also vary in whether to require multiple oscillations, a sharpwave and delta-wave as well as a ripple, NREM recordings, or hippocampal origin (see Table 2.1). Consequently, literature values for basic characteristics of human SWR vary widely.

Here, we identified human SWR in HC without IIS, and use their characteristics to guide separation of SWR from IIS in other patients. Human SWR were similar to rodent SWR in waveform, rate, intra-hippocampal topography, and concentration in NREM sleep. They differ from rodents in their ripple frequency, with significantly different densities in N2 vs N3 and in anterior vs posterior HC. Unlike rodents, human SWR seldom occur during waking and occur largely independently in the two hemispheres. Human SWR are usually also independent in

anterior vs posterior HC, but when related tend to spread from anterior to posterior, in contrast to rodents. Overall, human SWR are similar to rodent, but with significant differences that could influence their interaction with neocortex during consolidation.

Methods:

Patient selection

20 patients with long-standing drug-resistant partial seizures underwent SEEG depth electrode implantation in order to localize seizure onset and thus direct surgical treatment (see Table 2 for demographic and clinical information). Patients were selected from a group of 54 based on the following criteria: (1) age between 16 and 60 years; (2) globally typical SEEG rhythms in most channels (i.e., absence of diffuse slowing, widespread interictal discharges, highly frequent seizures, etc.); (3) electrode contacts in the HC as verified using non-invasive imaging (see below); (4) no previous excision of brain tissue or other gross pathology; (5) at least one HC contact in an HC not involved in the initiation of seizures. The resulting group of 20 patients includes 6 patients with an HC contact in a location with no interictal spikes, which were used to guide the protocols applied to the remaining 14 patients (Table 2.2). The 20 patients included 7 males, aged 29.8±11.9 years old (range 16-58). Electrode targets and implantation durations were chosen entirely on clinical grounds (Gonzalez-Martinez et al., 2013). All patients gave fully informed consent for data usage as monitored by the local Institutional Review Board, in accordance with clinical guidelines and regulations at Cleveland Clinic.

Electrode localization

After implantation, electrodes were located by aligning post-implant CT to preoperative 3D T1-weighted structural MRI with ~1mm^3 voxel size (Dykstra et al., 2012), using 3D Slicer

(RRID:SCR_005619). This allows visualization of individual contacts with respect to HC cross-sectional anatomy (e.g., Fig. 2.1*G*), which was interpreted in reference to the atlas of Duvernoy (Duvernoy, 1988). At most anterior-posterior levels, an electrode approaching human HC orthogonal to the sagittal plane passes through white matter, ventricle, alveus, and strata oriens, pyramidale, radiatum and lacunosum-moleculare, in that order. This progression was correlated anatomically by superposition of electrode contacts from post-implant CT onto preoperative MRI, and physiologically by observing activity typical of white matter, CSF or gray matter.

The assignment of depth contacts to anterior or posterior hippocampus (Ant-HC/Post-HC) was made with the posterior limit of the uncal head as boundary (Poppenk et al., 2013; Ding and Van Hoesen, 2015) (e.g., Fig. 2.4*D*). Recordings were obtained from 32 HC contacts, 20 anterior (11 left) and 12 posterior (7 left). In 4 patients, HC recordings were bilateral (3 anterior and 1 posterior), and in 8 patients, ipsilateral anterior and posterior HC were both recorded. The distance of each hippocampal contact from the anterior limit of the hippocampal head (e.g., Fig. 2.3*F*) was obtained in Freesurfer (RRID:SCR_001847).

Data collection and preprocessing

Continuous recordings from SEEG depth electrodes were made with cable telemetry system (JE-120 amplifier with 128 or 256 channels, 0.016-3000 Hz bandpass, Neurofax EEG-1200, Nihon Kohden) across multiple nights (Table 2.3) over the course of clinical monitoring for spontaneous seizures, with 1000 Hz sampling rate. The total NREM sleep durations vary across patients; while some difference is expected given intrinsic variability of normal human sleep duration (Carskadon and Dement, 2010) and clinically assigned sleep deprivation, we also confirmed that the percentages of NREM in total sleep from 28 sleeps across 16 of our patients were comparable to (i.e. within 2 standard deviation of) normative data in terms of N2 and N3

durations (Moraes et al., 2014) (Table 2.S1) ; Recordings were anonymized and converted into the European Data Format (EDF). Subsequent data preprocessing was performed in MATLAB (RRID:SCR_001622); the Fieldtrip toolbox (Oostenveld et al., 2011) was used for bandpass filters, line noise removal, and visual inspection. Separation of patient NREM sleep/wake states from intracranial LFP alone was achieved by previously described methods utilizing clustering of first principal components of delta-to-spindle and delta-to-gamma power ratios across multiple LFP-derived signal vectors (Gervasoni et al., 2004; Jiang et al., 2017), with the addition that separation of N2 and N3 was empirically determined by the proportion of down-states that are also part of slow oscillations (at least 50% for N3 (Silber et al., 2007)), since isolated down-states in the form of K-complexes are predominantly found in stage 2 sleep (Cash et al., 2009).

HC-SWR identification

Previous studies have used a variety of methods to identify SWR and distinguish them from IIS (Table 2.1). Previous studies did not require that a sharpwave be present. However, based on the fact that in rodents and macaques many ripples occur without a sharpwave (Buzsáki, 2015; Ramirez-Villegas et al., 2015), we explicitly tested for the presence of a sharpwave and following slow positivity, with the ripple needing to occur near the peak of the sharpwave. In order to identify ripples, previous studies detected outlier peaks in the amplitude or power in the putative ripple frequency range. However, such peaks can reflect a single sharp transient. Thus, unlike some previous studies (Table 2.1), in our study we followed detections of ripple-frequency amplitude peaks with tests for multiple discrete peaks at ripple frequency. Since IIS are characterized by a large fast spike component, the test for multiple oscillations helps distinguish them from SWR. Since the slower field potentials accompanying IIS have different waveforms than the characteristic sharpwave and later positivity, requiring that these waves be

present in their typical form also helps differential IIS from SWR. Nonetheless, due to the variability of IIS, it is important to visually examine the recordings in each patient to confirm the adequacy of IIS-rejection. These steps have seldom been taken by previous studies, some of which failed to even attempt to separate interictal spikes from SWR (Clemens et al., 2007, 2011). Some studies recorded entirely (Clemens et al., 2007, 2011) or mainly (Axmacher et al., 2008; Le Van Quyen et al., 2008) outside the hippocampus, although high frequency oscillations in rodents vary considerably between regions (Buzsáki, 2015). In our study, we recorded SWR exclusively from contacts which were confirmed to lie in the HC with CT/MRI localization. This localization was also used in our study to distinguish anterior from posterior HC recordings, which has not previously been done. This distinction is important given that these areas differ considerably in functional correlates and external anatomical connections (Ranganath and Ritchey, 2012; Strange et al., 2014). Finally, although most studies recorded human SWR in NREM sleep stages N2 and N3, some studies recorded mainly or entirely in other states, especially waking (Axmacher et al., 2008; Brázdil et al., 2015). Since it is unclear whether these are the same phenomena as classical SWR, we recorded during repeated 24-hour periods and after determining that SWR are essentially absent outside to N2 and N3, confined our quantitative analysis to those sleep stages.

In summary, we attempted to identify HC-SWR which were distinct from IIS and which possessed the ripple, sharpwave, and positive wave components of the SWR. Initially, an inclusive selection criterion (ripple selection based on amplitude from 65-180 Hz) was applied to HC recordings in the patients without IIS described above, in order to establish the parameters appropriate to use in the complete patient population. A minimum of 300 SWR were selected visually based on waveform and averaged in the time and time-frequency domains. Based on the

ripple frequency observed in this population, a bandpass of 60 to120 Hz was chosen for further processing (6th order Butterworth IIR bandpass filter). Root-mean-square (RMS) over time of the filtered signal was calculated using a moving average of 20 ms, with the 80th percentile of RMS values for each HC channel being set as a heuristic cut-off. Whenever a channel's signal exceeds this cut-off, a putative ripple event was detected. Adjacent putative ripple event indices less than 40ms apart were merged, with the center of the new event chosen by the highest RMS value within the merged time window. Each putative ripple event was then evaluated based on the number of distinct peaks in the HC LFP signal (low-passed at 120 Hz) surrounding the event center; a 40-ms time bin was shifted (5ms per shift) across ±50 ms, and at least one such time bin must include more than 3 peaks (the first and the last peak cannot be both less than 7ms away from the edges of this time bin) for the putative ripple event to be considered for subsequent analyses. In addition, the distance between two consecutive ripple centers must exceed 40 ms. To determine the duration of each ripple, the left edge was defined as the first time point before the ripple center where RMS value exceeded the percentile threshold used for initial ripple detection, and the right edge was defined as the first time point after the ripple center where RMS value fell below the threshold; all other time points within the duration of this ripple must exceed the RMS threshold.

Since RMS peaks may arise from artifacts or epileptiform activity, 2000 ms of hippocampal LFP data centered on each ripple event undergoes 1-D wavelet (Haar and Daubechies 1-5) decomposition for the detection and removal of sharp transients (i.e. signal discontinuities). For each wavelet decomposition, putative SWR were marked in ~10 min long NREM sleep period (marking ended sooner if 400 putative SWR had been found). A scale threshold was then established via iterative optimization for the best separation between hand-

marked true ripple events and interictal events in the same NREM sleep period. Each putative sharp transient was then rejected only if the 200 Hz highpassed data at that point exceeds an adaptive threshold (Bragin et al., 1999) of 3—or another number that allows best separation in agreement with visual inspection by human expert (between 0.5 and 5, and ~2 on average)—standard deviations above the mean for the 10-second data preceding the transient.

To identify which ripples were coupled to sharpwaves (i.e., SWR), we created patient-specific average templates (-100ms to +300ms around ripple center) from hand-marked exemplars (100-400 SWR) in NREM per patient) that resemble previously described primate sharpwave-ripples with biphasic LFP deflections (Skaggs et al., 2007; Ramirez-Villegas et al., 2015). We then evaluated whether each ripple qualifies as a SWR with the following two criteria: 1, the similarity of the peri-ripple LFP to the average template as quantified by the dot product between the template and the peri-ripple LFP (-100ms to +300ms). For each template-LFP pair, the similarity threshold was chosen so that it would reject at least 95% of the hand-marked ripples with no sharpwave. 2, the absolute difference between the LFP value at the ripple center and at the maximum/minimum value between +100ms and +250ms after ripple center was computed for each ripple; this difference must exceed 10% (or another value which excludes 95% of hand-marked ripples with no sharpwave) of the difference distribution created from hand-marked SWR. In addition, the distance between two consecutive SWR centers must exceed 200 ms. Time-frequency plots of HC LFP centered on detected SWR were then created in MATLAB with EEGLAB toolbox (Delorme and Makeig, 2004), each trial covering ±1500 ms around SWR and with -2000 ms to -1500ms as baseline (masked for significance at alpha = 0.05, 200 permutations).

Experimental design and statistical analysis

All statistical tests below have $\alpha = 0.05$ post FDR-correction for multiple comparisons (Benjamini and Hochberg, 1995), unless otherwise specified. We evaluated in patients with multiple hippocampal recording sites the extent to which SWR overlap (i.e. fall within 50ms of each other). This was tested both for two sites within the same hippocampus along the longitudinal axis (anterior and posterior), or in the two hemispheres (left and right, in the same longitudinal position). To test whether such overlaps differ from expected values due to chance alone (with variable overlap criteria being the time window size (ranging from 25 to 5000 ms) within which SWR from multiple HC sites co-occur), we estimated the co-occurrence rate for random SWR times, with the proviso that the total number of randomly-occurring SWR in each 5 min interval matches that actually observed. One-tailed 2-sample t-tests were then conducted between actual co-occurrences versus expected, with one pair of observations from each patient (N=8 for anterior vs posterior, and N=4 for left vs right). To test whether anterior led posterior HC-SWR in each patient we conducted a binomial test for the SWR pairs occurring in both sites within 200ms, against the null hypothesis of equal numbers from anterior vs posterior leads.

Results:

We identified human HC SWR from intracranial recordings, distinguished them from IIS, characterized their density, topography, and ripple frequency, and determined if their characteristics change between NREM stages N2 and N3, or between anterior and posterior HC sites. Morphologically normal ripples were isolated from >24 h continuous recordings in 20 stereoelectroencephalography (SEEG) patients with intractable focal epilepsy, with anterior (in 17 patients) and/or posterior HC contacts (in 11 patients).

<u>Comparison of SWR in patients with or without HC IIS</u>

Given the potential for contamination with epileptiform activity, our initial studies focused on six patients (8 HC locations, 5 in Ant-HC, 3 in Post-HC) that show no HC interictal spikes (IIS) over the course of the patient's hospitalization (Table 2.2). SWR were detected by applying patient-specific SWR templates built from hand-marked representatives to non-epileptiform high frequency oscillation events, we found that these patients showed SWR with the same characteristic waveform, rate (for anterior contacts, ~13.45/min in N2, ~19.89/min in N3, comparable to previous report (Le Van Quyen et al., 2008)), and association with NREM as reported in rodents and in non-human primates (Fig. 2.1*A*, Fig. 2.2, Fig. 2.3*A*). These characteristics were compared to those obtained in patients whose HC contacts showed occasional IIS. Events in these patients were accepted as SWR only after rigorous separation procedures from IIS based on amplitude, waveform, and spectral pattern (Fig. 2.2). The SWR in the patients with HC IIS were comparable to those with no IIS in waveform and rate (Fig. 2.1*B-C*, Fig. 2.3*A-D, F-G*). Further studies then included these patients and HC electrodes (24 unique contacts, 32 total including IIS-free patients).

Intrahippocampal SWR topography and ripple frequency

We observed in our data that intrahippocampal topography of the SWR in humans appears similar to that established in rodents: the maximum amplitude of the ripple is seen just after passing through the alveus into the presumptive stratum pyramidale, and that of the sharpwave and following delta wave more medially in presumed stratum radiatum (Fig. 2.1*D-F*, *G-I*). We further quantified the relative maximum amplitude of all ripples (that were part of SWR) and of their associated sharp-delta waves in radiatum versus pyramidale contacts in 10 subjects with both. For ripple, we computed for each SWR the proportion of increase for maximum LFP amplitude over mean LFP amplitude across ±20ms of ripple center; for sharp-

delta wave, we computed for each SWR the proportion of increase for maximum LFP amplitude over mean LFP amplitude across 1000 ms (-250~750 ms relative to ripple center). We found that the mean pyramidale relative ripple amplitude (0.68) was significantly greater than the mean radiatum relative ripple amplitude (0.63) ($p < 2.2 \times 10^{-16}$, paired two-tailed t-test), although the effect size was small (Cohen's $d = 0.05$) (Lakens, 2013). As expected from examples in Fig. 2.1, the mean radiatum relative sharp-delta wave amplitude (3.7) was significantly greater than the mean pyramidale relative sharp-delta wave amplitude (2.2) ($p < 2.2 \times 10^{-16}$, paired two-tailed t-test), with a medium effect size (Cohen's $d = 0.54$).

Time-frequency plots of SWR showed a concentration of ripple power at the oscillation frequency (Fig. 2.2*C*-*F*). The mean frequency of ripple oscillations in detected SWR was 81.5±9.7 Hz. This is lower than observed in rodents, but is consistent with previous studies in primates (Skaggs et al., 2007; Logothetis et al., 2012).

SWR density in different stages of NREM sleep, waking, and anterior versus posterior HC

Consistent with the occurrence of SWR during slow wave sleep in rodents, human SWR were largely confined to NREM sleep (Fig. 2.3*A*, *C*), with low mean waking SWR rates at 1.77/min for Ant-HC, and 2.16/min for Post-HC, not differing significantly from Ant-HC (p = 0.5433, two-tailed two-sample t-test). The mean occurrence rate of SWR was significantly greater in Ant-HC than in Post-HC, and more SWR occur in N3 than in N2 (Fig. 2.3*F*-*G*, Table 2.3). Specifically, for Ant-HC, the mean SWR rate was 11.59/min in N2, and significantly different at 17.01/min in N3 (two-tailed paired t-test, p = 0.0001); for Post-HC, the mean SWR rate was 6.75/min in N2, and significantly different at 10.71/min in N3 (two-tailed paired t-test, p = 0.0083). Comparing Ant-HC SWR rate to Post-HC SWR rate under different NREM stages, in turn, also yielded significant differences (two-tailed t-tests, p = 0.0038 for N2, p = 0.018 for N3).

In order to ensure that these results were not influenced by clinical sleep deprivation regimen, we also obtained the mean SWR rates in N2/N3 Ant-HC/Post-HC from only normal sleeps (i.e. N2 and N3 durations both fall within 2 standard deviations of normative data) across 12 of our patients (13 Ant-HC sites, 10 Post-HC sites). Similar to the overall results, in this normative population, for Ant-HC, the mean SWR rate was 11.97/min in N2, and significantly different at 18.29/min in N3 (two-tailed paired t-test, $p = 0.0089$); for Post-HC, the mean SWR rate was 6.85/min in N2, and significantly different at 10.02/min in N3 (two-tailed paired t-test, $p = 0.0166$). Also, similarly to the overall results, under different NREM stages, the mean SWR rates in Ant-HC were significantly different from those in Post-HC (two-tailed t-tests, $p = 0.0306$ for N2, $p = 0.0191$ for N3).

Spectral power changes surrounding SWR

Within the HC, SWR were surrounded by locally-decreased broadband spectral power (Fig. 2.2*C-F, I, J*). The post-SWR decrease occurs during the delta-wave which typically follows the sharpwave and, as previous studies in rodents have shown, is accompanied by hyperpolarization of HC pyramidal cells (English et al., 2014). However, here we observed an addition broadband decrease in spectral power which commonly began 500-1000 ms *prior* to the ripple. To further characterize the pre- and post-SWR spectral power decreases across HC sites from different subjects, we computed (separately for N2 and N3) the mean event-related spectral perturbation (ERSP) (Delorme and Makeig, 2004) from -650 ms to -150 ms before the SWR for three different frequency ranges: beta (10-30 Hz), low gamma (30-60 Hz), and high gamma (60-120 Hz). For all three frequency ranges, the mean pre-SWR ERSPs were significantly lower (two-tailed paired t-tests) than the baseline (-1500 ms to -1000 ms): in N2, for beta, a 1.0 dB decrease on average was observed ($p = 1.139 \times 10^{-5}$); for low gamma, a 0.85 dB decrease was

observed ($p = 1.166 \times 10^{-4}$); for high gamma, a 0.55 dB decrease was observed ($p = 6.762 \times 10^{-5}$). Similarly, in N3, for beta, a 0.96 dB decrease on average was observed from near-SWR to pre-SWR ($p = 1.171 \times 10^{-5}$); for low gamma, a 0.85 dB decrease was observed ($p = 1.012 \times 10^{-4}$); for high gamma, a 0.54 dB decrease was observed ($p = 1.390 \times 10^{-4}$). Thus, prior to the SWR, the local LFP is decreased across multiple frequency bands in both N2 and N3.

Co-occurrence of SWR in anterior and posterior HC

Although initial descriptions of SWR in rodents emphasized their co-occurrence throughout the entire extent of both hippocampi (Buzsaki et al., 1992), more detailed studies showed that isolated SWR could also occur (Patel et al., 2013). For patients (n = 8) with both Ant-HC and Post-HC contacts in the same HC (Fig. 2.4), the overlap (i.e. co-occurrence within 50 ms) between Ant-HC and Post-HC SWR was 5.6±3.0% in N2, and 7.3±5.9% in N3, compared to chance levels of 1.0±0.54% in N2 and 1.6±1.0% in N3. In both N2 and N3, the actual mean overlap percentages were significantly greater than the mean overlap percentages derived from chance ($p = 0.0018$ and $p = 0.011$, one-tailed paired t-tests). By varying the co-occurrence criterion range between 25 ms and 5000 ms, we observed greater-than-chance co-occurrence rates for Ant-HC and Post-HC SWR initially, but the actual co-occurrence rate tapered off exponentially (i.e. showed linear decay in log-log plots) towards chance level beyond ~100 ms for bilateral HC and beyond ~500 ms for Ant-/Post-HC (Fig. 2.4*B*).

Patel et al. (Patel et al., 2013) found in rodents that dorsal SWR often propagate to ventral, but ventral SWR often remain isolated. Accordingly, we tested if the probability of an Ant-HC SWR given a Post-HC SWR was greater than the probability of a Post-HC SWR given an Ant-HC SWR; we found this to be a trend, but not significantly so (n=8, one-tailed paired t-test, $p = 0.149$). We also evaluated if SWR propagate with preferred directionality within the

same hippocampus in humans, with binomial tests (chance at 50%) over the number of Post-HC SWR in N2+N3 that precede or follow Ant-HC SWR within 200 ms. While for 4 of these 8 patients, Ant-HC SWR preceded Post-HC SWR ($p < 2.20 \times 10^{-16}$ for patient 4, $p = 1.72 \times 10^{-10}$ for patient 5, $p < 2.20 \times 10^{-16}$ for patients 9 and 19) (Fig. 4*A*), the opposite was found for 3 patients ($p < 2.20 \times 10^{-16}$ for patient 6, $p = 5.79 \times 10^{-11}$ for patient 11, $p = 2.80 \times 10^{-8}$ for patient 13), and 1 showed no significant preference either way (patient 3, $p = 0.2082$).

Co-occurrence of SWR in left and right HC

The dominant and non-dominant hippocampal formations of humans are thought to be specialized for verbal and visuospatial memory, respectively (Gleiβner et al., 1998; Weber et al., 2006), and similar functional lateralization may also be present in animals (Shipton et al., 2014). This might predict distinct memory traces and thus low bilateral co-occurrence of SWR. We tested this prediction in patients (n = 4) with bilateral (left and right) HC contacts, placed in either both anterior or both posterior HC. In these patients, co-occurrence between HC in different hemispheres was 2.4±1.2% in N2, and 2.8±1.2% in N3. While this was less than that usually observed between two contacts within the same HC, it was still significantly greater than chance-derived overlap percentages (1.1±0.64% in N2, 1.4±0.77% in N3) for both N2 and N3 ($p = 0.0317$ and $p = 0.0105$, one-tailed paired t-test) (Fig. 2.4*C*). Thus, in humans, only a small proportion of SWR co-occur in both anterior and posterior hippocampal regions, and an even smaller proportion in both left and right hippocampi.

Discussion:

In this study, we defined the basic characteristics of human hippocampal sharpwave-ripples (HC-SWR), in order to better understand how they might contribute to memory consolidation. HC-SWR have previously been studied primarily in rodents (Buzsáki, 2015); in

humans recordings are rare and limited to those obtained from patients with epilepsy. Generally, such studies have not clearly isolated HC-SWR from epileptiform activity, have failed to use rigorous criteria for identification of HC-SWR, have recorded from sites that were adjacent to the HC but seldom from the HC itself, and/or have not clearly defined the patient's sleep/waking state (Table 2.1). Here, we selected patients whose hippocampal recordings appeared to be free of epileptic activity, and used rigorous selection criteria to clearly identify SWR. This allowed us to recognize SWR in a larger group of patients in HC with limited epileptiform activity. We then extensively characterized human HC-SWR so they could be compared to previous studies in rodents.

Human HC-SWR are similar to rodent's in most basic characteristics. In rodents, ripples are maximal in stratum pyramidale of CA1, and sharpwaves in stratum radiatum (Buzsáki, 2015). We observed a consistent topography from ripple to sharpwave maxima as the contacts progressed lateral to medially in humans.

Like most previous studies, we found a ripple center frequency between 80 and 90Hz, much lower than rodents (~140 Hz), but similar to monkeys (Skaggs et al., 2007; Logothetis et al., 2012; Ramirez-Villegas et al., 2015). Staba (Staba et al., 2004) found that bursts of power between 80-500Hz in human HC peaked at either 89 (ripple) or 263 (fast ripple). Both ripples and fast ripples occurred in the side contralateral to seizure onset, but the proportion of ripples was greater on that side. No requirement for an associated SW was imposed. We show that the lower center frequency characterizes ripples within sharpwaves, in HC without IIS. Ripples may comprise an exception to the general rule that frequencies of identifiable rhythms are fairly constant across mammalian species (Buzsáki et al., 2013). The functional implications of the lower frequency in humans is unclear. In rodents, 80-90Hz oscillations are seen when the

depolarization of CA1 pyramidal cells is less than during ripples (Sullivan et al., 2011). Alternatively, the lower frequency may reflect larger cells, lower packing density, and/or different channel time-constants in the human HC.

Ripple density in humans reported in previous studies ranges from 0.08/min (Staba et al., 2004) to 30/min, or even 115/min if patients with memory deficits are included (Jacobs et al., 2016) (Table 2.1). The average SWR density in this study ranged from ~7 to ~17/min, according to the stage of sleep or part of the hippocampus being recorded. This density was consistent across patients with no HC-IIS or seizures, versus those with some HC-IIS but no seizures, and lies within the range of previous human (Table 2.1) and animal studies (Buzsáki, 2015).

Our finding that HC-SWR are preceded by suppression of broadband oscillations in the putative CA1 is consistent with models that emphasize a role for sustained inhibition in the genesis of SWR (Buzsáki, 2015). As in rodents (Klausberger et al., 2003) putative inhibitory interneurons in human hippocampus fire before SWR (Le Van Quyen et al., 2008). The quiet background may increase the consistency of CA1 neural response to CA3 input which triggers SWR.

The long, tubular human hippocampus shows substantial differences in anatomical connections and function along its length (Poppenk et al., 2013; Strange et al., 2014). While primate dorsal HC has been obliterated during fetal development, it is unclear if the remaining HC corresponds to the rodent ventral HC only, or if the HC has rotated such that human posterior HC corresponds to rodent dorsal.

In rats, SWR density depend on the interaction of threshold and location on the dorso-ventral HC axis: smaller ripples occurred at ~15/min in the ventral HC and 5 in dorsal, whereas larger ripples the converse (Patel et al., 2013). Our SWR results in humans were similar to the

smaller ripples in rats: ~15/min for the anterior and 8/min for the posterior HC. Recently, (Staresina et al., 2015), recording mainly in posterior HC, reported that ripples were phase-coupled to HC spindles SS, rather than the sharpwaves typical in rodents. Combined with our results, this suggests that spindle-ripples rather than sharpwave-ripples may characterize posterior HC sites.

Human NREM is different than the rodent's, being nocturnal and quasi-continuous, and including distinct N2 and N3 stages. In each 90 min sleep cycle N2 precedes N3, but most N2 occurs later in the night, and they may make complementary contributions to memory consolidation (Wei et al., 2018). Only one previous study reported different rates for ripples in N2 (1.6/min) versus N3 (1.0/min); that study did not record from the HC, and explicitly included IIS with SWR (Clemens et al., 2007). In contrast, we found that human HC-SWR, excluding IIS, were lower density in N2, 9/min, than N3, 15/min. Traditionally, N2 is characterized by sleep spindles and K-complexes, and N3 by down-upstates (Silber et al., 2007), suggesting that SWR may be more strongly associated with down-upstates than spindles. However, spindles and down-upstates both occur in both stages (Cash et al., 2009; Mak-McCully et al., 2017), and both co-occur with SWR (Buzsáki, 2015). In any case, our results show that human HC-SWR are present in both sleep stages.

In rodents, SWR are common during Quiet Waking (Roumis and Frank, 2015), a behavioral state characterized by grooming or immobility and large cortical LFP in comparison to active waking (Poulet and Petersen, 2008). In humans, Axmacher (Axmacher et al., 2008) reported ripples during quiet waking, at a density (5.3/min) much higher than N3 (0.35/min). In contrast, Clemens (Clemens et al., 2007) reported lower ripple density in waking (0.85/min) versus N2/N3 (1.3/min), but these recordings were extra-HC and included IIS. Finally, Brázdil

(Brázdil et al., 2015), who recorded only during a task, reported high ripple density (19.4/min). We found that human HC-SWR are very rare during waking (1.9/min) compared to N2/N3 sleep (12/min). However, unlike the human studies cited above, we required that ripples be embedded in a sharpwave; when that requirement was removed, the density of ripples during waking was greater during waking than NREM (Fig. 2.3). The occurrence of ripples without a sharpwave has also been noted in rodents and macaques (Buzsáki, 2015; Ramirez-Villegas et al., 2015) It is possible that ripples during waking (as opposed to SWR) contribute to consolidation in humans, and conversely, there is no direct evidence that SWR during NREM contribute to memory consolidation in humans. Axmacher (Axmacher et al., 2008) found that ripples in rhinal cortex, mainly recorded during quiet waking, were correlated with consolidation. More recent human intracranial EEG studies (Jiang et al., 2017; Zhang et al., 2018) found during NREM a significant co-occurrence of human HC-SWR with replay of widespread cortical spatiotemporal high gamma patterns from the preceding waking period.

Although initial studies emphasized the synchrony of SWR across substantial portions of the hippocampus (Chrobak and Buzsáki, 1996; Buzsáki, 2015), a recent study found that HC-SWR seldom co-occurred in both dorsal and ventral HC (Patel et al., 2013). In humans, our study found that co-occurrence of SWR within 50 ms in anterior versus posterior HC was only ~5% above chance. When SWR do co-occur within an HC, in rats, propagation is more often in the dorso-ventral direction, whereas in humans the preference is less clear. This may be related to the higher SWR rate that we found in anterior HC, and its much larger volume in humans (Destrieux et al., 2013).

Co-occurrence of SWR between the left and right hippocampus is even rarer than within an HC. We found that bilateral SWR occurred only ~1.4% above chance, in contrast to rats

where ~50% are bilaterally synchronous (Chrobak and Buzsáki, 1996). Greater bilateral independence in humans would also agree with the small size of the hippocampal commissure in humans (Wilson et al., 1991), and the lack of bilateral activity propagation evoked by unilateral electrical stimulation (Wilson et al., 1990). Functional specialization of dominant versus nondominant hippocampi has been inferred from the selective impairment of verbal versus nonverbal memory observed after unilateral lesions (Gleiβner et al., 1998; Weber et al., 2006). Consistent with these long-standing neuropsychological observations, our study shows that a core physiological process hypothesized to support consolidation occurs largely independently in the two hippocampi.

Our study demonstrates that SWR occur in human hippocampi seemingly free from epileptiform activity, and that similar SWR occur in HC showing only effects of distant foci. Human HC-SWR are similar to rodents in their waveforms, distribution across putative lamina in CA1, concentration in NREM sleep, and overall density. Human HC-SWR differ from rodents in the oscillation frequency within ripples, and their absence during quiet waking. Human HC-SWR density differs between stages N2 and N3, a distinction not present in rodents. Human HC-SWR density and propagation patterns also differ between anterior and posterior HC. Unlike rodents, human HC-SWR occurrence is almost completely independent in the two hemispheres. Overall, this study provides a framework for, and imposes powerful constraints on, models for the hippocampal contribution to memory consolidation in humans.

Chapter 2, in full, is currently being prepared for submission for publication of the material. Jiang, Xi; Gonzalez-Martinez, Jorge; Cash, Sydney S.; Chauvel, Patrick; Halgren, Eric. The dissertation author was the primary investigator and author of this paper.

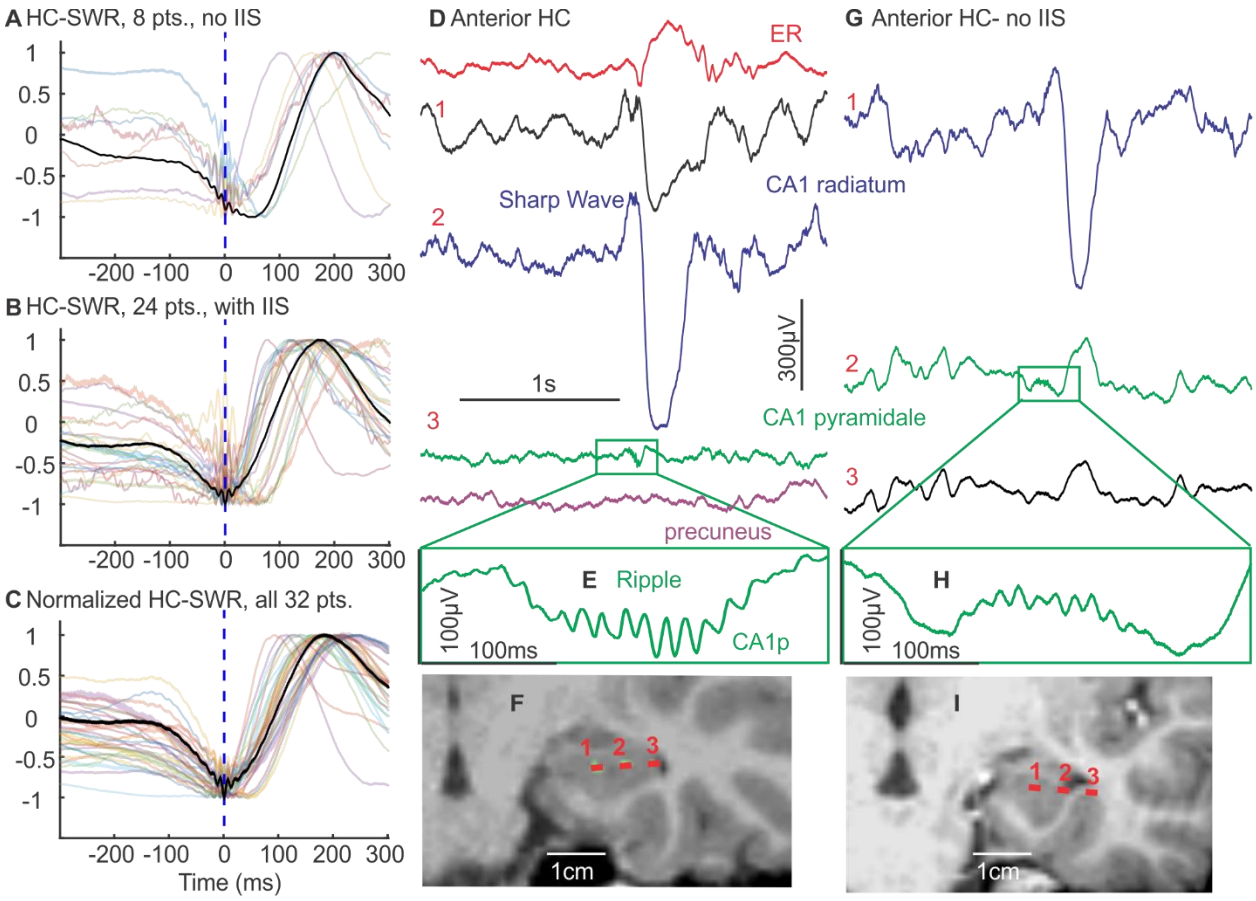

Figure 2.1: Distribution and characteristics of HC SWR. ***A-C***. Overlaid average waveforms of SWR across hippocampal contacts from different patients, with one representative patient bolded in black for clarity. ***A***. Hand-marked SWR exemplars from interictal-free patients. ***B***. Hand-marked SWR exemplars from other patients. ***C***. Automatically detected SWR from all patients. ***D***. Single sweep of HC and NC referential SEEG showing SWR. ***E***. Expanded time-base of ripple. ***F***. MRI with CT of SEEG contacts in ***D*** superimposed. ER: entorhinal. ***G-I*** are replicates of ***D-F***, but from another subject with no HC interictal activity. pts.: patients.

Figure 2.2: Spectral characteristics of HC SWR. ***A***. Average LFP of SWR accepted after the procedure in ***H***. ***B***. Average LFP of IISs originally classified as SWR based on high-frequency power from the same HC contact as ***A***, but rejected from further analysis. ***C-F***. Time-frequency plots showing typical frequency ranges of SWR, and broadband power decreases near SWR, from different NREM stages and example contacts in different HC locations. ***G***. time-frequency plot of the same IISs that make up ***B***; the power increase across all frequencies is not characteristic of true SWR (see ***C***, which was derived from true SWR in the same HC contact). ***H***. Schematic for the identification process of true SWR. Candidate LFP events (examples marked 1-5 and bound in orange dash line boxes) were first selected based on 60-120 Hz power. Putative ripples resembling event 2, i.e. those with less than 3 unique oscillation peaks, would be rejected first, followed by the removal of instances resembling event 3 (no distinct sharpwave that resembles hand-marked examples) and of those similar to event 1 (putative interictal spikes with high frequency power above ripple range). ***I***, ***J***: grand averages of all patients' time-frequency plots for N2 (***I***) and N3(***J***). Pt.: patient.

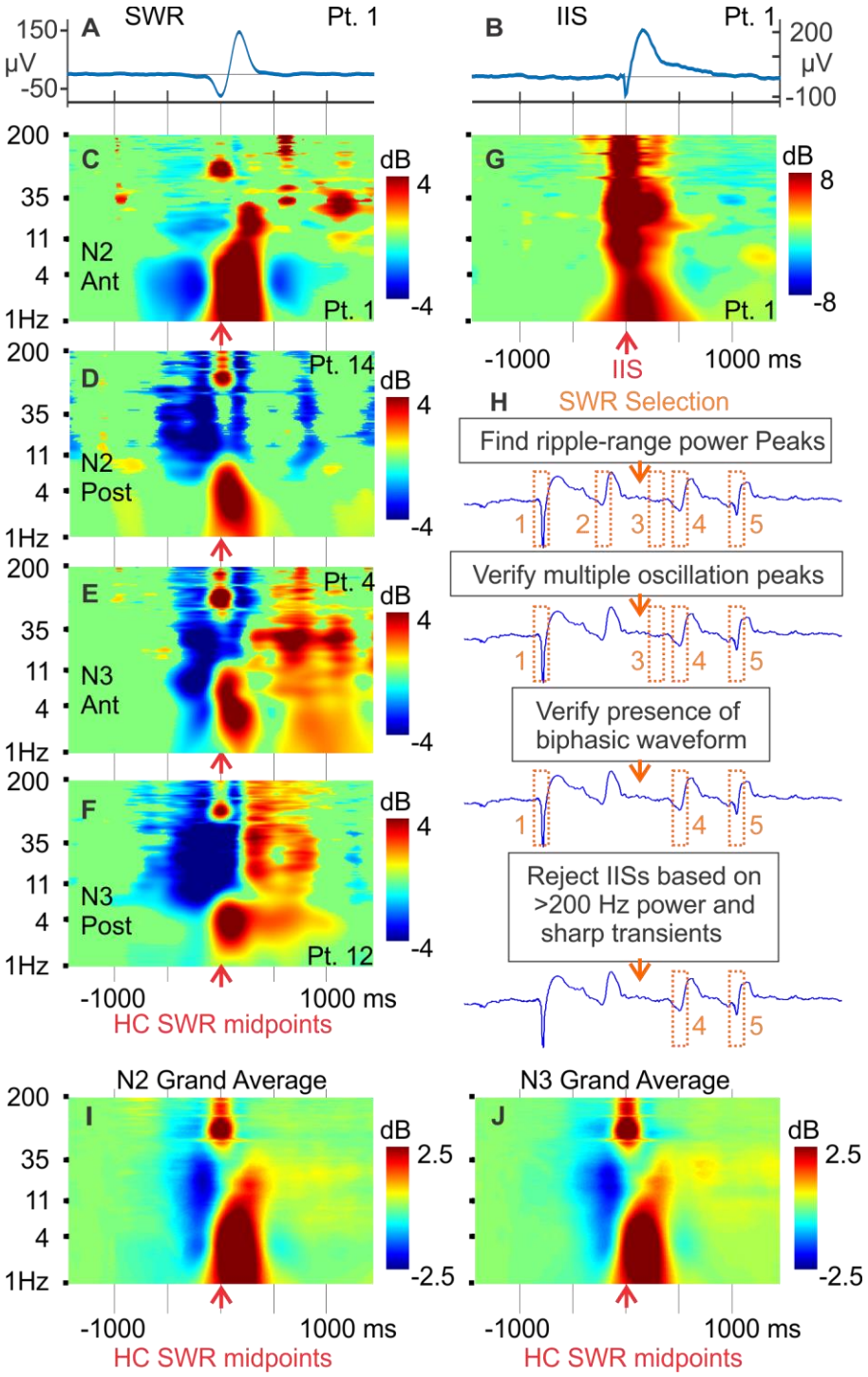
A
SWR
Pt. 1
150
μV
-50
B
IIS
Pt. 1
200
μV
-100
C
N2
Ant
Pt. 1
D
N2
Post
Pt. 14
E
N3
Ant
Pt. 4
F
N3
Post
Pt. 12
200
35
11
4
1Hz
dB
4
-4
G
Pt. 1
8
-8
-1000
1000 ms
IIS
HC SWR midpoints
H
SWR Selection
Find ripple-range power Peaks
Verify multiple oscillation peaks
Verify presence of biphasic waveform
Reject IISs based on >200 Hz power and sharp transients
1
2
3
4
5
N2 Grand Average
N3 Grand Average
I
J
2.5
-2.5

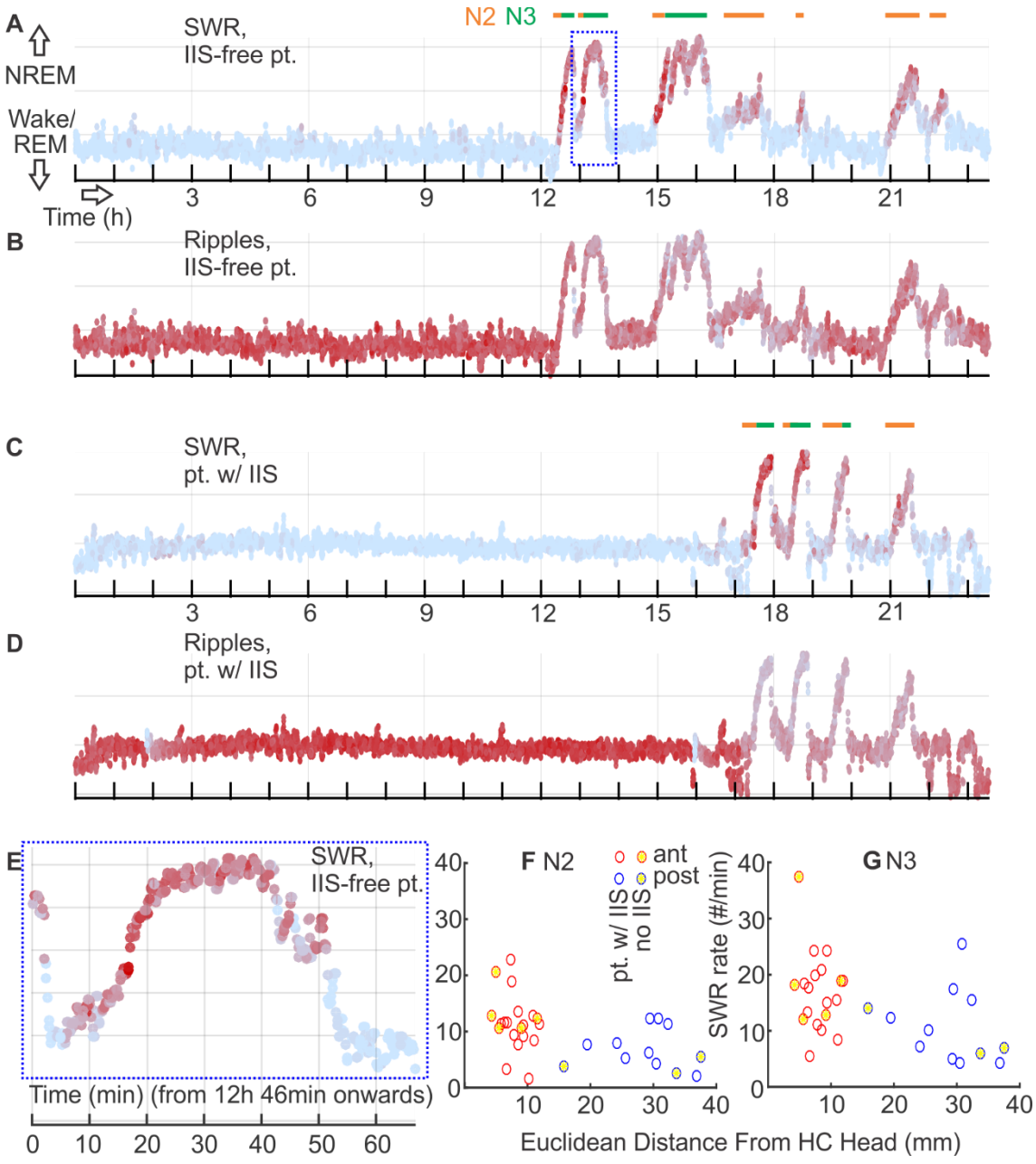

Figure 2.3: Distribution of HC SWR across stages of sleep and waking. ***A-D***. State plots showing the separation of NREM sleep in 24-hour LFP recording for both IIS-free (***A***, ***B***) and non-IIS-free (***C***, ***D***) patients, using the first principal component derived from 19 vectors (one per cortical bipolar SEEG channel) of frequency power ratios (0.5-3 Hz over 0.5-16 Hz) (Gervasoni et al., 2004; Jiang et al., 2017). SWR rate (***A***, ***C***) and plain ripple rate (***B***, ***D***) are color coded with red intensity, and N2/N3 periods are marked with orange/green horizontal lines, respectively. Deep blue dash line in ***A*** marks the close-up period in ***E***.***E***, close-up of one NREM cycle in ***A***. ***F***, ***G***. Distribution of SWR occurrence rates in different NREM stages across the HC longitudinal axis. Each circle represents data from one hippocampal contact. Red circles indicate contacts in Ant-HC; blue circles indicate those in Post-HC. Yellow fill marks the contacts from interictal-free patients.

Figure 2.4: Co-occurrence of SWR from HC site pairs. ***A***. In some patients, Ant-HC SWR tend to precede Post-HC SWR, while the opposite was found in others. Each panel contains peri-stimulus time histograms over ±200 ms, with Ant-HC SWR as triggers (time 0, red vertical lines). In four patients (marked green), Ant-HC SWR significantly preceded Post-SWR ($p < 2.2 \times 10^{-16}$ for Pt. 4, Pt. 9, and Pt. 19; $p = 1.72 \times 10^{-10}$ for Pt. 5); in three patients (marked orange), Post-HC SWR significantly preceded Ant-SWR ($p < 2.2 \times 10^{-16}$ for Pt. 6; $p = 5.79 \times 10^{-11}$ for Pt. 11, 2.80×10^{-8} for Pt. 13); in one patient, no significant precedence was observed either way ($p = 0.2082$) (two-tailed binomial tests for counts within ±200 ms). Pt.: patient. The average occurrence rate of SWRs over NREM (~0.002 per 10 ms bin). Green/Orange stars mark the time bin closest to when an Ant-HC/Post-HC SWR would reach Post-HC/Ant-HC, respectively, given the previously estimated intrahippocampal SWR propagation speed of 0.35 m/s (Patel et al., 2013). ***B***. For both bilateral HC site pairs and Ant-HC/Post-HC site pairs. SWR co-occurrence likelihood approaches chance as time window for co-occurrence expands. Blue filled circles mark (wrt. left y-axis) the ratios of actual over chance overlap proportions, and orange/brown unfilled circles mark (wrt. right y-axis) the corresponding actual (orange) and chance (brown) proportions. All axes for each panel are logarithmic. Bilat.: bilateral. AP: Ant-HC/Post-HC. ***C***. Sketch of SWR co-occurrence (with co-occurrence criterion being ± 50 ms) across Ant-HC and Post-HC, as well as across bilateral HCs. The occurrence rates are in numbers per minute. ***D***. Sagittal MRI showing the boundary between Ant-HC and Post-HC (marked in yellow), using the uncal apex criterion (Poppenk et al., 2013).

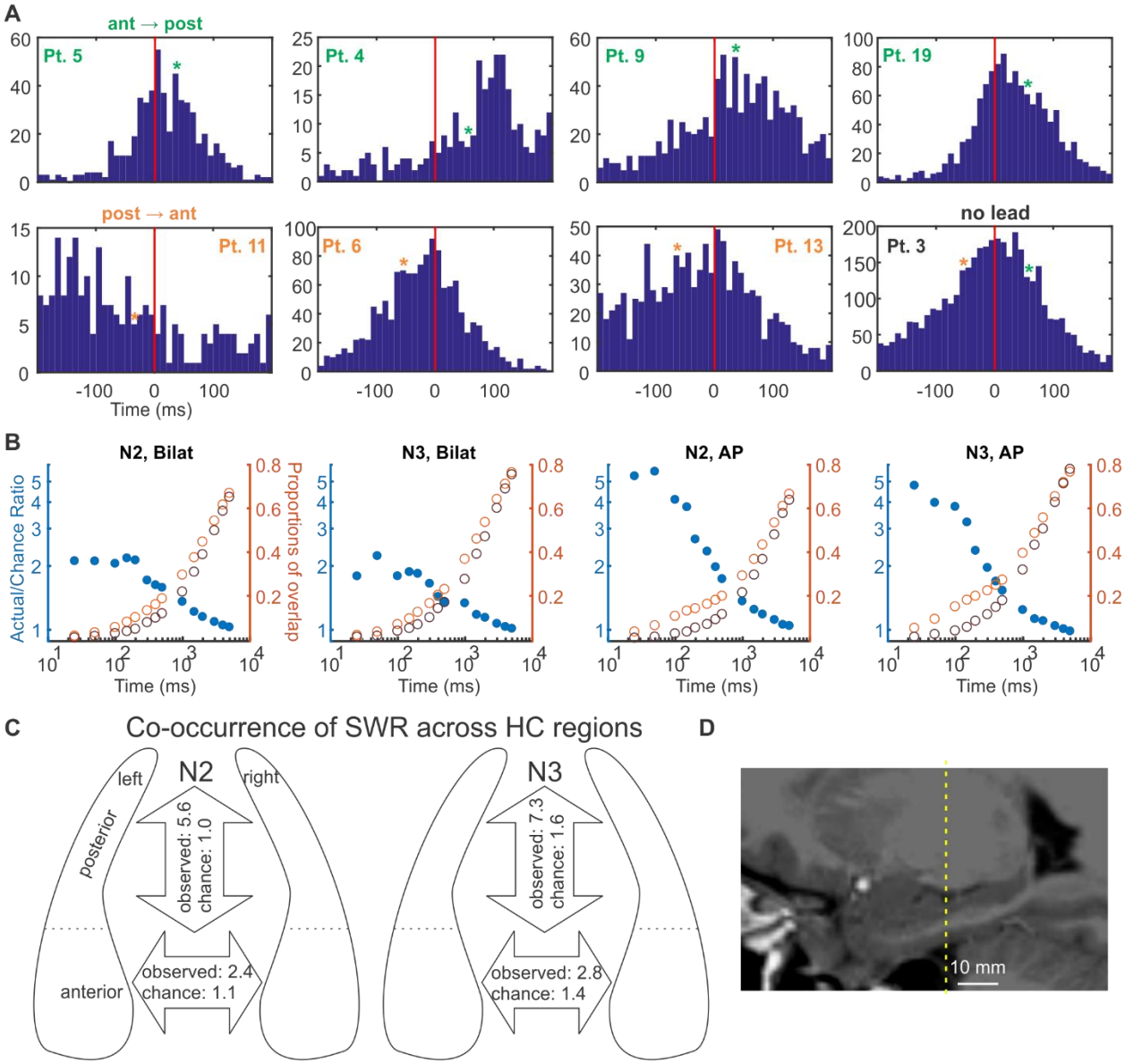
A
ant → post
Pt. 5
Pt. 4
Pt. 9
Pt. 19
post → ant
Pt. 11
Pt. 6
Pt. 13
no lead
Pt. 3
Time (ms)
B
N2, Bilat
N3, Bilat
N2, AP
N3, AP
Actual/Chance Ratio
Proportions of overlap
Time (ms)
C
Co-occurrence of SWR across HC regions
N2
N3
left
right
posterior
anterior
observed: 5.6
chance: 1.0
observed: 2.4
chance: 1.1
observed: 7.3
chance: 1.6
observed: 2.8
chance: 1.4
D
10 mm

Table 2.1: Previous studies reporting characteristics of human sharpwave-ripples.

reference	location[1]	units	ripple selection					epilepsy rejection				ripple characteristics				#patients with ripples[4]	state[5]	similar references from same group
			band pass	auto *vs.* visual[2]	minimum duration (ms)	min # waves	Sharp Wave required?	exclude ictal onset zone?	exclude large sharp events?	exclude HC with IIS?[3]	visual control?	ripple frequency	ripple duration (ms)	sleep rate /min	wake rate /min			
Axmacher et al, 2008	HC, pHCg	no	80-140	a	25	2	no[6]	yes	yes	no	no	85 [7]	x	0.35 [7a]	5.3	11	sleep, QW[8]	
Bragin et al, 1999	HC, pHCg	yes	50-200	v	60	x	no	no	no	no	yes	120	x	5 [8a]		4	sleep, QW	Bragin et al, 1999
Brázdil et al, 2015	HC	no	80-250	a	30	1	no	yes	no	no	no	x	83		19.4	10	waking task	
Clemens et al, 2007	pHCg (FO)	no	80-140	av	x	3	no	no[9]	no	no	no	84	27	1.3 [9a]	0.85 [7]	10	NREM (N2,N3)	Clemens et al, 2011
Jacobs et al, 2016	HC	no	80-250	v	x	x	no	yes[10]	yes	no	yes	x	x	30 [11]		10	NREM	
Le Van Quyen et al, 2008	HC, pHCg	yes	80-200	a	20	1	no	no	no	no	no	98	38	20.7 [8a]		11	NREM, QW	
Staba et al, 2004	HC	no	80-500	a	no	1	no	yes[10]	no	no	no	89	x	0.08 [7]	0.04	25	NREM	Staba et al, 2002
Staresina et al, 2015	HC	no	80-100	a	38	3	no[12]	yes	yes	no	yes	87	x	1.2		12	NREM (N2,N3)	
This study	HC[13]	no	60-120	av	25	4	yes[14]	yes	yes	yes[15]	yes	82	96	12 [16]	1.9	20	NREM (N2,N3)	

[1] HC-hippocampus; pHCg-parahippocampal gyrus (termed entorhinal or rhinal cortex by some); FO-recorded from cisterna ambiens with foramen ovale electrodes (all others are depth electrodes)

[2] av-automatic detection with visual validation; x-not reported

[3] IIS-interictal spike

[4] # of patients with ripples, in HC outside ictal onset zone, if reported separately

[5] QW-quiet waking

[6] ripple-triggered average shows small SW (~15μv)

[7] estimated from published figures

[7a] N3 only

[8] almost all ripples were recorded in waking

[8a] separate values not given for quiet waking

[9] ripples with vs without an IIS studied together

[9a] average of N2 and N3

[10] data reported separately for ictal zone

[11] for HC outside the ictal onset zone with intact memory (115 if memory impaired)

[12] from the reported co-occurrence of ripples, spindles and delta it appears that SWR were rare

[13] separate analyses for anterior and posterior HC

[14] visually-chosen SW at each electrode site used to construct a template

[15] data reported separately for HC lacking IIS

[16] average of posterior and anterior HC, and N2 and N3

Table 2.2: Patient demographics. Pt: patient. L: Left. R: Right.

Pt#	Age	Sex	Handedness	L Ant HC	L Post HC	R Ant HC	R Post HC	# Cortical Channels	Interictal-free?
1	20	M	R	x				19	N
2	51	F	R	x				12	N
3	58	F	R	x	x			24	N
4	42	M	L	x	x	x		17	N
5	18	F	L			x	x	21	Y
6	20	F	R			x	x	21	N
7	22	M	LR	x				19	Y
8	30	F	R			x		13	N
9	43	F	R	x	x			12	N
10	16	M	R			x		17	Y
11	32	F	R	x		x	x	30	N
12	36	M	L				x	25	Y
13	21	F	L	x	x	x		14	N
14	21	F	R		x			14	N
15	29	F	R		x		x	17	N
16	41	F	R			x		19	N
17	24	M	R	x				21	N
18	31	F	R	x				15	N
19	21	M	R	x	x			15	Y
20	19	F	R			x		21	Y
mean	**30**							**18**	**Total: 8**

Table 2.3: Patient sleep durations and ripple rates. Pt: patient. L: Left. R: Right. Dur.: duration. Std dev: standard deviation.

Pt#	# Sleep Periods	mean duration of NREM (h)	Std dev NREM (h)	Total N2 Dur. (h)	Total N3 Dur. (h)	SWR Rate, N2 Ant. (/min)	SWR Rate, N2 Post. (/min)	SWR Rate, N3 Ant. (/min)	SWR Rate, N3 Post (/min)
1	3	2.2	0.78	2.8	3.3	11.3		19	
2	4	7.5	1.87	27.3	0	1.56			
3	4	7.1	2.44	23.1	0.30	11.2	12	24	25
4	4	3.1	0.33	1.8	9.0	10	4.3	11	4.3
5	1	3.7		1.9	0.9	20.7	3.7	38	14
6	3	2.7	1.49	2.6	3.0	9.05	12	15	17
7	3	3.8	1.17	2.4	3.8	10.7		13	
8	5	5.2	1.26	6.5	14	18.9		20	
9	4	3.1	0.45	3.7	4.4	12.8	7.9	16	7.2
10	5	3.8	1.11	7.5	8.8	12.9		18	
11	3	5.1	3.43	8.4	2.8	7.32	7.7	12	12
12	4	5.2	1.48	11.6	6.5		5.5		7
13	3	6	0.47	14.7	1.1	12.5	6.2	19	4.9
14	8	3.7	1.1	16.9	9.3		11		15
15	4	2.5	1.31	5.4	2.7		3.6		7.2
16	3	4.6	0.72	7.4	4.4	9.38		11	
17	3	5.1	1.88	8.9	2.9	22.9		24	
18	6	6.1	1.18	24.2	3.8	7.77		10	
19	4	2.8	0.72	5.4	5.8	12.4	2.6	19	6.1
20	3	4.9	2.53	5.2	6.0	10.6		12	
mean	**4**	**4.4**		**9.39**	**4.64**	**11.9**	**7**	**18**	**11**

Table 2.S1: Comparison of patient sleep data to normative data. A patient's sleep is considered "normal" if its N2 and N3 durations both fall within 2 standard deviations of normative data.

Patient Data																		
Patient Data			Sleep 1		Sleep 2		Sleep 3		Sleep 4		Sleep 5		Sleep 6		Sleep 7		Sleep 8	
Patient	Age Range ID	# of Normal Sleep (s)	N2 Dur (h)	N3 Dur (h)	N2 Dur (h)	N3 Dur (h)	N2 Dur (h)	N3 Dur (h)	N2 Dur (h)	N3 Dur (h)	N2 Dur (h)	N3 Dur (h)	N2 Dur (h)	N3 Dur (h)	N2 Dur (h)	N3 Dur (h)	N2 Dur (h)	N3 Dur (h)
1	1	1	1.73 (2)	1.09 (2)	0.594 (4)	0.705 (2)	0.850 (3)	1.51 (1)										
2	7	0	4.91 (4)	0.0 (3)	9.29 (10)	0.0 (3)	7.57 (7)	0.0 (3)	8.14 (8)	0.0 (3)								
3	8	1	9.53 (8)	0.164 (2)	7.01 (5)	1.04 (1)	6.75(5)	0.0 (2)	3.56 (1)	0.360 (2)								
4	5	1	1.56 (2)	1.95 (2)	0.426 (3)	2.83 (4)	0.258 (4)	2.48 (4)	0.934 (3)	2.10 (2)								
5	1	1	2.79 (1)	0.914 (2)														
6	1	1	0.276 (4)	1.42 (1)	0.508 (4)	1.41 (1)	2.63 (1)	1.76 (1)										
7	1	2	0.477 (4)	1.94 (2)	2.14 (2)	2.30 (2)	2.60 (1)	1.83 (1)										
8	3	0	1.46 (2)	3.42 (5)	3.47 (1)	3.68 (6)	1.87 (2)	2.87 (4)	0.948 (3)	2.82 (4)	3.30 (1)	2.32 (3)						
9	5	2	1.14 (3)	1.52 (1)	1.92 (2)	1.61 (1)	2.35 (1)	1.01 (1)	1.12 (3)	1.56 (1)								
10	1	3	2.67 (1)	2.15 (2)	2.21 (2)	2.26 (2)	1.32 (3)	1.84 (1)	0.591 (4)	1.55 (1)	2.92 (1)	1.44 (1)						
11	3	1	7.87 (6)	0.79 (2)	3.66 (1)	1.23 (1)	0.550 (3)	1.25 (1)										
12	6	2	2.66 (1)	0.983 (1)	2.24 (1)	2.38 (3)	3.72 (1)	1.79 (2)	5.02 (3)	2.10 (2)								
13	1	0	5.58 (3)	0.74 (2)	5.33 (3)	0.983 (2)	5.15 (2)	0.35 (3)										
14	1	5	1.78 (2)	0.983 (2)	4.16 (1)	0.736 (2)	3.25 (1)	2.26 (2)	2.33 (2)	1.48 (1)	1.18 (3)	1.23 (1)	1.13 (3)	1.81 (1)	1.37 (3)	1.55 (1)	2.47 (2)	1.48 (1)
15	2	1	2.24 (2)	0.317 (3)	0.108 (4)	1.61 (1)	3.27 (1)	1.08 (1)	0.574 (4)	0.869 (2)								
16	5	2	3.35 (1)	0.718 (1)	2.94 (1)	2.46 (3)	2.33 (1)	1.94 (2)										
17	1	2	5.33 (3)	1.73 (1)	2.98 (1)	1.82 (1)	2.35 (2)	0.987 (2)										
18	3	2	7.36 (6)	0.37 (3)	5.50 (3)	1.24 (1)	4.06 (1)	1.28 (1)	3.67 (1)	0.600 (2)	5.18 (3)	0.82 (2)	5.18 (3)	0.82 (2)				
19	1	1	1.47 (3)	1.67 (1)	0.965 (3)	1.23 (1)	2.05 (2)	1.67 (1)	1.02 (3)	1.27 (1)								
20	1	0	6.28 (4)	1.49 (1)	0.450 (4)	2.58 (3)	0.759 (4)	3.13 (4)										
	Total Norm Sleeps	28																
	"Normal" when both N2 and N3 durations are within 2 std of normative data																	
	Each cell has "within # of std" in parenthesis																	

CHAPTER 3: Interaction between cortical sleep graphoelements and sharpwave-ripples

Title: Coordination of human hippocampal sharp-wave ripples during NREM sleep with cortical theta bursts, spindles, downstates and upstates

Abstract:

In rodents, firing patterns from waking are replayed in NREM sleep during hippocampal sharpwave-ripples (HC-SWR). This replay is correlated with neocortical graphoelements (NC-GE). NC-GE include theta-bursts, spindles, downstates and upstates. In humans, consolidation during sleep is correlated with scalp-recorded spindles and down-upstates, but HC-SWR cannot be recorded non-invasively. Here we examine the relationship of NREM NC-GE to HC-SWR in humans. SWR in both anterior and posterior HC co-occur with NC-GE of all kinds in all cortical areas, bilaterally, with some quantitative differences. The proportion of SWR-GE pairs that were significantly related was three times higher for downstates or upstates than theta bursts or spindles, 44% higher in N2 than N3, and 37% higher in posterior than anterior HC. Frontal GE co-occurred with HC-SWR ~25% more, and lateral occipital ~45% less than average. Frontal spindles co-occurred frequently with posterior HC-SWR in N2. Cortical theta bursts tend to precede HC-SWR, and thus are positioned to help define potential cortical cues for HC-SWR firing. HC-SWR tend to occur after cortical downstates, and are typically surrounded by locally-decreased broadband power, potentially indicating cortical facilitation of hippocampal synchrony that underlies HC-SWR. Widespread cortical upstates and spindles follow HC-SWR, consistent with the hypothesis that hippocampal firing during HC-SWR helps define the content of increased cortical firing during upstates and spindles. The sequence of post-SWR cortical upstates tends to be stereotyped, often proceeding from medial to lateral. Overall, our results

describe how coordinated hippocampal and cortical oscillations may support and organize memory consolidation in humans.

Introduction:

Neocortical declarative memory consolidation depends on hippocampal input (Squire et al., 2001) during non-rapid eye movement (NREM) sleep (Rasch and Born, 2013). NREM sleep is characterized by large stereotyped neocortical (NC) population events ("graphoelements", or GE) including theta bursts (TB) (Gonzalez et al., 2018), sleep spindles (SS) (Mak-McCully et al., 2017), downstates (DS) (Cash et al., 2009), and upstates (US) (Sanchez-Vives and McCormick, 2000). The hippocampus (HC) generates sharpwave-ripples (SWR) during NREM: a large negative ~50-100 ms "sharp wave" with superimposed 80-200 Hz "ripples", followed by ~200 ms positive wave (Buzsáki, 2015). During SWR, HC pyramidal cells "replay" spatio-temporal firing patterns from waking (Wilson and McNaughton, 1994), and coordinated replay occurs in visual (Ji and Wilson, 2007) and prefrontal (Peyrache et al., 2009; Johnson et al., 2010) cortices. Thus, hippocampal replay during SWR could inform neocortical firing patterns which directly underlie consolidation (Buzsáki, 2015). Furthermore, the co-occurrence of NC-GE with HC-SWR in NREM sleep may help coordinate the consolidation process (Siapas and Wilson, 1998; Mölle et al., 2006). This is supported by experiments where disrupting hippocampal replay (de Lavilléon et al., 2015), HC-SWR (Ego-Stengel and Wilson, 2010; Suh et al., 2013; Rothschild et al., 2016), or NC-SS—especially when they occur with DS-US (Schreiner and Rasch, 2015; Maingret et al., 2016; Latchoumane et al., 2017)—impaired consolidation.

The experiments above were in rodents, but NC-GE and HC-SWR may occur in all mammals (Buzsáki et al., 2013). In humans, SS, DS-US, and especially their co-occurrences recorded with scalp-EEG are correlated with successful memory consolidation (Niknazar et al.,

2015). Thus, the coordinated occurrence of HC-SWR with NC-GE may also support memory replay and consolidation in humans. However, although HC-SWR (Bragin et al., 1999; Staba et al., 2004; Axmacher et al., 2008; Le Van Quyen et al., 2008; Jacobs et al., 2016) and NC-GE (Cash et al., 2009; Csercsa et al., 2010; Nir et al., 2011; Mak-McCully et al., 2017; Piantoni et al., 2017; Gonzalez et al., 2018) have been recorded with intracranial electrodes in humans being evaluated for epilepsy, little is known about their relationship. Clemens *et al*. (Clemens et al., 2007, 2011) found that a mixture of interictal spikes and ripples recorded near the parahippocampal gyrus co-occurred with scalp-recorded SS. Similarly, Staresina *et al*. (Staresina et al., 2015) found a 5% increase in ripple-band power within 250ms of scalp-recorded SS centers.

Here, we report the relationship of HC-SWR to NC-TB, SS, DS and US. To ensure that HC-SWR are not contaminated by epileptiform activity we include a subgroup with HC recordings that appear to be epilepsy-free. To maximize similarity to rodent HC-SWR, we require multiple oscillations occurring in a systematic relationship to the sharpwave and following delta wave. Ventral versus dorsal HC in rodents and anterior versus posterior HC in humans have distinct anatomical connections and functional properties (Ranganath and Ritchey, 2012; Patel et al., 2013; Strange et al., 2014). Furthermore, NREM sleep stages N2 and N3 are highly distinct, with SS and isolated DS-US sequences prominent in N2, and sustained DS-US oscillations characterizing N3 (Silber). Thus, we characterize the SWR-GE relationship separately for anterior vs posterior HC, different cortical areas, and different sleep stages.

We demonstrate widespread co-occurrence of NC-GE with HC-SWR for all GE types, NREM stages, cortical and hippocampal regions, with strong quantitative differences. The specific NC sites whose GE co-occurred with each HC site varied significantly between HC sites

and GE types, possibly reflecting the selection of HC-NC networks participating in the consolidation of a particular memory. In particular, NC-TB tended to precede HC-SWR and NC-US tended to follow. TB-DS-SS "triplets" preferentially co-occurred with HC-SWR in the canonical order proposed in earlier reports (Mak-McCully et al., 2017; Gonzalez et al., 2018). We propose that NC-TB could help define potential cortical cues for HC-SWR firing, as well as trigger NC-DS (Gonzalez et al., 2018), which in turn may trigger NC-SS/NC-DS to support and organize consolidation of specific memories.

Methods:

Overview

Peri-stimulus time histograms were constructed of neocortical graphoelement (NC-GE) occurrence times with respect to the hippocampal sharpwave-ripples (HC-SWR). Separate histograms were constructed for each: NC-HC channel pair, each GE (TB, SS, DS, and US), and for each sleep-stage (N2 or N3). Significant co-occurrences were tabulated, their peak latencies determined, and collated across NC-HC pairs. Changes in co-occurrence frequency and anatomical pattern were examined across GE type, HC location (anterior versus posterior), sleep stage, and their combinations.

Patient selection

20 patients with long-standing drug-resistant partial seizures underwent SEEG depth electrode implantation in order to localize seizure onset and thus direct surgical treatment (see Chapter 2, Table 2.2 for demographic and clinical information). Patients were selected from a group of 54 as previously described in Chapter 2. The resulting group of 20 patients includes 6 patients with an HC contact in a location with no interictal spikes, which were used to guide the

protocols applied to the remaining 14 patients (Table 2.2). The 20 patients included 7 males, aged 29.8±11.9 years old (range 16-58). Electrode targets and implantation durations were chosen entirely on clinical grounds (Gonzalez-Martinez et al., 2013). All patients gave fully informed consent for data usage as monitored by the local Institutional Review Board, in accordance with clinical guidelines and regulations at Cleveland Clinic.

Electrode localization

After implantation, electrodes were located by aligning post-implant CT to preoperative 3D T1-weighted structural MRI with ~1mm^3 voxel size (Dykstra et al., 2012), using 3D Slicer (RRID:SCR_005619). This allows visualization of individual contacts with respect to HC cross-sectional anatomy, which was interpreted in reference to the atlas of Duvernoy (Duvernoy, 1988). The assignment of depth contacts to anterior or posterior hippocampus (Ant-HC/Post-HC) was made with the posterior limit of the uncal head as boundary (Poppenk et al., 2013; Ding and Van Hoesen, 2015). Recordings were obtained from 32 HC contacts, 20 anterior (11 left) and 12 posterior (7 left). In 4 patients, HC recordings were bilateral (3 anterior and 1 posterior), and in 8 patients, ipsilateral anterior and posterior HC were both recorded. The distance of each hippocampal contact from the anterior limit of the hippocampal head was obtained in Freesurfer (RRID:SCR_001847). The CT-visible cortical contacts were compared to the MRI-visible cortical ribbon in order to identify pairs of contacts which are on the pial and white matter sides of the same cortical patch. These anatomically-selected pairs were confirmed physiologically by the presence of mainly polarity-inverted local field potentials in the referential recordings. Subsequent analysis was then confined to recordings between such bipolar transcortical pairs, yielding local field potential gradients. We have previously shown that referential recordings of

sleep graphoelements can yield misleading localization, but that activity recorded by bipolar transcortical pairs is locally generated (Mak-McCully et al., 2015).

Electrode contacts were rejected from analysis if they were involved in the early stages of the seizure discharge, had frequent interictal activity or abnormal spontaneous local field potentials. From the total of 2844 contacts implanted in the 20 patients, 366 transcortical pairs (18.3±4.7 per patient) were accepted for further analysis. Polarity of the pairs was adjusted if necessary to 'pial surface minus white matter' according to MRI localization, confirmed with decreased high gamma power during surface-negative downstates (see below).

Freesurfer (Dale et al., 1999; Fischl et al., 1999a, 2004) was used to reconstruct from individual MRI scans the cortical pial and inflated surfaces, as well as automatic parcellation of the cortical surface into anatomical areas (Desikan et al., 2006), after a sulcal-gyral alignment process. In order to test for differences in HC-NC relationships between cortical locations, standard FreeSurfer ROIs were combined into 12 composite ROIs, and these were further combined across the two hemispheres in homologous ROIs (Table 3.S5; Figure 3.4*A*). In order to test for HC-NC effects within vs between hemispheres, the ROIs were combined into Fronto-Central and Non-Frontal for each hemisphere (Table 3.S5). An average surface for all 20 patients was then generated to serve as the basis of all 3D maps. While each cortical SEEG electrode contact's location was obtained through direction correlation of CT and MRI as described earlier in this section, we obtained the cortical parcellation labels corresponding to each contact by morphing the Right-Anterior-Superior-oriented anatomical coordinates from individual surfaces to the average surface space (Fischl et al., 1999b). In addition, the nearest vertices on the average surface to the morphed coordinates would be identified for subsequent plotting of 2D projections onto the left lateral view. For the 2D projections only, to optimize visualization (i.e. minimize

multiple contact overlap) while preserving anatomical fidelity, positions of contacts with significant HC-NC GE correlation were allowed to shift within a 5 mm radius. All visualizations were created with custom scripts in MATLAB 2016b.

Data collection and preprocessing

Continuous recordings from SEEG depth electrodes were made with cable telemetry system (JE-120 amplifier with 128 or 256 channels, 0.016-3000 Hz bandpass, Neurofax EEG-1200, Nihon Kohden) across multiple nights (Chapter 2, Table 2.3) over the course of clinical monitoring for spontaneous seizures, with 1000 Hz sampling rate. The total NREM sleep durations vary across patients; while some difference is expected given intrinsic variability of normal human sleep duration (Carskadon and Dement, 2010), patients undergoing seizure monitoring experience additional disruption due to the hospital environment and clinical care. In order to examine the potential effect of sleep disruption on our results, we identified 28 nights in 16 patients in which the percentages of NREM were comparable to (i.e. within 2 standard deviation of) normative data (Moraes et al., 2014). Recordings were anonymized and converted into the European Data Format (EDF). Subsequent data preprocessing was performed in MATLAB (RRID:SCR_001622); the Fieldtrip toolbox (Oostenveld et al., 2011) was used for bandpass filters, line noise removal, and visual inspection. Separation of patient NREM sleep/wake states from intracranial LFP alone was achieved by previously described methods utilizing clustering of first principal components of delta-to-spindle and delta-to-gamma power ratios across multiple LFP-derived signal vectors (Gervasoni et al., 2004; Jiang et al., 2017), with the addition that separation of N2 and N3 was empirically determined by the proportion of down-states that are also part of slow oscillations (at least 50% for N3 (Silber et al., 2007)), since

isolated down-states in the form of K-complexes are predominantly found in stage 2 sleep (Cash et al., 2009).

Hippocampal sharpwave-ripple (HC-SWR) selection

Previous studies have used a variety of approaches to identifying HC-SWR, with regard to how they distinguish epileptiform interictal spikes from HC-SWR (or even if they do distinguish them), whether they require that multiple oscillations are present in a ripple or simple a peak in ripple-band power, whether they require that the ripple occur at the peak of a HC sharpwave and followed by a slower wave of opposite polarity, whether recordings are obtained in NREM sleep stages N2 and N3, and whether the event are recorded in the hippocampus per se or a nearby structure (see Chapter 2 for review). The HC-SWR studied here were clearly distinguished from epileptiform activity by multiple criteria, possessed multiple peaks within the ripple and the ripple itself was located within a characteristic low frequency LFP. The SWR were all recorded in the HC during NREM sleep stages N2 and N3.

Specifically, HC LFP data were band-pass filtered between 60 and120 Hz (6th order Butterworth IIR bandpass filter). This band was chosen based on examination of the time-frequency plots of visually-selected SWR in patients with no HC interictal spikes. Root-mean-square (RMS) over time of the filtered signal was calculated using a moving average of 20 ms, with the 80th percentile of RMS values for each HC channel being set as a heuristic cut-off. Whenever a channel's signal exceeds this cut-off, a putative ripple event was detected. Adjacent putative ripple event indices less than 40ms apart were merged, with the center of the new event chosen by the highest RMS value within the merged time window. Each putative ripple event was then evaluated based on the number of distinct peaks in the HC LFP signal (low-passed at 120 Hz) surrounding the event center; a 40-ms time bin was shifted (5ms per shift) across ±50

ms, and at least one such time bin must include more than 3 peaks (the first and the last peak cannot be both less than 7ms away from the edges of this time bin) for the putative ripple event to be considered for subsequent analyses. In addition, the distance between two consecutive ripple centers must exceed 40 ms.

Since RMS peaks may arise from artifacts or epileptiform activity, 2000 ms of hippocampal LFP data centered on each ripple event undergoes 1-D wavelet (Haar and Daubechies 1-5) decomposition for the detection and removal of sharp transients (i.e. signal discontinuities). For each wavelet decomposition, putative HC-SWR were marked in ~10 min long NREM sleep period (marking ended sooner if 400 putative HC-SWR had been found). A scale threshold was then established via iterative optimization for the best separation between hand-marked true ripple events and interictal events in the same NREM sleep period. Each putative sharp transient was then rejected only if the 200 Hz highpassed data at that point exceeds an adaptive threshold (Bragin et al., 1999) of 3—or another number that allows best separation in agreement with visual inspection by human expert (between 0.5 and 5, and ~2 on average)—standard deviations above the mean for the 10-second data preceding the transient.

To identify ripples coupled to sharpwaves, we created patient-specific average templates (-100ms to +300ms around ripple center) from hand-marked exemplars (100-400 HC-SWR) in NREM per patient) that resemble previously described primate sharpwave-ripples with biphasic LFP deflections (Skaggs et al., 2007; Ramirez-Villegas et al., 2015). We then evaluated whether each ripple qualifies as a SWR based on its accompanying biphasic waveform, as described in Chapter 2.

Neocortical graphoelement (NC-GE) selection

Automatic cortical theta burst (TB) detection was performed as previously described (Gonzalez et al., 2018): a 5-9 Hz bandpass was applied to the LFP data, and a channel-wise cutoff set at mean +3 s.d. was applied to each channel's Hilbert envelope (smoothed with 300 ms Gaussian kernel) to identify local maxima that would be "peaks" of putative TBs, and make start/stop edge cut-offs at mean +1 s.d.. The resulting TBs were only accepted for further analyses if their durations fall between 400 ms and 1000 ms, with their number-of-zero-crossings-based frequency estimate falling within the bandpass frequency range as well, i.e. for each putative TB, the number of zero crossings should yield a rate between 10 and 18Hz.

Automatic cortical spindle (SS) detection was performed using previously published methods for SEEG spindle identification (Mak-McCully et al., 2017): a 10–16 Hz bandpass was applied to the LFP data, and the analytic amplitude of the bandpassed signal was convolved with an average Tukey window of 600 ms. A channel-wise cutoff set at mean +2 s.d. was applied to each channel's convolved bandpass envelope to identify local maxima that would be "peaks" of putative spindles. A 400 ms Tukey window was then applied to the previously computed Hilbert amplitude to define the onset and offset of putative SSs; the maximum FFT amplitude of the putative SS signal at the SS peak was used to set edge thresholds (50 % of peak amplitude). Finally, the putative SS segments were evaluated with four different criteria for rejection: 1, the spindle duration needs to be longer than 400 ms; 2, the spectral power outside the spindle frequency band on the lower end (4-8 Hz) or the higher end (18-30 Hz) should not exceed 14 dB; 3, each spindle should consist of at least 3 unique oscillation peaks in the 10-16 Hz bandpass; 4, the time between successive zero-crossings should be within the range of 40-100 ms.

Downstates (DSs) and upstates (USs) were identified as follows: for each cortical LFP signal, a zero-phase eighth order Butterworth filter from 0.1 to 4 Hz was applied. Consecutive

zero crossings of opposite slope separated by 250 to 3000 ms were then selected as delineating putative graphoelements. For each putative graphoelement, the amplitude peak between zero crossing was computed; only the top 10% of peaks were retained. The polarity of each signal was inverted if necessary to assure that NC-DS were negative, as confirmed with a high gamma (70-190 Hz) power decrease exceeding 1 dB within ±250 ms of the negative NC-DS peaks.

Experimental design and statistical analysis: Co-occurrence of HC-SWR and NC-GE

All statistical tests below have $\alpha = 0.05$ post FDR-correction for multiple comparisons (Benjamini and Hochberg, 1995), unless otherwise specified.

Peri-stimulus time histograms were constructed for each NC-HC channel pair, separately for each graphoelement (GE; TB, SS, DS, and US), and for each sleep-stage (N2 or N3), each histogram comprising the occurrence times of a given NC-GE during the ±2s interval surrounding midpoints of HC-SWR (see Fig. 3.1 for examples). The significance of peaks and troughs in each histogram was tested by comparing them to distributions derived from histograms constructed under the null hypothesis of no relationship between the NC-GE and HC-SWR using the following randomization procedure. Null-hypothesis histograms (N=1000) were constructed of NC-GE occurrences relative to a number of random times equal to the number of HC-SWR. For each 200ms time bin with 100ms overlap comprising the 4-second trial duration, the actual counts are then compared to the distribution under the null hypothesis.

The latencies of the largest significant peaks identified in the individual histograms constructed as described above, were used to create summary histograms for each NC-GE, sleep stage, and HC-SWR origin in anterior versus posterior HC. These are plotted in Fig. 3.2 and Figure 3.S1, and tabulated in Table 3.1. To test if, overall, a given type of cortical graphoelement significantly precedes or follows HC-SWR, two-tailed binomial tests with chance probability of

0.5 were performed on the number of channel-pairs with peak latencies in the 500ms before vs the 500ms after the reference HC-SWR. Since certain graphoelements, such as cortical theta, tend to yield peak latencies centered around zero, we also tested with Kolmogorov-Smirnov (KS) tests whether, overall, for a given cortical-GE, the distribution of peak latencies significantly related to HC-SWR differs from chance.

Experimental design and statistical analysis: Differences in anatomical patterns of HC-SWR to NC-GE between anterior vs posterior and left vs right HC

For every HC site across all patients, we tested the following: 1. whether the anatomical distribution of HC-SWR coupling to NC-GE across NC sites was different from chance for a given HC site. Subsequently, we tested the following: 2. whether the significantly-different-from chance distributions of NC sites from 1 would also differ between HC site pairs. An HC site pair could be either Ant-HC and Post-HC in the same hippocampus, or left HC and right HC (either both Ant-HC or both Post-HC) in the same patient; 3. whether any difference seen in 2 could be seen on the basis of different NC-GE types; 4. whether for the NC sites that have coupled GE to both members of the HC pair (Ant-HC and Post-HC, or left HC and right HC), the occurrence rate of a particular type of NC-GE within 500 ms of HC-SWR in both HC sites would be different from the occurrence rate of that NC-GE within 500 ms of HC-SWR in only one of the HC sites in the pair. For 1, we performed a chi-square test of homogeneity for each HC site with regard to each NC-GE type, i.e. for a given patient with multiple NC sites, a 2 x N contingency table was made for each NC site, N being the number of NC sites, one column of table containing the number of NC-GE overlapping with (i.e. falling within 500 ms of) HC-SWR for each NC, the other containing the number of NC-GE that do not. A significant chi-square would therefore indicate a significant non-random distribution for that particular HC site and NC-GE

type. For 2, we performed Wilcoxon signed rank tests on the data obtained in 1 to evaluate whether for a given NC-GE type (for which 1 yielded significance for both members of an HC site pair), the proportions of NC-GE from significantly coupled NC sites that overlapped with Ant-HC/left HC-SWR differ from the proportions for Post-HC/right HC-SWR. Each test required that both members of a HC site pair were required to have significant chi-square test result from 1. For 3, we repeated the procedure in 2, but instead of comparing proportions between HC site pairs, we compared between NC-GE types for each HC site. Each test required that for a given HC site, both NC-GE types were required to have significant chi-square test result from 1. Analyses 1-3 were performed with N2 and N3 combined. For 4, we computed the correlation of HC-SWR overlap rates for different NC-GE types, with each data point of the correlation derived from a different NC site. In addition, we computed across NC sites from all patients chi-square tests of independence for whether there could be a significant relationship between the anatomical distributions of different NC-GE types' respective NC sites that significantly coupled to HC-SWR.

Experimental design and statistical analysis: Anatomical sequences of NC-US following HC-SWR

We observed that multiple cortical upstates commonly occurred after a given HC-SWR; to test whether a given two-upstate sequence (involving two different cortical channels) within 500 ms after HC-SWR occurred more often than chance, we performed bootstrapping with 1000 random trials in N2 and N3 sleep, where each random trial involved random time points as pseudo-SWR, with both the same total number and the same occurrence rate for each 5-minute interval as HC-SWR from the original data. The number of two-upstate sequences following pseudo-SWR for each random trial was then tallied, and unique (in terms of both channels

involved and the temporal order in which NC-US from each channel occurred) sequences that were found more often in the original data than in 95% of the random trials were considered to occur significantly more often than chance.

In addition, the bootstrapping test results allowed us to tally (under the following conditions: N2 Ant-HC, N2 Post-HC, N3 Ant-HC, and N3 Post-HC) the number of significantly occurring two-US sequences found in the actual data versus found with 1000 sets of pseudo-SWR. We examined the consistently recurring NC-US sequence population further for preferred directionality across the cortex by counting the number of unique sequences in N2/N3 and Ant-HC/Post-HC where the first NC-US for each sequence was in the medial or lateral cortex. Binomial tests were then performed to determine whether the no-directionality-preference null hypothesis could be rejected for medial-versus-lateral leading sequences that originate from temporal, frontal, parietal, or occipital lobes.

Experimental design and statistical analysis: Modulation of HC-SWR with GE-DS co-occurrence by number of DS

HC-SWR were observed to commonly be surrounded by broadband decreased spectral power, suggesting a possible relationship to NC-DS. To test whether multiple NC-DS are more likely than single NC-DS to co-occur with HC-SWR, we generated the baseline occurrence rate of single DS and multiple DS (averages derived from 200 permutations with pseudo-SWR) within ±500 ms of SWR for all HC contacts in all patients. We then obtained the ratios between the numbers of actual single DS / multiple DS and the baselines, followed by paired t-tests against the null hypothesis of equal mean for single DS and multiple DS ratios across patients.

Experimental design and statistical analysis: Canonical sequences of NC-GE

Previous studies have identified canonical sequences of different NC-GE in human NREM SEEG, specifically TB-DS-SS (Mak-McCully et al., 2017; Gonzalez et al., 2018). Accordingly, we identified triplet sequences (involving one TB, one DS, and one SS from NC) near HC-SWR, with the temporal limitation that TB start, SS start, and DS peak all must fall within -1500 ms and +1000 ms of an HC-SWR to yield a GE triplet. To test whether previously observed canonical order (would be preferred for these triplets near HC-SWR, we tallied the number of triplets occurring in each of the six possible orders and performed binomial tests against chance (1/6).

Experimental design and statistical analysis: Modulation of HC-SWR co-occurrence with NC-GE by sleep stage (N2 vs N3), cortical site (anatomical ROI), HC site (anterior vs posterior), and laterality (HC-NC ipsilateral or contralateral to each other)

We further explored the spatial distribution of the NC-HC relationship by tallying the proportion of significant HC-NC channel pairs across different NC regions, with respect to different NC-GE types and different HC-SWR sources (Table 3.2). To characterize the apparent variability in Table 3.2, we performed a 4-way ANOVA to compare the main effects of GE type (TB, SS, DS, US), NREM stage (N2 vs. N3), Ant- or Post-HC origin of HC-SWR, and NC ROIs (coverage listed in Table 3.2 and Table 3.S5), as well as the 2-way and 3-way interaction effects. Similarly, given the lateralization of human hippocampal function, we were interested in examining whether ipsilateral HC-NC channel pairs would show different relationships from contralateral pairs across GE types, NREM stages, or NC ROIs. Due to a sparse representation of contralateral channel pairs for individual ROIs, we calculated proportions for larger regions by combining both HC and NC sites: Ant-HC and Post-HC channels were combined into a single HC category, and the 10 NC ROIs used in previous analysis were collapsed into two: “fronto-

central" and "non-frontal" (Table 3.S5). We then computed for each ROI the proportion of NC channels significantly coupled to HC-SWR (Table 3.3), and performed 4-way ANOVA as previously described, with the ipsilateral/contralateral factor replacing the Ant/Post-HC factor. All post-hoc analyses for both ANOVAs were performed with Tukey's range test. For each ANOVA, we checked the normality assumption by conducting the Lilliefors test on the residuals.

Results:

Hippocampal sharpwave-ripples (HC-SWR) occurrences are significantly associated with all categories of neocortical graphoelements (NC-GE), including theta bursts (TB), downstates (DS), upstates (US), and sleep spindles (SS)

We identified human HC-SWR from intracranial recordings and aligned them with simultaneously recorded cortical events in NREM sleep, in order to determine if their occurrences are related and have a consistent order, and whether their relations change between NREM stages N2 and N3, between anterior and posterior HC sites, or between ipsilateral versus contralateral NC targets. Morphologically normal ripples were isolated from >24 h continuous recordings in 20 stereoelectroencephalography (SEEG) patients with intractable focal epilepsy, with anterior (in 17 patients) and/or posterior HC contacts (in 11 patients), and related to sleep graphoelements (GE) in 12-30 NC bipolar recording channels per patient. Several patients (n = 8) had both Ant-HC and Post-HC contacts in the same HC, and/or with bilateral (left and right) HC contacts (n=4) placed in either both anterior or both posterior HC.

In order to examine the relationship between HC-SWR and NC-GE, different categories of GE (TB, DS, US, and SS) were identified in simultaneous recordings from NC in all lobes. These recording channels were differential derivations between adjacent contacts spanning the

cortical ribbon, and were thus assured of being locally-generated. Detection algorithms have all been extensively validated in our previous studies (Mak-McCully et al., 2015, 2017; Gonzalez et al., 2018). Down-to-upstate transitions (D2U) were also identified. However, the results for the D2U event were largely redundant with those for DS and US, and thus are only included in Fig. 3.S2.

In order to display the regularities in our data, we constructed histograms of the occurrence times of each GE (TB onset, SS onset, DS peak, and US peak) between each pair of (non-epileptogenic) HC (n=32) and NC (n=366) channels (n=20 patients). Separate analyses were carried out for stages N2 vs. N3, for SWR recorded in Ant-HC vs. Post-HC, and for HC-NC pairs in the same vs. opposite hemispheres. Altogether, there were 598 unique HC-NC pairs (458 ipsilateral, 140 contralateral), and 8 histograms for each pair (one for each sleep stage, times each of the 4 GEs), for a total of 4784 histograms. Overall, each of these histograms plots the occurrence times of 3048±4221 NC-GEs (+2.84 skewness) with respect to 2080±2502 HC-SWR (+2.1 skewness); a total of 14.6 million NC-GE events and 9.95 million HC-SWR were used for histogram construction. Detailed breakdown of histogram contents by GE types and SWR sources (N2 vs. N3, Ant-HC vs. Post-HC, ipsilateral vs. contralateral) can be found in Table 3.S1.

Of the 598 HC-NC pairs, 551 (92%) of all pairs had at least one histogram showing a significant relationship between the HC-SWR and a NC-GE ($p<.0.05$ post FDR-correction, randomization test, see section “Experimental design and statistical analysis” in Methods). The proportion was slightly greater when the HC and NC sites were in the same hemisphere (432 (94%) of the ipsilateral pairs and 119 (85%) of the contralateral pairs). Of the entire set of 4784 histograms, 1722 (36%) showed a significant association between the HC-SWR and NC-GE.

The significant histograms (examples are shown in Fig. 3.1) include all types of cortical GE from channels across all cortical lobes. The peak of the histogram represented a mean increase of 71%, or median increase of 49% above baseline (measured as the mean height of non-significant bins).

We summarized these data further by constructing histograms of peak latencies from the histograms described above. Specifically, we determined the latency of peak occurrence rate relative to HC-SWR time for each significant HC-SWR/NC-GE histogram, and plotted these as a histogram for each GE, separately for N2 vs. N3 and Ant-HC vs. Post-HC (Fig. 3.2, Fig. 3.S1). Each of these 16 histograms of histogram peaks (N2/N3 x Ant/Post x 4 GEs) summarizes the significant latencies from 108±54 HC-NC channel pair histograms, comprising a total of 4.03 x 10^5±3.78 x 10^5 HC-NC events (range 2.44 x 10^4-1.35 x 10^6). As noted previously in Chapter 2, N2 and posterior HC sites had fewer HC-SWR. Results were also summarized by plotting each cortical channel after morphing to a standardized brain (Fig. 3.2, Fig. 3.S1).

In the summary histograms, significant temporal relationships were found between HC-SWR and each of the GE types. As shown in Table 3.S2, we tested for the presence of a significantly non-random distribution of NC-GE peak times with respect to HC-SWR (column 4), and found significant results for both N2 and N3, and both Ant-HC and Post-HC, for TB, DS and US. NC-SS and HC-SWR were significantly related in N2 Post-HC with a trend in N3 Post-HC, reflecting both the preferred occurrence of NC-SS during N2, and a tighter coupling between NC-SS and Post-HC as compared to Ant-HC, which we will explore in a future publication.

<u>NC-TB typically precede, while NC-US and SS typically follow HC-SWR</u>

We also examined if the peak latency in the summary histograms between HC-SWR and NC-GE differed significantly from zero, using both the mean of the included HC-NC channel pairs (column 5 of Table 3.1), or a fitted distribution (column 6 of Table 3.1). Significant effects were found for SS in N2, which followed HC-SWR by 169ms (mean) or 244ms (fitted). DS were also significantly later than HC-SWR in the Post-HC by 157ms (mean) or 290ms (fitted). Finally, US were significantly later than HC-SWR in both N2/N3 and Ant/Post-HC by 112ms (mean) or 179ms (fitted). The same conditions also showed a significant difference in the proportion of NC-GE events in the 500ms before versus after the HC-SWR (columns 7 and 8 of Table 3.1).While only trends were noted for TB to precede Post-HC SWR (column 7 of Table 3.1), possibly due to the relatively low count of NC sites showing significant HC-SWR to NC-TB coupling (Fig. 3.2, Fig. 3.S1), overall TB precedence was indeed significant (column 8 of Table 3.1).

Different types of NC-GEs had different typical latencies with respect to HC-SWR; for example, TB occurred at about the same time but with a tendency to precede HC-SWR, especially for Post-HC, and spindle onsets were often found about ~300 ms after Post-HC SWR. Overall, the latencies of different NC-GEs with respect to SWR shown in Fig. 3.2 and Table 3.1 were consistent with the typical sequence we established in our previous studies of cortical NC-GE during NREM sleep (Mak-McCully et al., 2015, 2017; Gonzalez et al., 2018). In N2, this sequence begins with the NC-TB which increases in strength to terminate as the negative peak of the NC-DS, and the NC-SS then begins on the upslope to the NC-US. An example of a canonical sequence is shown in Fig. 3.3*A* together with an HC-SWR between the NC-DS and NC-SS.

Although generally consistent with the canonical sequence, the temporal ordering of NC-GE would be obscured by the fact that they are not necessarily associated with the same SWRs.

Thus, we performed an analysis limited to events wherein NC-TB, NC-DS and NC-SS all occurred in proximity (-1500 ms to +1000 ms) to the same HC-SWR. We found that the canonical order (NC-TB→NC-DS→NC-SS) was about twice as common as other orders ($p=0.0001$, two-tailed paired t-test for in-category vs out-category over all NC channels, combining N2/N3/Ant/Post). Furthermore, in the canonical sequences, the latencies of the successive NC-GE and HC-SWR were highly stereotyped (Fig. 3.3*B*), especially in the events anchored by an Ant-HC SWR.

Multiple NC-DS are more likely than single NC-DS to co-occur with HC-SWR

In previous studies with SEEG, we showed that NC-DS vary in the extent of cortex which they engage (Mak-McCully et al., 2015, 2017), with the NC-DS involving greater cortical extents being more likely to evoke a thalamic DS (Mak-McCully et al., 2015, 2017). As previously noted (Chapter 2), HC-SWR tend to occur on the background of a broadband spectral power decrease, suggestive of a DS-like state in the HC, and this in turn suggests that the NC-HC relationship may be similar to the NC-thalamic interactions previously examined. Thus, we predicted that HC-SWR may be associated with the convergence of NC-DS from multiple cortical locations. Indeed, we found that multiple NC-DS are significantly more likely than single DS to co-occur with HC-SWR from N2 Post-HC (15% increase), N3 Ant-HC (13% increase), and N3 Post-HC (18% increase) ($p = 0.0021$, 0.0026, and 0.0029, respectively, one-tail paired t-tests). In the case of N2 Ant-HC, there was a trend for multiple NC-DS to co-occur with HC-SWR more often (5% increase, $p = 0.075$, one-tail paired t-tests).

NC-US following HC-SWR tend to occur in medial and then lateral cortex

Prominent models of memory consolidation posit that the information from the HC to the NC driven by the replay firing during the HC-SWR trigger the re-activation of the

spatiotemporal patterns in the NC and thus memory consolidation (Buzsáki, 2015). Given our observation that NC-US reliably follow HC-SWR from both Ant-HC and Post-HC, and in both N2 and N3, we set out to determine whether signs of sequential cortical activation can be detected after HC-SWR, and if so, whether any regularities in this spread can be ascertained. First, we found that pairs of NC-US in different NC locations falling within 500 ms after the same HC-SWR occurred at rates higher than one would expect from the rate of single NC-US ($p < 0.001$, bootstrapping test). Furthermore, these NC-US sequences tended to be in a particular order from medial to lateral sites. At a threshold of $p < 0.05$ for NC-US sequences occurring more often than chance, when the medial/lateral preference was considered for each unique channel pair, trends of medial temporal and medial frontal leading preferences were observed for N3 Ant-HC ($p = 0.064$ and $p = 0.056$, two-tailed binomial), whereas medial parietal and medial occipital leading were significantly preferred for N2 Post-HC ($p = 0.044$ and $p = 0.0001$, two-tailed binomial).

The NC sites whose GE co-occur with SWR in a given HC site are not random

The results presented above demonstrate that for a given HC site, a particular category of GEs will significantly co-occur in some but not other NC sites. Indeed, the striking positive skewness both in general and in specific categories (Table 3.S1) suggests that, in addition to high variability in co-occurrence rates of NC-GEs with SWRs, a small population of histograms for particular HC-NC-GE-state combinations (shown in Fig. 3.1) may contain a disproportionately large number of events. However, they would not bias the main results (Figs. 3.2, 3.S1) where each of the significant HC-NC channel pairs provide a single count.

We further examined this issue by performing a chi-square test of homogeneity for each HC site with regard to co-occurrence of each NC-GE, across NC sites. We found that most HC

sites were coupled to NC-GE with NC site distributions that significantly differ from chance (Table 3.S2): out of 32 unique HC sites, 21 were coupled to non-homogeneous distributions of NC sites with significant TB-SWR relationships, 21 were coupled to significant SS-SWR NC site distributions, and all 32 were coupled to significant DS and US distributions.

Different anatomical patterns of NC sites have DS or US that co-occur significantly with SWR from multiple simultaneously recorded HC sites

The NC sites where GE co-occur with HC-SWR from a particular HC location constitute an anatomical network which could have functional significance during consolidation. Having determined above that the HC-NC co-occurrences are not randomly distributed across the recorded NC sites, we then examined if the distribution differed between HC sites. This analysis was conducted in patients with multiple HC contacts either in the same hippocampus (Ant-HC and Post-HC) or bilaterally in both anterior or both posterior HC. Again, we repeated this analysis for each of the NC-GE categories, provided that both HC sites had a significantly non-random pattern of co-occurrence with NS sites. For a given NC-GE, analysis was limited to those NC sites that significantly co-occurred with both HC sites (i.e., both Ant- and Post-HC, or both left and right HC, in a given patient).

Specifically, Wilcoxon signed rank tests were performed on the proportions of NC-GE that co-occurred with anterior versus posterior HC-SWR, or in a separate analysis, that co-occurred with left versus right HC-SWR. In total, 8 Ant-Post HC pairs and 4 Left-Right HC pairs were examined. We found a tendency for Ant-Post HC pairs to yield significantly different NC-HC coupling distributions, with NC-DS and NC-US showing stronger effects than NC-TB and NC-SS: 2 of the 5 qualified pairs for NC-TB showed significant difference (and an additional 2 showed a trend, i.e. $p < 0.1$), 1 in 3 for NC-SS (and 1 with a trend), 5 in 8 for NC-DS (and 2 with

a trend), and 7 in 8 for NC-US (Table 3.S3). Similarly, for Left-Right HC pairs, all 4 of the qualified pairs for NC-TB, NC-SS, and NC-US showed significant differences, and all 3 of the qualified pairs did for NC-DS (Table 3.S3).

Similar anatomical patterns of NC sites co-occur significantly with SWR from multiple simultaneously recorded HC sites for different GE types

We then repeated this procedure, but instead of comparing proportions between HC site pairs, we compared between NC-GE types for each HC site (Table 3.S4). Each test required that for a given HC site, both NC-GE types needed to have a significantly non-random co-occurrence pattern across the NC sites, as described above. For two of the six possible NC-GE site pairs (TB vs. SS, DS vs. US), we found remarkably few HC sites showing significant difference, with another (SS vs. DS) showing mixtures of significant and non-significant HC sites, suggesting that the distributions of NC sites—specifically those coupled to multiple NC-GE types—tend not to differ significantly across these NC-GE type pairs for a given HC site. In contrast, most HC sites tested showed significant difference for TB vs. DS, TB vs. US, and SS vs. US; in other words, for these NC-GE type pairs, the distributions of NC sites coupled to one NC-GE type tend to differ from distributions of NC sites coupled to the other.

We also computed the correlation of HC-SWR overlap rates for different NC-GE types, with each data point of the correlation derived from a different NC site. In addition, we computed across NC sites from all patients chi-square tests of independence for whether there could be a significant relationship between the anatomical distributions of different NC-GE types' respective NC sites that significantly coupled to HC-SWR. Remarkably, for most NC-GE type pairs, strong correlations in proportions of NC-GE overlapping with HC-SWR were found (Fig. 3.4*A*). The chi-square tests in both N2 and N3 also indicated that NC sites that tended to

show significant temporal correlation with HC-SWR for one NC-GE type also tended to associate with another NC-GE type, with some exceptions: TB vs. SS only showed a trend, and SS vs. US in N2 was non-significant. Specifically, for N2 and N3 respectively, we found $p = 0.0822$ and $p = 0.0694$ for TB vs. SS, $p = 1.785 \times 10^{-11}$ and $p = 9.355 \times 10^{-8}$ for TB vs. DS, $p = 3.191 \times 10^{-15}$ and $p = 2.264 \times 10^{-7}$ for TB vs. US, $p = 0.0187$ and $p = 0.0106$ for SS vs. DS, $p = 0.4350$ and $p = 5.267 \times 10^{-5}$ for SS vs. US, $p = 5.036 \times 10^{-32}$ and 9.509×10^{-32} for DS vs. US.

HC-SWR co-occur with NC-GE more often for DS/US than TB/SS, in NREM sleep stage N2 than N3, in posterior than anterior HC, and in frontal than occipital regions

While the summaries in Fig. 3.2 and Table 3.1 gave us an overview of NC-GE and HC-SWR relations, we noted that the maps in Fig. 3.2 revealed apparent regional differences across NC in co-occurrence strength. We also considered the possibility that "hot spots" may exist in NC and contribute to the widespread positive skewness seen in Table 3.S1. We therefore explored the spatial distribution of NC-HC relationship further by tallying the proportion of significant HC-NC channel pairs across different NC regions, with respect to different NC-GE types and different HC-SWR sources (Table 3.2). To explore the apparent variability in Table 3.2, we performed a 4-way ANOVA to compare the main effects of GE type (TB, SS, DS, US), NREM stage (N2 vs. N3), Ant- or Post-HC origin of SWRs, and NC ROIs (coverage listed in Table 3.2 and Table 3.S5), as well as the 2-way and 3-way interaction effects. All post-hoc analyses were performed with Tukey's range test. We checked the normality assumption by conducting the Lilliefors test on the residuals, and the null hypothesis of normality could not be rejected ($p = 0.1653$).

All 4 main effects were significant. The main effect for GE yielded $F = 136.87$, $p = 1.93 \times 10^{-16}$, indicating that some NC-GE types were more related to HC-SWR than others. Post-hoc

analysis across GE types showed that, while the mean proportions of SWR-responsive HC-NC channel pairs did not differ between TB and SS ($p = 0.7852$), nor between DS and US ($p = 0.9968$), they did differ between TB/SS and DS/US ($p = 3.774 \times 10^{-9}$ for TB and DS, same for TB and US; $p = 3.773 \times 10^{-9}$ for SS and DS; same for SS and US). The mean proportions were 0.1655 for TB, 0.1852 for SS, 0.5136 for DS, and 0.5299 for US; thus, TB and SS were related in a smaller proportion of NC sites to SWRs than DS and US were.

The main effect for NREM stage yielded $F = 61.38$, $p = 2.01 \times 10^{-8}$, and together with mean proportions of 0.412 for N2 versus 0.294 in N3, suggested that more HC-NC channel pairs were significantly related to SWRs in N2 than in N3. This was despite SWRs occurring more often in N3 (Chapter 2). The fact that the durations of N2 were about twice those of N3 in our recordings may have contributed to this unexpected observation.

The main effect of HC-SWR longitudinal origin yielded $F = 41.457$, $p = 6.72 \times 10^{-7}$, and together with mean proportions of 0.316 for Ant-HC and 0.414 for Post-HC, suggested that more of NC were related to Post-HC SWR than to Ant-HC SWR, despite the density of SWR being about twice as high in Ant-HC versus in Post-HC (see Chapter 2, Fig. 2.3).

The main effect of NC ROIs yielded $F = 10.56$, $p = 8.47 \times 10^{-7}$, indicating that different NC regions were coordinated with/by HC-SWR to different extents. When the sum of mean proportions across NREM stages and Ant/Post-HC for each ROI were sorted, there appeared to be an anterior-to-posterior gradient, whereby the more frontal an NC region, the higher the sum tended to be (Fig. 3.4*B*-*C*). The exception was cingulate, which had the largest sum overall, and post-hoc analysis across NC ROIs confirmed that, except for orbitofrontal and prefrontal ($p = 0.6885$ and $p = 0.6787$, respectively), the mean proportion for cingulate was significantly greater than all other NC ROIs ($p = 0.0099$ for lateral temporal, $p = 0.0235$ for paracentral, $p = 0.0005$

for medial temporo-occipital, $p = 0.0106$ for medial parietal, $p = 0.0171$ for insula, $p = 3.211 \times 10^{-7}$ for lateral occipital, $p = 0.0007$ for lateral parietal). In contrast, the most posterior ROI (lateral occipital) had the smallest sum overall, and except for lateral parietal ($p = 0.0714$) and medial temporo-occipital ($p = 0.0879$), the mean proportion for lateral occipital was significantly less than all other NC ROIs ($p = 0.0062$ for lateral temporal, $p = 0.0025$ for paracentral, $p = 1.958 \times 10^{-5}$ for prefrontal, $p = 0.0058$ for medial parietal, $p = 0.0035$ for insula, $p = 1.880 \times 10^{-5}$ for orbitofrontal, $p = 3.211 \times 10^{-7}$ for cingulate).

NREM stage, GE type, anterior vs posterior HC-SWR origin, and NC ROI, have interacting effects on SWR-GE co-occurrence

With the exception of GE * NREM stage, all 2-way interaction effects from the ANOVA were significant. The interaction effect of GE * HC-SWR longitudinal origin yielded $F = 4.57$, $p = 0.0103$, indicating that certain NC-GE types could be related to Ant-HC and Post-HC to different extents. When averaged across ROIs and separately for N2/N3, the proportions of significant HC-NC channel pairs were greater for Post-HC than for Ant-HC in all GE types, with the exception of SS N3 (Ant-HC proportion was 1.3 times greater than Post-HC). For NC-TB, in particular, Post-HC proportions were twice as large as Ant-HC proportions. As expected, post-hoc analysis for GE * Ant-/Post-HC interaction supported the significant difference between Ant-HC and Post-HC proportions for NC-TB ($p = 0.0005$), but not for NC-SS ($p \approx 1$), likely due to the confounding effect of different NREM stages. Significant Ant/Post difference was also found for DS ($p = 0.0049$), and a trend was present for US ($p = 0.0564$).

The interaction effect of GE * NC ROI yielded $F = 3.314$, $p = 0.0014$, in line with our observation that certain NC regions, e.g. insula, cingulate, and orbitofrontal, could be more related to some NC-GE types than others (Table 3.2, Fig. 3.4*D*). Post-hoc analysis indicated that

cingulate TB were significantly more related to HC than paracentral ($p = 0.0373$), medial temporo-occipital ($p = 0.0184$), medial parietal ($p = 0.0139$), and lateral occipital ($p = 0.0030$) ones were. Orbitofrontal SS were significantly more related to HC than lateral temporal ($p = 0.0089$), paracentral ($p = 0.0082$), insula ($p = 0.0002$), and lateral occipital ($p = 0.0036$) ones were. In contrast, for DS and US, the HC-NC relationship across ROIs appeared less variable overall, with the exception that cingulate DS and US were significantly more related to HC than lateral occipital ones were ($p = 0.0277$ for DS, $p = 0.0121$ for US).

The interaction effect of NREM stage * Ant-/Post-HC yielded $F = 8.822$, $p = 0.0062$, as we observed in Fig. 3.4*E* where, with the exception of NC-SS in N3, the degree to which Post-HC proportion was higher than Ant-HC appeared attenuated in N3 compared to N2. Post-hoc analysis confirmed that the difference between Post-HC and Ant-HC proportions was significant in N2 ($p = 2.283 \times 10^{-6}$) but not in N3 ($p = 0.0910$). This may be related to the preference of NC-TB for Post-HC (as mentioned earlier for interaction effect of GE * Ant-/Post-HC) and NC-SS for N2 (as known in literature (Andrillon et al., 2011)).

The interaction effect of NREM stage * NC ROI yielded $F = 6.763$, $p = 4.93 \times 10^{-5}$, indicating that certain NC regions could be more related to HC-SWR in N2 than in N3, or vice versa. Overall, the proportions of significant channels were greater in N2, especially orbitofrontal, while cingulate appeared to be the exception (Fig. 3.4*C*). Post-hoc analysis showed that among the individual ROIs, only orbitofrontal and insula had significantly greater proportions in N2 than in N3 ($p = 3.528 \times 10^{-6}$ for orbitofrontal, $p = 0.0051$ for insula). Notably, the proportion of orbitofrontal channels with significant SS-SWR relationship was the highest among ROIs (Fig. 3.4*D*), possibly contributing to orbitofrontal's N2 preference as described above.

The interaction effect of Ant-/Post-HC * NC ROI yielded $F = 2.946$, $p = 0.0143$. Thus, while both Ant-HC and Post-HC appeared to engage the whole cortex (Fig. 3.2, Fig. 3.4), some ROIs could preferentially communicate with Ant- or Post-HC, with cingulate and prefrontal being possible examples (Fig. 3.4*C*). Post-hoc analysis indicated that no significant Ant/Post preference was present within most individual ROIs, with the exception being prefrontal, where Post-HC was preferred ($p = 0.0103$).

As previously mentioned, the interaction effect of GE * NREM stage was not significant, despite the fact the NC-TB and NC-SS occur more often in N2 (Andrillon et al., 2011; Gonzalez et al., 2018), while NC-DS and NC-US occur more often in N3 (Cash et al., 2009). This observation suggested that the GEs which did occur in the sleep stage where they occurred less often overall might not change in how related they were to the HC-SWR, i.e. the NC-HC relationships (as estimated from GE-SWR correlations) were consistent over time in NREM.

Among the 3-way interaction effects, only NREM stage * Ant-/Post-HC * NC ROI was significant ($F = 2.958$, $p = 0.0140$), as one might expect given that certain ROIs appeared to prefer Post-HC (prefrontal) and N2 (orbitofrontal). Indeed, post-hoc analysis revealed that for individual ROIs, only prefrontal and orbitofrontal showed significant differences among the four SWR sources (N2 Ant-HC, N2 Post-HC, N3 Ant-HC, N3 Post-HC): for prefrontal, N2 Post-HC had a significantly greater proportion of related HC-NC channel pairs than N3 Ant-HC ($p = 0.0328$); for orbitofrontal, N2 Post-HC had a significantly greater proportion of related channel pairs than other SWR sources ($p = 0.0003$ for N2 Ant-HC, $p = 7.559 \times 10^{-6}$ for N3 Ant-HC, $p = 4.582 \times 10^{-6}$ for N3 Post-HC).

<u>HC-SWR/NC-GE co-occurrence is stronger within hemisphere than between hemispheres</u>

Given the well-known lateralization of human hippocampal function (Weber et al., 2006; Iglói et al., 2010), we were interested in examining whether ipsilateral HC-NC channel pairs would show different relationships from contralateral pairs across NC-GE types, NREM stages, or NC ROIs. Due to a sparse representation of contralateral channel pairs for individual ROIs, we calculated proportions for larger regions by combining both HC and NC sites. Anterior and posterior HC channels were combined into a single HC category. The 10 NC ROIs used in previous analysis were collapsed into two: "fronto-central", which included the previous cingulate, orbitofrontal, prefrontal, and paracentral ROIs; and "non-frontal", which included the previous lateral temporal, medial temporo-occipital, medial occipito-parietal, insula, lateral occipital, and lateral parietal ROIs. We then computed for each ROI the proportion of NC channels significantly coupled to HC-SWR (Table 3.3), and performed 4-way ANOVA as previously described, with the ipsilateral/contralateral factor replacing the Ant-/Post-HC factor. All post-hoc analyses were performed with Tukey's range test. We checked the normality assumption by conducting the Lilliefors test on the residuals, and the null hypothesis of normality could not be rejected ($p = 0.0950$).

All 4 main effects were significant. As our previous ANOVA already revealed significant main effects for GE type and NREM stage, we focused our attention on the remaining two factors (i.e. ipsilateral/contralateral and combined NC ROI). The main effect of ipsilateral/contralateral channel pair types yielded $F = 65.058$, $p = 0.0040$. and together with mean proportions of 0.395 for ipsilateral and 0.282 for contralateral (a 40% increase), indicating that NC-GE in more channels significantly co-occurred with ipsilateral HC-SWR than contralateral HC-SWR. The main effect of ROIs yielded $F = 28.267$, $p = 0.0130$, indicating that the more frontal/cingulate parts of NC were significantly more likely to show significant GE-

SWR correlations than the posterior regions (mean proportion of 0.376 for fronto-central versus 0.301 for non-frontal).

Of the 2-way interaction effects, only laterality * GE and laterality * NC ROI were significant. No 3-way interactions were significant. Post-hoc analysis of the significant laterality * GE interaction ($F = 14.98$, $p = 0.0261$) revealed a stronger laterality effect for NC-US ($p = 0.0287$). However, the proportions for contralateral pairs were not themselves small compared to those for other NC-GE types (Fig. 3.4*F*). We also computed the proportions of ipsilateral versus contralateral HC-NC channel pairs with significant HC-SWR coupling to each NC-GE type. The ratios of contralateral over ipsilateral proportions for NC-TB (0.37), NC-DS (0.64), and NC-US (0.51) indicated a reduction of likelihood for contralateral HC-NC channel pairs to show significant HC-NC association compared to ipsilateral pairs, but the ratio of proportions for NC-SS was 1.02, i.e. there was a remarkably specific lack of ipsi/contra-lateral difference regarding HC-SWR to NC-SS association. Post-hoc analysis of the significant laterality * ROI interaction ($F = 10.450$, $p = 0.0481$) indicated a stronger laterality effect for the non-frontal ROI ($p = 0.0124$). Thus, the proportion of ipsilateral channels whose NC-GE significantly co-occur with HC-SWR is 40% greater than contralateral, and this effect is greater for NC-US and non-frontal locations.

Discussion:

Overall, our study demonstrates that human hippocampal sharpwave-ripples (SWR) are significantly associated with all categories of neocortical sleep grapho-elements (NC-GE) occurring in non-rapid-eye-movement (NREM) sleep, including theta bursts (TB), downstates (DS), upstates (US), and sleep spindles (SS). This coordination extends to all recorded NC areas, but for any given HC site only includes a minority of the cortex. The spatial intensity and

topography of HC-NC coordination differs across GE category, NREM sleep stage (N2 versus N3), HC location (anterior versus posterior), and NC area (frontal versus posterior). In addition, the HC-NC interactions are temporally-organized, with HC-SWR tending to follow TB, occur during DS, and precede SS and US (Fig. 3.3, Fig. 3.5). We discuss here how these spatio-temporal characteristics of the interaction of HC-SWR with NC-GE may assist in memory consolidation by coordinating information transfer between HC and NC, and processing within these structures.

Spatial organization of HC-SWR interactions with NC-GE.

SWR in both anterior and posterior HC co-occur with NC-GE of all kinds in all cortical areas, but there are some quantitative differences. The proportion of ipsilateral channels whose NC-GE significantly co-occur with HC-SWR is 40% greater than contralateral, and this effect is greater for US and non-frontal locations. This finding is consistent with the well-known lateralization of human hippocampal function (Weber et al., 2006; Iglói et al., 2010).

Frontal-GE co-occurred with HC-SWR ~25% more than average, whereas the lateral occipital GE co-occurred ~45% less. The frontal lobe has been considered to play a prominent role in declarative memory, especially in forming recollection cues, and integrating context with content (Fletcher and Henson, 2001; Badre et al., 2010). Similarly, memory consolidation during sleep is especially strong for inferential implications of events rather than their perceptual content (Zeithamova et al., 2012). Consistent with our observations, medial temporal lobe connections in primates target association and prefrontal areas more strongly than early sensory cortex (Van Hoesen, 1995; Suzuki and Amaral, 2004).

The proportion of SWR-GE pairs that were significantly related was 37% higher for SWR occurring in posterior than in anterior HC. In rodents, the dorsal but not ventral HC is

needed for spatial memory (Strange et al., 2014). While the ventral HC no doubt also has memory functions, they are less well understood. Rodent dorsal and ventral HC have similar internal anatomy but different external connections (Strange et al., 2014); corresponding differences are observed in primates and humans (Strange et al., 2014; Ding and Van Hoesen, 2015), implying that the dorsal-ventral distinction in rodents corresponds to the posterior-anterior in primates. If so, then our finding may reflect a tighter coupling of replaying HC events with cortical GE in posterior than anterior HC. Although anatomical data in primates is limited, the anterior-HC is mainly connected to limbic structures including amygdala and orbital cortex, whereas posterior-HC is more connected to posterior cingulate and parietal cortices. The implication that these areas would contain higher proportions of connected locations with anterior versus posterior HC was only partially supported: whereas posterior-HC-SWR co-occurred frequently with NC-GE in cingulate and parietal cortices, it also did with orbitofrontal cortex.

The proportion of HC-NC channel pairs whose HC-SWR/NC-GE significantly co-occurred was 44% higher in N2 than N3, despite the lower rate of HC-SWR in N2 than N3 (See Chapter 2, Fig. 2.3). Classically, isolated SS and K-Complexes predominate in N2, and the Slow Oscillation during N3 (Silber et al., 2007). However, intracranial recordings show that the principle difference is that in N2, NC-GE occur in TB-DS-SS-US sequences (known as K-complexes (Cash et al., 2009)), whereas in N3, abbreviated TB-SS are sandwiched between continuously alternating DS-US comprising the Slow Oscillation (Mak-McCully et al., 2017; Gonzalez et al., 2018). Consequently, SS and TB are about equally dense in N3 as N2, but have fewer oscillations (Mak-McCully et al., 2017; Gonzalez et al., 2018). Apparently, HC-SWR are more consistently associated with the TB-DS-SS-US complexes when they occur in relative

isolation in N2 than more continuously in N3. Alternatively, the relative lack of significant associations may reflect a statistical difficulty in distinguishing temporal correlations because of the high rates of both HC-SWR and DS-US in N3. If the difference is indeed physiological, it would imply that co-occurring HC-SWR with NC-GE are more common later in the night, when N2 predominates. Furthermore, in each ~90 min sleep cycle, N2 precedes N3, suggesting that the HC-NC engagement may become more selective over the course of each cycle.

The proportion of SWR-GE pairs that were significantly related was three times higher for NC-DS or NC-US than NC-TB or NC-SS. This could suggest that the HC-NC pairs related during TB and SS exchange more specific information whereas the HC-NC pairs related during NC-DS and NC-US reflect more contextual information, and/or provide an overall oscillatory context supporting large-scale timing and synchronization. This interpretation is consistent with the higher density and greater long-range coherence of NC-DS and NC-US than NC-TB and NC-SS (Mak-McCully et al., 2017; Gonzalez et al., 2018; Halgren et al., 2018).

The NC sites where GE co-occur with HC-SWR from a particular HC location constitute an anatomical network which could have functional significance during consolidation. In our data, the HC-NC co-occurrences were not randomly distributed across the recorded NC sites. Furthermore, if two HC locations were recorded simultaneously, their SWR co-occurred with NC-GE in different anatomical sites. However, for a given HC site, the NC sites with significant SWR-GE co-occurrence did not differ significantly across categories of NC-GE. Together, these results suggest that the SWR in a particular HC location engage with all categories of GE within the same, selected group of NC sites.

Previously we found that NC-US sequences occur during waking in particular sequences across large parts of the cortex (Jiang et al., 2017). A significantly greater proportion of these

spatiotemporal sequences occur more frequently in the sleep periods following the waking period where they were found, as compared to the sleep from preceding nights. These "replaying" events were associated with SWR-like events in the HC of 3 patients. In the current study, we did not compare spatiotemporal US sequences from waking to those in sleep. However, we did find that HC-SWRs did tend to be followed by multiple NC-US, and that these tended to exhibit a consistent structure, often proceeding from medial to lateral cortical areas.

Temporal organization of HC-SWR interactions with NC-GE.

While NC-TB, DS, US, and SS can occur separately from each other, they often occur in that order (Mak-McCully et al., 2017; Gonzalez et al., 2018). Typically, the sequence begins with an NC-TB whose oscillations grow into an NC-DS. Thalamic-DS follow NC-DS, especially when there multiple NC-DS are present. Thalamic-SS onset is coupled to the thalamic-DS peak. Thus, when the TH-SS is projected back to the NC, it arrives on the upslope of the NC-SS and continues through the NC-US (Fig. 3.5).

We found that within this sequence, NC-TB tend to precede HC-SWR, and thus are positioned to help define potential cortical cues for SWR firing. Several studies have found that waking NC-TB occur during cognitive processing, phase coupled with neuronal firing, as indexed by high gamma (Canolty et al., 2006; Sato et al., 2014; Alekseichuk et al., 2016). NC-TB when asleep have a similar laminar profile and are also phase coupled with high gamma (Gonzalez et al., 2018; Halgren et al., 2018). The final inhibitory peak of the NC-TB coincides with the local NC-DS, consistent with NC-DS sometimes being triggered by TB (Gonzalez et al., 2018).

The occurrence of NC-DS following NC-TB would tend to decrease the excitatory NC input to HC. This is consistent with our previous observation that HC-SWR tend to be

surrounded by locally-decreased broadband power (see Chapter 2, Fig. 2.2). Inhibitory interneurons in CA1 play a prominent role in the genesis of HC-SWR (Buzsáki, 2015), and in humans begin to fire prior to the HC-SWR (Le Van Quyen et al., 2008). The global decrease in membrane fluctuations prior to the HC-SWR may help create a more stable background upon which the exceptional synchrony underlying SWR can emerge.

Regardless of their influence on the local neuronal background, the most important function of NC-DS may be to synchronize activity across different structures. The tight coupling of thalamic-SS onset to the most hyperpolarized peak of the thalamic-DS suggests that the h and T currents, thought to be necessary for spindle generation (Bonjean et al., 2011), are not chronically available during NREM, but require the additional hyperpolarization consequent to decreased excitatory cortical input during NC-DS. This interpretation is supported by the observations that NC-DS consistently precede thalamic-DS, and that the probability of thalamic-DS is substantially higher when there are multiple NC-DS (Mak-McCully et al., 2017). Similarly, we found here that HC-SWR were more likely in conjunction with multiple than isolated NC-US. In addition to this indirect triggering of NC-SS by NC-DS projected to the thalamus, NC-US are directly triggered as a rebound from the profound hyperpolarization during NC-DS. The implication that converging NC-DS may trigger DS in the HC and thalamus, and consequently synchronized HC-SWR and thalamic-SS, is consistent with the finding that HC-SWR-triggered BOLD in monkeys shows thalamic suppression (Logothetis et al., 2012).

A striking finding of the current study were the widespread NC-US and NC-SS which consistently follow HC-SWR. During the NS-US, cortical cells fire at levels comparable to waking (Steriade, 2001). NC-SS tend to occur on the US, and there is a phasic additional increase in firing at their peaks (Mak-McCully et al., 2017; Gonzalez et al., 2018). The increased

firing within narrow temporal windows would create the conditions for Spike Timing Dependent Plasticity (Froemke and Dan, 2002), as would the strong inward Ca^{+2} current in the apical dendrites of cortical pyramidal cells during NC-SS (Seibt et al., 2017). In rodents, HC pyramidal cells replay sequences of firing from the preceding waking period during HC-SWR (Wilson and McNaughton, 1994), and this has been shown to be important for memory consolidation (Suh et al., 2013; de Lavilléon et al., 2015). Our results imply that the information encoded in these firing patterns arrives in an NC prepared to construct firing patterns and consolidate the consequent networks by virtue of the coincident NC-SS and NC-US (Fig. 3.5).

Chapter 3, in full, is currently being prepared for submission for publication of the material. Jiang, Xi; Gonzalez-Martinez, Jorge; Halgren, Eric. The dissertation author was the primary investigator and author of this paper.

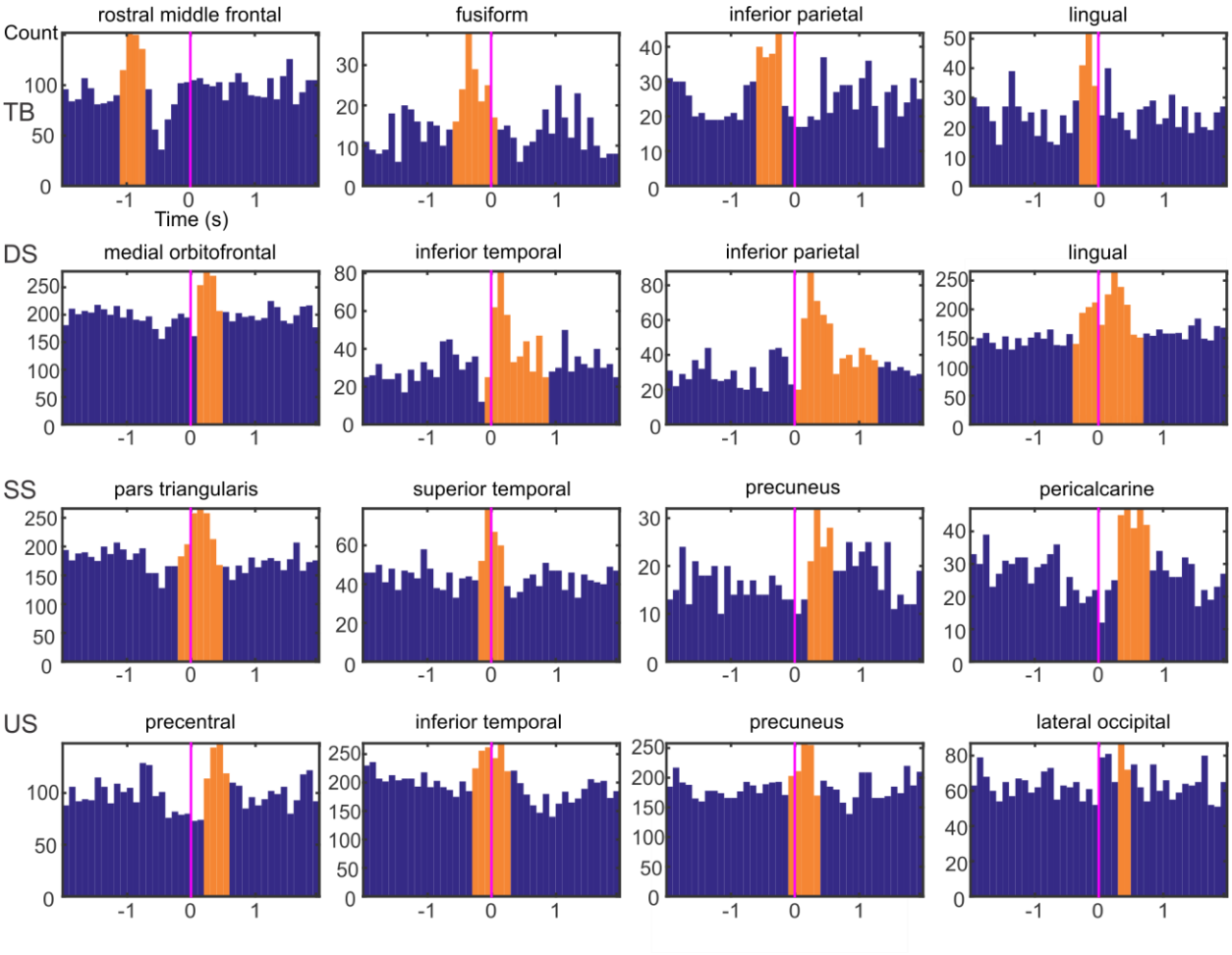

Figure 3.1: Neocortical graphoelements (NC-GE) in relation to HC-SWR, for example channel-pairs. Each row of histograms is for a different type of GE: theta burst onsets (TB), downstate peaks (DS), spindle onsets (SS), and upstate peaks (US). The four columns of plots show example histograms with significant temporal correlations between HC-SWR and NC-GE from the frontal, temporal, parietal, and occipital lobes, respectively. Magenta vertical lines indicate trigger (SWR) location for the peri-stimulus histograms. Orange bars indicate the time ranges with both peak NC-GE occurrence rate and significant correlation.

Figure 3.2: GEs across NC tend to co-occur with HC-SWR at consistent latencies. ***A-C***. *Top*: Histograms of peak latencies for HC-NC channel pairs with significant temporal correlations between HC-SWRs and NC-GE. Each count is the peak latency of a particular HC-NC channel pair (see Fig. 3.1 for examples). *Bottom*: maps of peak latency between SWR and GE for cortical channels. Circles indicate where GE-SWR relationships are significant, while plus signs represent non-significant channels. The intensity of each circle corresponds to the strength of GE-SWR coupling estimated (as in Fig. 3.1), and the color of each circle indicates peak latency: red for GE before SWR, blue for GE after SWR, and yellow for GE co-occurring with SWR (i.e. within 100 ms of each other). Both hemispheres and medial and lateral cortical sites are superimposed in each plot. ***A***. NC-US tend to follow both Ant-HC and Post-HC SWR in both N2 and N3. ***B***. NC-TB tend to precede Post-HC SWR, while other NC-GEs tend to follow. ***C***. NC-TB tends to precede Ant-HC SWRs, while NC-DS and NC-SS tend to follow. ***B-C.*** Stage N2 NREM sleep. Stage N3 results are shown in Figure 3.S1.

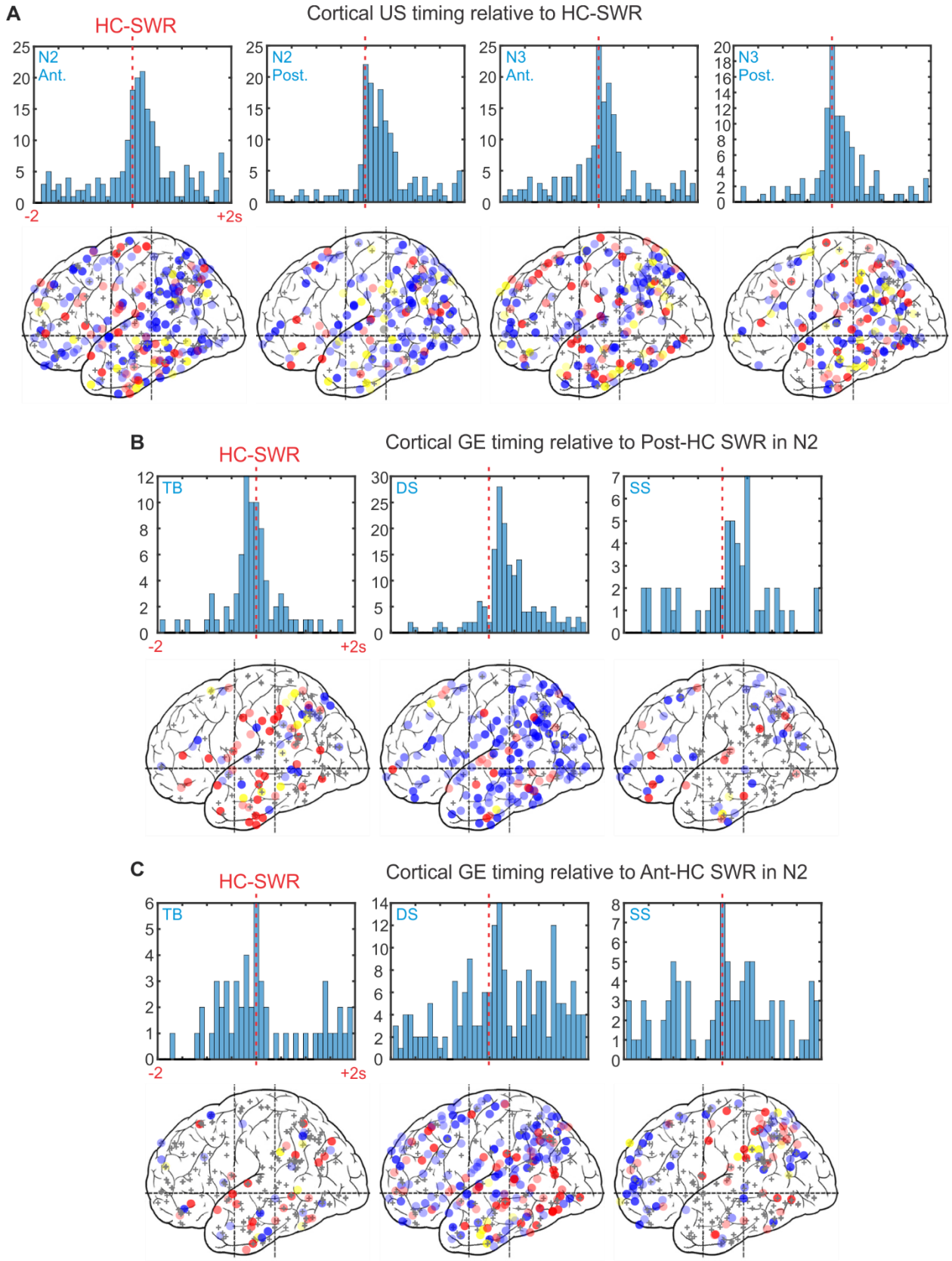
A
Cortical US timing relative to HC-SWR
HC-SWR
N2 Ant.
N2 Post.
N3 Ant.
N3 Post.
-2
+2s
B
Cortical GE timing relative to Post-HC SWR in N2
HC-SWR
TB
DS
SS
-2
+2s
C
Cortical GE timing relative to Ant-HC SWR in N2
HC-SWR
TB
DS
SS
-2
+2s

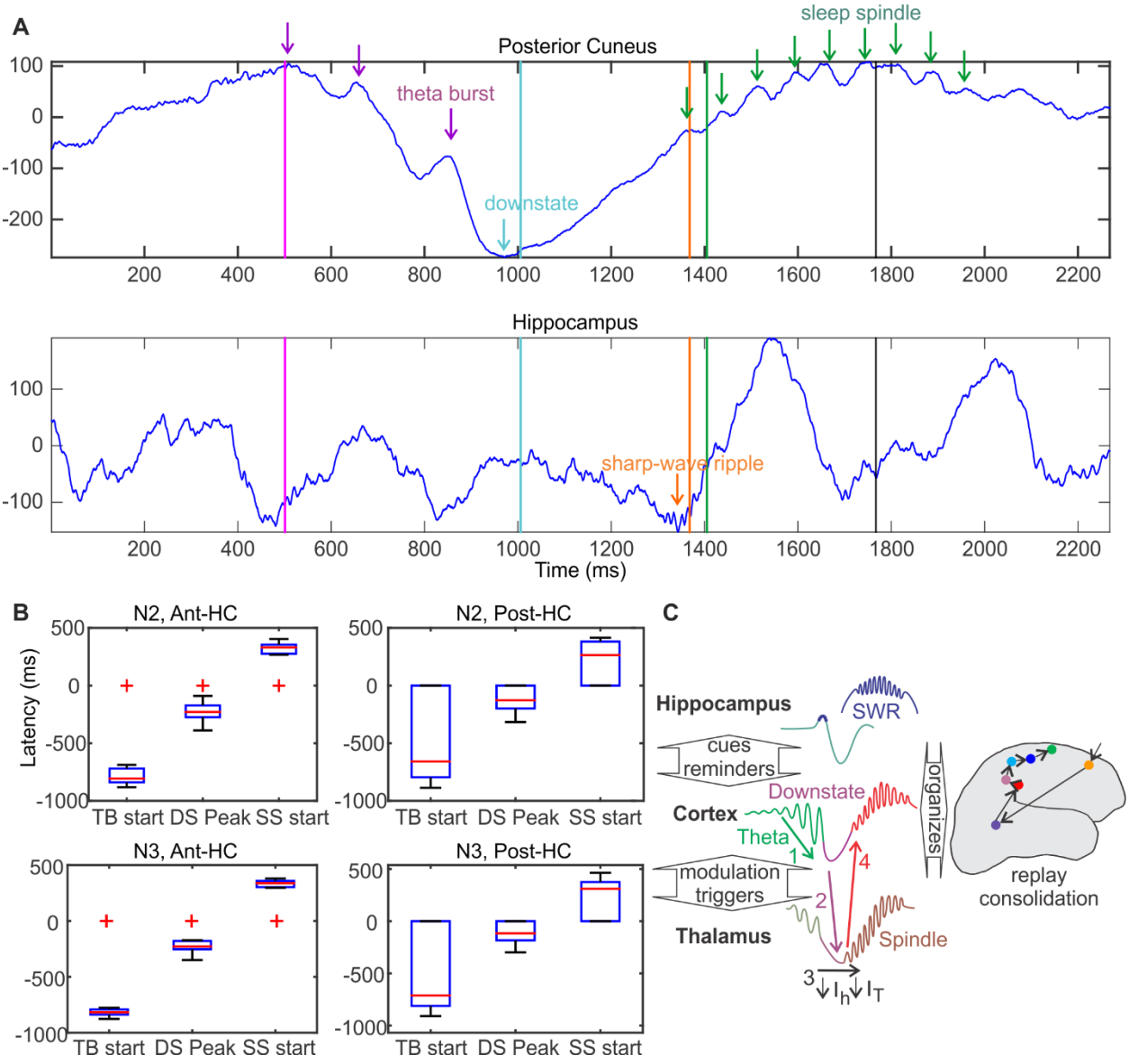

Figure 3.3: HC-SWR are associated with stereotyped NC-GE sequences. ***A***. Example LFP traces of a HC-NC channel pair where TB, DS, SWR, and SS occur in sequence. Vertical colored lines indicate automatically detected NC-GE locations (TB start, DS peak, SWR center, and SS start). ***B***. In TB→DS→SS sequences that co-occur with HC-SWR, the latencies between NC GEs and SWRs are stereotyped, with TB starts almost always preceding HC-SWR and SS starts almost always following. ***C***. Hypothesized schema of thalamo-cortico-hippocampal coordination based on co-occurrences of HC-SWR and NC-GEs. I_h, I_T: thalamic H-current and T-current, respectively, which are key in regulating NC-US (Mak-McCully et al., 2017).

Figure 3.4: Strength of HC-NC association varies across NC regions (*C*, *D*, F), NREM stages (C, *E*, *F*), GE types (*A*, *D*, *E*, *F*), and anterior vs posterior (*E*) or ipsilateral vs contralateral (*F*) SWR sources. ***A***. Proportions of co-occurring HC-SWR with NC-GE for different NC channels show strong correlation across NC-GE type pairs (TB vs. SS, TB vs. DS, etc.), especially for DS vs. US. Each marker in a given scatter plot panel represents one HC-NC channel pair. Linear regression best fit lines were marked for each scatterplot in grey. ***B***. Map of NC ROIs ***C***, ***F***. Stacked bar graph of mean proportions of significant HC-NC channel pairs. Channels with significant (as evaluated in Fig. 3.1) HC-NC co-occurrences are more common in fronto-central (FC) than non-frontal (NF) cortex (***C***, ***D***, ***F***), N2 than N3 (***C***, ***E***, ***F***), DS and US than TB and SS (***D***, ***E***, ***F***), with posterior than anterior HC-SWR (***E***), and with ipsilateral than contralateral HC-SWR (***F***). Within these general patterns, interactions can be observed, such as the relatively high co-occurrence of orbitofrontal GE with Post-HC SWR in N2 (***C***). Proportions are relative to total channels in each ROI (***C***, ***D***), all ROIs (***E***), or fronto-central or non-frontal ROIs in the ipsilateral vs contralateral hemisphere (***F***). For correspondence of ROIs to FreeSurfer labels, and their amalgamation to fronto-central and non-frontal, see Table 3.S5.

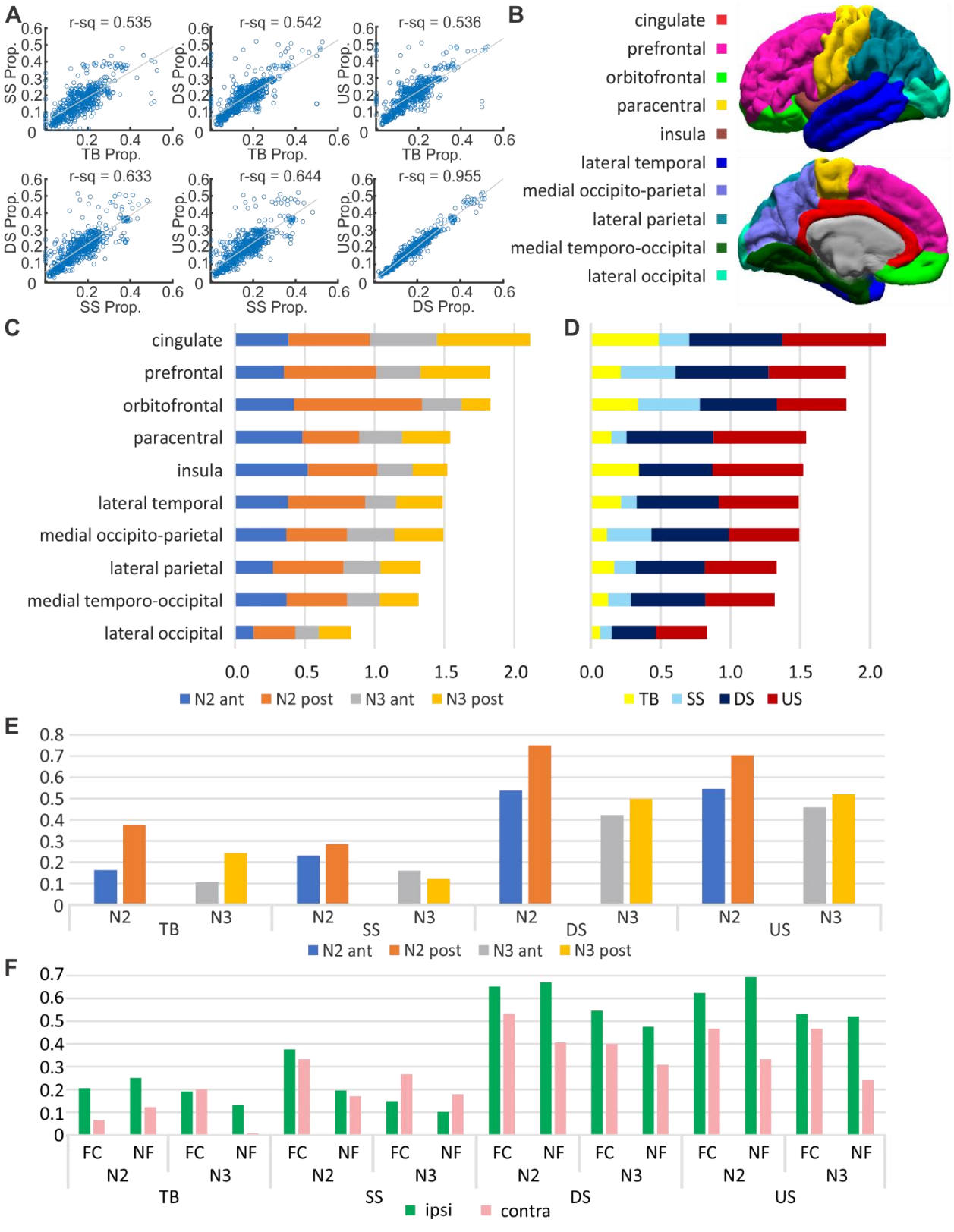
A
r-sq = 0.535
r-sq = 0.542
r-sq = 0.536
r-sq = 0.633
r-sq = 0.644
r-sq = 0.955
SS Prop.
DS Prop.
US Prop.
TB Prop.
SS Prop.
DS Prop.
B
cingulate
prefrontal
orbitofrontal
paracentral
insula
lateral temporal
medial occipito-parietal
lateral parietal
medial temporo-occipital
lateral occipital
C
N2 ant
N2 post
N3 ant
N3 post
D
TB
SS
DS
US
E
N2
N3
TB
SS
DS
US
F
FC
NF
ipsi
contra

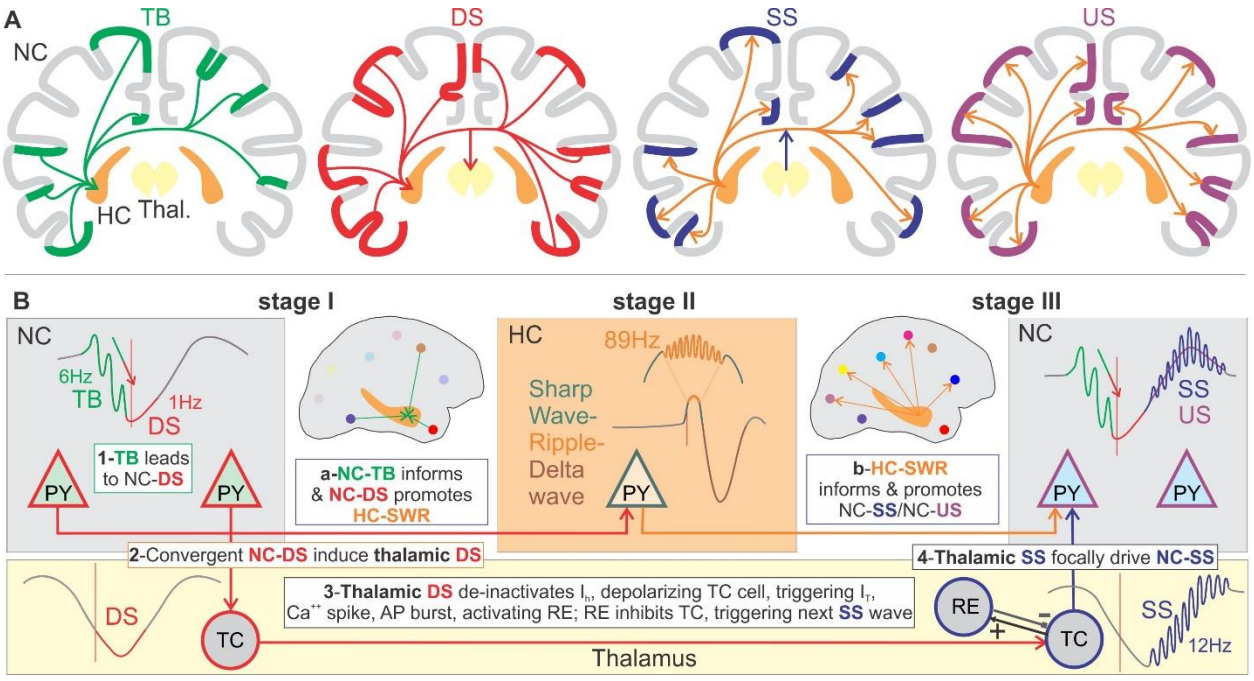

Figure 3.5: Summary of HC-SWR interactions with NC-GE in the context of previous findings of NC-thalamus interactions during GE. ***A***. NC areas whose GE co-occur with SWR in a particular HC location are widespread, and more distributed for DS and US than TB and SS. For a given HC site, the NC locations which co-occur with different GE are overlapping but distinct. Generally, NC-TB precede HC-SWR, whereas other NC-GE follow. ***B***. Thalamic interactions. **1**- NC-TB precede NC-DS and sometimes may help trigger them. **2**- Converging NC-DS appear to trigger thalamic-DS. **3**- the resulting hyperpolarization of thalamo-cortical (TC) cells appears to be a necessary condition to make the voltage-gated T and h currents available, which in interaction with thalamic reticular nucleus cells (RE) results in SS generation. **4**- SS are projected from thalamus to NC. **a**- We found that NC-TB precede HC-SWR and propose that they may enfold NC firing that helps select HC traces that are activated in SWR. The NC-DS that may follow NC-TB could be the source of the decreased HC-LFP surrounding the SWR. **b**- Information contained in the HC replay during the consequent SWR would thus arrive at the NC in the same time frame as the SS and US are providing a favorable environment for synchronous activation of NC neurons. In sum, we propose 3 stages in the spatiotemporal organization of memory consolidation. In **stage I**, NC-TB induce NC-DS, which converge on thalamus and HC. In **stage II**, thalamic-DS result in thalamic-SS, and HC-DS in HC-SWR. In **stage III**, thalamic SS are projected to the NC where they meet the US (rebound from the preceding NC-DS) and the trace information activated by the HC-SWR.

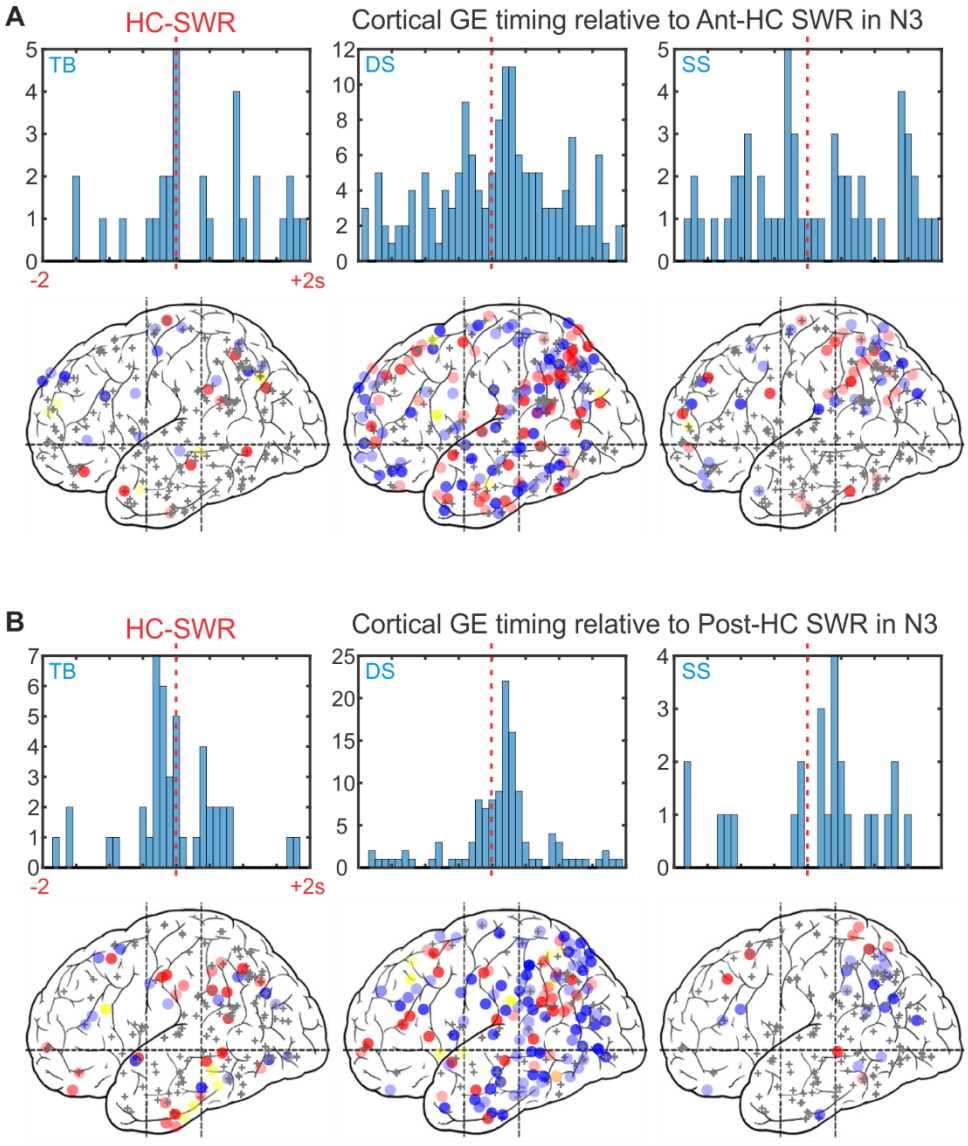

Figure 3.S1: GEs across NC tend to occur with consistent latencies from HC-SWR in stage N3. ***A-B***. Top: Histograms of peak latencies for HC-NC channel pairs with significant temporal correlations between HC-SWR and NC-GE in N3. Each count is the peak latency of a particular HC-NC channel pair. Bottom: maps of peak latency between SWR and GE for cortical channels. Circles indicate where GE-SWR relationships are significant, while plus signs represent non-significant channels. The intensity of each circle corresponds to the strength of the coupling, and the color indicates latency: red for NC-GE before HC-SWR, blue for NC-GE after HC-SWR, and yellow for NC-GE co-occurring with HC-SWR (i.e. within 100 ms of each other). ***A***. NC-DS tend to follow Ant-HC SWR. ***B***. NC-TB tend to precede Post-HC SWR, while NC-DS and NC-SS tend to follow.

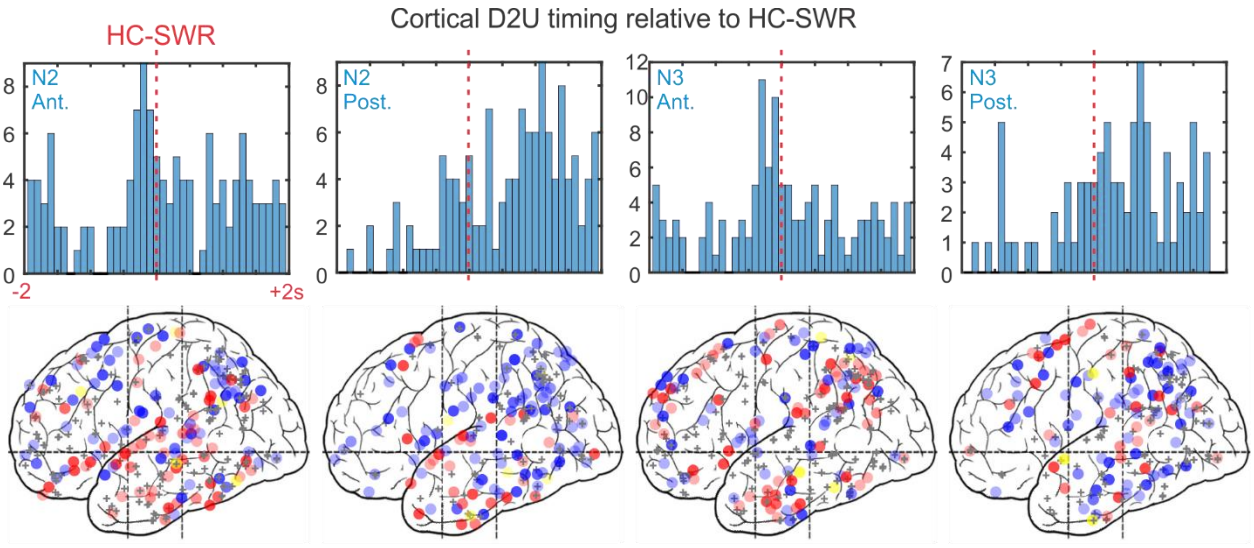

Figure 3.S2: D2U across NC sites co-occur with HC-SWR, but with variable latencies. Top: Histograms of peak latencies for HC-NC channel pairs with significant temporal correlations between HC-SWR and NC-D2U in N3. Each count is the peak latency of a particular HC-NC channel pair. Bottom: maps of peak latency between HC-SWR and NC-D2U for cortical channels. Circles indicate where D2U-SWR relationships are significant, while plus signs represent non-significant channels. The intensity of each circle corresponds to the strength of the coupling, and the color indicates latency: red for NC-D2U before HC-SWR, blue for NC-D2U after HC-SWR, and yellow for NC-D2U co-occurring with HC-SWR (i.e. within 100 ms of each other).

Table 3.1: Relation of HC-SWR to NC-GE. Separate values and statistical significance tests are shown for NREM sleep stages N2 vs. N3, for anterior vs. posterior HC, and for different graphoelements (TB- theta bursts; DS- downstates; SS- sleep spindles; US- upstates). Tests indicate if there was a significant association between the times of occurrence of the SWR and GE (fourth column); if the GE occurred significantly before the SWR (negative numbers) or before, when measuring the peak latency as the mean value across cortico-HC pairs (fifth column), or as the peak of an extreme value distribution fitted over the ±500 ms histogram-of-histograms in Fig. 2 and in Fig. 2-1 (sixth column). The seventh column shows if there is a significant difference in the number of GE occurring 500ms before vs. 500ms after the SWR. The eighth column contains results from the same test as the seventh column, but applied to data with N2/N3/Ant/Post combined. **BOLD** indicates significant values; *italics* indicate trends. For columns 4, 7, and 8, extremely small (< 0.0001) p-values are represented by 0 for clarity.

GE Type	Sleep Stage	HC Longi-tudinal Axis	SWR v. GE related (KS test p-value)	Peak Latency (ms), Mean	Peak Latency (ms), DistPeak	Non-zero Latency, binomial p-value	Non-zero Latency, binomial p-value, overall
TB	N2	Ant	**0.023**	-92	-104	0.238	**0.0011**
TB	N2	Post	**0**	*-45*	*-123*	*0.065*	
TB	N3	Ant	**0.023**	0	-95	0.508	
TB	N3	Post	**0.003**	*-62*	*-209*	*0.052*	
DS	N2	Ant	**0**	0	94	0.228	**0**
DS	N2	Post	**0**	**186**	**356**	**0**	
DS	N3	Ant	**0.002**	*35*	*236*	*0.091*	
DS	N3	Post	**0**	**128**	**224**	**0**	
SS	N2	Ant	0.115	**150**	**179**	**0.009**	**0.0002**
SS	N2	Post	**0.02**	**187**	**309**	**0.001**	
SS	N3	Ant	0.452	-32	-229	0.481	
SS	N3	Post	*0.073*	*238*	*342*	*0.092*	
US	N2	Ant	**0**	**126**	**216**	**0**	**0**
US	N2	Post	**0**	**164**	**279**	**0**	
US	N3	Ant	**0**	**76**	**134**	**0**	
US	N3	Post	**0**	**81**	**85**	**0.013**	

Table 3.2: Numbers of HC-NC channel pairs by NC regions of interest (ROIs) and proportions of HC-NC channel pairs with significant GE-SWR relationships across NC. Ch. pairs: HC-NC channel pairs. Ant.: Ant-HC. Post.: Post-HC.

			Proportion of channels with significant HC-SWR co-occurring with NC-GE types															
GE Type	Total# Ch. pairs		TB				DS				SS				US			
			N2		N3		N2		N3		N2		N3		N2		N3	
ROI	Ant.	Post.	Ant.	Post.	Ant.	Post.	Ant.	Post.	Ant.	Post.	Ant.	Post.	Ant.	Post.	Ant.	Post.	Ant.	Post.
Lateral occipital	15	15	0.067	0.067	0.000	0.133	0.200	0.467	0.200	0.400	0.000	0.067	0.267	0.000	0.267	0.600	0.200	0.400
Medial temporo-occipital	31	26	0.194	0.077	0.032	0.192	0.516	0.808	0.387	0.423	0.129	0.231	0.097	0.192	0.645	0.615	0.419	0.308
Lateral parietal	74	51	0.081	0.412	0.041	0.137	0.392	0.686	0.365	0.529	0.203	0.157	0.203	0.059	0.419	0.765	0.446	0.431
Medial occipito-parietal	34	27	0.029	0.259	0.059	0.111	0.500	0.667	0.529	0.519	0.529	0.185	0.265	0.296	0.412	0.630	0.500	0.481
Lateral temporal	86	54	0.186	0.407	0.070	0.204	0.558	0.889	0.372	0.537	0.140	0.222	0.047	0.037	0.640	0.685	0.407	0.556
Insula	11	6	0.455	0.667	0.091	0.167	0.909	0.667	0.364	0.167	0.000	0.000	0.000	0.000	0.727	0.667	0.545	0.667
Paracentral	29	16	0.103	0.250	0.172	0.063	0.724	0.625	0.517	0.625	0.276	0.125	0.034	0.000	0.828	0.625	0.517	0.688
Orbitofrontal	23	6	0.217	0.667	0.130	0.333	0.565	1.000	0.478	0.167	0.435	1.000	0.174	0.167	0.478	1.000	0.348	0.167
Prefrontal	49	14	0.061	0.286	0.082	0.429	0.551	0.857	0.469	0.786	0.367	0.714	0.204	0.286	0.429	0.786	0.510	0.500
Cingulate	13	6	0.231	0.667	0.385	0.667	0.462	0.833	0.538	0.833	0.231	0.167	0.308	0.167	0.615	0.667	0.692	1.000
Total# Ch. Pairs across NC / Average Proportion	365	221	0.162	0.376	0.106	0.244	0.538	0.750	0.422	0.499	0.231	0.287	0.160	0.120	0.546	0.704	0.459	0.520

Table 3.3: Proportions of HC-NC channel pairs with significant GE-SWR relationships across NC, separated by ROI, NREM stage, GE type, and ipsilateral/contralateral NC-HC pairings. ipsi: ipsilateral. contra: contralateral.

	Proportion of channels with significant HC-SWR co-occurring with NC-GE types															
GE Type	TB				DS				SS				US			
	N2		N3		N2		N3		N2		N3		N2		N3	
ROI \ SWR Source	ipsi	contra	ipsi	contra	ipsi	contra	ipsi	contra	ipsi	contra	ipsi	contra	ipsi	contra	ipsi	contra
Fronto-central	0.206	0.067	0.191	0.200	0.652	0.533	0.546	0.400	0.376	0.333	0.149	0.267	0.624	0.467	0.532	0.467
Non-frontal	0.251	0.122	0.134	0.008	0.671	0.407	0.476	0.309	0.195	0.171	0.101	0.179	0.694	0.333	0.521	0.244

Table 3.S1: Summary of number of events in NC-GE to HC-SWR histograms. Each cell is formatted as follows: Mean±Standard Deviation (Skewness). Ant: anterior. Post: posterior. Ipsi: ipsilateral. Contra: contralateral.

	NC-GE Type		NC-TB		NC-SS		NC-DS		NC-US	
Stage	Ant/ Post	Ipsi/ Contra	NC-GE	HC-SWR	NC-GE	HC-SWR	NC-GE	HC-SWR	NC-GE	HC-SWR
N2	Ant	Ipsi	803± 1032 (1.9)	714± 911 (1.9)	1077± 1604 (2.6)	911± 1280 (2.3)	2992± 2918 (1.4)	2249± 2221 (1.4)	2962± 2862 (1.5)	2115± 2015 (1.5)
N2	Ant	Contra	931± 949 (1.3)	832± 833 (1.3)	1531± 2048 (1.7)	1286± 1649 (1.6)	3813± 3171 (0.4)	2921± 2327 (0.4)	3914± 3091 (0.6)	2862± 2163 (0.4)
N2	Post	Ipsi	927± 1127 (1.7)	822± 995 (1.7)	989± 1732 (3.0)	857± 1448 (2.8)	3131± 3627 (1.5)	2382± 2740 (1.5)	3120± 3412 (1.5)	2260± 2498 (1.5)
N2	Post	Contra	383± 585 (3.2)	335± 501 (3.1)	325± 407 (1.6)	286± 350 (1.4)	1277± 1238 (1.3)	970± 935 (1.3)	1376± 1305 (1.4)	948± 871 (1.3)
N3	Ant	Ipsi	1480± 1894 (2.7)	1276± 1573 (2.6)	1537± 2255 (2.7)	1297± 1785 (2.5)	7673± 6550 (1.5)	4576± 3377 (1.3)	8467± 6712 (1.5)	4573± 3124 (1.2)
N3	Ant	Contra	1325± 1211 (1.8)	1177± 1030 (1.7)	2221± 2799 (1.6)	1864± 2247 (1.6)	7134± 4298 (1.0)	4996± 2687 (0.8)	8229± 4324 (1.3)	5226± 2424 (1.0)
N3	Post	Ipsi	1145± 1057 (1.1)	1003± 906 (1.1)	1078± 2208 (6.5)	918± 1686 (5.2)	5148± 5003 (3.0)	3355± 3047 (2.7)	5754± 5283 (2.7)	3392± 2945 (2.6)
N3	Post	Contra	678± 696 (2.5)	591± 593 (2.5)	583± 712 (1.4)	509± 591 (1.3)	3381± 2495 (2.0)	2253± 1574 (2.5)	4196± 2811 (2.5)	2417± 1520 (2.7)

Table 3.S2: P-values for chi-square tests of homogeneity (α = 0.05 post FDR-correction applied over each column), conducted for each HC site with regard to each NC-GE's coupling to HC-SWR in NREM. A: anterior. P: posterior. Cells marked 2.20E-016 are placeholders for $p < 2.2 \times 10^{-16}$. # signif.: number of HC sites with a non-homogeneous anatomical distribution of significantly coupled NC sites. Dist.: anatomical distribution (of NC sites).

Patient	HC Site	Significance of (SWR x TB) NC site dist.	Significance of (SWR x DS) NC site dist.	Significance of (SWR x SS) NC site dist.	Significance of (SWR x US) NC site dist.
1	A	2.20E-016	2.20E-016	2.20E-016	2.20E-016
2	A	2.20E-016	2.20E-016	4.48E-13	2.20E-016
3	A	2.20E-016	2.20E-016	2.20E-016	2.20E-016
	P	2.20E-016	2.20E-016	2.20E-016	2.20E-016
4	A	2.20E-016	2.8E-14	0.0005	2.20E-016
	P	0.2403	0.0028	0.0151	0.0003
	A	2.20E-016	1E-15	1.0891E-08	2.20E-016
5	A	4.99E-08	2.20E-016	2.20E-016	2.20E-016
	P	0.0014	2.20E-016	1.70E-008	2.5E-14
6	A	2.20E-016	1.379E-11	7.2022E-10	0.0002
	P	0.0005	0.0202	2.28E-006	0.0665
7	A	0.0003	2.20E-016	2.20E-016	2.20E-016
8	A	2.20E-016	2.20E-016	2.20E-016	2.20E-016
9	A	2.60E-008	1E-15	2.2857E-06	4.86003E-05
	P	2.20E-016	2.20E-016	2E-15	2.20E-016
10	A	8.2285E-11	2.20E-016	1.0309E-10	2.20E-016
11	A	2.20E-016	2.20E-016	2.20E-016	2.20E-016
	A	2.4554E-11	1.7733E-07	1.8223E-05	0.0006
	P	2.20E-016	2.20E-016	3.3E-14	2.20E-016
12	P	2.20E-016	1.9301E-09	2.20E-016	2.20E-016
13	A	2.20E-016	1.679E-10	2.2232E-08	2.20E-016
	P	2.20E-016	2.20E-016	2.4805E-06	2.20E-016
	A	2.20E-016	6.3974E-11	3.3886E-10	2.20E-016
14	P	2.20E-016	2.20E-016	2.20E-016	7.86692E-09
15	P	0.0158	0.0008	0.0083	8.78129E-05
	P	0.0011	0.1182	0.0003	0.0069
16	A	2.20E-016	2.2276E-09	0.0006	2.20E-016
17	A	8.3641E-10	2.20E-016	2.5371E-11	1.11717E-10
18	A	2.0809E-06	2.8456E-08	2.20E-016	0.0001
19	A	3.4393E-10	0.0255	3E-15	2.60652E-09
	P	6.7389E-10	2.20E-016	2.20E-016	2.452E-12
20	A	2.20E-016	2.20E-016	2.2857E-06	2.20E-016
# signif. HC sites (/32)		31	31	32	31

Table 3.S3: Proportions of NC-GE from significantly coupled NC sites that overlapped with Ant-HC SWR differ from the proportions for Post-HC SWR, and proportions of NC-GE that overlapped with Left-HC SWR differ from the proportions for Right-HC SWR. Wilcoxon signed rank tests were performed on the data obtained for Table 3.S2. Each patient's test (whose p-value was tabulated above) required that both members of a HC site pair must have significant chi-square test result from Table 3.S2; otherwise, the corresponding cell would be filled with NA. # signif.: number of significant tests (in total number of qualified patients).

	Diff. b/t coupled NC site dist., Ant-HC vs. Post-HC				Diff. b/t coupled NC site dist., Left-HC vs. Right-HC			
Patient	NC-TB	NC-DS	NC-SS	NC-US	NC-TB	NC-DS	NC-SS	NC-US
3	0.1099	0.0001	0.0004	0.0001	NA	NA	NA	NA
4	NA	0.0003	0.0004	0.0003	0.0049	0.0003	0.0003	0.0003
5	0.0002	0.0001	0.0002	0.0001	NA	NA	NA	NA
6	0.0002	0.0001	0.0002	NA	NA	NA	NA	NA
9	0.1099	0.0005	0.0674	0.0005	NA	NA	NA	NA
11	1.39E-005	1.39E-005	2.05E-005	1.39E-005	6.94E-006	6.94E-006	6.94E-006	6.94E-006
13	0.0004	0.0002	0.0002	0.0002	0.0002	0.0002	0.0002	0.0003
15	NA	NA	NA	NA	0.0004	NA	0.0003	0.0003
19	0.0002	0.0001	0.0002	0.0001	NA	NA	NA	NA
# signif.	5 in 7	8 in 8	7 in 8	7 in 7	4 in 4	3 in 3	4 in 4	4 in 4

Table 3.S4: Anatomical distributions of NC sites significantly coupled with HC-SWR in terms of different NC-GE types tend to be similar for some NC-GE type pairs (TB vs. SS, DS vs. US) and different for other pairs. Wilcoxon signed rank tests were performed on the data obtained for Table 3.S2. Each test (whose p-value was tabulated above) required that the corresponding cell in Table 3.S2 for that particular HC site must have significant chi-square test result from Table 3.S2 (thereby counting towards Qualif. Sites); otherwise, the corresponding cell would be filled with NA. # signif.: number of significant tests (in total number of qualified patients).

Patient	HippSite	TB vs SS	TB vs DS	TB vs US	SS vs DS	SS vs US	DS vs US
1	LA	0.2719	0.0012	0.0009	0.0048	0.0033	0.0256
2	LA	0.0035	0.0230	0.9697	0.0810	0.0014	0.0256
3	LA	0.0032	0.0036	0.0098	0.1703	0.0917	0.6582
	LP	0.1162	0.1585	0.7348	0.5658	0.0928	0.1085
4	LA	0.0807	0.1114	0.0141	0.0908	0.6490	0.1576
	LP	NA	NA	NA	0.0348	0.6002	0.1106
	RA	0.1671	0.0603	0.0078	0.8590	0.0908	0.2979
5	RA	0.6581	0.0054	0.0075	0.0005	0.0007	0.3207
	RP	0.4383	0.0104	0.0119	0.0012	0.0008	0.3430
6	RA	0.4656	0.0029	0.0008	0.0032	0.0011	0.0072
	RP	0.3482	0.0020	NA	0.0031	NA	NA
7	LA	0.7667	0.0045	0.0034	0.0521	0.0033	0.0659
8	RA	0.0666	0.0021	0.0010	0.1643	0.7599	0.1085
9	LA	0.4383	0.0230	0.0024	0.0732	0.0066	0.4108
	LP	0.0757	0.0029	0.0220	0.9097	0.3173	0.4108
10	RA	0.0066	0.7022	0.4867	0.0014	0.0011	0.4643
11	LA	0.0481	0.0002	8.6275E-05	0.0112	0.0033	0.8681
	RA	0.1071	0.0012	0.0001	0.2201	0.0441	0.0659
	RP	0.8899	0.0030	0.0094	0.0002	0.0006	0.3433
12	RP	0.9464	0.0127	0.0016	0.1305	0.0441	0.1576
13	LA	0.2096	0.3286	0.1561	0.2486	0.7160	0.7728
	LP	0.0066	0.0030	0.0065	0.1402	0.0766	0.9163
	RA	0.1165	0.0845	0.0385	0.8590	0.8077	0.9341
14	LP	0.6928	0.0015	0.0024	0.0014	0.0048	0.0171
15	LP	0.0035	0.4658	0.0553	0.0014	0.0011	0.0723
	RP	0.1162	NA	0.1806	NA	0.0102	NA
16	RA	0.1162	0.8092	0.0098	0.0222	0.0014	0.0072
17	LA	0.0035	0.0029	0.0024	0.0647	0.1139	0.6582
18	LA	0.1162	0.0009	0.0006	0.0005	0.0006	0.2979
19	LA	0.4453	0.0030	0.0009	0.0110	0.0014	0.0659
	LP	0.0035	0.0722	0.0575	0.0005	0.0006	0.9341
20	RA	0.0035	0.0081	0.0011	0.0745	0.0917	0.2979
	Qualif. Sites	31	30	30	31	31	30
	Signif. Sites	8	21	23	15	20	5
	Signif. Ratio	0.2581	0.7000	0.7667	0.4839	0.6452	0.1667
p-values (1-tailed binomial), # Signif. Sites vs. # Non-signif. Sites		0.9983	0.0214	0.0026	0.6399	0.0748	1.0000

Table 3.S5: ROIs for statistical analyses of spatio-temporal differences across NC regions in NC-SWR relationships.

Combined ROI	Original Freesurfer Label(s)
Lateral temporal	Banks of superior temporal gyrus, inferior temporal, middle temporal, superior temporal, temporal pole, transverse temporal
Cingulate	Caudal anterior cingulate, rostral anterior cingulate, isthmus cingulate, posterior cingulate
Orbitofrontal	Frontal pole, lateral orbitofrontal, medial orbitofrontal, pars orbitalis
Prefrontal	Caudal middle frontal, pars opercularis, pars triangularis, rostral middle frontal, superior frontal
Paracentral	Paracentral, postcentral, precentral
Medial temporo-occipital	Entorhinal, fusiform, lingual
Medial occipito-parietal	Cuneus, pericalcarine, precuneus
Insula	Insula
Lateral occipital	Lateral occipital
Lateral parietal	Inferior parietal, superior parietal, supramarginal
Fronto-central	All labels for the following Combined ROIs: Cingulate, orbito-frontal, prefrontal, paracentral
Non-frontal	All labels for the following Combined ROIs: Lateral temporal, medial temporo-occipital, medial occipito-parietal, insula, lateral occipital, lateral parietal

CHAPTER 4: Hippocampal spindle-ripples and cortico-hippocampal communication

Title: Hippocampal-cortical interactions during NREM sleep in humans vary across the hippocampal longitudinal axis

Abstract:

The human anterior and posterior hippocampus (Ant-HC, Post-HC) differ in their functional correlates. This has been explained as mainly resulting from different external connections rather than intrinsic physiology. However, the activities of human Ant-HC versus Post-HC have not been compared when they are performing what is presumed to be their primary function: memory consolidation. Here we confirm previous reports that during NREM sleep the HC generates sharpwave-ripples (SWR: as in rodents), as well as spindle-ripples (SSR: ripples phase-locked to local spindles). We found that SSR comprise 51% of Post-HC ripples, as compared to only 14% in Ant-HC. Both SWR and SSR co-occur with neocortical theta bursts (TB), downstates (DS), spindles (SS) and upstates (US), which are thought to coordinate cortico-hippocampal interactions and facilitate consolidation. Within the cortex, these typically occur in the order TB-DS-SS-US, with SWR most often occurring with DS, and SSR during SS. In contrast to SWR which most often co-occurred with frontal DS and US, Post-HC SSR were strongly phase-locked to SS in medial and lateral posterior parietal cortices. Our results suggest that replay events in human anterior hippocampus resemble those of rodents. In contrast, human posterior hippocampal ripples are embedded within spindles tightly coupled to specific cortical areas associated with recollective experience in neuroimaging and lesion studies. Human SWR, and any associated replay events, are separated by ~5s. In contrast, ripples on successive SSR peaks are separated by ~80ms, potentially supporting a different mode of plasticity leading to consolidation of specific details supporting conscious recollection.

Introduction:

Hippocampal sharpwave-ripples (HC-SWR) are striking complexes of local field potentials (LFP) recorded in the hippocampus during NREM sleep and rest periods (Buzsáki, 2015). HC-SWR consist of an initial negative component lasting 40-100 ms in the CA1 stratum radiatum, accompanied by a faster 110-200 Hz oscillation maximal in stratum pyramidale termed a "ripple" and typically followed by a ~200 ms duration positive wave in stratum radiatum. Pyramidal cell firing during HC-SWR tends to reproduce the spatio-temporal patterns established during the preceding active periods; this 'replay' is hypothesized to help guide cortical activity as it consolidates memories (Wilson and McNaughton, 1994; Skaggs and McNaughton, 1996; Nádasdy et al., 1999). Disruption of HC-SWR impairs memory consolidation (Girardeau et al., 2009; Maingret et al., 2016). The coordination of HC ripples with cortical consolidation is thought to be orchestrated by neocortical LFP graphoelements (NC-GE) such as sleep spindles (SS), down- and upstates (DS, US), and possibly theta bursts (TB) (Gonzalez et al., 2018). Specifically, in rodents, evidence suggests that coordination between HC-SWR and NC-SS (Siapas and Wilson, 1998; Sirota et al., 2003; Peyrache et al., 2009) and DS/US (Battaglia et al., 2004; Mölle et al., 2006; Headley et al., 2016) is central to replay (Diekelmann and Born, 2010; O'Neill et al., 2010; Girardeau and Zugaro, 2011).

HC-SWR have been extensively studied in rodents. However, two studies in macaques have confirmed the presence of HC-SWR during NREM sleep with the typical biphasic negative-positive waves in radiatum, and ~100 Hz ripples in pyramidale (Skaggs et al., 2007; Ramirez-Villegas et al., 2015). HC-SWR have also been observed in recordings from hippocampal electrodes implanted in humans to identify epileptogenic tissue. In a series of studies, Bragin described HC-SWR but mainly focused on the use of ripples to identify

epileptogenic tissue (Bragin et al., 1997, 1999; Staba et al., 2002). Axmacher (Axmacher et al., 2008) described HC ripples which occurred mainly in waking but were phase-locked to delta. Previously, we described typical SWR in human HC (Chapter 2).

Recently, Staresina (Staresina et al., 2015) reported that HC ripples in humans during NREM are tightly phase-coupled to hippocampal SS (HC-SS). HC-SS (without specific reference to ripples) were later reported to occur in both NREM and REM (Carpentier et al., 2017; Lestra et al., 2018). We will henceforth refer to ripples associated with HC-SS as hippocampal sleep spindle-ripples (HC-SSR). Staresina et al. suggested that HC-SS modulation of ripples could indicate their origin—and possibly function—being uniquely human, in contrast to HC-SWR in mammals; however, other interpretations of the data are possible. First, while not explicitly stated, their recordings were mainly in the posterior HC, whereas previous recordings were mainly in anterior where most of the human hippocampal volume lies (Destrieux et al., 2013). Thus, Staresina's findings could be reconciled with earlier studies if HC-SSR were specifically and/or mainly a property of posterior HC. Second, Staresina's recordings did not use a bipolar configuration within the hippocampus, but a referential recording to a somewhat distant location. While that is not likely to affect their ripple recordings, it is possible that their SS and US sometimes arose outside of the hippocampus (Mak-McCully et al., 2017). Third, it could be that both classical SWR and SSR exist within the HC, as well as transitional forms.

We report here that, indeed, both SWR and SSR exist in the HC, as do transitional forms. HC-SSR and HC-SS are largely confined to the posterior HC. The posterior hippocampal SSs tend to co-occur with NC-SS. Both HC-SSR and HC-SS are embedded in a sequence beginning with NC theta bursts, then downstates, spindles and upstates, in that order. Hippocampal and parietal spindles are initially incoherent but gradually achieve high levels of synchrony in about

2 cycles. Posterior HC-SS interacting in close synchrony with parietal NC-SS within the context of more widespread cortical rhythms provides another possible mechanism for hippocampo-cortical coordination of memory consolidation.

Methods:

Patient selection

20 patients with long-standing drug-resistant partial seizures underwent SEEG depth electrode implantation in order to localize seizure onset and thus direct surgical treatment. Patients were selected from a group of 54 as previously described (in Chapter 2) criteria for minimal pathology. The resulting group of 20 patients includes 6 patients with an HC contact in a location with no interictal spikes, which were used to guide the protocols applied to the remaining 14 patients. The 20 patients included 7 males, aged 29.8±11.9 years old (range 16-58). Electrode targets and implantation durations were chosen entirely on clinical grounds (Gonzalez-Martinez et al., 2013). All patients gave fully informed consent for data usage as monitored by the local Institutional Review Board, in accordance with clinical guidelines and regulations at Cleveland Clinic.

Electrode localization

After implantation, electrodes were located by aligning post-implant CT to preoperative 3D T1-weighted structural MRI with ~1mm^3 voxel size (Dykstra et al., 2012), using 3D Slicer (RRID:SCR_005619). This allows visualization of individual contacts with respect to HC cross-sectional anatomy, which was interpreted in reference to the atlas of Duvernoy (Duvernoy, 1988). The assignment of depth contacts to anterior or posterior hippocampus (Ant-HC/Post-HC) was made with the posterior limit of the uncal head as boundary (Poppenk et al., 2013; Ding and

Van Hoesen, 2015). Recordings were obtained from 32 HC contacts, 20 anterior (11 left) and 12 posterior (7 left). In 4 patients, HC recordings were bilateral (3 anterior and 1 posterior), and in 8 patients, ipsilateral anterior and posterior HC were both recorded. The distance of each hippocampal contact from the anterior limit of the hippocampal head was obtained in Freesurfer (RRID:SCR_001847). The CT-visible cortical contacts were then identified as previously described (see Chapter 2 Methods), in order to ensure that activity recorded by bipolar transcortical pairs is locally generated (Mak-McCully et al., 2015). Electrode contacts were rejected from analysis if they were involved in the early stages of the seizure discharge, had frequent interictal activity or abnormal spontaneous local field potentials. From the total of 2844 contacts implanted in the 20 patients, 366 transcortical pairs (18.3±4.7 per patient) were accepted for further analysis. Polarity of the pairs was adjusted if necessary to 'pial surface minus white matter' according to MRI localization, confirmed with decreased high gamma power during surface-negative downstates (see below).

Freesurfer (Dale et al., 1999; Fischl et al., 1999a, 2004) was used to reconstruct from individual MRI scans the cortical pial and inflated surfaces, as well as automatic parcellation of the cortical surface into anatomical areas (Desikan et al., 2006), after a sulcal-gyral alignment process. An average surface for all 20 patients was then generated to serve as the basis of all 3D maps. While each cortical SEEG electrode contact's location was obtained through direction correlation of CT and MRI as described earlier in this section, we obtained the cortical parcellation labels corresponding to each contact by morphing the Right-Anterior-Superior-oriented anatomical coordinates from individual surfaces to the average surface space (Fischl et al., 1999b). In addition, the nearest vertices on the average surface to the morphed coordinates would be identified for subsequent plotting of 2D projections onto the left lateral view (Figures 3

and 4). For the 2D projections only, to optimize visualization (i.e. minimize multiple contact overlap) while preserving anatomical fidelity, positions of contacts with significant HC-NC GE correlation were allowed to shift within a 5 mm radius. All visualizations were created with custom scripts in MATLAB 2016b.

Data collection and preprocessing

Continuous recordings from SEEG depth electrodes were made with cable telemetry system (JE-120 amplifier with 128 or 256 channels, 0.016-3000 Hz bandpass, Neurofax EEG-1200, Nihon Kohden) across multiple nights (see Table 2.3 in Chapter 2) over the course of clinical monitoring for spontaneous seizures, with 1000 Hz sampling rate. The total NREM sleep durations vary across patients; while some difference is expected given intrinsic variability of normal human sleep duration (Carskadon and Dement, 2010) and clinically assigned sleep deprivation, we also confirmed that the percentages of NREM in total sleep from 28 sleeps across 16 of our patients were comparable to (i.e. within 2 standard deviation of) normative data (Moraes et al., 2014) in terms of N2 and N3 durations. Recordings were anonymized and converted into the European Data Format (EDF). Subsequent data preprocessing was performed in MATLAB (RRID:SCR_001622); the Fieldtrip toolbox (Oostenveld et al., 2011) was used for bandpass filters, line noise removal, and visual inspection. Separation of patient NREM sleep/wake states from intracranial LFP alone was achieved by previously described methods utilizing clustering of first principal components of delta-to-spindle and delta-to-gamma power ratios across multiple LFP-derived signal vectors (Gervasoni et al., 2004; Jiang et al., 2017), with the addition that separation of N2 and N3 was empirically determined by the proportion of down-states that are also part of slow oscillations (at least 50% for N3 (Silber et al., 2007)), since

isolated down-states in the form of K-complexes are predominantly found in stage 2 sleep (Cash et al., 2009).

Hippocampal graphoelement selection

To identify hippocampal spindles, we applied a previously reported spindle detector (Mak-McCully et al., 2017) to hippocampal LFP signals from NREM: a 10–16 Hz bandpass was applied to the LFP data, and the analytic amplitude of the bandpassed signal was convolved with an average Tukey window of 600 ms. A channel-wise cutoff set at mean +2 s.d. was applied to identify local maxima that would be "peaks" of putative spindles, with spindle edges defined at 50 % of peak amplitude. The putative HC-SS segments were accepted for subsequent analyses if they were longer than 400 ms, had less than 14dB power in the nearby frequency bands (4-8 Hz and 18-30 Hz), and contained at least 3 unique oscillation peaks with 40-100 ms gaps. Hippocampal SWR were obtained as previously described (see Chapter 2), on the basis of 60-120 Hz power, number of distinct (at least 3) peaks in the HC LFP signal, and similarity to hand-marked non-epileptic exemplars. Prior to the SWR similarity evaluation, putative ripples were also examined for whether a given ripple center falls within a hippocampal spindle duration in the same signal; if positive, such ripples were then deemed SSR. Since a single ripple could qualify as both SWR and SSR, such a ripple would then be termed SXR where appropriate (e.g. Fig. 4.1).

Cortical graphoelement selection

Automatic cortical theta burst (TB) detection was performed as previously described (Gonzalez et al., 2018): a 5-9 Hz bandpass was applied to the LFP data, and a channel-wise cutoff set at mean +3 s.d. was applied to each channel's Hilbert envelope (smoothed with 300 ms Gaussian kernel) to identify local maxima that would be "peaks" of putative TBs, and make

start/stop edge cut-offs at mean +1 s.d.. The resulting TBs were only accepted for further analyses if their durations fall between 400 ms and 1000 ms, with their number-of-zero-crossings-based frequency estimate falling within the bandpass frequency range as well.

Automatic cortical spindle (SS) detection was performed in the same matter as previously described for hippocampal spindles. Downstates (DS) and upstates (US) were identified as follows: for each cortical LFP signal, a zero-phase eighth order Butterworth filter from 0.1 to 4 Hz was applied. Consecutive zero crossings of opposite slope separated by 250 to 3000 ms were then selected as delineating putative graphoelements. For each putative graphoelement, the amplitude peak between zero crossing was computed; only the top 10% of peaks were retained. The polarity of each signal was inverted if necessary to assure that DS were negative, as confirmed with a high gamma (70-190 Hz) power decrease exceeding 1 dB within ±250 ms of the negative DS peaks.

Experimental design and statistical analysis

All statistical tests below have $\alpha = 0.05$ post FDR-correction for multiple comparisons (Benjamini and Hochberg, 1995), unless otherwise specified.

Peri-stimulus time histograms were constructed for each NC-HC channel pair, separately for each graphoelement (GE; TB, SS, DS, and US), and for each sleep-stage (N2 or N3), each histogram comprising the occurrence times of a given NC-GE during the ±2s interval surrounding midpoints of HC-GE (i.e. HC-SSR and HC-SS, see Fig. 4.2 for examples). The significance of peaks and troughs in each histogram was tested by comparing them to distributions derived from histograms constructed under the null hypothesis of no relationship between the NC-GE and HC-GE using the following randomization procedure. Null-hypothesis histograms (N=1000) were constructed of NC-GE occurrences relative to a number of random

times equal to the number of HC-GEs. For each 200ms time bin with 100ms overlap comprising the 4-second trial duration, the actual counts are then compared to the distribution under the null hypothesis.

The latencies of the largest significant peaks identified in the individual histograms constructed as described above, were used to create summary histograms for each GE, sleep stage, and HC-GE origin in anterior versus posterior HC. These are plotted in Fig. 4.3 and Fig. 4.S3, and tabulated in Table 4.2. To test if, overall, a given type of cortical graphoelement significantly precedes or follows HC-GE, two-tailed binomial tests with chance probability of 0.5 were performed on the number of channel-pairs with peak latencies in the 2000 ms before vs the 2000 ms after the reference HC-GE. Since certain graphoelements, such as cortical theta, tend to yield peak latencies centered around zero, we also tested with Kolmogorov-Smirnov (KS) tests whether, overall, for a given NC-GE, the distribution of peak latencies significantly related to HC-GE differs from chance.

To evaluate the phase relationship between cortical and hippocampal spindle oscillations, we computed phase-locking values (PLV) (Lachaux et al., 1999) between each cortical and hippocampal channel pairing over 3-second trials centered on all hippocampal spindle event starts in NREM (N2+N3). Only hippocampal graphoelements that overlapped with cortical spindle for at least 160 ms were included. We also computed PLV for the same cortical-hippocampal channel pairs over the same number of trials centered on random times in NREM to create a baseline estimate, and for each non-overlapping 50ms time bin, a two-sample t-test was performed between the actual PLV and the baseline estimate, with the resulting p-values undergoing FDR correction. A given channel pair would be considered significantly phase-locking if: 1, more than 40 trials were used in the PLV computation, since small sample size is

known to introduce bias (Aydore et al., 2013); 2, at least 3 consecutive time bins yield post-FDR p-values below 0.05.

For intra-hippocampal coupling between ripple-frequency amplitude (70-100 Hz) and spindle (10-16 Hz) phase, we applied previously published methods for evaluating event-related phase-amplitude coupling (ERPAC) and estimating subsequently ERPAC significance over time from intracranial LFP data (Voytek et al., 2013). The events were NREM hippocampal spindle starts, and each ERPAC trial covers -1000 ms to +1500 ms peri-event. Each trial was also marked as either overlapping with NC-SS (by more than one spindle cycle) or not. Statistical evaluation of significant coupling was done using permutation tests that kept the actual analytic amplitude and phase values at each time point, but randomized the trial labels 1,000 times so that the amplitude values are matched to phase values from random trials. To generate the comodulogram in Fig. 4.1, we concatenated the hippocampal data across spindle events and applied previously published phase-amplitude coupling algorithm (Colgin et al., 2009) implemented within the Pactools software package (Tour et al., 2017) under Python 3.6 (RRID:SCR_008394).

In order to explore the anatomical distribution of NC-HC GE co-occurrences, we tested the following: 1. whether the distribution of significantly SSR- or HC SS-coupled NC sites was different from chance for a given HC site; 2. whether the significantly-different-from chance distributions of NC sites from 1 would also differ between Ant-/Post-HC site pairs; 3. whether the NC sites showing significant HC-NC correlation with one NC-GE type tended to also show correlation with another NC-GE type.

For 1, we performed a chi-square test of homogeneity for each HC site with regard to each GE, i.e. for a given patient with multiple NC sites, a 2 x N contingency table was made for

each NC site, N being the number of NC sites, one row of table containing the number of NC-GE overlapping with (i.e. occurring within 1500 ms of) HC-GE for each NC, the other containing the number of NC-GE that do not. A significant chi-square would therefore indicate a significant non-random distribution for that particular HC site and NC-GE type.

For 2, we performed Wilcoxon signed rank tests on the data obtained in 1 to evaluate whether for a given NC-GE type (for which 1 yielded significance for both members of an HC site pair), the proportions of GE from significantly coupled NC sites that overlapped with Ant-HC SSR/SS differ from the proportions for Post-HC SSR/SS. Each test required that both members of a HC site pair have a significant chi-square test result from 1.

For 3, we computed the correlation of HC-GE overlap rates for different NC-GE types, with each data point of the correlation derived from a different NC site. In addition, we computed across NC sites from all patients chi-square tests of independence for whether there could be a significant relationship between the anatomical distributions of different GE types' respective NC sites that significantly coupled to HC-SSR/HC-SS.

We further explored the spatial distribution of NC-HC relationship by tallying the proportion of significant HC-NC channel pairs across different NC regions, with respect to different NC-GE types and different HC-GE sources (Table 4.5, Table 4.S4). To characterize the apparent variability in Table 4.5, we performed 4-way ANOVAs to compare the main effects of GE type (TB, SS, DS, US), NREM stage (N2 vs. N3), Ant- or Post-HC origin of HC-GE, and NC ROIs (coverage listed in Table 4.S3) as well as the 2-way and 3-way interaction effects (Table 4.6, Table 4.S6). Similarly, given the lateralization of human hippocampal function, we were interested in examining whether ipsilateral HC-NC channel pairs would show different relationships from contralateral pairs across GE types, NREM stages, or NC ROIs. Due to a

sparse representation of contralateral channel pairs for individual ROIs, we calculated proportions for larger regions by combining both HC and NC sites: Ant-HC and Post-HC channels were combined into a single HC category, and the 10 NC ROIs used in previous analysis were collapsed into two: "fronto-central" and "non-frontal" (Table 4.S3). We then computed for each ROI the proportion of NC channels significantly coupled to HC-GE (Table 4.S5), and performed 4-way ANOVA as previously described, with the ipsilateral/contralateral factor replacing the Ant/Post-HC factor. All post-hoc analyses for both ANOVAs were performed with Tukey's range test. For each ANOVA, we checked the normality assumption by conducting the Lilliefors test on the residuals.

Results:

In this paper, we considered the hippocampal HC-SS and HC-SSR (HC-GE collectively) in humans, and their relationship to NC-GE. We noted above the study of Staresina which reported that human ripples occur within the context of spindles rather than sharpwaves in humans. We found that indeed, HC-SSR do occur in the human hippocampus, but they are preferentially located in the posterior HC sites (Fig. 4.1). Like HC-SWR (see Chapter 3), HC-SSR were strongly related to the NC-GE (Fig. 4.2, Fig. 4.3). The histograms and brain maps in Fig. 4.3 show a strong relationship in stage N2 between posterior HC-SS and NC-TB, DS, SS and US. The relative latencies are consistent with the order we have established in earlier studies of NC and thalamic GE (Mak-McCully et al., 2017; Gonzalez et al., 2018), i.e. TB→ DS→SS→US (Fig. 4.3, Fig. 4.4), and HC-SS tends to coincide with NC-SS (Fig. 4.4). Preferential co-occurrence, strong coherence, and phase-locking were noted between posterior HC-SS and NC-SS in the posterior parietal and retrosplenial cortices (Fig. 4.5, Fig. 4.6).

<u>Characterization of human HC-SS and SSR in NREM</u>

We identified human HC-SWR, SSR and SS from intracranial recordings and aligned them with simultaneously recorded cortical events in NREM sleep, in order to determine if their occurrences are related and have a consistent order, and whether their relations change between NREM stages N2 and N3, or between anterior and posterior HC sites. Morphologically normal ripples were isolated from >24 h continuous recordings in 20 stereoelectroencephalography (SEEG) patients with intractable focal epilepsy, with anterior (in 17 patients) and/or posterior HC contacts (in 11 patients), and related to sleep NC-GE in 12-30 bipolar recording channels per patient. Some ripples were found to co-occur with classical sharpwaves (Fig. 4.1*A*), and others did not (Fig. 4.1*B*). The latter could sometimes be observed as HC-SSR nestled within HC-SS (Fig. 4.1*C*-*F*), as previously reported (Staresina et al., 2015). Time-frequency analysis showed that, while HC-SWR tended to be surrounded by a broad-band power decrease, HC-SSR and HC-SS did not (Fig. 4.1*G*-*I*). Similar to NC-SS and HC-SWR, HC-SSR and HC-SS in humans were mostly absent in waking (Fig. 4.1*J*-*K*, Fig. 4.S1). However, HC-SSR and HC-SS did not appear to concentrate in NREM to the same extent as SWRs, in agreement with a recent report on human HC-SS in REM (Lestra et al., 2018). Time-frequency plots locked to HC spindle peaks yielded ripple power increases that appeared modulated by spindle frequency phase (Fig. 4.1*E*-*F*); this was further supported by intrahippocampal phase-amplitude coupling (Fig. 4.1*L*).

We found that, while HC sites produce both HC-SWR and HC-SS/HC-SSR (Table 4.1), the occurrence rates (#/min) of HC-SSR were remarkably lower than those of HC-SWR in Ant-HC (2.049 vs. 11.59 in N2, $p = 1.602 \times 10^{-7}$; 2.523 vs. 17.01 in N3, $p = 7.682 \times 10^{-8}$; two-tailed paired t-tests). No similar difference was observed for Post-HC, however (8.053 vs. 6.750 in N2, $p = 0.4911$; 10.00 vs. 10.71 in N3, $p = 0.8038$; two-tailed paired t-tests). HC-SSR tended to occur more often in Post-HC than in Ant-HC ($p = 0.0018$ in N2, $p = 0.0027$ in N3, two-tailed

two-sample t-tests), and this Post-HC preference was observed for HC-SS as well (2.758 / min in Ant-HC vs. 7.537 / min in Post-HC for N2, $p = 0.0002$; 3.318 in Ant-HC vs. 9.683 in Post-HC for N3, $p = 0.0004$; two-tailed two-sample t-tests) (Fig. 4.1*M-P*). Transitional forms ("SXR") that were detected as both SWR and SSR constituted a minority of SSR (21.4% in N2 Ant-HC, 26.9 % in N3 Ant-HC, 9.7% in N2 Post-HC, 13.0% in N3 Post-HC), and the proportion of SXR among SSR was greater in Ant-HC than in Post-HC ($p = 0.0045$ for N2, $p = 0.0060$ for N3, two-tailed two-sample t-tests), in line with the SWR rate reduction in Post-HC. Notably, while cortical spindles tend to occur more often in N2, we observed an increase in both HC-SS and HC-SSR in N3, and this increase was restricted to Post-HC only ($p = 0.0752$ and $p = 0.0857$ for Ant-HC SSR and SS, respectively; $p = 0.0088$ and 0.0061 for Post-HC SSR and SS, respectively; two-tailed paired t-tests).

Since HC-SS could co-occur with multiple ripples in different spindle cycles, as could be seen in Fig. 4.1*D*, we tallied the numbers of HC ripples within the duration of HC-SS in N2 and N3. We found in our data that up to 9 ripples could occur within one HC-SS in N2 (up to 10 in N3), although in both N2 and N3, only ~10% of the HC-SS had 3 ripples or more nestled within. Given the potential locality of HC ripples (Patel et al., 2013) and the SS phase modulation of high gamma amplitude (Fig. 4.1*L*), these ripple counts might be underestimates if each spindle cycle could contain a ripple. More than half (53% in N2, 57% in N3) of the HC-SS overlapped with at least one ripple from the same HC site, and this N2 vs. N3 percentage difference was significant (Fisher's exact test, $p < 2.20 \times 10^{-16}$). Among the population of HC-SS with at least one co-occurring ripple, 62% and 69% had more than one ripple within the SS duration for N2 and N3, respectively. Again, the N2 vs. N3 percentage difference was significant (Fisher's exact test, $p = 2.070 \times 10^{-12}$).

Co-occurrence of HC-SS and HC-SSR in anterior and posterior, or left and right HC

Although initial descriptions of SWR in rodents emphasized their co-occurrence throughout the entire extent of both hippocampi (Buzsaki et al., 1992), more detailed studies showed that isolated SWR are more common (Patel et al., 2013). The dominant and non-dominant hippocampal formations of humans are thought to be specialized for verbal and visuospatial memory, respectively (Gleiβner et al., 1998; Weber et al., 2006), which might predict distinct memory traces and thus low bilateral co-occurrence of HC-GE. Analogously, the extent to which HC-SSR and/or HC-SS co-occur within the same hippocampus and/or bilaterally ought to be investigated. We found that, for patients (n = 8) with both Ant-HC and Post-HC contacts in the same HC, the overlap (i.e. co-occurrence within 50 ms) between Ant-HC and Post-HC SSR was 1.6±1.8% in N2, and 1.7±2.3% in N3, compared to chance levels of 0.59±0.58% in N2 and 0.65±0.73% in N3. In both N2 and N3, the actual mean overlap percentage tended to be greater than the mean overlap percentage derived from chance, but not significantly so for N3 ($p = 0.0418$ and $p = 0.0674$, respectively; one-tailed paired t-tests). Similarly, the overlap between Ant-HC and Post-HC SS was significantly greater than chance in both N2 and N3 ($p = 0.0082$ and $p = 0.0188$, respectively; one-tailed paired t-tests); the mean percentages were 3.6±2.8% in N2, and 3.8±3.6% in N3, compared to chance levels of 0.61±0.37% in N2 and 0.79±0.61% in N3. We also evaluated HC-NC GE overlap in patients (n = 4) with bilateral (left and right) HC contacts, placed in either both anterior or both posterior HC. In these patients, co-occurrence of SSRs between HC in different hemispheres was minuscule: 0.38±0.49% in N2, and 0.73±0.86% in N3. This was much less than that usually observed between two contacts within the same HC, and not significantly greater than chance-derived overlap percentages (0.13±0.13% in N2, 0.30±0.21% in N3) for either N2 or N3 (p =

0.1673 and p = 0.1955, one-tailed paired t-tests). Co-occurrence of HC-SS was also rare but more frequent than that of HC-SSR: 1.1±0.73% in N2, and 0.90±0.56% in N3. These small percentages nonetheless tend to be greater than chance (0.40±0.31% in N2, 0.27±0.13% in N3), and significantly so in N2 (p = 0.036) but not in N3 (p = 0.0501, one-tailed paired t-tests). Thus, in humans, a small but significant proportion of HC-SSR and HC-SS co-occurs in both anterior and posterior hippocampal regions, and only a minuscule (but still greater than chance for HC-SS) proportion of HC-SS and HC-SSR co-occur in both left and right hippocampi, with the differences from chance being greater in N2 than in N3.

Furthermore, by varying the co-occurrence criterion range between 25 ms and 5000 ms, we observed greater-than-chance co-occurrence rates for Ant-HC and Post-HC SSR/SS (as well as for left and right HC SSR/SS) initially (Fig. 4.S2), but the actual co-occurrence rate tapered off exponentially (i.e. showed linear decay in log-log plots) towards chance level beyond 1000 ms. For bilateral HC, high variability in the ratio between actual and chance proportions (of overlapping HC-GE) was observed, likely due to the relatively small sample size.

Associations of cortical graphoelements with HC-SSR and HC-SS

In order to examine the relationship between HC graphoelements (HC-GE, i.e. SS and SSR) and cortical activity, different graphoelements (NC-GE, including theta bursts (TB), downstates (DS), upstates (US), and spindles (SS)) were identified in simultaneous recordings from neocortex (NC) in all lobes. These recording channels were differential derivations between adjacent contacts spanning the cortical ribbon, and were thus assured of being locally-generated. Detection algorithms have all been extensively validated in our previous studies (Mak-McCully et al., 2015, 2017; Gonzalez et al., 2018). To display the regularities in our data, we constructed histograms of the occurrence times of each NC-GE (TB onset, SS onset, DS peak, US peak)

between each pair of (non-epileptogenic) HC (n = 32) and NC (n = 366) channels (n = 20 patients). Separate analyses were carried out for stages N2 vs. N3, for HC-GE recorded in Ant-HC vs. Post-HC, and for HC-NC pairs in the same vs. opposite hemispheres.

Altogether, there were 598 unique HC-NC pairs (458 ipsilateral, 140 contralateral), and 16 histograms for each pair (one for each sleep stage, times each of the 4 GE types, for HC-SS or SSR), for a total of 9568 histograms. Overall, each of these histograms plots the occurrence times of 1386±2565 NC-GEs (+3.86 skewness) with respect to 861±1581 SSRs (+3.57 skewness) and to 1022±1642 HCSSs (+3.61 skewness); a total of 13.2 million NC-GE events, 4.12 million HC-SSR, and 4.89 HC-SS were plotted. Detailed breakdown of histogram contents by GE types and HC-GE sources (N2 vs. N3, Ant-HC vs. Post-HC, ipsilateral vs. contralateral) can be found in Table 4.S1. The striking positive skewness both in general and in specific categories (Table 4.S1) suggests that, in addition to high variability in co-occurrence rates of NC-GE with HC-SS and with HC-SSR, a small population of histograms may contain a disproportionately large number of NC and HC events. For both HC-SS and HC-SSR, across all NC-GE types, in both N2 and N3, the NC-HC associations appeared to be more frequently involving Post-HC than Ant-HC, as reflected in the elevation of NC-GE counts (Table 4.S1); this agrees with our earlier observation that HC-SS and HC-SSR predominantly occurred in Post-HC.

Of the 598 HC-NC channel pairs, 555 (93%) of all pairs (429 (94%) of the ipsilateral pairs and 126 (90%) of the contralateral pairs) had at least one histogram showing a significant relationship between the HC-GE and a NC-GE ($p<.0.05$ post FDR-correction, randomization test, see section “Experimental design and statistical analysis” in Methods). The percentages of significant ipsilateral and contralateral pairs were not significantly different (Fisher’s exact test, $p = 0.1888$). Of the entire set of 4784 histograms involving HC-SSR and NC-GE, 1247 (26%)

showed a significant association; for those involving HC-SS and NC-GE, 2033 (43%) showed a significant association, which is significantly greater than the proportion of histograms coupled to HC-SSR ($p = 1.385 \times 10^{-64}$, Fisher's exact test). The significant histograms (examples are shown in Fig. 4.2) include all types of NC-GE from channels across all cortical lobes. For HC-SSR, the peak of the histogram represented a mean increase of 157%, or median increase of 86.7% above baseline (measured as the mean height of non-significant bins), with standard deviation of 250%, and positive skew value of 6.40. For HC-SS, the peak of the histogram represented a mean increase of 147%, or median increase of 91.3% above baseline, with standard deviation of 220%, and positive skew value of 9.19. The large positive skew values indicate the presence of long right tails in the distributions of HC-SSR and HC-SS histogram peak elevations, i.e. the presence of a HC-NC channel pair population with much stronger HC-NC GE co-occurrence than other channel pairs.

We summarized these data further by constructing histograms of peak latencies from the histograms described above. Specifically, we determined the latency of peak occurrence rate relative to HC-SSR or HC-SS time for each significant HC-NC-GE histogram, and plotted these as a histogram for each NC-GE type, separately for N2 vs. N3 and Ant-HC vs. Post-HC (Fig. 4.3, Fig. 4.4, Fig. 4.S3, Fig. 4.S4). Each of the 16 histograms of histogram peaks (N2/N3 x Ant/Post x 4 NC-GE) for HC-SSR summarizes the significant latencies from 78±41 HC-NC channel pair histograms, comprising a total of $1.37 \times 10^5 \pm 1.45 \times 10^5$ HC-NC events (range 7.18×10^3-4.04×10^5). Each of the 16 histograms of histogram peaks for HC-SS summarizes the significant latencies from 126±63 HC-NC channel pair histograms, comprising a total of $2.46 \times 10^5 \pm 2.07 \times 10^5$ HC-NC events (range 1.24×10^4-6.23×10^5). As noted above, N2 and posterior

HC sites had more HC-SSR and HC-SS. Results were also summarized by plotting each cortical channel after morphing to a standardized brain (Fig. 4.3, Fig. 4.4, Fig. 4.S3, Fig. 4.S4).

In the summary histograms, significant temporal relationships were found between HC-SSR and each of the NC-GE types. As shown in Table 4.2, we tested for the presence of a significantly non-random distribution of NC-GE peak times with respect to HC-SSR (column 4), and found significant results for both N2 and N3, and both Ant-HC and Post-HC, for NC-SS and NC-US. NC-TB and HC-SSR were significantly related in N2, but not in N3, possibly due to NC-TB being more abundant and more related to NC-DS in N2 (Gonzalez et al., 2018). NC-DS and HC-SSR were significantly related in N2 for both Ant-HC and Post-HC, but only for Post-HC in N3, which may reflect the preference of HC-SSR to occur in Post-HC. Similarly, in the summary histograms, significant temporal relationships were found between HC-SS and each of the NC-GE types. We also tested for the presence of a significantly non-random distribution of NC-GE peak times with respect to HC-SS (column 8 in Table 4.2); we found significant results for both N2 and N3, and both Ant-HC and Post-HC, for NC-TB, DS, SS, and US.

We also examined if the peak latency in the summary histograms between HC-GE and NC-GE differed significantly from zero, and computed both the mean of the included HC-NC channel pairs (columns 5 and 9 of Table 4.2) and the center of a distribution fitted over the peak latencies (columns 6 and 10 of Table 4.2). With HC-SSR, significant effects were found for NC-TB in N2, which preceded HC-SSR by 398 ms (mean) or 741 ms (fitted). For Ant-HC in N2, NC-DS was significantly earlier than HC-SSR by 185 ms (mean) or 575 ms (fitted), while NC-SS and NC-US latencies were not significantly biased either way (i.e. earlier or later than HC-SSR). For Post-HC in both N2 and N3, NC-SS was significantly earlier than HC-SSR—by 211 ms (mean) or 353 ms (fitted) in N2, and by 241 ms (mean) or 425 ms (fitted) in N3—while NC-

DS was significantly earlier than HC-SSR by 288 ms (mean) or 489 ms (fitted) in N3, but not in N2. However, it should be noted that NC-DS distribution appeared bimodal for N2 Post-HC SSR (Fig. 4.3*B*), which likely distorted the mean and distribution peak estimations. The larger pre-trigger peak of the NC-DS latency distribution for N2 Post-HC SSR, like the NC-DS distribution peak in N3, preceded that of the NC-SS latency distribution (~700 ms pre-SSR for NC-DS vs. 353 ms for NC-SS). Thus, at least among the NC-GE that preceded HC-SSR, there appeared to be a reliable sequence of TB-DS-SS for both Ant-HC and Post-HC in N2. Similarly, for Post-HC in N3, the TB-DS-SS persisted. Finally, while NC-US were significantly coupled to HC-SSR across N2 and N3 for both Ant-HC and Post-HC, there were no significant biases to precede or follow HC-SSR, indicating that NC-US tended to co-occur with HC-SSR and were likely to be the last in the sequence of NC-GE types we observed, i.e. TB→ DS→SS→US. These observations are consistent with previously established order in earlier studies of NC and thalamic GE (Mak-McCully et al., 2017; Gonzalez et al., 2018).

HC-NC GE co-occurrence patterns are anatomically selective

Since several of our patients have HC contacts in both anterior and posterior parts of the same hippocampus, we investigated whether these HC sites have similar or different anatomical distributions over NC locations in terms of their preferred associations with different GE types. In particular, we asked the following: 1. whether the distribution of significantly SSR/HCSS-coupled NC sites was different from chance for a given HC site; 2. whether the significantly-different-from chance distributions of NC sites from 1 would also differ between Ant-HC and Post-HC site pairs; 3. whether the NC sites showing significant HC-NC correlation with one NC GE type tended to also show correlation with another NC GE type.

For 1, we performed a chi-square test of homogeneity for each HC site with regard to each GE, and we found that most of the HC sites were indeed coupled to NC-GEs with NC site distributions that significantly differ from chance in N2 (Table 4.3, Table 4.S2): out of 32 unique HC sites, 24 / 25 were coupled to non-homogeneous distributions of NC sites with significant TB to HC-GE relationships, respectively; similarly, 21 / 26 were coupled to NC-SS site distributions, 22 / 30 were coupled to DS distributions, and 21 / 28 were coupled to US distributions. In contrast, out of 32 x 4 = 128 distributions of NC channels showing NC-GE to HC-GE association in N3, only 43 were significantly different from chance for HC-SSR, and 61 were significantly different from chance for HC-SS. We further confirmed that the proportion of significant distributions were indeed significantly greater in N2 for both SSR and HC-SS (Fisher's exact tests, $p = 2.754 \times 10^{-8}$ for SSR, $p = 2.212 \times 10^{-10}$ for HC-SS).

For 2, we performed Wilcoxon signed rank tests on the data obtained in 1 to evaluate whether for a given GE type, the proportions of GEs from significantly coupled NC sites that overlapped with Ant-HC SSR/SS differ from the proportions for Post-HC SSR/SS. Each test required that both members of a HC site pair have a significant chi-square test result from 1. In total, 8 Ant-Post HC pairs were examined. We found that, for all the qualified Ant-Post HC pairs, the distributions of significantly associated NC channels for Ant-HC and for Post-HC differed significantly (Table 4.4).

For 3, we computed the correlation of HC GE overlap rates for different NC GE types, with each data point of the correlation derived from a different NC site. In addition, we computed across NC sites from all patients chi-square tests of independence for whether there could be a significant relationship between the anatomical distributions of different GE types' respective NC sites that significantly coupled to SSRs/HCSSs. Remarkably, for all GE type

pairs, strong correlations were found (Fig. 4.5*A*), and the chi-square tests in both N2 and N3 indicated that NC sites that tended to show significant temporal correlation with SSR/HC-SS for one NC-GE type also tended to associate with another NC-GE type (with the sole exception of TB vs. SS in N3 with HC-SSR): with regard to HC-SSR, for N2 and N3 respectively, we found $p = 0.0005$ and $p = 0.6642$ for TB vs. SS, $p = 4.319 \times 10^{-6}$ and $p = 6.885 \times 10^{-6}$ for TB vs. DS, $p = 1.538 \times 10^{-15}$ and $p = 2.775 \times 10^{-6}$ for TB vs. US, $p = 3.509 \times 10^{-5}$ and $p = 0.0094$ for SS vs. DS, $p = 0.0026$ and $p = 6.130 \times 10^{-5}$ for SS vs. US, $p = 2.506 \times 10^{-27}$ and 7.927×10^{-14} for DS vs. US. Similarly, with regard to HC-SS, for N2 and N3 respectively, we found $p = 2.589 \times 10^{-8}$ and $p = 3.742 \times 10^{-5}$ for TB vs. SS, $p = 5.242 \times 10^{-25}$ and $p = 6.132 \times 10^{-17}$ for TB vs. DS, $p = 2.675 \times 10^{-23}$ and $p = 5.475 \times 10^{-12}$ for TB vs. US, $p = 0.0053$ and $p = 4.782 \times 10^{-8}$ for SS vs. DS, $p = 0.0042$ and $p = 1.483 \times 10^{-13}$ for SS vs. US, $p = 6.153 \times 10^{-29}$ and 9.211×10^{-41} for DS vs. US.

Differences in NC-HC SSR relationship across NC regions, NREM stages, HC sites, and GEs

While the summaries in Figs. 4.3 and 4.4 and Tables 4.3, 4.4, and 4.5 gave us an overview of NC-GE and HC-GE relations, we noted that there appeared to be regional differences across NC in the strength of temporal correlations. We also considered the possibility that "hot spots" may exist in NC and contribute to the widespread positive skewness in the distributions of GE counts across individual NC-HC GE histograms (Table 4.S1). We therefore explored the spatial distribution of NC-HC relationship further by tallying the proportion of significant HC-NC channel pairs across different NC regions, with respect to different NC-GE types and different SSR/HC-SS sources (Table 4.5, Table 4.S4). We then performed two 4-way ANOVAs (one for SSR, another for HC-SS) to compare the main effects of NC-GE type (TB, SS, DS, US), NREM stage (N2 vs. N3), Ant- or Post-HC origin of HC-GE, and NC ROIs (Fig. 4.5*B*, coverage listed in Table 4.S3), as well as the 2-way and 3-way interaction effects. All post-

hoc analyses were performed with Tukey's range test. We checked the normality assumption by conducting the Lilliefors test on the residuals, and the null hypothesis of normality could not be rejected ($p = 0.2058$ for HC-SSR, $p = 0.0935$ for HC-SS). Both the ANOVA and post-hoc analyses' results (F-statistics and p-values) are summarized in Table 4.6.

For the ANOVA performed over proportions of NC channels showing significant NC-GE to HC-SSR temporal correlations, all 4 main effects were significant. The main effect for GE indicated that some NC-GE were more related to HC-SSR than others. Post-hoc analysis across NC-GE types showed that, while the mean proportions of SSR-responsive HC-NC channel pairs did not differ between NC-DS and NC-US, they did differ for the rest of NC-GE type pairs. The mean proportions were 0.1252 for TB, 0.2822 for SS, 0.3591 for DS, and 0.3874 for US; thus, TB and SS were related in a smaller proportion of NC sites to HC-SSR than DS and US were, and TB was less related to HC-SSR than SS overall. The significant main effect for NREM stage, together with mean proportions of 0.3784 for N2 versus 0.1985 in N3, suggested that more HC-NC channel pairs were significantly related to HC-SSR in N2 than in N3. The significant main effect of HC-SSR longitudinal origin, and together with mean proportions of 0.2152 for Ant-HC and 0.3617 for Post-HC, suggested that more of NC were related to Post-HC SSRs than to Ant-HC SSR, in line with our previous observation that the density of HC-SSR was much higher in Post-HC than in Ant-HC.

The significant main effect of NC ROIs indicated that different NC regions were coordinated with/by HC-SSR to different extents. When the sum of mean proportions (of NC channels significantly coupled to HC-SSR) across NREM stages and Ant/Post-HC for each ROI were computed, the NC region with the strongest HC-NC association appeared to be prefrontal, followed by cingulate, orbitofrontal, and medial occipito-parietal cortices; in contrast, lateral

occipital and lateral temporal regions had the least and second least sum, particularly in N3 (Fig. 4.5*C*). Post-hoc analysis across NC ROIs confirmed that, except for lateral temporal, the mean proportion for lateral occipital was significantly less than all other NC ROIs. Similarly, according to post-hoc analysis, the mean proportion for prefrontal ROI was not significantly different from cingulate, orbitofrontal, or medial occipito-parietal, but was significantly greater than the rest of the ROIs.

Except for GE * ROI, all 2-way interaction effects from the SSR ANOVA were significant. None of the 3-way interaction effects were significant. The lack of significance for GE * ROI interaction suggests that, overall, HC-NC association with respect to different NC-GE types tended to involve similar populations of NC channels; this agrees with our previous results regarding the significantly more than chance likelihoods of NC sites with multiple GE types showing association with HC-SSR, as well as the strong correlations in proportions of different types of NC-GE to co-occur with HC-SSR (Fig. 4.5*A*). However, one cannot exclude the possibility of specific ROIs being more involved with one type of NC GE-HC SSR association (e.g. NC-SS with HC-SSR) than other ROIs, as we shall demonstrate in subsequent analyses.

The interaction effect of GE * NREM stage indicated that certain NC-GE type could preferentially couple to HC-SSR in N2 and/or N3 compared to other NC-GE types. Post-hoc analysis revealed that, in N2, while the DS and US mean proportions were not significantly different from each other, they both exceeded TB and SS proportions significantly; in contrast, while N3 DS and US mean proportions still did not differ significantly, SS mean proportion in N3 also did not differ from those for DS/US. In both N2 and N3, TB mean proportions were significantly less than those for other NC-GE types.

The interaction effect of GE * HC-SSR longitudinal origin suggested that certain NC-GE types could be related to Ant-HC and Post-HC SSRs to different extents. When averaged across ROIs and separately for N2/N3, the proportions of significant HC-NC channel pairs were greater for Post-HC than for Ant-HC in all NC-GE types, except for TB in N3. For SS, in particular, Post-HC proportions were about twice as large as Ant-HC proportions in N2, and about three times as large in N3 (Fig. 4.5*E*). As expected, post-hoc analysis for GE * Ant-/Post-HC interaction supported the significant difference between Ant-HC and Post-HC proportions for SS, DS, and US ($p = 0.0001$), but not for TB.

The interaction effect of NREM stage * Ant-/Post-HC could be observed in Fig. 4.5*E* where, except for NC-TB (where Ant-HC proportion was greater than Post-HC), the degree to which Post-HC proportion was higher than Ant-HC appeared less in N2 compared to N3. Post-hoc analysis confirmed that the difference between Post-HC and Ant-HC proportions was significant in both N2 and N3, with the difference between Ant-HC and Post-HC means in N2 being greater than that in N3 (0.1841 vs. 0.1090).

Since the interaction effect of NREM stage * NC ROI is significant, certain NC regions could be more related to HC-SSR in N2 than in N3, or vice versa. Overall, the proportions of significant channels were greater in N2, especially in orbitofrontal and lateral temporal ROIs, while cingulate appeared to show the least N2/N3 difference (Fig. 4.5*C*). Post-hoc analysis showed that, as expected, orbitofrontal and lateral temporal ROIs had significantly greater mean proportions in N2 than in N3. Similarly, prefrontal, paracentral, and insula all had significantly greater mean proportions in N2, while the other (generally more posterior) ROIs showed no significant difference either way.

Given the interaction effect of Ant-/Post-HC * NC ROI, while both Ant-HC and Post-HC SSR appeared to engage the whole cortex (Fig. 4.2*A*, Fig. 4.3, Fig. 4.S3), some ROIs could preferentially communicate with Ant- or Post-HC compared to others. In fact, the mean proportions across ROIs appeared higher for Post-HC, only differing in the extent (Fig. 4.5*C*). Post-hoc analysis indicated that significant Ant/Post preference was present for cingulate, prefrontal, and medial occipito-parietal, but not for the other ROIs.

Differences in NC-HC SS relationship across NC regions, NREM stages, HC sites, and NC-GE types

We repeated the analysis described above for HC-SSR, but for HC-SS, and summarized the results below (with F-statistics and p-values in Table 4.S6). For the ANOVA performed over proportions of NC channels with significant NC-GE to HC-SS temporal correlation, all 4 main effects were significant. The main effect for GE suggested that some NC-GE were more related to HC-SS than others. Post-hoc analysis across NC-GE types showed that, while the mean proportions of HC-SS-responsive HC-NC channel pairs did not differ between DS and US or between TB and SS, they did differ for the rest of NC-GE pairs. The mean proportions were 0.3165 for TB, 0.3160 for SS, 0.5484 for DS, and 0.5658 for US; thus, TB and SS were related in a smaller proportion of NC sites to HC-SS than DS and US were. The main effect for NREM stage, together with mean proportions of 0.5507 for N2 versus 0.3226 in N3, suggested that more HC-NC channel pairs were significantly related to HC-SS in N2 than in N3. The main effect of HC-SS longitudinal origin, and together with mean proportions of 0.3826 for Ant-HC and 0.4907 for Post-HC, suggested that more of NC were related to Post-HC SS than to Ant-HC SS, in line with our previous observation that the density of HC-SS was much higher in Post-HC than in Ant-HC (Fig. 4.1*M-N*). All the above effects were comparable to their counterparts in the

previous ANOVA regarding HC-SSR, with the exception that NC-SS were significantly more related to HC-SSR than NC-TB were, but no such significant difference was observed for HC-SS overall. Thus, HC-SSR could involve a subset of HC-SS with preferential coupling to NC-SS.

The main effect of NC ROIs indicated that different NC regions were coordinated with/by HC-SS to different extents. When the sum of mean proportions (of NC channels significantly coupled to HC-SS) across NREM stages and Ant/Post-HC for each ROI were computed, the NC regions with the strongest HC-NC relationship appeared to be cingulate; in contrast, lateral occipital had the least sum (Fig. 4.5*D*). Post-hoc analysis across NC ROIs confirmed that, except for medial temporo-occipital and insula, the mean proportion for lateral occipital was significantly less than all other NC ROIs. Similarly, according to post-hoc analysis, the mean proportion for cingulate ROI was not significantly different from orbitofrontal or prefrontal, but was significantly greater than the rest of the ROIs. These results agree with their counterparts from the HC-SSR ANOVA, where lateral occipital was also found to be the least involved in HC-NC association, and prefrontal, cingulate, and orbitofrontal were found to be the most involved.

Out of the six 2-way interaction effects from the HC-SS ANOVA, half were significant (GE * Ant-HC/Post-HC, GE * ROI, NREM stage * ROI), and the other half were not (GE * NREM stage, NREM stage * Ant-HC/Post-HC, Ant-HC/Post-HC * ROI). The lack of significance for GE * NREM stage interaction suggests that, overall, HC-NC association with respect to different NC-GE types tended to be consistent across N2 and N3. Indeed, regardless of NC-GE type, more NC channels show NC-GE co-occurring with HC-SS in N2 than in N3 (Fig. 4.5*F*). The lack of significance for NREM stage * Ant-HC/Post-HC interaction suggests that, overall, NC association with Ant-HC and with Post-HC was consistent across N2 and N3. This

can be observed in Fig. 4.5*F* for NC-TB and NC-SS, where the relative differences between mean proportions of NC channels significantly coupled to Ant-HC and those of NC channels coupled to Post-HC were not apparently different; however, the Ant-HC/Post-HC differences appeared exaggerated in N3 compared to N2 for NC-DS and NC-US. Thus, a mixture of trends across NC-GE types may have contributed to the weak NREM stage * Ant-HC/Post-HC interaction effect. The lack of significance for Ant-HC/Post-HC * ROI indicates that HC-NC association across ROIs for Ant-HC resembled that for Post-HC regarding HC-SS, despite the higher density of Post-HC SS compared to Ant-HC SS. One could thereby propose that the relative rarity of HC-SS in Ant-HC might not preclude their importance.

The interaction effect of GE * Ant-HC/Post-HC indicated that certain NC-GE types could be related to Ant-HC and Post-HC SS to different extents. When averaged across ROIs and separately for N2/N3, the proportions of significant HC-NC channel pairs were greater for Post-HC than for Ant-HC for NC-SS in both N2 and N3, for DS in N3, and for US in N3. For NC-SS, in particular, Post-HC proportions were about twice as large as Ant-HC proportions in N2, and more than twice as large in N3 (Fig. 4.5*G*). As expected, post-hoc analysis for GE * Ant-/Post-HC interaction supported the significant difference between Ant-HC and Post-HC proportions for SS. In addition, significant difference was found for DS, but not for TB or US.

Given the significant interaction effect of GE * ROI, certain NC-GE types could be related to different NC ROIs more or less often than other NC-GE types. The insula, for instance, had greater proportions of channels showing DS to HC-SS and US to HC-SS associations (mean proportions across Ant-HC/Post-HC and N2/N3 of 0.5833 and 0.3485, respectively) than TB to HC-SS and NC-HC SS associations (mean proportions of 0.2197 and 0.1742, respectively). Post-hoc analysis showed that, indeed, several ROIs were showing preferential associations of certain

NC-GE types with HC-SS, e.g. DS and US were significantly preferred over NC-SS to associate with HC-SS for lateral temporal, among others.

The interaction effect of NREM stage * NC ROI indicated that certain NC regions could be more related to HC-SS in N2 than in N3, or vice versa. Overall, the proportions of significant channels were greater in N2, especially in orbitofrontal and insula ROIs, while cingulate and lateral occipital appeared to show the least N2/N3 difference (Fig. 4.5*D*). Post-hoc analysis showed that, as expected, orbitofrontal and insula ROIs had significantly greater mean proportions in N2 than in N3. Lateral temporal, prefrontal, paracentral, and lateral parietal ROIs all had significantly greater mean proportions in N2, while the other ROIs showed no significant difference either way. Notably, for both HC-SSR and HC-SS ANOVAs, regarding the interaction effect of NREM stage * NC ROI, all ROIs involving occipital cortices (medial temporo-occipital, medial occipito-parietal, and lateral occipital) showed consistent associations with HC across N2 and N3, while orbitofrontal, prefrontal, paracentral, lateral temporal, and insula ROIs showed preferential associations in N2.

Among the 3-way interaction effects, the following two were significant: GE * NREM stage * Ant-/Post-HC, and NREM stage * Ant-/Post-HC * NC ROI. GE * NREM stage * Ant-/Post-HC interaction was present in Fig. 4.5*F*, where e.g. N2 Post-HC dominated for NC-SS relations, and N3 Ant-HC was low for both DS and US. Post-hoc analysis confirmed that the mean proportion of NC channels with significant HC-NC SS associations was greater for N2 Post-HC than for the three other HC-SS sources. Similarly, DS and US were much less likely to associate with HC-SS from N3 Ant-HC than with those from other sources. NREM stage * Ant-/Post-HC * NC ROI interaction was in line with Fig. 4.5*D*, where N2 Post-HC proportion was dominant in some ROIs (e.g. orbitofrontal), while others appeared more balanced (e.g. cingulate,

lateral occipital). Post-hoc analysis revealed a more complicated picture, with no ROI showing significantly more association with one HC-SS source over all others (e.g. N2 Post-HC over N2 Ant-HC, N3 Ant-HC, and N3 Post-HC), but some ROIs comes close (e.g. orbitofrontal, $p = 0.1354$ for N2 Post-HC vs. N2 Ant-HC, $p = 1.138 \times 10^{-5}$ for N2 Post-HC vs. N3 Ant-HC, and $p = 4.444 \times 10^{-6}$ for N3 Post-HC). On the other hand, cingulate and lateral occipital ROIs did turn out as expected, i.e. no significant differences in HC-NC associations across N2/N3 and Ant-/Post-HC; medial temporo-occipital was similarly unaffected.

Relationships between NC-GE and HC-GE in ipsilateral versus contralateral HC-NC channel pairs

Given the well-known lateralization of human hippocampal function (Weber et al., 2006; Iglói et al., 2010), we were interested in examining whether ipsilateral HC-NC channel pairs would show different relationships from contralateral pairs across NC-GE types, NREM stages, or NC ROIs. Due to a sparse representation of contralateral channel pairs for individual ROIs, we combined the 10 NC ROIs used in previous analysis into two: “fronto-central”, which included the previous cingulate, orbitofrontal, prefrontal, and paracentral ROIs; and “non-frontal”, which included the previous lateral temporal, medial temporo-occipital, medial occipito-parietal, insula, lateral occipital, and lateral parietal ROIs. We then computed for each ROI the proportion of NC channels significantly coupled to HC-SSR/HC-SS (Table 4.S5) and tallied the numbers of NC channels with or without significant HC-NC associations for each NC-GE type across N2 and N3 (Table 4.7).

We checked the normality assumption for ANOVA by conducting the Lilliefors test on the residuals; while the null hypothesis of normality could not be rejected for HC-SS ($p = 0.5000$), the null hypothesis was rejected for SSR ($p = 0.0030$). Nevertheless, we could observe

in Table 4.7 a consistent reduction in the proportions of NC channels showing significant temporal correlation with HC-SSR, by 13-45% for each NC-GE type (separately in N2 or N3) from ipsilateral to contralateral, with NC-TB in N3 showing the least drop and DS in N2 showing the most. Similarly, for HC-SS, we observed a consistent reduction across NC-GE types in both N2 and N3; with the exception of NC-TB in N3 (40% drop for HC-SS vs. 13% for HC-SSR), the ipsilateral-to-contralateral drop (11-20%) in HC-NC association proportions was smaller with respect to HC-SS than to HC-SSR. This suggests that spindle phase-modulated HC-NC communication preferentially take place ipsilaterally, and our subsequent phase-amplitude coupling analyses appeared to support this (Fig. 4.6), as we would describe in detail later in the Results.

We performed 4-way ANOVA as previously described for NC-GE to HC-SS associations, with the ipsilateral/contralateral factor replacing the Ant-/Post-HC factor. All post-hoc analyses were performed with Tukey's range test. All 4 main effects were significant, but none of the interaction effects were. As our previous ANOVA already revealed significant main effects for NC-GE type and NREM stage, we focused our attention on the remaining two factors (i.e. ipsilateral/contralateral and combined NC ROI), which substantially differed from those for the previous ANOVA. The main effect of ipsilateral/contralateral channel pair types yielded $F = 12.55$, $p = 0.0383$. and together with mean proportions of 0.454 for ipsilateral and 0.400 for contralateral, suggested that more of NC were related to ipsilateral HC-SS than to contralateral HC-SS, although the difference was modest. The main effect of ROIs yielded $F = 28.90$, $p = 0.0126$. Since only two ROIs were included in this ANOVA, this result suggested that the more frontal/cingulate parts of NC were significantly more likely to show significant associations

between NC-GE and HC-SS than the posterior regions (mean proportion of 0.468 for fronto-central versus 0.386 for non-frontal).

HC-SS phase-lock to NC-SS and modulate ripple-frequency activity

A previous report of human HC-SS suggested that scalp-recorded NC-SS could phase-lock with HC-SS, which modulated ripple activity (Staresina et al., 2015). We observed earlier in the results that hippocampal ripples could indeed co-occur with and appeared modulated by HC-SS (Fig. 4.1*C*, *D*, *L*), and we found widespread NC channels showing significant NC-HC SS temporal correlations, particularly in N2 with respect to Post-HC (Fig. 4.4*B*, Fig. 4.5*F*). To further evaluate spindle-mediated HC-NC coupling, we computed phase-locking values over 3-second trials where NC-SS overlapped with HC-SS for at least one cycle (examples shown in Fig. 4.6*A*), and computed event-based ("events" being HC-SS) phase-amplitude coupling within Ant-HC or Post-HC using HC-SS from all patients in NREM (N2+N3) (Fig. 4.6*D*). After PLV computation, for each non-overlapping 50ms time bin, a two-sample t-test was performed between the actual PLV and the baseline estimate, with the resulting p-values undergoing FDR correction. A given HC-NC channel pair would be considered significantly phase-locking if: 1, more than 40 trials were used in the PLV computation, since small sample size is known to introduce bias (Aydore et al., 2013); 2, at least 3 consecutive time bins yield post-FDR p-values below 0.05. We found that significant HC-NC SS phase-locking (over 10-16 Hz, with maximum PLV ranging from 0.3 to 0.9) could be found across widespread NC regions (Fig. 4.6*B*, *C*; Fig. 4.S5), and maximum PLV tended to be reached at ~300-700 ms after HC-SS onsets.

We observed a higher density of NC channels showing significant PLV with Post-HC than with Ant-HC. In particular, 37% of NC channels phase-locked with HC, and out of this channel population, 67% phase-locked with Post-HC in N2, and 70% in N3. For both N2 and

N3, this Post-HC preference among NC channels with significant SS PLV was significant (Fisher's exact tests, $p = 4.991 \times 10^{-9}$ for N2, $p = 2.377 \times 10^{-7}$ for N3). While HC-NC SS phase-locking was observed across NC, only a small proportion had sustained large PLV (e.g. rightmost panel of Fig. 4.6*A*). Specifically, only 3% of all NC channels had a peak HC-NC SS PLV value above 0.5; in this small population of high PLV channels, ~70% were parietal (an even mix of precuneus/superior parietal and inferior parietal lobule). In addition, for patients with both Ant-HC and Post-HC contacts in the same hippocampus, NC channels phase-locked to Post-HC tended not to show significant phase-locking with Ant-HC as well (e.g. Fig. 4.6*A*), suggesting that HC-NC coupling mediated by spindle phase could be strongly localized along the HC longitudinal axis, which appears in agreement with the rare overlap between Ant-HC and Post-HC SSR/SS reported in the beginning of the Results section.

Remarkably, for the population of NC channels from the 8 patients with multiple HC contacts in the same hippocampi, 15 out of 16 (94%) NC channels showing significant SS phase-locking with Ant-HC also phase-lock with Post-HC significantly in N2, while conversely only 15 out of 43 (35%) NC channels showing significant SS phase-locking with Post-HC also phase-lock with Ant-HC; in N3, this Ant/Post imbalance in percentages of concurrently coupled NC sites was preserved (7 out of 10 (70%) with Ant-HC vs. 7 out of 24 (29%) with Post-HC). Thus, if Ant-HC phase-locks with an NC site, then Post-HC does also, but not *vice versa*.

Strong ipsilateral preference for phase-locked HC-NC channel pairs was also observed in the patients with bilateral Post-HC contacts, with example PLV plots shown in Fig. 4.6*A*, where the right precuneus preferentially coupled with right Post-HC. Within the channel pairs showing significant SS PLV involving Ant-HC, in N2, only 5% were contralateral (thus 95% were ipsilateral); in N3, all of the channel pairs with significant PLV involving Ant-HC were

ipsilateral. Similarly, for phase-locking channel pairs involving Post-HC, 89% were ipsilateral in N2, and 90% were ipsilateral in N3. This strong preference for ipsilateral HC-NC SS phase-locking is larger than the preference for ipsilateral co-occurrence of HC-SS and HC-SSR with NC-GE described above.

Finally, we computed intra-hippocampal event-related phase-amplitude coupling (ERPAC) between spindle (10-16 Hz) phase and ripple (60-120 Hz) amplitude, using previously published methods (Voytek et al., 2013). All HCSSs in NREM across all patients were included in the computation, separated by longitudinal origin (Ant-HC/Post-HC), with aligned events being HCSS starts. As we expected from Fig. 4.1*L* earlier, we found significant event-related modulation of hippocampal ripple amplitude by HC-SS phase (Fig. 4.6*D*), with the effect being much more prominent in Post-HC (two-tailed paired t-test over mean ERPAC values from 0 to 1000 ms post-trigger, $p < 2.20 \times 10^{-16}$, Cohen's $d = 1.74$).

Discussion:

In this study, our investigation began with a previously published claim that HC-SSR—i.e. ripples co-occurring with human hippocampal spindles (HC-SS)—represented a uniquely human phenomenon that could play a similar role in memory consolidation as sharpwave-ripples (HC-SWR) in animals (Staresina et al., 2015). We noted, however, that Staresina *et al*.'s site selection criteria resulted in their (unremarked) concentration of recordings from the posterior hippocampus (Post-HC) which may not be typical of the human HC, whose volume is predominantly anterior (Poppenk et al., 2013). In addition, anterior and posterior HC are quite distinct in their external connections (Strange et al., 2014). Based on our previous work where typical HC-SWR were demonstrated with an anterior hippocampus (Ant-HC) preference (see Chapter 2), we propose an alternative interpretation wherein both HC-SWR and HC-SSR exist,

but are concentrated in anterior and posterior HC (Post-HC), respectively. We confirm that hypothesis here, and demonstrate properties of Post-HC SSR which may distinguish its contribution to memory consolidation.

The presence of human HC-SS itself was known from early intracranial studies (Montplaisir et al., 1981) and was considered possibly pathological. However, their non-epileptic nature was supported by subsequent reports of HC-SS in animals (Siapas and Wilson, 1998; Sirota et al., 2003; Miyawaki and Diba, 2016), human NREM (Malow et al., 1999; Andrillon et al., 2011; Carpentier et al., 2017), and, surprisingly, REM sleep (Lestra et al., 2018)—as we also observed (Fig. 4.1). Given the prominent presence and functional relevance of sleep spindles (SS) in the neocortex (NC) in NREM sleep (Mednick et al., 2013), particular in stage 2 (N2) for humans (Niknazar et al., 2015), the modulation of HC activity by HC-SS and HC-NC SS coordination constitute a candidate mechanism for HC-NC information transfer, as proposed by Staresina *et al*., among others (Siapas and Wilson, 1998; Sirota et al., 2003; Staresina et al., 2015). While our results do provide further evidence for the importance of SSR/HC-SS coordination with NC-SS, we also report for the first time the relative dearth of SSR/HC-SS in human Ant-HC, and offer further electrophysiological characterizations that set SSR apart from SWR, particularly in terms of LFP event morphology (Fig. 4.1) and preferential association with posterior cortices (Fig. 4.5, 4.6).

Animal studies indicated a present but not well defined temporal relationship between HC-SWR and NC-SS; while SS could reach the hippocampus via entorhinal cortex and phase-modulate HC firing (Sirota et al., 2003; Isomura et al., 2006), HC-SWR were typically found to precede NC spindles (Siapas and Wilson, 1998; Peyrache et al., 2011). In addition, different NC-SS and HC-SWR origins might predicate different temporal (and by extension functional)

relationship (Buzsáki, 2015). From our results concerning the SSR/HC-SS as HC events distinguishable from SWR in morphology and distribution, we propose an alternative resolution where HC-SWR tend to precede NC-SS (see Chapter 3) and SSR/HC-SS tend to co-occur with NC-SS (Fig. 4.3, 4.4). In support of this, we would like to note that methodology of earlier reports on HC ripples being modulated by either HC or NC-SS tends to rely on high-frequency power alone and to lack verification of ripples co-occurring with sharpwave waveform, thereby likely permits mixed population of SWR and SSR in analyses. (Sirota et al., 2003; Wierzynski et al., 2009; Staresina et al., 2015; Maingret et al., 2016; Latchoumane et al., 2017).

Clemens *et al*. (Clemens et al., 2011) reported that ripples (including both interictal spikes as well as physiological activity) recorded medially to the parahippocampal gyrus are phase modulated by parietal scalp spindles. Similarly, Staresina *et al*. (Staresina et al., 2015) found a 5% increase in HC ripple band power +/-250ms to Cz SS center. However, the current report appears to be the first to provide the first direct electrophysiological evidence of human HC-NC-SS phase-locking. HC and parietal spindles may become phase-locked via the direct anatomical connections from CA1 to area 7a, demonstrated in primates (Clower et al., 2001). Although pulvinar spindles drive posterior parietal in humans (Mak-McCully et al., 2017), it is the nucleus reuniens which projects to the HC in primates (Amaral and Cowan, 1980). In humans, spindles modulate cortical firing (Hagler et al., 2018), synergistically with the increase associated with the upstate that they ride (Csercsa et al., 2010; Mak-McCully et al., 2017; Gonzalez et al., 2018). In rodents, spindles themselves (Seibt et al., 2017), and especially those riding on upstates (Niethard et al., 2018), are associated with strong Ca^{2+} influx in NC pyramidal cell apical dendrites, presumably supporting the plasticity observed during these waves (Steriade and Timofeev, 2003). Behavioral consolidation in rodents has been found to depend on NC

spindles and down-upstates, coupled with each other and with HC-SWR (Maingret et al., 2016; Latchoumane et al., 2017). Similarly, scalp SS and SS-US complexes are associated with consolidation in humans (Marshall et al., 2006; Mednick et al., 2013; Niknazar et al., 2015).

The distinctive behavioral contributions of the ventral vs. dorsal HC in rodents, or Ant-HC vs. Post-HC in humans, have been characterized in multiple ways. In rodents, ventral HC lesions impair contextual emotional learning, consistent with its connections with amygdala, orbitofrontal, and hypothalamic areas, whereas dorsal lesions impair spatial learning, consistent with its connections with retrosplenial and parietal areas (Fanselow and Dong, 2010). Although ventral HC neurons also exhibit place fields, they are less frequent and larger than dorsal HC (Strange et al., 2014), and the relatively decreased dentate gyrus presence in ventral HC is consistent with coarser pattern separation (Poppenk et al., 2013). The anatomical contrasts between ventral and dorsal HC in rodents have been confirmed with resting state BOLD connectivity measures (Ranganath and Ritchey, 2012). The functional imaging studies are generally consistent with greater involvement of anterior HC in learning the gist of events, and posterior the details, a characterization perhaps consistent with the broader encoding by its cells in rodents (Poppenk et al., 2013; Strange et al., 2014).

The preponderance of SSR in the posterior HC has not been reported in rodents. Indeed, if anything, SWR are more dense and stronger in dorsal than ventral rodent HC (Patel et al., 2013). This raises the possibility that Post-HC SSR are a species-specific phenomenon in humans. In this context, it is interesting that the cortical areas (angular g., precuneus, and retrosplenial cortex) strongly phase-locked with Post-HC SSR, as well as the HC itself, are all associated with episodic memory, which Tulving (Tulving and Markowitsch, 1998) has argued is unique to humans. Lesions restricted to the HC but sparing adjoining temporal cortical areas

severely impair episodic memory while allowing declarative memories to be formed (Vargha-Khadem et al., 1997). Similarly, angular gyrus lesions impair recollective experience without necessarily impairing familiarity judgements (Papagno, 2018). Recollective experience is correlated with PET and fMRI activation in these areas (Gilmore et al., 2015), as well as unit-increases (Rutishauser et al., 2017). This has been interpreted as indicating a role of 7a+ in directing attention (Davis et al., 2018), or in actually storing details of the memories (Rugg and King, 2018). Recollection is also associated with a late parietal positive event-related potential, which is dependent on HC integrity (Smith and Halgren, 1989), and correlated across trials with Post-HC and retrosplenial BOLD activation (Hoppstädter et al., 2015). HC stimulation can induce intense feelings that current experience is being re-lived (*déjà vu*) as well as vivid recollections of previous experiences (Halgren et al., 1978; Curot et al., 2017).

The ratio of hippocampal to neocortical pyramidal cells is ~1:33 in rats, and ~1:2246 in humans (Korbo et al., 1990; West and Gundersen, 1990; West et al., 1991; Pakkenberg and Gundersen, 1997). Yet, a central feature of HC-dependent memory is its ability to unify arbitrary elements, and this is presumed to require the HC to interact with all or most of the NC (McNaughton, 2010). Indeed, we have shown that the HC-SWR co-occur with NC-SS/US across widespread cortical areas in all lobes. Furthermore, HC-SWR only occur ~12 times per minute, and thus most cortical activity would develop in the absence of HC input. Nonetheless, HC-SWR tend to occur at the time of the NC-DS, i.e., at the beginning of the NC-SS and US, and thus can set the stage for subsequent elaboration of the NC↔NC network. Thus, the wide HC→NC fanout and low HC-SWR density as well as its timing, might be expected to limit the influence of HC input to setting the general context of with respect to NC network evolution rather than its precise content.

In contrast to Ant-HC SWR, Post-HC SSR produce multiple ripple bursts to a focal cortical target during the process of NC cell-assembly. We found that multiple ripples commonly occur over the course of a single Post-HC SWR, with their centers separated by ~80ms, compared to HC-SWR which are separated by ~5s. Furthermore, in contrast to the co-occurrence of HC-SWR with widespread NC areas, Post-HC SSR have a very high level of phase-locking with a relatively highly restricted target in area 7a. Finally, the Post-HC SSR provides input over a sustained period to the NC, during the SS-US, as opposed to a single punctate input from HC-SWR at the beginning of the SS-US. Thus, while the HC-SWR input is well-suited to provide guiding input to widespread NC areas comprising the "gist" of a recent event, the Post-HC SSR may be better suited to impress specific details through repeated inputs to focal NC areas.

Chapter 4, in full, is currently being prepared for submission for publication of the material. Jiang, Xi; Gonzalez-Martinez, Jorge; Halgren, Eric. The dissertation author was the primary investigator and author of this paper.

Figure 4.1: Hippocampal spindles (HC-SS) co-ordinate ripples and are found predominantly in posterior HC. ***A***-***B***. Overlaid average waveforms of HC-SWR (***A***) and of ripples not coupled to sharpwaves (***B***) across hippocampal contacts from different patients, with one representative patient bolded in black for clarity. ***C***. Example LFP trace of a ~14 Hz HC-SS (red section), bipolar recording in the posterior HC. ***D***. Expanded time-base plot of the spindle shown in ***C***; a 80-90 Hz ripple occurs preferentially at some peaks of the spindle waves. ***E***. Example averaged time-frequency plot triggered on the center peak of HC-SS from the same channel in ***C*** (n=1086). ***F***. The average LFP of events in ***E***. ***G***-***I***. Event-related spectral power is contrasted for SWR (***G***), SSR (***H***), and SS (***I***) from the same HC site, with corresponding average LFP traces below the time-frequency plots. The high frequency ripple burst is seen for SWR and SSR but not prominently so in SS. Prolong spindle activity is seen for SSR and SS but not SWR. ***J***-***K***. Example state plots showing the separation of NREM sleep from waking/REM in ~8-hour LFP recording, using the first principal component derived from vectors (one per cortical bipolar SEEG channel) of frequency power ratios (0.5-3 Hz over 0.5-16 Hz) (Gervasoni et al., 2004; Jiang et al., 2017). SWR rate (***J***) and SSR rate (***K***) are color coded with red intensity, and N2/N3 periods are marked with orange/green horizontal lines, respectively. Light blue arrow marks the beginning of NREM sleep. ***L***. Phase-amplitude coupling within HC between HC-SS phase and ripple amplitude (bandpassed between 50 and 150 Hz). ***M***-***P***. Distribution of HC-SS and HC-SSR occurrence rates in different NREM stages across the HC longitudinal axis. Each circle represents data from one hippocampal contact. Red circles indicate contacts in Ant-HC; blue circles indicate those in Post-HC. Yellow highlights mark the contacts from interictal-free patients.

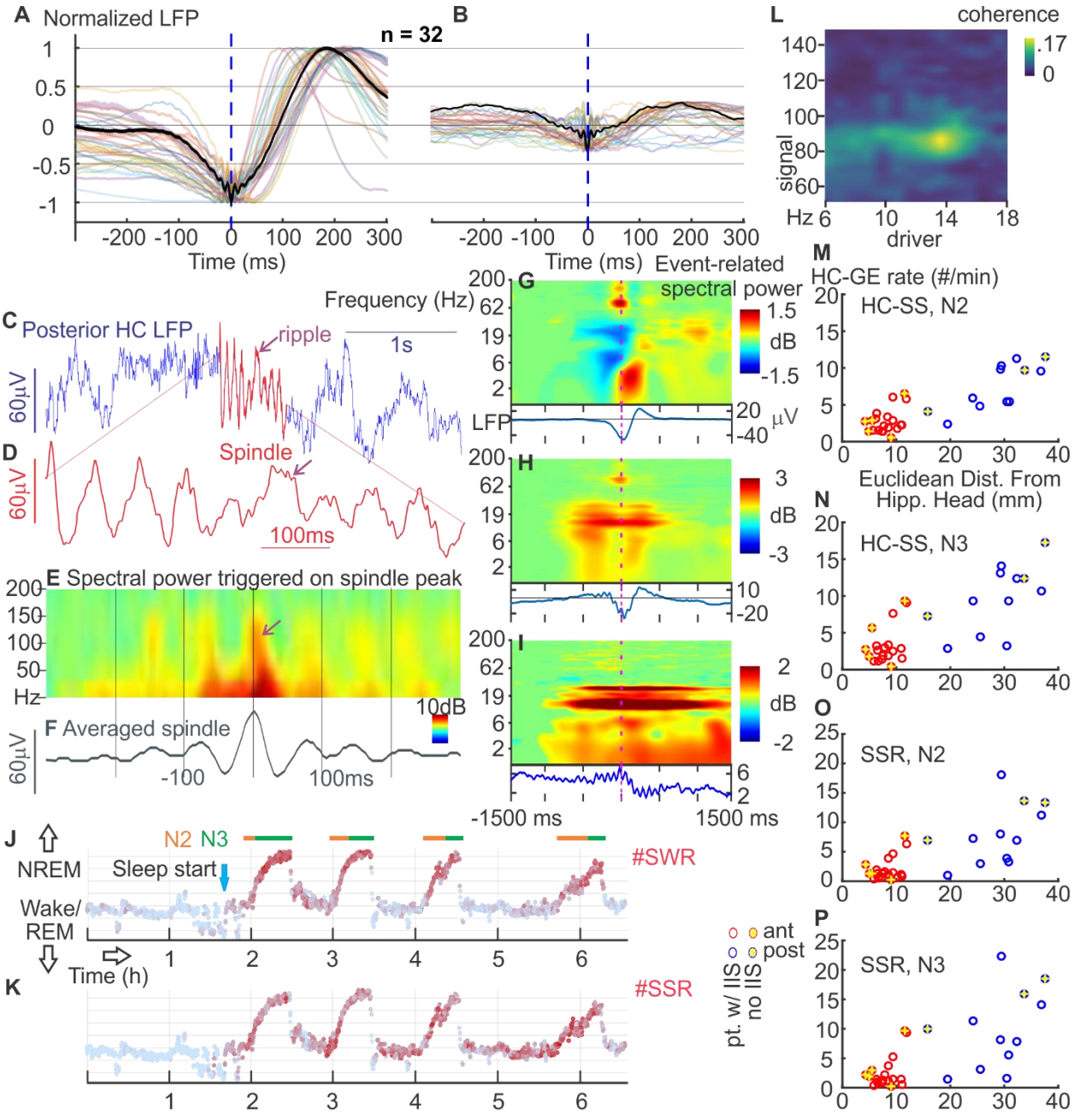
A Normalized LFP
n = 32
B
Time (ms)
L coherence
signal
driver
Hz
C Posterior HC LFP
ripple
1s
60μV
D
Spindle
100ms
E Spectral power triggered on spindle peak
F Averaged spindle
Frequency (Hz)
G Event-related spectral power
LFP
H
I
-1500 ms
1500 ms
M HC-GE rate (#/min)
HC-SS, N2
Euclidean Dist. From Hipp. Head (mm)
N HC-SS, N3
O SSR, N2
P SSR, N3
J
NREM
Wake/ REM
N2 N3
Sleep start
Time (h)
#SWR
K
#SSR
ant
post
pt. w/ IIS
no IIS

Figure 4.2: Neocortical graphoelements (NC-GE) in relation to HC-SSR (*A*) and HC-SS (*B*), for example channel-pairs. Each row of histograms is for a different type of NC-GE: theta burst onsets (TB), downstate peaks (DS), spindle onsets (SS), and upstate peaks (US). Each column of plots shows example histograms with significant temporal correlations between HC-GE and NC-GE from the same NC region in (from left to right) frontal, temporal, parietal, and occipital lobes. Magenta vertical lines indicate trigger (HC-GE) location for the peri-stimulus histograms. Orange bars indicate the time ranges with both peak NC-GE occurrence rate and significant correlation.

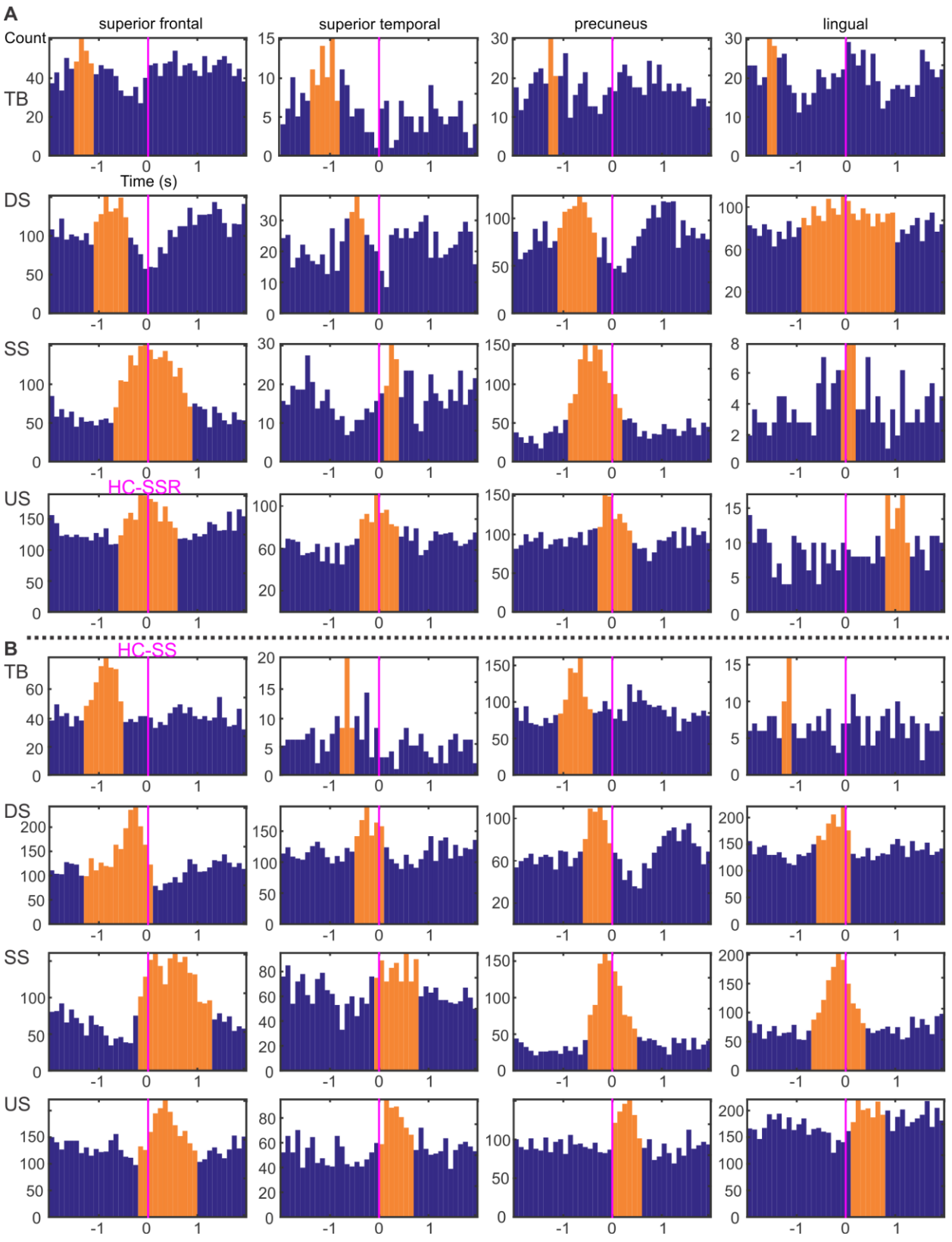
A
superior frontal
superior temporal
precuneus
lingual
Count
TB
DS
SS
US
Time (s)
HC-SSR
B
HC-SS
TB
DS
SS
US

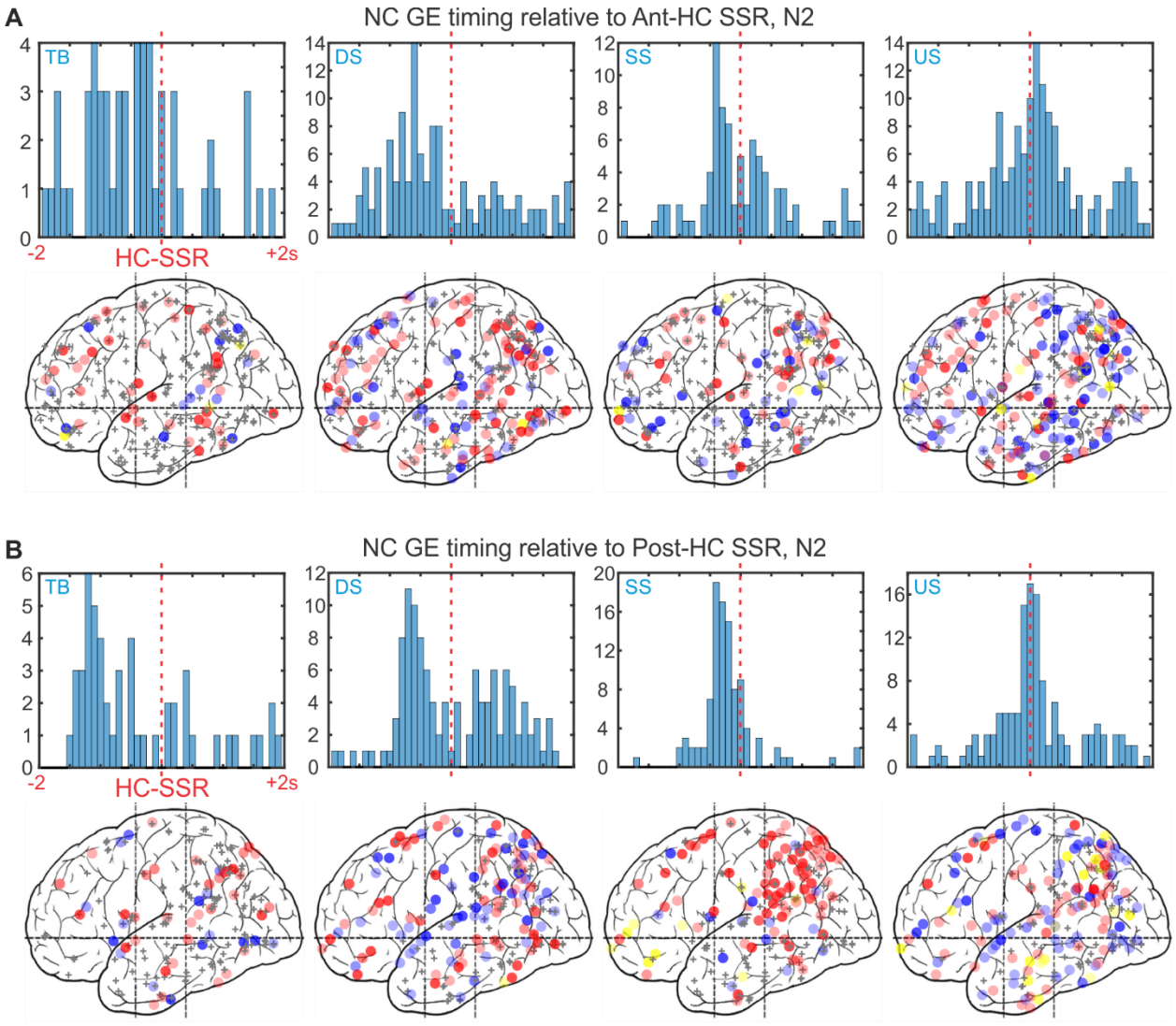

Figure 4.3: GEs across NC tend to occur with consistent latencies from HC-SSR. ***A*-*B***. Top: Histograms of peak latencies for HC-NC channel pairs with significant temporal correlations between HC-SSR and NC-GE. Each count is the peak latency of a particular HC-NC channel pair. Bottom: maps of peak latency between HC-SSR and NC-GE for cortical channels. Circles indicate where NC-GE relationships with HC-SSR are significant, while plus signs represent non-significant channels. The intensity of each circle corresponds to the strength of HC-SSR to NC-GE coupling estimated (as in Fig. 4.2), and the color of each circle indicates peak latency: red for NC-GE before HC-SSR, blue for NC-GE after HC-SSR, and yellow for NC-GE co-occurring with HC-SSR (i.e. within 100 ms of each other). Both hemispheres and medial and lateral cortical sites are superimposed in each plot. ***A***. In N2, with Ant-HC SSR as reference, NC-GE tend to occur in the following order: TB starts → DS peaks ~= SS starts → US peaks. ***B***. In N2, with Post-HC SSR as reference, NC-GE tend to occur in the following order: TB starts → DS peaks ~= SS starts → US peaks; NC-US peaks tend to co-occur with HC-SSR.

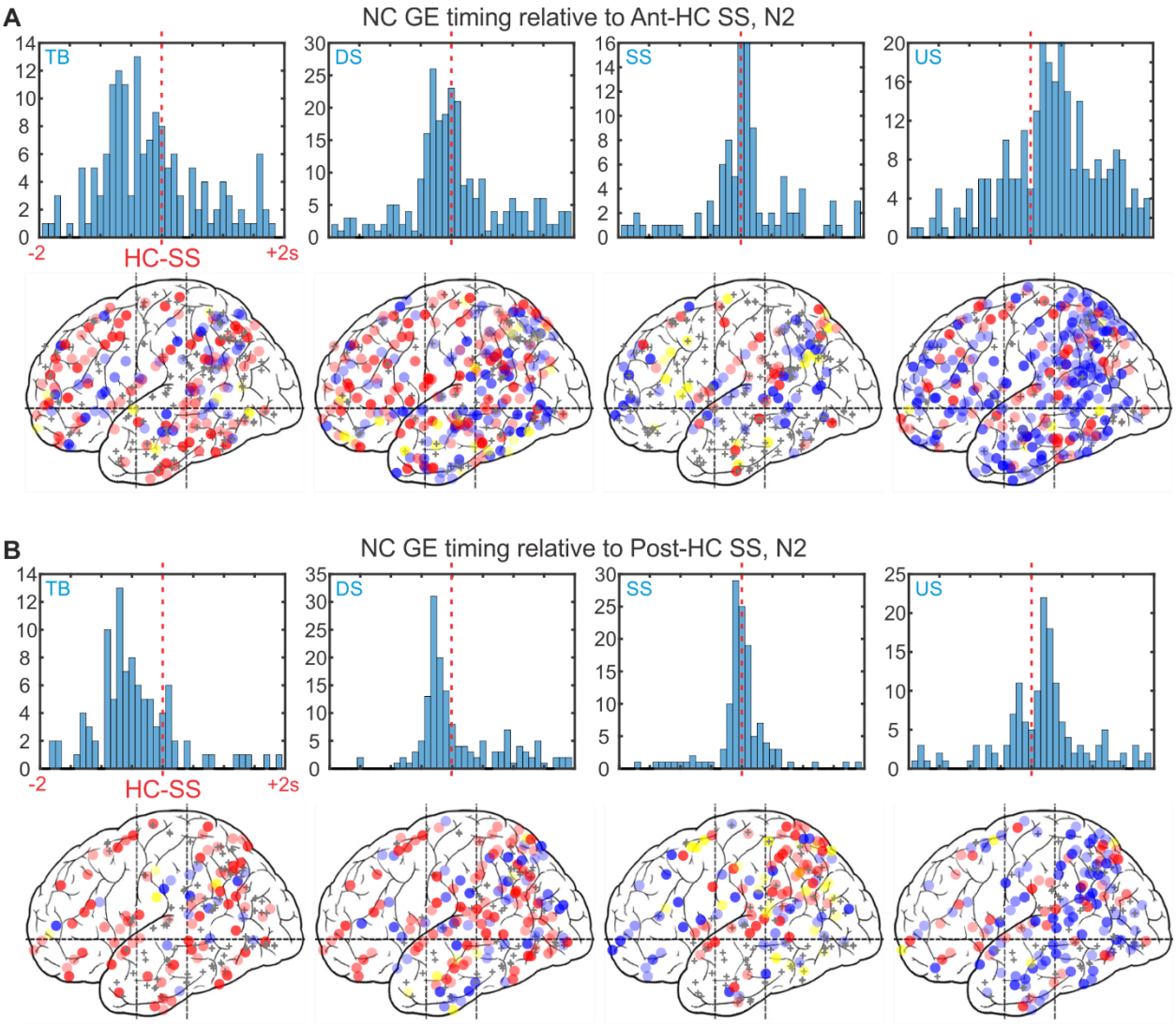

Figure 4.4: GEs across NC tend to occur with consistent latencies from HC-SS. ***A***-***B***. Top: Histograms of peak latencies for HC-NC channel pairs with significant temporal correlations between HC-SS and NC-GE. Each count is the peak latency of a particular HC-NC channel pair. Bottom: maps of peak latency between HC-SS and NC-GE for cortical channels. Circles indicate where HC-NC relationships are significant, while plus signs represent non-significant channels. The intensity of each circle corresponds to the strength of NC-GE to HC-SS coupling estimated (as in Fig. 4.2), and the color of each circle indicates peak latency: red for NC-GE before HC-SS, blue for NC-GE after HC-SS, and yellow for NC-GE co-occurring with HC-SS (i.e. within 100 ms of each other). Both hemispheres and medial and lateral cortical sites are superimposed in each plot. ***A***. In N2, with Ant-HC SS as reference, NC-GE tend to occur in the following order: TB starts → DS peaks → SS starts → US peaks. ***B***. In N2, with Post-HC SS as reference, NC-GE tend to occur in the following order: TB starts → DS peaks → SS starts → US peaks. In both ***A*** and ***B***, NC-SS tend to co-occur with HC-SS, and widespread NC-US tend to follow.

Figure 4.5: Strength of HC-NC association shows both correlativity and variability across GE types, NREM stages, HC-GE sources, and NC regions. ***A***. Proportions of HC-SSR events co-occurring with NC-GE (upper row) or HC-SS events with NC-GE, compared for different NC channels across NC-GE type pairs (TB vs. SS, TB vs. DS, etc.). Co-occurrence rates are highly correlated between all NC-GE types, especially for DS vs. US. Each marker in a given scatter plot panel represents one HC-NC channel pair. Linear regression best fit lines were marked for each scatterplot in grey. ***B***. Map of NC ROIs used for analysis (see Table 4.S3). ***C***, ***D***. Stacked bar graph of mean significant (evaluated as in Fig. 4.2) HC-NC channel pair proportions with regard to all channels found in each ROI. Data in ***C*** was obtained by averaging across GE types for each SSR origin (different NREM stages and HC contact positions); similarly, data in ***D*** was obtained by averaging across NC-GE types for each HC-SS origin. ***E***, ***F***. Global (i.e. across all NC ROIs) proportions of significant HC-NC channel pairs for HC-SSR (***E***) and for HC-SS (***F***). Panels ***C***-***F*** share the same color legend.

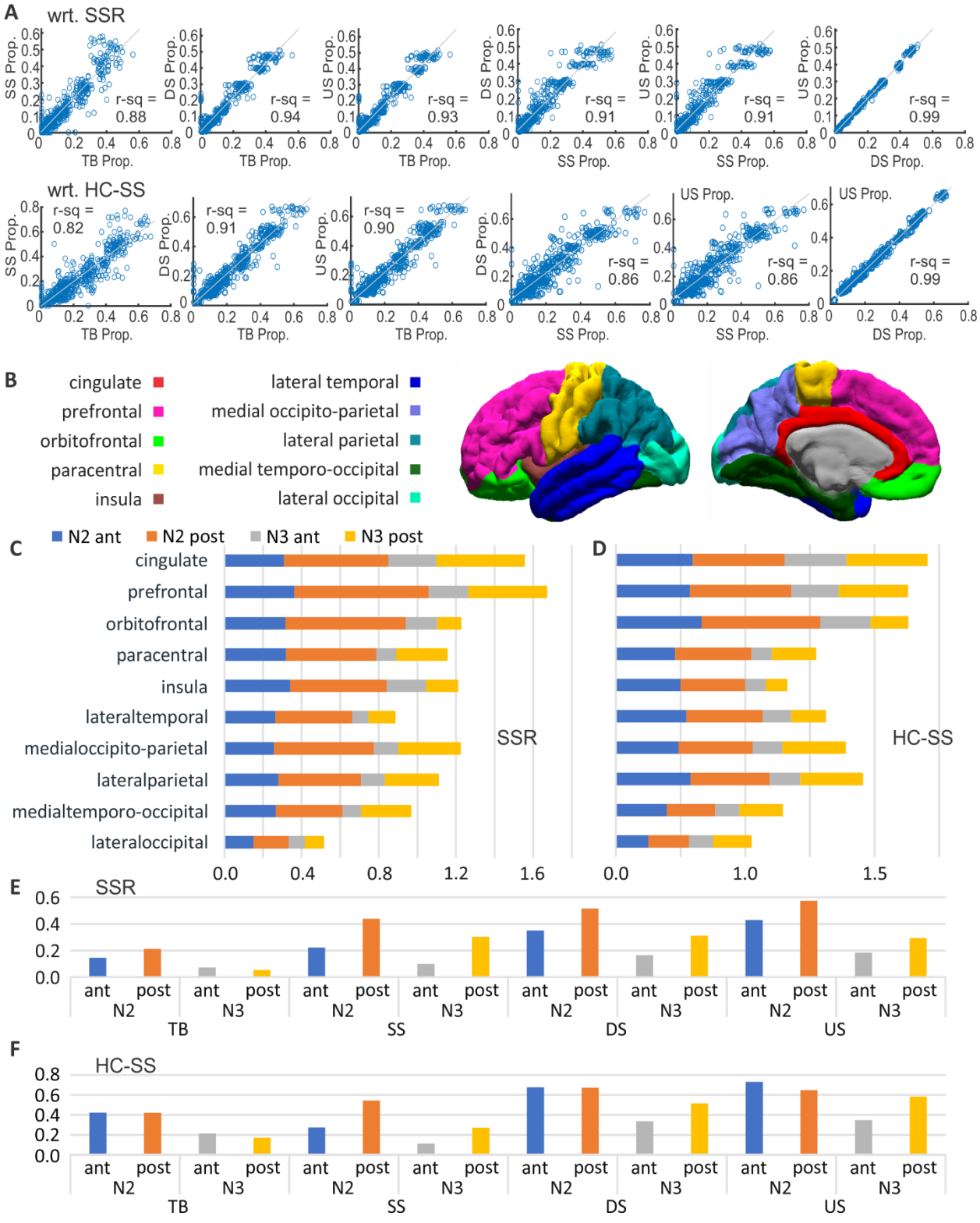
A
wrt. SSR
SS Prop.
DS Prop.
US Prop.
TB Prop.
SS Prop.
DS Prop.
r-sq = 0.88
r-sq = 0.94
r-sq = 0.93
r-sq = 0.91
r-sq = 0.91
r-sq = 0.99
wrt. HC-SS
r-sq = 0.82
r-sq = 0.91
r-sq = 0.90
r-sq = 0.86
r-sq = 0.86
r-sq = 0.99
B
cingulate
prefrontal
orbitofrontal
paracentral
insula
lateral temporal
medial occipito-parietal
lateral parietal
medial temporo-occipital
lateral occipital
C
N2 ant
N2 post
N3 ant
N3 post
cingulate
prefrontal
orbitofrontal
paracentral
insula
lateraltemporal
medialoccipito-parietal
lateralparietal
medialtemporo-occipital
lateraloccipital
SSR
0.0
0.4
0.8
1.2
1.6
D
HC-SS
0.0
1.0
1.5
E
SSR
ant
post
N2
N3
TB
SS
DS
US
F
HC-SS

Figure 4.6: Hippocampal spindles phase-lock to neocortical spindles and modulate hippocampal ripple activity. ***A***. HC-SS phase-locking with NC-SS tends to be localized along the longitudinal axis and prefers ipsilateral HC-NC channel pairs. Each panel shows two traces of phase-locking values (PLV); blue trace marks average PLV computed over three-second trials with overlapping HC- and NC-SS, centered on the starts of HC-SS; black trace marks average PLV computed over an equal number of pseudo-trials centered on random time points in NREM (N2+N3). From left to right, panels 1 and 2 show phase-locking to the same NC channel in (left) superior parietal cortex; panels 3 and 4 show phase-locking to the same NC channel in right precuneus. LA: left anterior. LP: left posterior. RP: right posterior. ***B***, ***C***. 2d projection maps of medial (***B***) and lateral (***C***) NC channels showing significant spindle phase-locking with HC. Each blue circle marks a significant NC channel, with color intensity corresponding to peak PLV amplitude. Plus signs mark channels with no significant phase-locking. ***D***. Intra-hippocampal event-related phase-amplitude coupling (ERPAC) was computed over all HC-SS in NREM across all patients, separated by longitudinal origin (Ant-HC/Post-HC), with aligned events being HC-SS starts (red vertical lines), between spindle (10-16 Hz) phase and ripple (60-120 Hz) amplitude. Green line segments mark the time segments with significant coupling ($p < 0.001$).

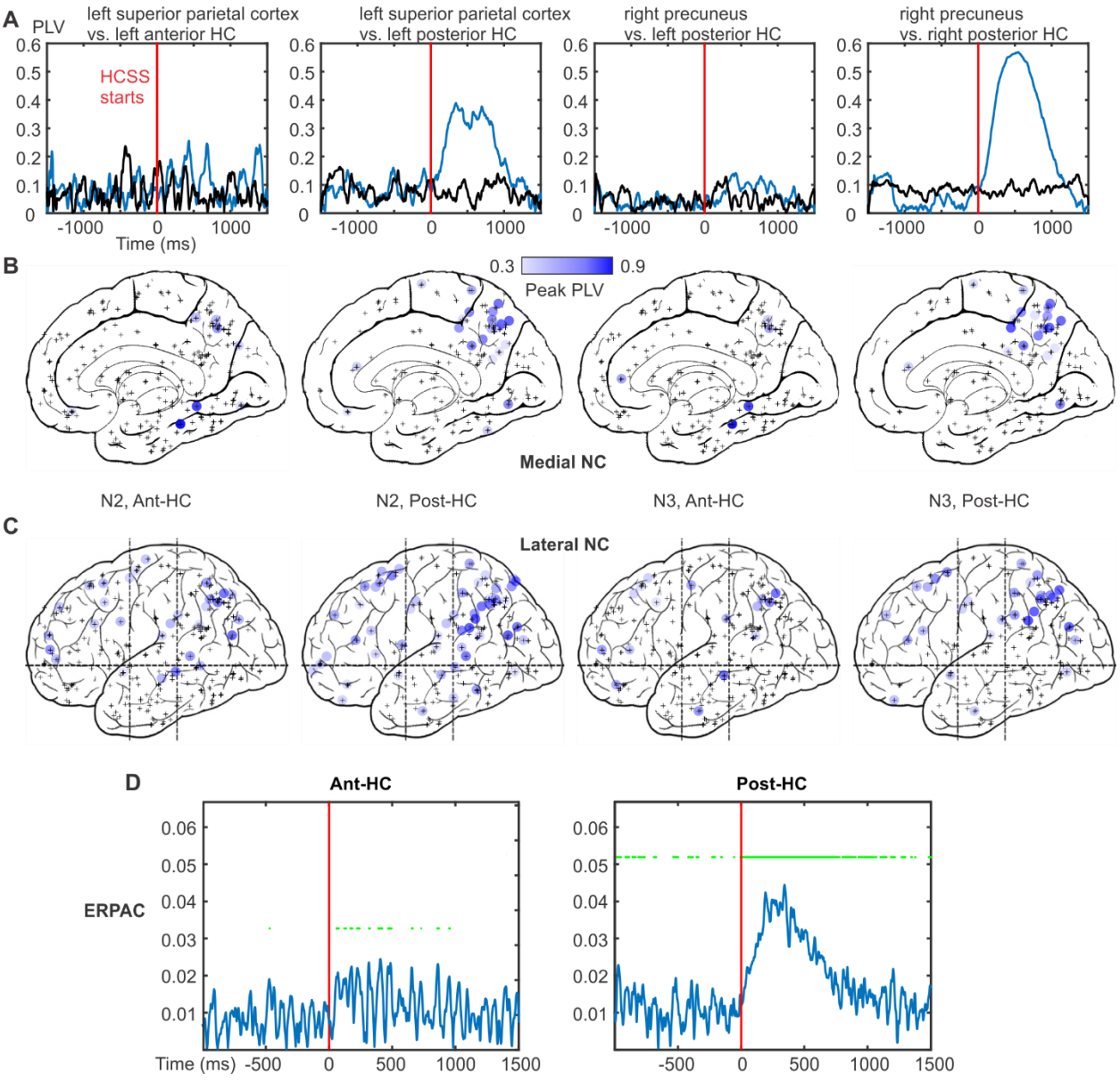
A
PLV
left superior parietal cortex
vs. left anterior HC
left superior parietal cortex
vs. left posterior HC
right precuneus
vs. left posterior HC
right precuneus
vs. right posterior HC
HCSS
starts
0.6
0.5
0.4
0.3
0.2
0.1
0
-1000
0
1000
Time (ms)
B
0.3
0.9
Peak PLV
Medial NC
N2, Ant-HC
N2, Post-HC
N3, Ant-HC
N3, Post-HC
C
Lateral NC
D
Ant-HC
Post-HC
ERPAC
0.06
0.05
0.04
0.03
0.02
0.01
Time (ms)
-500
0
500
1000
1500

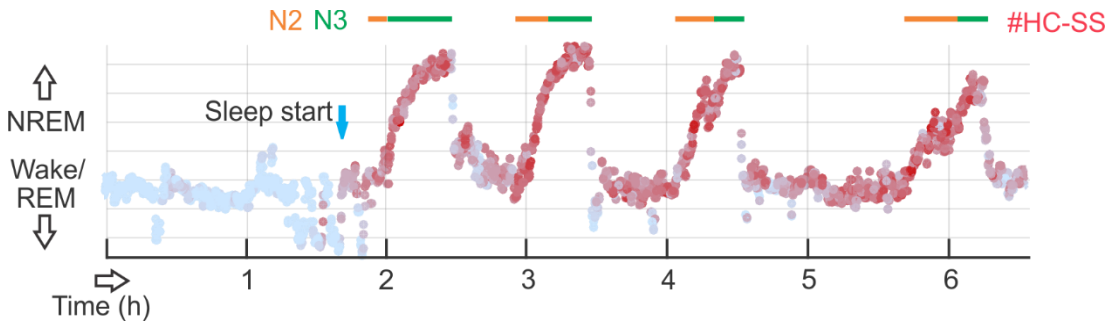

Figure 4.S1: Example state plot showing the separation of NREM sleep from waking/REM in ~8-hour LFP recording and HC-SS occurrence rate (color coded with red intensity) over time. N2/N3 periods are marked with orange/green horizontal lines, respectively. Light blue arrow marks the beginning of NREM sleep.

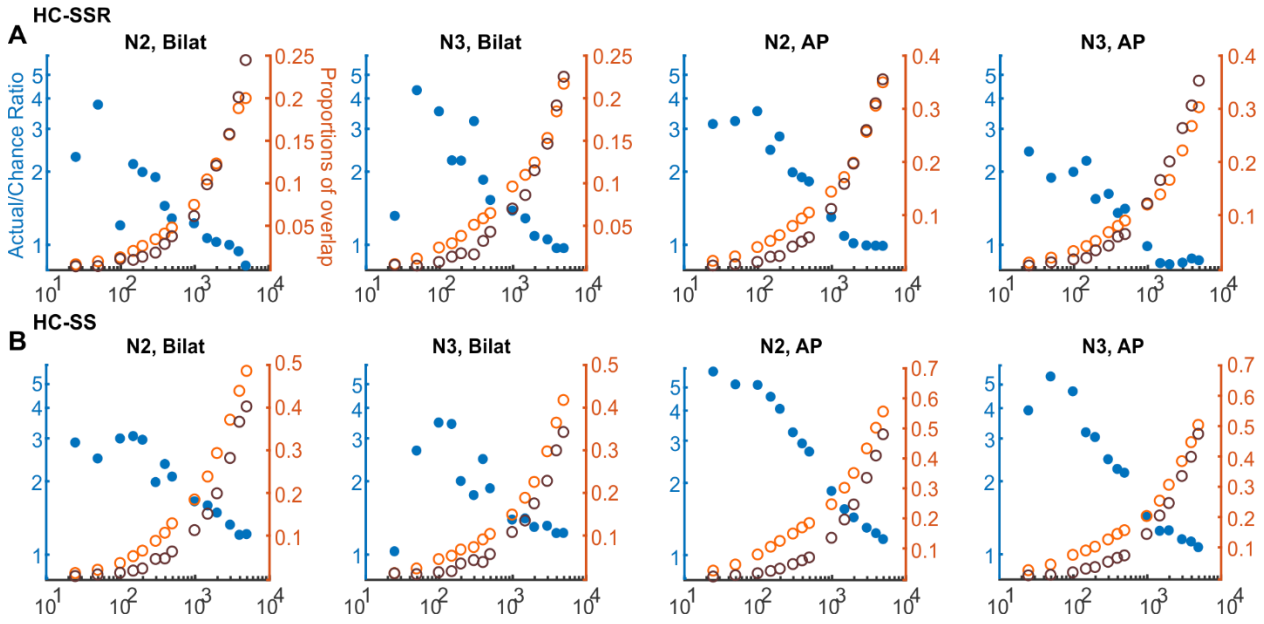

Figure 4.S2: For both bilateral HC site pairs and Ant-HC/Post-HC site pairs, SSR (*A*) and HC-SS (*B*) co-occurrence likelihood approaches chance as time window for co-occurrence expands. Blue filled circles mark (wrt. left y-axis) the ratios of actual over chance overlap proportions, and orange/brown unfilled circles mark (wrt. right y-axis) the corresponding actual (orange) and chance (brown) proportions. All axes for each panel are logarithmic. Bilat.: bilateral. AP: Ant-HC/Post-HC.

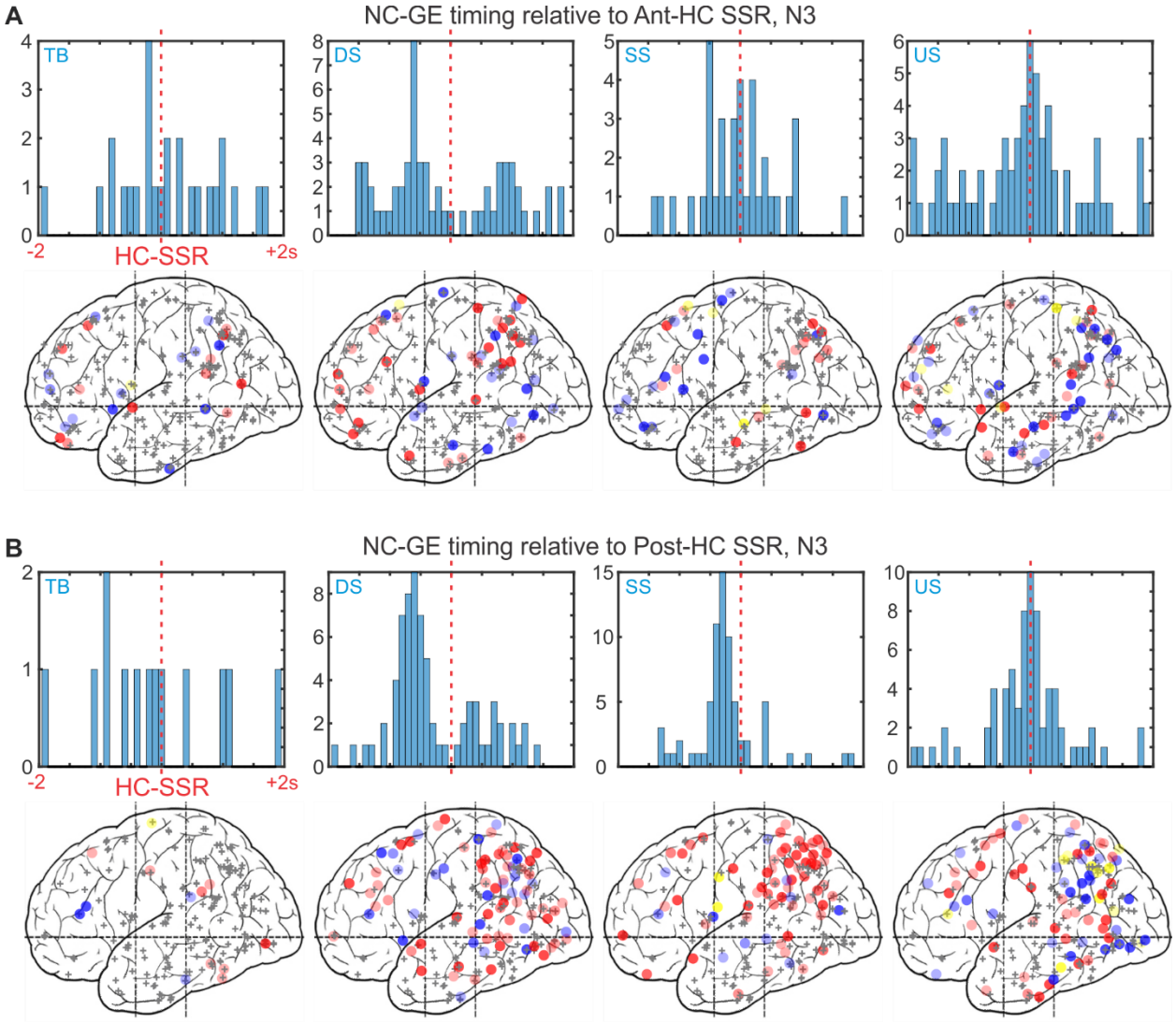

Figure 4.S3: DS, SS, and US across NC tend to occur with consistent latencies from HC-SSR in N3. ***A***-***B***. Top: Histograms of peak latencies for HC-NC channel pairs with significant temporal correlations between HC-SSR and NC-GE. Each count is the peak latency of a particular HC-NC channel pair. Bottom: maps of peak latency between HC-SSR and HC-GE for cortical channels. Circles indicate where GE-SSR relationships are significant, while plus signs represent non-significant channels. The intensity of each circle corresponds to the strength of GE-SSR coupling estimated (as in Fig. 4.2), and the color of each circle indicates peak latency: red for NC-GE before HC-SSR, blue for NC-GE after HC-SSR, and yellow for NC-GE co-occurring with HC-SSR (i.e. within 100 ms of each other). Both hemispheres and medial and lateral cortical sites are superimposed in each plot. ***A***. In N3, with Ant-HC SSR as reference, NC-GE tend to occur in the following order: DS peaks → SS starts → US peaks. ***B***. In N3, with Post-HC SSR as reference, NC-GE tend to occur in the following order: DS peaks → SS starts → US peaks. In both ***A*** and ***B***, US peaks tend to co-occur with HC-SSR.

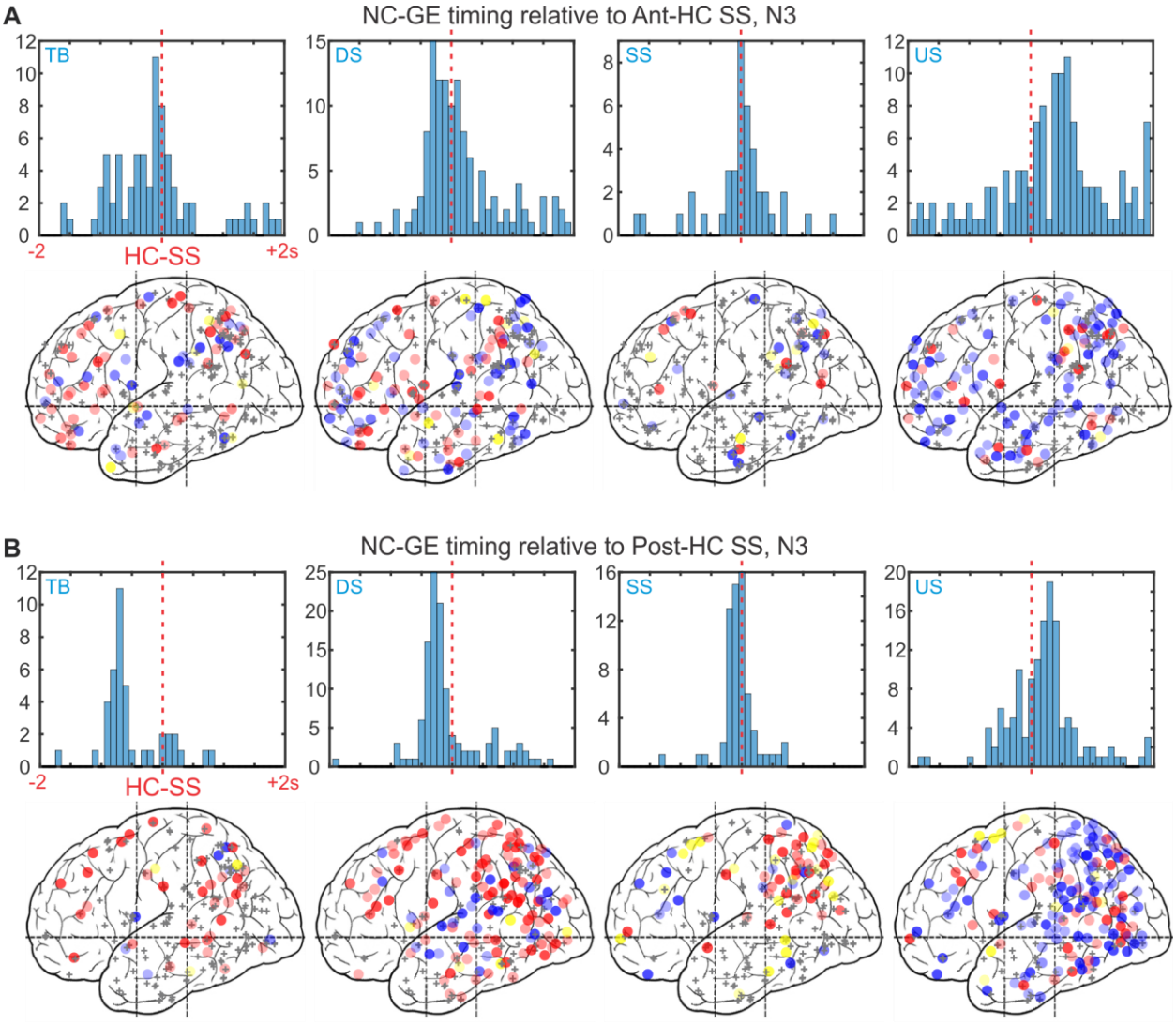

Figure 4.S4: GEs across NC tend to occur with consistent latencies from HC-SS in N3. ***A-B***. Top: Histograms of peak latencies for HC-NC channel pairs with significant temporal correlations between HC-SS and NC-GE. Each count is the peak latency of a particular HC-NC channel pair. Bottom: maps of peak latency between HC-SS and NC-GE for cortical channels. Circles indicate where GE-SS relationships are significant, while plus signs represent non-significant channels. The intensity of each circle corresponds to the strength of NC-GE to HC-SS coupling estimated (as in Fig. 4.2), and the color of each circle indicates peak latency: red for NC-GE before HC-SS, blue for NC-GE after HC-SS, and yellow for NC-GE co-occurring with HC-SS (i.e. within 100 ms of each other). Both hemispheres and medial and lateral cortical sites are superimposed in each plot. ***A***. In N3, with Ant-HC SS as reference, NC-GE tend to occur in the following order: DS peaks → SS starts → US peaks. ***B***. In N3, with Post-HC SS as reference, NC-GE tend to occur in the following order: TB starts → DS peaks → SS starts → US peaks. In both ***A*** and ***B***, NC-SS tend to co-occur with HC-SS, and widespread NC-US tend to follow.

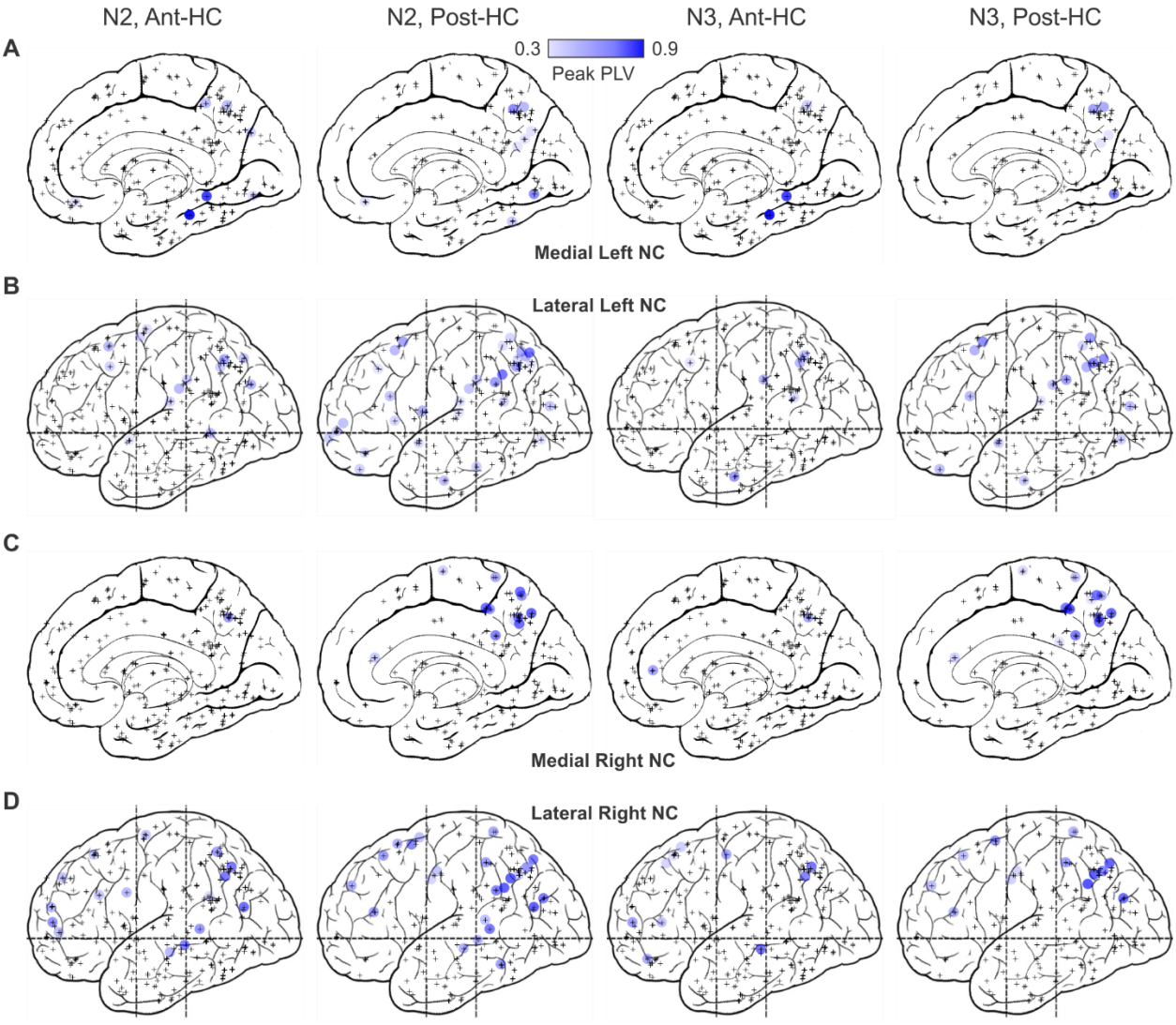

Figure 4.S5: 2D projection maps of left hemisphere medial (*A*), left hemisphere lateral (*B*), right hemisphere medial (*C*), and right hemisphere lateral (*D*) NC channels showing significant spindle phase-locking with HC. Each blue circle marks a significant NC channel, with color intensity corresponding to peak PLV amplitude. Plus signs mark channels with no significant phase-locking.

Table 4.1: List of patient-wise occurrence rates of hippocampal graphoelements. Pt: patient. L: Left. R: Right.

Pt#	L Ant HC	L Post HC	R Ant HC	R Post HC	SWR Rate, N2 Ant.	SWR Rate, N2 Post.	SWR Rate, N3 Ant.	SWR Rate, N3 Post	SSR Rate, N2 Ant.	SSR Rate, N2, Post.	SSR Rate, N3, Ant.	SSR Rate, N3, Post.	HC-SS Rate, N2 Ant.	HC-SS Rate, N2, Post.	HC-SS Rate, N3, Ant.	HC-SS Rate, N3, Post.
1	x				11		19		6.3		9.4		5.8		9	
2	x				1.6				0.67				1.7			
3	x	x			11	12	24	25	1.4	3.4	1.4	5.6	2.8	5.4	2.6	9.3
4	x	x	x		10	4.3	11	4.3	1.4	3.8	1.1	1.6	2.6	5.5	2.4	3.2
5			x	x	21	3.7	38	14	1.3	7	1.9	9.9	1.4	4	1.8	7.2
6			x	x	9	12	15	17	4.6	18	5.2	22	6.1	10	7.6	14
7	x				11		13		0.27		0.26		0.52		0.43	
8			x		19		20		1.2		1.3		1.4		1.9	
9	x	x			13	7.9	16	7.2	1.1	7.2	1.5	11	2.2	5.9	2.8	9.3
10			x		13		18		2.7		2.2		2.7		2.7	
11	x		x	x	7.3	7.7	12	12	0.44	1.1	0.49	1.5	1.5	2.4	1.1	2.8
12				x		5.5		7		13.4		19		12		17
13	x	x	x		13	6.2	19	4.9	2.6	8	2.4	8.2	3.6	9.8	3	13
14		x				11		15		7		7.9		11		12
15		x		x		3.6		7.2		7.1		8.6		7.2		7.6
16			x		9.4		11		1.6		2.2		2.2		3	
17	x				23		24		0.75		0.89		1.4		1.4	
18	x				7.8		10		1.2		1.1		1.9		1.9	
19	x	x			12	2.6	19	6.1	7.7	14	9.7	16	6.6	9.7	9.3	12
20			x		11		12		1.3		3		2.9		5.6	
mean					**12**	**7**	**18**	**11**	**2.1**	**8.2**	**2.8**	**10**	**2.8**	**7.5**	**3.5**	**9.8**

Table 4.2: Relation of HC-GE to NC-GE. Separate values and statistical significance tests are shown for NREM sleep stages N2 vs. N3, for anterior vs. posterior HC, and for different graphoelements (TB- theta bursts; SS- sleep spindles; DS- downstates; US- upstates). Tests indicate if there was a significant association between the times of occurrence of the SSR/HCSS and GE (fourth column); if the NC-GE occurred significantly before the SSR/HC-SS (negative numbers) or before, when measuring the peak latency as the mean value across cortico-HC pairs (fifth column), or as the peak of an extreme value distribution fitted over the ±2000 ms histogram-of-histograms in Fig. 3 and in Fig. 3-1 (sixth column). The seventh column shows if there is a significant difference in the number of NC-GE occurring 2000 ms before vs. 2000 ms after the SSR/HC-SS. Extremely small (< 0.0001) p-values are represented by 0 for clarity.

NC-GE Type	Sleep Stage	HC Longi-tudinal Axis	HC-SSR v. NC-GE related (KS test p-value)	Peak Latency from HC-SSR (ms), Mean	Peak Latency from HC-SSR (ms), DistPeak	Non-zero Latency from HC-SSR, binomial p-value	HC-SS v. NC-GE related (KS test p-value)	Peak Latency from HC-SS (ms), Mean	Peak Latency from HC-SS (ms), DistPeak	Non-zero Latency from HC-SS, binomial p-value
TB	N2	Ant	0	-398	-741	0	0	-164	-392	0
TB	N2	Post	0.002	-386	-1074	0.011	0	-455	-698	0
TB	N3	Ant	0.129	123	206	1	0	-96	-338	0.006
TB	N3	Post	0.654	-131	-346	0.388	0	-512	-646	0
DS	N2	Ant	0	-185	-575	0	0	55	-65	0.232
DS	N2	Post	0	38	31	0.519	0	105	-167	0.001
DS	N3	Ant	0.216	-95	-426	0.117	0	148	-57	1
DS	N3	Post	0	-288	-489	0.001	0	-64	-184	0
SS	N2	Ant	0	-16	-163	0.213	0	80	73	0.086
SS	N2	Post	0	-211	-353	0	0	-19	-106	0.368
SS	N3	Ant	0.017	-32	-142	0.728	0.003	-10	12	0.377
SS	N3	Post	0	-241	-425	0	0	-45	-32	0.013
US	N2	Ant	0	35	93	0.221	0	348	534	0
US	N2	Post	0	68	62	0.643	0	165	212	0
US	N3	Ant	0.013	-131	-180	0.609	0	338	568	0
US	N3	Post	0	-49	-71	0.699	0	199	111	0

Table 4.3: P-values for chi-square tests of homogeneity (α = 0.05 post FDR-correction applied over each column), conducted for each HC site with regard to each NC-GE type's coupling to HC-SSR. Ant.: Ant-HC. Post: Post-HC. Cells marked 2.20E-016 are placeholders for $p < 2.2 \times 10^{-16}$. # signif.: number of HC sites with a non-homogeneous anatomical distribution of significantly coupled NC sites.

HC-SSR	NC-GE Type	TB	DS	SS	US	TB	DS	SS	US
Patient	HippSite	N2	N2	N2	N2	N3	N3	N3	N3
1	Ant.	0.0350	1.96E-005	0.0013	0.0112	4.56E-008	0.0026	0.1016	0.0216
2	Ant.	4.26E-012	4.17E-014	0.0007	4.62E-013	1	1	1	1
3	Ant.	0.0284	2.72E-005	1.11E-008	7.41E-005	0.9876	0.9956	0.9596	1
	Post.	7.67E-011	2.20E-016	2.20E-016	2.20E-016	0.9876	1	0.6746	0.9311
4	Ant.	0.1174	0.0605	0.9073	0.1010	0.0361	0.0001	0.2911	0.0037
	Post.	1.27E-010	6.43E-011	2.08E-005	1.78E-015	6.28E-014	1.01E-009	2.59E-013	2.20E-016
	Ant.	0.0378	0.3110	0.5857	0.0090	0.0665	0.2191	0.6746	0.1673
5	Ant.	0.0225	0.0003	4.22E-007	0.1711	0.8922	1	0.3795	0.7614
	Post.	0.1661	3.13E-013	0.0006	6.42E-010	0.0693	1	0.9596	1
6	Ant.	0.3037	7.98E-007	0.1041	0.0035	3.99E-011	8.68E-009	0.0179	0.0006
	Post.	1.27E-010	2.20E-016	6.59E-006	2.20E-016	2.20E-016	1.31E-010	0.0137	7.25E-011
7	Ant.	0.1116	0.9558	0.5720	0.9631	0.9030	0.8851	0.9596	0.9630
8	Ant.	0.1022	1.96E-009	6.59E-006	9.70E-012	0.1896	3.20E-014	1.35E-013	1.21E-005
9	Ant.	0.0215	0.3618	0.9819	0.2716	0.0759	0.5351	0.6076	0.3635
	Post.	0.0353	0.2274	0.0042	0.8674	0.0002	0.5351	0.0474	0.0053
10	Ant.	0.4424	0.0190	0.3806	0.0345	0.1350	0.0095	0.0725	0.0019
11	Ant.	1.71E-007	0.0579	9.12E-006	8.46E-005	0.2322	1	0.9596	1
	Ant.	1.21E-007	3.66E-008	5.26E-006	1.97E-007	0.0281	1	0.3795	1
	Post.	5.69E-010	3.40E-012	1.79E-009	3.62E-005	0.5437	0.9377	0.4875	1
12	Post.	2.20E-016	7.32E-011	2.20E-016	6.99E-011	2.20E-016	6.55E-007	2.20E-016	0.0006
13	Ant.	6.25E-007	2.72E-005	0.1443	0.0200	0.5779	0.9377	0.3483	1
	Post.	1.42E-011	5.59E-013	0.0001	0.0866	0.7241	0.0167	0.6218	0.8924
	Ant.	4.26E-012	0.0003	0.2241	0.5459	0.4472	0.9509	0.9786	0.8924
14	Post.	2.37E-015	2.20E-016	9.12E-009	2.20E-016	0.0001	0.0025	0.0116	0.7384
15	Post.	1.01E-005	0.0003	0.5282	0.0006	0.7241	0.9377	0.0147	0.9874
	Post.	0.0148	0.4608	1.22E-008	0.1932	0.9505	0.5189	1.16E-009	0.9630
16	Ant.	1.78E-015	2.64E-007	1.79E-009	5.64E-010	0.0006	0.9265	0.1499	0.8924
17	Ant.	0.6359	0.2852	0.2241	0.5079	0.4262	0.9509	0.9102	0.2694
18	Ant.	4.86E-010	9.96E-009	0.0017	2.67E-011	0.0665	0.7863	0.1309	0.4451
19	Ant.	0.5133	0.7507	0.2811	0.2495	0.9876	0.9377	0.9596	1
	Post.	0.0284	0.0001	0.0011	7.58E-006	7.89E-011	0.2566	0.0116	4.44E-005
20	Ant.	4.07E-010	0.2530	0.0005	0.8674	0.0003	2.84E-014	0.0474	1.40E-009
# signif. HC sites (/32)		24	22	21	21	11	11	10	11

Table 4.4: Proportions of NC-GE from significantly coupled NC sites that overlapped with Ant-HC SSR/SS differ from the proportions for Post-HC SSR/SS. Wilcoxon signed rank tests were performed on the data obtained for Table 4. Each test (whose p-value was tabulated above) required that both members of a HC site pair must have significant chi-square test result from Table 4 (for HC-SSR) or Table 4-1 (for HC-SS); otherwise, the corresponding cell would be filled with NA. # signif.: number of significant tests (in total number of qualified patients).

	HC-SSR				HC-SS			
Patient	NC-TB	NC-DS	NC-SS	NC-US	NC-TB	NC-DS	NC-SS	NC-US
3	0.0001	0.0001	0.0001	0.0001	0.0001	0.0001	0.0001	0.0001
4	0.0005	3.35E-004	NA	0.0003	0.0005	3.35E-004	0.0005	0.0003
5	NA	NA	0.0003	NA	NA	NA	0.0005	0.0001
6	0.0002	0.0001	0.0001	0.0001	0.0002	0.0001	0.0002	0.0001
9	0.0005	NA	NA	NA	0.0005	0.0005	0.0342	0.0005
11	4.72E-005	1.39E-005	8.65E-005	NA	2.53E-005	1.39E-005	2.81E-005	1.39E-005
13	0.0002	0.0002	NA	0.0002	0.0002	0.0002	0.0002	0.0002
19	NA	NA	NA	NA	0.0002	NA	0.0002	0.0001
# signif.	6 in 6	5 in 5	4 in 4	4 In 4	7 in 7	6 in 6	8 in 8	8 in 8

Table 4.5: Numbers of HC-NC channel pairs by NC regions of interest (ROIs) and proportions of HC-NC channel pairs with significant NC-GE/HC-SSR relationships across NC. Ant.: Ant-HC. Post.: Post-HC.

NC-GE Type	Total# Ch. pairs		Proportion of channels with significant HC-SSR co-occurring with NC-GE types															
			TB				DS				SS				US			
			N2		N3		N2		N3		N2		N3		N2		N3	
ROI	Ant.	Post.	Ant.	Post.	Ant.	Post.	Ant.	Post.	Ant.	Post.	Ant.	Post.	Ant.	Post.	Ant.	Post.	Ant.	Post.
Lateral occipital	15	15	0.000	0.000	0.000	0.067	0.267	0.333	0.067	0.200	0.133	0.133	0.133	0.067	0.200	0.267	0.133	0.067
Medial temporo-occipital	31	26	0.129	0.231	0.032	0.115	0.452	0.385	0.129	0.385	0.129	0.231	0.097	0.154	0.355	0.538	0.129	0.385
Lateral parietal	74	51	0.135	0.176	0.081	0.039	0.297	0.451	0.203	0.353	0.216	0.549	0.041	0.373	0.473	0.529	0.176	0.353
Medial occipito-parietal	34	27	0.118	0.259	0.059	0.037	0.176	0.630	0.206	0.370	0.324	0.630	0.059	0.556	0.412	0.556	0.176	0.333
Lateral temporal	86	54	0.128	0.241	0.035	0.019	0.314	0.444	0.081	0.222	0.186	0.333	0.070	0.148	0.430	0.574	0.151	0.167
Insula	11	6	0.273	0.333	0.182	0.000	0.636	0.500	0.273	0.167	0.091	0.500	0.000	0.167	0.364	0.667	0.364	0.333
Paracentral	29	16	0.207	0.313	0.069	0.063	0.345	0.625	0.172	0.313	0.276	0.313	0.034	0.375	0.448	0.625	0.138	0.313
Orbitofrontal	23	6	0.174	0.000	0.174	0.000	0.348	1.000	0.087	0.000	0.261	0.667	0.130	0.333	0.478	0.833	0.261	0.167
Prefrontal	49	14	0.204	0.214	0.102	0.143	0.510	0.929	0.224	0.500	0.265	0.714	0.245	0.571	0.469	0.929	0.245	0.429
Cingulate	13	6	0.077	0.333	0.077	0.167	0.385	0.500	0.385	0.500	0.308	0.667	0.308	0.500	0.462	0.667	0.231	0.667
Total# Ch. pairs across NC / Average Proportion	365	221	0.144	0.210	0.081	0.065	0.373	0.580	0.183	0.301	0.219	0.474	0.112	0.324	0.409	0.618	0.200	0.321

Table 4.6: Summary of 4-way ANOVA results with respect to NC-GE and HC-SSR associations. LO: lateral occipital; LT: lateral temporal; CG: cingulate; OF: orbitofrontal; PF: prefrontal; PC: paracentral; MTO: medial temporo-occipital; MOP: medial occipito-parietal; IS: insula; LP: lateral parietal. N.S.: not significant (for post-hoc Tukey's range tests, $p > 0.1$).

Source	F	p-value	Post-hoc analysis (if any) and corresponding p-value (Tukey's range test)													
GE	64.7383	1.87×10^{-12}	TB vs. SS	TB vs. DS	TB vs. US	SS vs. DS	SS vs. US	DS vs. US								
			2.119×10^{-7}	3.828×10^{-9}	3.777×10^{-9}	0.0048	0.0001	0.5301								
Stage	151.6419	1.37×10^{-12}	N/A													
AP	100.5432	1.34×10^{-10}	N/A													
ROI	12.5037	1.55×10^{-7}		LT	CG	OF	PF	PC	MTO	MOP	IS	LP	LO			
			LO vs.	N.S.	7.149×10^{-7}	0.0003	2.024×10^{-7}	0.0014	0.0478	0.0004	0.0005	0.0034	N/A			
			PF vs.	7.566×10^{-7}	N.S.	0.0541	N/A	0.0153	0.0004	0.0514	0.0413	0.0064	2.024×10^{-7}			
GE*Stage	6.5194	0.0018		TB vs. SS		TB vs. DS		TB vs. US		SS vs. DS		SS vs. US		DS vs. US		
			N2	9.110×10^{-5}		6.217×10^{-8}		6.005×10^{-8}		0.0029		0.0001		N.S.		
			N3	0.0008		9.315×10^{-5}		1.733×10^{-5}		N.S.		N.S.		N.S.		
GE*AP	8.9952	0.0003	Ant- vs. Post-HC		TB		DS		SS				US			
					N.S.		0.0002		4.101×10^{-7}				0.0001			
GE*ROI	1.3691	0.2098	N/A													
Stage*AP	6.6064	0.0160	Ant- vs. Post-HC				N2				N3					
							1.312×10^{-8}				8.236×10^{-5}					
Stage*ROI	2.8821	0.0160	N2 vs. N3	LT	CG	OF	PF	PC	MTO	MOP	IS	LP	LO			
				0.0051	N.S.	3.528×10^{-6}	0.0060	0.0117	N.S.	N.S.	0.0030	N.S.	N.S.			
AP*ROI	2.7922	0.0187	Ant- vs. Post-HC	LT	CG	OF	PF	PC	MTO	MOP	IS	LP	LO			
				N.S.	0.0063	N.S.	0.0004	N.S.	N.S.	0.0039	N.S.	N.S.	1.0000			
GE*Stage*AP	0.1449	0.9321	N/A													
GE*Stage*ROI	1.1404	0.3676	N/A													
GE*AP*ROI	1.3006	0.2497	N/A													
Stage*AP*ROI	1.7914	0.1165	N/A													

Table 4.7: Numbers and proportions of ipsilateral (ipsi) and contralateral (contra) NC channels showing significant NC-HC GE coupling. Overall, across all GEs, the proportions of significant channels were lower for contralateral than for ipsilateral.

	Stage	N2						N3					
	(Ant and Post combined)	ipsi			contra			ipsi			contra		
HC-GE Type	NC-GE Type	# sig chan	# nonsig chan	proportion	# sig chan	# nonsig chan	proportion	# sig chan	# nonsig chan	proportion	# sig chan	# nonsig chan	proportion
SSR	TB	81	367	0.1808	19	119	0.1377	30	418	0.0670	8	130	0.0580
	DS	207	241	0.4621	35	103	0.2536	102	346	0.2277	27	111	0.1957
	SS	143	305	0.3192	35	103	0.2536	88	360	0.1964	15	123	0.1087
	US	230	218	0.5134	54	84	0.3913	108	340	0.2411	24	114	0.1739
SS	TB	196	252	0.4375	51	87	0.3696	98	350	0.2188	18	120	0.1304
	DS	317	131	0.7076	79	59	0.5725	191	257	0.4263	46	92	0.3333
	SS	176	272	0.3929	44	94	0.3188	81	367	0.1808	20	118	0.1449
	US	322	126	0.7188	88	50	0.6377	204	244	0.4553	52	86	0.3768

Table 4.S1: Summary of events in NC-GE to HC-SSR/SS histograms. Each cell is formatted as follows: Mean±Standard Deviation (Skewness). I: ipsilateral. C: contralateral. A: Ant-HC. P: Post-HC.

GE	TB			SS			DS			US		
	NC-GE	HC-SSR	HC-SS	NC-GE	HC-SSR	HC-SS	NC-GE	HC-SSR	HC-SS	NC-GE	HC-SSR	HC-SS
N2, A, I	209±246 (1.7)	132±155 (1.8)	231±243 (1.4)	227±326 (2.6)	155±210 (2.2)	230±309 (2.2)	753±788 (1.6)	410±419 (1.6)	679±654 (1.2)	774±801 (1.8)	388±385 (1.7)	666±630 (1.3)
N2, A, C	196±269 (2.0)	130±214 (2.6)	212±245 (1.6)	213±325 (2.6)	142±233 (2.4)	217±299 (2.3)	657±791 (1.6)	371±528 (1.9)	597±586 (1.4)	706±823 (2.2)	361±499 (2.0)	621±565 (1.6)
N2, P, I	821±917 (1.6)	684±787 (1.8)	759±805 (1.2)	920±1285 (2.6)	759±989 (1.9)	824±1126 (2.4)	2710±2378 (0.88)	1851±1520 (0.65)	2187±1923 (0.69)	2701±2258 (0.77)	1737±1394 (0.67)	2083±1755 (0.63)
N2, P. C	526±700 (1.8)	451±589 (1.5)	469±635 (2.0)	482±786 (2.8)	413±702 (2.8)	435±645 (2.3)	1850±2154 (1.5)	1343±1541 (1.3)	1434±1635 (1.5)	2037±2345 (1.6)	1321±1457 (1.2)	1422±1590 (1.5)
N3, A, I	368±464 (1.9)	244±336 (2.7)	377±408 (1.4)	278±408 (2.8)	207±313 (3.0)	262±339 (2.2)	1680±1897 (1.9)	837±1012 (2.3)	1124±966 (1.4)	1874±1966 (1.7)	837±965 (2.1)	1148±923 (1.2)
N3, A, C	243±277 (1.6)	157±210 (1.9)	264±237 (1.2)	258±327 (2.1)	166±221 (1.9)	265±297 (1.8)	980±818 (0.87)	500±491 (1.2)	836±483 (0.47)	1148±882 (1.0)	509±473 (1.3)	902±430 (0.67)
N3, P, I	1266±1776 (2.3)	1100±1575 (2.2)	1095±1437 (2.1)	1218±2125 (3.7)	1037±1640 (2.4)	1045±1766 (3.5)	5499±5499 (1.1)	3489±3406 (0.91)	3586±3562 (1.2)	6058±5851 (0.97)	3476±3333 (0.89)	3586±3456 (1.2)
N3, P, C	818±1105 (2.0)	714±990 (1.9)	715±936 (2.2)	711±1223 (3.4)	588±1078 (3.4)	651±986 (2.8)	3926±4209 (1.9)	2606±2907 (1.8)	2661±2634 (2.0)	4709±4596 (1.7)	2702±2845 (1.6)	2795±2559 (1.9)

Table 4.S2: P-values for chi-square tests of homogeneity (α = 0.05 post FDR-correction applied over each column), conducted for each HC site with regard to each NC-GE type's coupling to HC-SS. Ant.: Ant-HC. Post: Post-HC. Cells marked 2.20E-016 are placeholders for $p < 2.2 \times 10^{-16}$. # signif.: number of HC sites with a non-homogeneous anatomical distribution of significantly coupled NC sites.

HC-SS	NC-GE Type	TB	DS	SS	US	TB	DS	SS	US
Patient	HC Site	N2	N2	N2	N2	N3	N3	N3	N3
1	Ant.	2.0582E-11	2.20E-016	2.20E-016	2.20E-016	0.0002	2.8534E-06	3.88E-13	0.0673
2	Ant.	2.20E-016	2.20E-016	2.20E-016	2.20E-016	2	2	2	2
3	Ant.	2.20E-016	2.20E-016	2.20E-016	2.20E-016	0.8466	0.9361	0.5576	1.0137
	Post.	2.20E-016	2.20E-016	2.20E-016	2.20E-016	0.9836	1.0220	0.5173	1.0137
4	Ant.	0.0327	0.0006	0.4236	0.0143	2.20E-016	2.20E-016	0.0002	2.284E-09
	Post.	0.0151	0.0001	0.0003	7.4779E-05	2.20E-016	1E-15	2.20E-016	2.20E-016
	Ant.	1.6218E-05	0.0006	0.1293	2.20E-016	2.20E-016	2.20E-016	2.20E-016	2.20E-016
5	Ant.	0.0018	0.0006	7.163E-11	0.0001	0.4797	1.0220	0.2163	0.2900
	Post.	0.2584	9.12E-13	0.0116	4.5188E-07	0.4797	1.0220	0.5981	1.0137
6	Ant.	0.4663	0.0085	0.0004	0.0110	8.6751E-10	3.78E-12	0.0041	0.0025
	Post.	5.8316E-08	1.0874E-11	1.07001E-08	3.2769E-10	2.20E-016	1.1269E-08	2.0565E-05	2.3435E-07
7	Ant.	0.2521	0.5388	0.0207	0.0794	0.7412	0.9361	0.3746	1.0137
8	Ant.	3.0439E-11	2.20E-016	2.20E-016	2.20E-016	1E-15	2.20E-016	2.20E-016	2.20E-016
9	Ant.	0.0011	0.0028	0.0065	0.1653	0.0946	0.0007	0.2163	0.0025
	Post.	0.0193	0.0614	0.0011	0.4801	2.2815E-05	0.4151	0.0016	0.3327
10	Ant.	0.2872	0.0007	0.7490	0.0003	0.0019	9.1424E-10	0.2163	2.07E-13
11	Ant.	2.20E-016	2.20E-016	2.20E-016	2.20E-016	0.0006	0.5080	3.0068E-05	1.0137
	Ant.	2.20E-016	2.20E-016	2.20E-016	2.20E-016	0.0050	0.9361	0.5554	0.9961
	Post.	2.20E-016	2.20E-016	2.20E-016	2.20E-016	4.58E-13	2.1548E-09	0.0621	0.6495
12	Post.	2.20E-016	2.20E-016	2.20E-016	2.20E-016	2.20E-016	1.2071E-11	2.20E-016	4.9348E-11
13	Ant.	1.3833E-10	2.20E-016	0.0018	2.20E-016	0.3811	0.9361	0.5131	0.4685
	Post.	2.20E-016	2.20E-016	5.6889E-11	2.20E-016	0.0065	4.5893E-07	0.2163	0.0004
	Ant.	7.2137E-07	9.6215E-07	0.6631	1.0715E-09	0.4423	0.2714	1.0296	0.6284
14	Post.	2.3919E-06	0.0094	0.0391	7.005E-12	0.0006	0.3934	0.1484	0.0163
15	Post.	2.20E-016	2.20E-016	1.15463E-06	2.20E-016	0.0746	0.1119	0.3089	0.2105
	Post.	9.9E-13	0.0011	3.18663E-08	0.0114	0.8466	0.6007	2.3449E-07	1.0137
16	Ant.	6.9395E-10	2.20E-016	2.20E-016	2.20E-016	0.0429	3.4673E-07	7.5853E-08	1.0745E-07
17	Ant.	0.0916	0.0004	0.1249	0.1974	0.0012	0.4151	0.5981	1.0137
18	Ant.	2.20E-016	2.20E-016	2.20E-016	2.20E-016	0.0006	0.1444	0.1139	0.2101
19	Ant.	0.2090	0.0002	0.2387	0.0004	0.8466	1.0220	0.5554	1.0137
	Post.	0.0783	0.0003	0.0019	3.7003E-05	3.7947E-10	0.2660	0.0031	0.0004
20	Ant.	2.20E-016	2.20E-016	2.20E-016	2.20E-016	2.20E-016	2.20E-016	2.20E-016	2.20E-016
# signif. HC sites (/32)		25	30	26	28	20	14	13	14

Table 4.S3: ROIs for statistical analyses of spatio-temporal differences across NC regions in NC-SWR relationships. This table is identical to Table 3.S5, but is included again here for convenience.

Combined ROI	Original Freesurfer Label(s)
Lateral temporal	Banks of superior temporal gyrus, inferior temporal, middle temporal, superior temporal, temporal pole, transverse temporal
Cingulate	Caudal anterior cingulate, rostral anterior cingulate, isthmus cingulate, posterior cingulate
Orbitofrontal	Frontal pole, lateral orbitofrontal, medial orbitofrontal, pars orbitalis
Prefrontal	Caudal middle frontal, pars opercularis, pars triangularis, rostral middle frontal, superior frontal
Paracentral	Paracentral, postcentral, precentral
Medial temporo-occipital	Entorhinal, fusiform, lingual
Medial occipito-parietal	Cuneus, pericalcarine, precuneus
Insula	Insula
Lateral occipital	Lateral occipital
Lateral parietal	Inferior parietal, superior parietal, supramarginal
Fronto-central	All labels for the following Combined ROIs: Cingulate, orbito-frontal, prefrontal, paracentral
Non-frontal	All labels for the following Combined ROIs: Lateral temporal, medial temporo-occipital, medial occipito-parietal, insula, lateral occipital, lateral parietal

Table 4.S4: Numbers of HC-NC channel pairs by NC regions of interest (ROIs) and proportions of HC-NC channel pairs with significant relationships between NC-GE and HC-SS. Ch. pairs: HC-NC channel pairs. Ant.: Ant-HC. Post.: Post-HC.

			Proportion of channels with significant HC-SS co-occurring with NC-GE types															
NC-GE Type	Total# Ch. pairs		TB				DS				SS				US			
			N2		N3		N2		N3		N2		N3		N2		N3	
ROI	Ant.	Post.	Ant.	Post.	Ant.	Post.	Ant.	Post.	Ant.	Post.	Ant.	Post.	Ant.	Post.	Ant.	Post.	Ant.	Post.
Lateral occipital	15	15	0.200	0.133	0.133	0.000	0.200	0.600	0.067	0.467	0.133	0.200	0.133	0.133	0.467	0.333	0.400	0.600
Medial temporo-occipital	31	26	0.194	0.269	0.161	0.231	0.613	0.500	0.194	0.423	0.194	0.192	0.129	0.154	0.581	0.538	0.258	0.538
Lateral parietal	74	51	0.432	0.412	0.176	0.176	0.757	0.706	0.311	0.608	0.324	0.706	0.095	0.353	0.797	0.627	0.365	0.804
Medial occipito-parietal	34	27	0.324	0.370	0.147	0.185	0.529	0.630	0.265	0.556	0.324	0.667	0.147	0.556	0.765	0.630	0.353	0.667
Lateral temporal	86	54	0.442	0.463	0.163	0.148	0.733	0.722	0.349	0.444	0.221	0.444	0.070	0.093	0.791	0.722	0.302	0.389
Insula	11	6	0.364	0.333	0.182	0.000	0.727	0.833	0.273	0.500	0.364	0.333	0.000	0.000	0.545	0.500	0.182	0.167
Paracentral	29	16	0.414	0.438	0.138	0.188	0.655	0.500	0.241	0.563	0.172	0.688	0.103	0.188	0.586	0.750	0.138	0.438
Orbitofrontal	23	6	0.739	1.000	0.435	0.167	0.783	1.000	0.565	0.167	0.261	0.833	0.087	0.333	0.870	0.833	0.478	0.500
Prefrontal	49	14	0.531	0.714	0.367	0.286	0.694	0.857	0.449	0.571	0.367	0.714	0.163	0.571	0.694	0.857	0.490	0.714
Cingulate	13	6	0.385	0.500	0.385	0.333	0.692	0.667	0.692	0.833	0.385	1.000	0.308	0.500	0.923	0.667	0.538	0.833
Total# Ch. pairs across NC / Average Proportion	365	221	0.402	0.463	0.229	0.171	0.638	0.701	0.341	0.513	0.274	0.578	0.124	0.288	0.702	0.646	0.350	0.565

Table 4.S5: Proportions of HC-NC channel pairs with significant GE-SSR or GE-HC SS relationships across NC, separated by ROI, NREM stage, NC-GE type, and ipsilateral/contralateral NC-HC pairings. ipsi: ipsilateral. contra: contralateral.

		Proportion of channels with significant HC-GE co-occurring with NC-GE types															
	NC-GE Type	TB				DS				SS				US			
	Stage	N2		N3		N2		N3		N2		N3		N2		N3	
HC-GE Type	ROI \ SWR Source	ipsi	contra	ipsi	contra	ipsi	contra	ipsi	contra	ipsi	contra	ipsi	contra	ipsi	contra	ipsi	contra
SSR	frontocentral	0.206	0.133	0.099	0.133	0.518	0.467	0.234	0.333	0.362	0.200	0.255	0.200	0.553	0.467	0.270	0.200
	nonfrontal	0.169	0.138	0.052	0.049	0.436	0.228	0.225	0.179	0.300	0.260	0.169	0.098	0.495	0.382	0.228	0.171
SS	frontocentral	0.560	0.467	0.305	0.267	0.716	0.600	0.475	0.467	0.433	0.333	0.206	0.267	0.738	0.800	0.461	0.400
	nonfrontal	0.381	0.358	0.179	0.114	0.704	0.569	0.404	0.317	0.375	0.317	0.169	0.130	0.710	0.618	0.453	0.374

Table 4.S6: Summary of 4-way ANOVA results with respect to NC-GE and HC-SS associations. LO: lateral occipital; LT: lateral temporal; CG: cingulate; OF: orbitofrontal; PF: prefrontal; PC: paracentral; MTO: medial temporo-occipital; MOP: medial occipito-parietal; IS: insula; LP: lateral parietal. N.S.: not significant (for post-hoc Tukey's range tests, $p > 0.1$).

Source	F	p-value	Post-hoc analysis (if any) and corresponding p-value (Tukey's range test)									
GE	90.4008	3.37×10^{-14}	TB vs. SS	TB vs. DS	TB vs. US	SS vs. DS	SS vs. US	DS vs. US				
			N.S.	3.843×10^{-9}	3.787×10^{-9}	3.840×10^{-9}	3.786×10^{-9}	N.S.				
Stage	242.4623	5.19×10^{-15}	N/A									
AP	54.5554	6.04×10^{-8}	N/A									
ROI	24.8837	7.77×10^{-11}		LT	CG	OF	PF	PC	MTO	MOP	IS	LP	LO
			LO vs.	0.0052	1.295×10^{-7}	1.567×10^{-7}	1.583×10^{-7}	0.0208	N.S.	0.0002	N.S.	1.815×10^{-5}	N/A
			CG vs.	8.018×10^{-5}	N/A	N.S.	N.S.	1.895×10^{-5}	2.822×10^{-7}	0.0017	4.092×10^{-7}	0.0217	1.295×10^{-7}
GE*Stage	0.1744	0.9128	N/A									
GE*AP	10.9085	0.0001	Ant- vs. Post-HC	TB	DS	SS	US					
				1.0000	0.0085	4.203×10^{-7}	0.1645					
GE*ROI	2.0318	0.0354		LT	CG	OF	PF	PC	MTO	MOP	IS	LP	LO
			TB vs. SS	N.S.	N.S.	N.S.	N.S.	N.S.	N.S.	N.S.	N.S.	N.S.	N.S.
			TB vs. DS	N.S.	0.0144	N.S.	N.S.	N.S.	N.S.	N.S.	0.0029	0.0333	N.S.
			TB vs. US	N.S.	0.0071	N.S.	N.S.	N.S.	N.S.	0.0054	N.S.	0.0050	0.0089
			SS vs. DS	0.0040	N.S.	N.S.	N.S.	N.S.	N.S.	N.S.	0.0005	N.S.	N.S.
			SS vs. US	0.0060	N.S.	0.0392	N.S.	N.S.	0.0197	N.S.	N.S.	N.S.	0.0293
			DS vs. US	N.S.	N.S.	N.S.	N.S.	N.S.	N.S.	N.S.	N.S.	N.S.	N.S.
Stage*AP	1.1129	0.3008	N/A									
Stage*ROI	7.0965	3.28×10^{-5}	N2 vs. N3	LT	CG	OF	PF	PC	MTO	MOP	IS	LP	LO
				2.696×10^{-5}	N.S.	9.627×10^{-7}	0.0047	0.0003	N.S.	0.0824	1.304×10^{-5}	0.0032	N.S.
AP*ROI	1.7693	0.1213	N/A									
GE*Stage*AP	11.1324	0.0001		N2 Ant-HC	N2 Post-HC	N3 Ant-HC	N3 Post-HC						
			NC-SS, N2 Post-HC	7.634×10^{-6}	N/A	5.141×10^{-7}	1.653×10^{-5}						
			NC-DS, N3 Ant-HC	1.038×10^{-5}	7.725×10^{-7}	N/A	0.0196						
			NC-US, N3 Ant-HC	9.516×10^{-7}	1.190×10^{-5}	N/A	0.0016						
GE*Stage*ROI	1.0388	0.4610	N/A									
GE*AP*ROI	1.6853	0.0907	N/A									
Stage*AP*ROI	2.9611	0.0139	Mostly N.S., see Results section "Differences in NC-HC SS relationship across NC regions, NREM stages, HC sites, and NC-GE types"									

REFERENCES

Alekseichuk I, Turi Z, Amador de Lara G, Antal A, Paulus W (2016) Spatial working memory in humans depends on theta and high gamma synchronization in the prefrontal cortex. Curr Biol 26:1513–1521.

Amaral DG, Cowan WM (1980) Subcortical afferents to the hippocampal formation in the monkey. J Comp Neurol 189:573–591.

Andrillon T, Nir Y, Staba RJ, Ferrarelli F, Cirelli C, Tononi G, Fried I (2011) Sleep spindles in humans: insights from intracranial EEG and unit recordings. J Neurosci Off J Soc Neurosci 31:17821–17834.

Axmacher N, Elger CE, Fell J (2008) Ripples in the medial temporal lobe are relevant for human memory consolidation. Brain J Neurol 131:1806–1817.

Aydore S, Pantazis D, Leahy RM (2013) A note on the phase locking value and its properties. NeuroImage 74:231–244.

Badre D, Kayser AS, D'Esposito M (2010) Frontal cortex and the discovery of abstract action rules. Neuron 66:315–326.

Battaglia FP, Sutherland GR, McNaughton BL (2004) Hippocampal sharp wave bursts coincide with neocortical "up-state" transitions. Learn Mem Cold Spring Harb N 11:697–704.

Benjamini Y, Hochberg Y (1995) Controlling the false discovery rate: a practical and powerful approach to multiple testing. J R Stat Soc Ser B Methodol 57:289–300.

Bonjean M, Baker T, Lemieux M, Timofeev I, Sejnowski T, Bazhenov M (2011) Corticothalamic feedback controls sleep spindle duration in vivo. J Neurosci Off J Soc Neurosci 31:9124–9134.

Bragin A, Engel J, Wilson CL, Fried I, Buzsáki G (1999) High-frequency oscillations in human brain. Hippocampus 9:137–142.

Bragin A, Penttonen M, Buzsáki G (1997) Termination of epileptic afterdischarge in the hippocampus. J Neurosci Off J Soc Neurosci 17:2567–2579.

Brázdil M, Cimbálník J, Roman R, Shaw DJ, Stead MM, Daniel P, Jurák P, Halámek J (2015) Impact of cognitive stimulation on ripples within human epileptic and non-epileptic hippocampus. BMC Neurosci 16 Available at: https://www.ncbi.nlm.nih.gov/pmc/articles/PMC4513957/ [Accessed July 16, 2018].

Buzsáki G (2015) Hippocampal sharp wave-ripple: A cognitive biomarker for episodic memory and planning. Hippocampus 25:1073–1188.

Buzsaki G, Horvath Z, Urioste R, Hetke J, Wise K (1992) High-frequency network oscillation in the hippocampus. Science 256:1025–1027.

Buzsáki G, Logothetis N, Singer W (2013) Scaling brain size, keeping timing: evolutionary preservation of brain rhythms. Neuron 80:751–764.

Canolty RT, Edwards E, Dalal SS, Soltani M, Nagarajan SS, Kirsch HE, Berger MS, Barbaro NM, Knight RT (2006) High gamma power is phase-locked to theta oscillations in human neocortex. Science 313:1626–1628.

Carpentier N, Cecchin T, Koessler L, Louis-Dorr V, Jonas J, Vignal J-P, Carpentier M, Szurhaj W, Bourgin P, Maillard L (2017) Stereo-electroencephalography identifies N2 sleep and spindles in human hippocampus. Clin Neurophysiol Off J Int Fed Clin Neurophysiol 128:1696–1706.

Carskadon MA, Dement WC (2010) Monitoring and staging human sleep. In: Principles and practice of sleep medicine, 5th ed. (Kryger MH, Roth T, Dement WC, eds), pp 16–26. St. Louis: Elsevier Saunders.

Cash SS, Halgren E, Dehghani N, Rossetti AO, Thesen T, Wang C, Devinsky O, Kuzniecky R, Doyle W, Madsen JR, Bromfield E, Erőss L, Halász P, Karmos G, Csercsa R, Wittner L, Ulbert I (2009) The human K-complex represents an isolated cortical down-state. Science 324:1084–1087.

Chrobak JJ, Buzsáki G (1996) High-frequency oscillations in the output networks of the hippocampal-entorhinal axis of the freely behaving rat. J Neurosci Off J Soc Neurosci 16:3056–3066.

Clemens Z, Mölle M, Eross L, Barsi P, Halász P, Born J (2007) Temporal coupling of parahippocampal ripples, sleep spindles and slow oscillations in humans. Brain J Neurol 130:2868–2878.

Clemens Z, Mölle M, Eross L, Jakus R, Rásonyi G, Halász P, Born J (2011) Fine-tuned coupling between human parahippocampal ripples and sleep spindles. Eur J Neurosci 33:511–520.

Clower DM, West RA, Lynch JC, Strick PL (2001) The inferior parietal lobule is the target of output from the superior colliculus, hippocampus, and cerebellum. J Neurosci Off J Soc Neurosci 21:6283–6291.

Colgin LL, Denninger T, Fyhn M, Hafting T, Bonnevie T, Jensen O, Moser M-B, Moser EI (2009) Frequency of gamma oscillations routes flow of information in the hippocampus. Nature 462:353.

Csercsa R et al. (2010) Laminar analysis of slow wave activity in humans. Brain J Neurol 133:2814–2829.

Curot J, Busigny T, Valton L, Denuelle M, Vignal J-P, Maillard L, Chauvel P, Pariente J, Trebuchon A, Bartolomei F, Barbeau EJ (2017) Memory scrutinized through electrical

brain stimulation: A review of 80 years of experiential phenomena. Neurosci Biobehav Rev 78:161–177.

Dale AM, Fischl B, Sereno MI (1999) Cortical surface-based analysis. I. Segmentation and surface reconstruction. NeuroImage 9:179–194.

Davis SW, Wing EA, Cabeza R (2018) Contributions of the ventral parietal cortex to declarative memory. Handb Clin Neurol 151:525–553.

de Lavilléon G, Lacroix MM, Rondi-Reig L, Benchenane K (2015) Explicit memory creation during sleep demonstrates a causal role of place cells in navigation. Nat Neurosci 18:493–495.

Delorme A, Makeig S (2004) EEGLAB: an open source toolbox for analysis of single-trial EEG dynamics including independent component analysis. J Neurosci Methods 134:9–21.

Desikan RS, Ségonne F, Fischl B, Quinn BT, Dickerson BC, Blacker D, Buckner RL, Dale AM, Maguire RP, Hyman BT, Albert MS, Killiany RJ (2006) An automated labeling system for subdividing the human cerebral cortex on MRI scans into gyral based regions of interest. NeuroImage 31:968–980.

Destrieux C, Bourry D, Velut S (2013) Surgical anatomy of the hippocampus. Neurochirurgie 59:149–158.

Diekelmann S, Born J (2010) The memory function of sleep. Nat Rev Neurosci 11:114–126.

Ding S-L, Van Hoesen GW (2015) Organization and detailed parcellation of human hippocampal head and body regions based on a combined analysis of cyto- and chemoarchitecture. J Comp Neurol 523:2233–2253.

Duvernoy H (1988) The human hippocampus: an atlas of applied anatomy. Munich, BY: J.F. Bergmann-Verlag.

Dykstra AR, Chan AM, Quinn BT, Zepeda R, Keller CJ, Cormier J, Madsen JR, Eskandar EN, Cash SS (2012) Individualized localization and cortical surface-based registration of intracranial electrodes. NeuroImage 59:3563–3570.

Ego-Stengel V, Wilson MA (2010) Disruption of ripple-associated hippocampal activity during rest impairs spatial learning in the rat. Hippocampus 20:1–10.

English DF, Peyrache A, Stark E, Roux L, Vallentin D, Long MA, Buzsáki G (2014) Excitation and inhibition compete to control spiking during hippocampal ripples: intracellular study in behaving mice. J Neurosci Off J Soc Neurosci 34:16509–16517.

Fanselow MS, Dong H-W (2010) Are the dorsal and ventral hippocampus functionally distinct structures? Neuron 65:7.

Fischl B, Sereno MI, Dale AM (1999a) Cortical surface-based analysis. II: Inflation, flattening, and a surface-based coordinate system. NeuroImage 9:195–207.

Fischl B, Sereno MI, Tootell RB, Dale AM (1999b) High-resolution intersubject averaging and a coordinate system for the cortical surface. Hum Brain Mapp 8:272–284.

Fischl B, van der Kouwe A, Destrieux C, Halgren E, Ségonne F, Salat DH, Busa E, Seidman LJ, Goldstein J, Kennedy D, Caviness V, Makris N, Rosen B, Dale AM (2004) Automatically parcellating the human cerebral cortex. Cereb Cortex 14:11–22.

Fletcher PC, Henson RNA (2001) Frontal lobes and human memoryInsights from functional neuroimaging. Brain 124:849–881.

Froemke RC, Dan Y (2002) Spike-timing-dependent synaptic modification induced by natural spike trains. Nature 416:433–438.

Gervasoni D, Lin S-C, Ribeiro S, Soares ES, Pantoja J, Nicolelis MAL (2004) Global forebrain dynamics predict rat behavioral states and their transitions. J Neurosci Off J Soc Neurosci 24:11137–11147.

Gilmore AW, Nelson SM, McDermott KB (2015) A parietal memory network revealed by multiple MRI methods. Trends Cogn Sci 19:534–543.

Girardeau G, Benchenane K, Wiener SI, Buzsáki G, Zugaro MB (2009) Selective suppression of hippocampal ripples impairs spatial memory. Nat Neurosci 12:1222–1223.

Girardeau G, Zugaro M (2011) Hippocampal ripples and memory consolidation. Curr Opin Neurobiol 21:452–459.

Gleiβner U, Helmstaedter C, Elger CE (1998) Right hippocampal contribution to visual memory: a presurgical and postsurgical study in patients with temporal lobe epilepsy. J Neurol Neurosurg Psychiatry 65:665–669.

Gonzalez C, Mak-McCully R, Rosen B, Cash SS, Chauvel P, Bastuji H, Rey M, Halgren E (2018) Theta bursts precede, and spindles follow, cortical and thalamic downstates in human NREM sleep. J Neurosci Off J Soc Neurosci.

Gonzalez-Martinez J, Bulacio J, Alexopoulos A, Jehi L, Bingaman W, Najm I (2013) Stereoelectroencephalography in the “difficult to localize” refractory focal epilepsy: early experience from a North American epilepsy center. Epilepsia 54:323–330.

Hagler DJ, Ulbert I, Wittner L, Erőss L, Madsen JR, Devinsky O, Doyle W, Fabo D, Cash SS, Halgren E (2018) Heterogeneous origins of human sleep spindles in different cortical layers. J Neurosci Off J Soc Neurosci.

Halgren E, Walter RD, Cherlow DG, Crandall PH (1978) Mental phenomena evoked by electrical stimulation of the human hippocampal formation and amygdala. Brain J Neurol 101:83–117.

Halgren M, Fabó D, Ulbert I, Madsen JR, Erőss L, Doyle WK, Devinsky O, Schomer D, Cash SS, Halgren E (2018) Superficial slow rhythms integrate cortical processing in humans. Sci Rep 8:2055.

Headley DB, Kanta V, Paré D (2016) Intra- and interregional cortical interactions related to sharp-wave ripples and dentate spikes. J Neurophysiol 117:556–565.

Hoppstädter M, Baeuchl C, Diener C, Flor H, Meyer P (2015) Simultaneous EEG-fMRI reveals brain networks underlying recognition memory ERP old/new effects. NeuroImage 116:112–122.

Iglói K, Doeller CF, Berthoz A, Rondi-Reig L, Burgess N (2010) Lateralized human hippocampal activity predicts navigation based on sequence or place memory. Proc Natl Acad Sci U S A 107:14466–14471.

Isomura Y, Sirota A, Ozen S, Montgomery S, Mizuseki K, Henze DA, Buzsáki G (2006) Integration and segregation of activity in entorhinal-hippocampal subregions by neocortical slow oscillations. Neuron 52:871–882.

Jacobs J, Banks S, Zelmann R, Zijlmans M, Jones-Gotman M, Gotman J (2016) Spontaneous ripples in the hippocampus correlate with epileptogenicity and not memory function in patients with refractory epilepsy. Epilepsy Behav EB 62:258–266.

Ji D, Wilson MA (2007) Coordinated memory replay in the visual cortex and hippocampus during sleep. Nat Neurosci 10:100–107.

Jiang X, Shamie I, Doyle W, Friedman D, Dugan P, Devinsky O, Eskandar E, Cash SS, Thesen T, Halgren E (2017) Replay of large-scale spatio-temporal patterns from waking during subsequent NREM sleep in human cortex. Sci Rep 7:17380.

Johnson L, Euston D, Tatsuno M, McNaughton B (2010) Stored-trace reactivation in rat prefrontal cortex is correlated with down-to-up state fluctuation density. J Neurosci Off J Soc Neurosci 30:2650–2661.

Klausberger T, Magill PJ, Márton LF, Roberts JDB, Cobden PM, Buzsáki G, Somogyi P (2003) Brain-state- and cell-type-specific firing of hippocampal interneurons in vivo. Nature 421:844–848.

Korbo L, Pakkenberg B, Ladefoged O, Gundersen HJ, Arlien-Søborg P, Pakkenberg H (1990) An efficient method for estimating the total number of neurons in rat brain cortex. J Neurosci Methods 31:93–100.

Lachaux JP, Rodriguez E, Martinerie J, Varela FJ (1999) Measuring phase synchrony in brain signals. Hum Brain Mapp 8:194–208.

Lakens D (2013) Calculating and reporting effect sizes to facilitate cumulative science: a practical primer for t-tests and ANOVAs. Front Psychol 4 Available at:

https://www.ncbi.nlm.nih.gov/pmc/articles/PMC3840331/ [Accessed September 18, 2018].

Latchoumane C-FV, Ngo H-VV, Born J, Shin H-S (2017) Thalamic spindles promote memory formation during sleep through triple phase-locking of cortical, thalamic, and hippocampal rhythms. Neuron.

Le Van Quyen M, Bragin A, Staba R, Crépon B, Wilson CL, Engel J (2008) Cell type-specific firing during ripple oscillations in the hippocampal formation of humans. J Neurosci Off J Soc Neurosci 28:6104–6110.

Lestra P, Peter-Derex L, Salin P, Comte J-C (2018) Hippocampus and prefrontal cortex exhibit spindle-like waves during REM sleep. Neurophysiol Clin 48:135–136.

Logothetis NK, Eschenko O, Murayama Y, Augath M, Steudel T, Evrard HC, Besserve M, Oeltermann A (2012) Hippocampal-cortical interaction during periods of subcortical silence. Nature 491:547–553.

Maingret N, Girardeau G, Todorova R, Goutierre M, Zugaro M (2016) Hippocampo-cortical coupling mediates memory consolidation during sleep. Nat Neurosci 19:959–964.

Mak-McCully RA, Rolland M, Sargsyan A, Gonzalez C, Magnin M, Chauvel P, Rey M, Bastuji H, Halgren E (2017) Coordination of cortical and thalamic activity during non-REM sleep in humans. Nat Commun 8:ncomms15499.

Mak-McCully RA, Rosen BQ, Rolland M, Régis J, Bartolomei F, Rey M, Chauvel P, Cash SS, Halgren E (2015) Distribution, amplitude, incidence, co-occurrence, and propagation of human K-complexes in focal transcortical recordings. eneuro 2 Available at: http://eneuro.org/content/2/4/ENEURO.0028-15.2015.abstract.

Malow BA, Carney PR, Kushwaha R, Bowes RJ (1999) Hippocampal sleep spindles revisited: physiologic or epileptic activity? Clin Neurophysiol 110:687–693.

Marshall L, Helgadóttir H, Mölle M, Born J (2006) Boosting slow oscillations during sleep potentiates memory. Nature 444:610–613.

McNaughton BL (2010) Cortical hierarchies, sleep, and the extraction of knowledge from memory. Artif Intell 174:205–214.

Mednick SC, McDevitt EA, Walsh JK, Wamsley E, Paulus M, Kanady JC, Drummond SPA (2013) The critical role of sleep spindles in hippocampal-dependent memory: a pharmacology study. J Neurosci Off J Soc Neurosci 33:4494–4504.

Miyawaki H, Diba K (2016) Regulation of hippocampal firing by network oscillations during sleep. Curr Biol CB 26:893–902.

Mölle M, Yeshenko O, Marshall L, Sara SJ, Born J (2006) Hippocampal sharp wave-ripples linked to slow oscillations in rat slow-wave sleep. J Neurophysiol 96:62–70.

Montplaisir J, Leduc L, Laverdière M, Walsh J, Saint-Hilaire JM (1981) Sleep spindles in the human hippocampus: normal or epileptic activity? Sleep 4:423–428.

Moraes W, Piovezan R, Poyares D, Bittencourt LR, Santos-Silva R, Tufik S (2014) Effects of aging on sleep structure throughout adulthood: a population-based study. Sleep Med 15:401–409.

Nádasdy Z, Hirase H, Czurkó A, Csicsvari J, Buzsáki G (1999) Replay and time compression of recurring spike sequences in the hippocampus. J Neurosci 19:9497–9507.

Niethard N, Ngo H-VV, Ehrlich I, Born J (2018) Cortical circuit activity underlying sleep slow oscillations and spindles. Proc Natl Acad Sci:201805517.

Niknazar M, Krishnan GP, Bazhenov M, Mednick SC (2015) Coupling of thalamocortical sleep oscillations are important for memory consolidation in humans. PLOS ONE 10:e0144720.

Nir Y, Staba RJ, Andrillon T, Vyazovskiy VV, Cirelli C, Fried I, Tononi G (2011) Regional slow waves and spindles in human sleep. Neuron 70:153–169.

O'Neill J, Pleydell-Bouverie B, Dupret D, Csicsvari J (2010) Play it again: reactivation of waking experience and memory. Trends Neurosci 33:220–229.

Oostenveld R, Fries P, Maris E, Schoffelen J-M (2011) FieldTrip: Open source software for advanced analysis of MEG, EEG, and invasive electrophysiological data. Comput Intell Neurosci 2011:156869.

Pakkenberg B, Gundersen HJ (1997) Neocortical neuron number in humans: effect of sex and age. J Comp Neurol 384:312–320.

Papagno C (2018) Memory deficits. In: The Parietal Lobe, pp 377–393 Handbook of Clinical Neurology. Elsevier B. V.

Patel J, Schomburg EW, Berényi A, Fujisawa S, Buzsáki G (2013) Local generation and propagation of ripples along the septotemporal axis of the hippocampus. J Neurosci Off J Soc Neurosci 33:17029–17041.

Pavlides C, Winson J (1989) Influences of hippocampal place cell firing in the awake state on the activity of these cells during subsequent sleep episodes. J Neurosci Off J Soc Neurosci 9:2907–2918.

Peyrache A, Battaglia FP, Destexhe A (2011) Inhibition recruitment in prefrontal cortex during sleep spindles and gating of hippocampal inputs. Proc Natl Acad Sci U S A 108:17207–17212.

Peyrache A, Khamassi M, Benchenane K, Wiener SI, Battaglia FP (2009) Replay of rule-learning related neural patterns in the prefrontal cortex during sleep. Nat Neurosci 12:919–926.

Piantoni G, Halgren E, Cash SS (2017) Spatiotemporal characteristics of sleep spindles depend on cortical location. NeuroImage 146:236–245.

Poppenk J, Evensmoen HR, Moscovitch M, Nadel L (2013) Long-axis specialization of the human hippocampus. Trends Cogn Sci 17:230–240.

Poulet JFA, Petersen CCH (2008) Internal brain state regulates membrane potential synchrony in barrel cortex of behaving mice. Nature 454:881–885.

Ramirez-Villegas JF, Logothetis NK, Besserve M (2015) Diversity of sharp-wave–ripple LFP signatures reveals differentiated brain-wide dynamical events. Proc Natl Acad Sci 112:E6379–E6387.

Ranganath C, Ritchey M (2012) Two cortical systems for memory-guided behaviour. Nat Rev Neurosci 13:713–726.

Rasch B, Born J (2013) About sleep's role in memory. Physiol Rev 93:681–766.

Rothschild G, Eban E, Frank LM (2016) A cortical-hippocampal-cortical loop of information processing during memory consolidation. Nat Neurosci advance online publication Available at: http://www.nature.com/neuro/journal/vaop/ncurrent/full/nn.4457.html [Accessed December 21, 2016].

Roumis DK, Frank LM (2015) Hippocampal sharp-wave ripples in waking and sleeping states. Curr Opin Neurobiol 35:6–12.

Rugg MD, King DR (2018) Ventral lateral parietal cortex and episodic memory retrieval. Cortex 107:238–250.

Rutishauser U, Aflalo T, Rosario ER, Pouratian N, Andersen RA (2017) Single-neuron representation of memory strength and recognition confidence in left human posterior parietal cortex. Neuron.

Sanchez-Vives MV, McCormick DA (2000) Cellular and network mechanisms of rhythmic recurrent activity in neocortex. Nat Neurosci 3:1027–1034.

Sato W, Kochiyama T, Uono S, Matsuda K, Usui K, Inoue Y, Toichi M (2014) Rapid, high-frequency, and theta-coupled gamma oscillations in the inferior occipital gyrus during face processing. Cortex 60:52–68.

Schreiner T, Rasch B (2015) Boosting vocabulary learning by verbal cueing during sleep. Cereb Cortex 25:4169–4179.

Seibt J, Richard CJ, Sigl-Glöckner J, Takahashi N, Kaplan DI, Doron G, Limoges D de, Bocklisch C, Larkum ME (2017) Cortical dendritic activity correlates with spindle-rich oscillations during sleep in rodents. Nat Commun 8:684.

Shipton OA, El-Gaby M, Apergis-Schoute J, Deisseroth K, Bannerman DM, Paulsen O, Kohl MM (2014) Left–right dissociation of hippocampal memory processes in mice. Proc Natl Acad Sci 111:15238–15243.

Siapas AG, Wilson MA (1998) Coordinated interactions between hippocampal ripples and cortical spindles during slow-wave sleep. Neuron 21:1123–1128.

Silber M, Ancoli-Israel S, Bonnet M, Chokroverty S, Grigg-Damberger M, Hirshkowitz M, Kapen S, Keenan S, Kryger M, Penzel T, Pressman M, Iber C (2007) The visual scoring of sleep in adults. J Clin Sleep Med JCSM 3:121–131.

Sirota A, Csicsvari J, Buhl D, Buzsáki G (2003) Communication between neocortex and hippocampus during sleep in rodents. Proc Natl Acad Sci U S A 100:2065–2069.

Skaggs WE, McNaughton BL (1996) Replay of neuronal firing sequences in rat hippocampus during sleep following spatial experience. Science 271:1870–1873.

Skaggs WE, McNaughton BL, Permenter M, Archibeque M, Vogt J, Amaral DG, Barnes CA (2007) EEG sharp waves and sparse ensemble unit activity in the macaque hippocampus. J Neurophysiol 98:898–910.

Smith M, Halgren E (1989) Dissociation of recognition memory components following temporal lobe lesions. J Exp Psychol Learn Mem Cogn 15:50–60.

Squire LR, Clark RE, Knowlton BJ (2001) Retrograde amnesia. Hippocampus 11:50–55.

Staba RJ, Wilson CL, Bragin A, Fried I, Engel J (2002) Quantitative analysis of high-frequency oscillations (80-500 Hz) recorded in human epileptic hippocampus and entorhinal cortex. J Neurophysiol 88:1743–1752.

Staba RJ, Wilson CL, Bragin A, Jhung D, Fried I, Engel J (2004) High-frequency oscillations recorded in human medial temporal lobe during sleep. Ann Neurol 56:108–115.

Staresina BP, Bergmann TO, Bonnefond M, van der Meij R, Jensen O, Deuker L, Elger CE, Axmacher N, Fell J (2015) Hierarchical nesting of slow oscillations, spindles and ripples in the human hippocampus during sleep. Nat Neurosci 18:1679–1686.

Steriade M (2001) Impact of network activities on neuronal properties in corticothalamic systems. J Neurophysiol 86:1–39.

Steriade M, Timofeev I (2003) Neuronal plasticity in thalamocortical networks during sleep and waking oscillations. Neuron 37:563–576.

Strange BA, Witter MP, Lein ES, Moser EI (2014) Functional organization of the hippocampal longitudinal axis. Nat Rev Neurosci 15:655–669.

Suh J, Foster DJ, Davoudi H, Wilson MA, Tonegawa S (2013) Impaired hippocampal ripple-associated replay in a mouse model of schizophrenia. Neuron 80:484–493.

Sullivan D, Csicsvari J, Mizuseki K, Montgomery S, Diba K, Buzsáki G (2011) Relationships between hippocampal sharp waves, ripples, and fast gamma oscillation: influence of dentate and entorhinal cortical activity. J Neurosci 31:8605–8616.

Suzuki WA, Amaral DG (2004) Functional neuroanatomy of the medial temporal lobe memory system. Cortex J Devoted Study Nerv Syst Behav 40:220–222.

Tour TD la, Tallot L, Grabot L, Doyère V, Wassenhove V van, Grenier Y, Gramfort A (2017) Non-linear auto-regressive models for cross-frequency coupling in neural time series. PLOS Comput Biol 13:e1005893.

Tulving E, Markowitsch HJ (1998) Episodic and declarative memory: role of the hippocampus. Hippocampus 8:198–204.

Van Hoesen GW (1995) Anatomy of the medial temporal lobe. Magn Reson Imaging 13:1047–1055.

Vargha-Khadem F, Gadian DG, Watkins KE, Connelly A, Van Paesschen W, Mishkin M (1997) Differential effects of early hippocampal pathology on episodic and semantic memory. Science 277:376–380.

Voytek B, D'Esposito M, Crone N, Knight RT (2013) A method for event-related phase/amplitude coupling. NeuroImage 64:416–424.

Weber B, Wellmer J, Reuber M, Mormann F, Weis S, Urbach H, Ruhlmann J, Elger CE, Fernández G (2006) Left hippocampal pathology is associated with atypical language lateralization in patients with focal epilepsy. Brain 129:346–351.

Wei Y, Krishnan GP, Komarov M, Bazhenov M (2018) Differential roles of sleep spindles and sleep slow oscillations in memory consolidation. PLOS Comput Biol 14:e1006322.

West MJ, Gundersen HJ (1990) Unbiased stereological estimation of the number of neurons in the human hippocampus. J Comp Neurol 296:1–22.

West MJ, Slomianka L, Gundersen HJ (1991) Unbiased stereological estimation of the total number of neurons in thesubdivisions of the rat hippocampus using the optical fractionator. Anat Rec 231:482–497.

Wierzynski CM, Lubenov EV, Gu M, Siapas AG (2009) State-dependent spike-timing relationships between hippocampal and prefrontal circuits during sleep. Neuron 61:587–596.

Wilson CL, Isokawa M, Babb TL, Crandall PH (1990) Functional connections in the human temporal lobe. I. Analysis of limbic system pathways using neuronal responses evoked by electrical stimulation. Exp Brain Res 82:279–292.

Wilson CL, Isokawa M, Babb TL, Crandall PH, Levesque MF, Engel J (1991) Functional connections in the human temporal lobe. II. Evidence for a loss of functional linkage between contralateral limbic structures. Exp Brain Res 85:174–187.

Wilson MA, McNaughton BL (1994) Reactivation of hippocampal ensemble memories during sleep. Science 265:676–679.

Wilson SB, Emerson R (2002) Spike detection: a review and comparison of algorithms. 113:1873–1881.

Zeithamova D, Schlichting ML, Preston AR (2012) The hippocampus and inferential reasoning: building memories to navigate future decisions. Front Hum Neurosci 6 Available at: https://www.ncbi.nlm.nih.gov/pmc/articles/PMC3312239/ [Accessed October 9, 2018].

Zhang H, Fell J, Axmacher N (2018) Electrophysiological mechanisms of human memory consolidation. Nat Commun 9:4103.